GLOBAL CHANGE & ECOSYSTEMS

Volume 1: Predictions on Terrestrial Ecosystems

Otmar Urban
Karel Klem

Global Change Research Centre
Czech Academy of Sciences, v.v.i.

Brno 2015

GLOBAL CHANGE & ECOSYSTEMS

Volume 1: Predictions on Terrestrial Ecosystems

Otmar Urban
Karel Klem

Global Change Research Centre
Czech Academy of Sciences, v.v.i.

Brno 2015

Publication of this book was supported by the Ministry of Education, Youth and Sports of the Czech Republic within the National Programme for Sustainability I, grant No. LO1415.

Title: Global Change & Ecosystems

Volume 1: Predictions on Terrestrial Ecosystems

Editors: Otmar Urban, Karel Klem

Published by: Global Change Research Centre, Czech Academy of Sciences, v.v.i.

Bělidla 986/4a, 60300 Brno, Czech Republic

First edition

Brno 2015

Contact person: Otmar Urban, T: +420511192250, E: urban.o@czechglobe.cz

ISBN: 978-80-87902-14-1

Contents

Preface

According to the United Nations Framework Convention on Climate Change, global climate change is "a change of climate which is attributed directly or indirectly to human activity that alters the composition of the global atmosphere and which is in addition to natural climate variability observed over comparable time periods".

Ecosystems are among the most important and most vulnerable of the Earth's resources, as they are critical for sustaining life on the planet. The benefits that living organisms derive from ecosystems are mostly related to energy, carbon, and water cycling, but such other elements as nitrogen and phosphorus are also of great importance. Global climate change will unquestionably affect the major cycles comprising the ways in which energy and chemicals flow through plants, herbivores, micro-organisms, and other living organisms. Depending upon ecosystems' sensitivity to the manifestations of global climate change, these impacts can be either slowed or accelerated. Ecosystems are complex systems which are difficult to model, and our ability to predict responses to global climate change is limited. Therefore, a complex study of ecosystems that combines long-term monitoring, climate manipulation experiments, and modelling is essential to mitigating, minimizing, and ameliorating the effects of global climate change on ecosystems.

In this book, we present our current knowledge of climate change scenarios at global and regional scales (chapters 1–3), their potential impacts on terrestrial, and in particular forest, grassland, and agricultural, ecosystems as well as advanced experimental approaches to investigating these impacts (chapters 4, 5, and 17). In particular, we present the results of monitoring studies and manipulation experiments documenting the effects of light (chapters 4, 6, and 9), elevated atmospheric CO_2 concentration (chapters 7 and 8), drought (chapters 10 and 11), temperature (Chapter 12), ozone (Chapter 13), and acidity (Chapter 14) on the physiology, growth, and health status of plants and ecosystems. The final chapters of the book then deal with the impacts of climate change on biodiversity (chapters 15 and 16) and land-use changes (chapters 17 and 18), including changes in ecosystem services provided by ecosystems (Chapter 18).

The book's chapters thus cover areas of atmospheric, environmental, and social sciences. We believe this book will be valuable to all those studying climatology, plant physiology, agriculture, forestry, ecology, and other related disciplines particularly from the perspective of ongoing global climate change.

In closing, we would like to extend our special thanks to the reviewers Irena Marková (Mendel University in Brno, Czech Republic), Katarína Střelcová (University of Technology in Zvolen, Slovakia), and Tatiana Kluvánková (Slovak University of Technology & Slovak Academy of Sciences, Slovakia) for their valuable critical comments which have helped us to improve all of the chapters presented in this book.

Otmar Urban, Karel Klem (editors)

Chapter 1

Climate change and future scenarios

Alexander Ač[1], Lenka Krupková[2], Michal V. Marek[1]

[1]*Laboratory of Plant Ecological Physiology, Global Change Research Centre, Czech Academy of Sciences, Bělidla 4a, CZ-60300 Brno, Czech Republic*

[2]*Department of Matters and Energy Fluxes, Global Change Research Centre, Czech Academy of Sciences, Bělidla 4a, CZ-60300 Brno, Czech Republic*

1. INTRODUCTION

In the past, Earth's climate underwent large climatic changes as a result of only natural factors. During the past several hundred thousand years, climate variability was driven largely by changes in orbital forcing, which resulted in long periods of colder climate, or ice ages, interrupted by shorter periods of warmer climate, or interglacials. This regular pattern, wherein interglacials were repeating each ca 120,000 years, was explained by the Milankovitch theory of orbital cycles (Milankovitch 1941). Other natural factors which can substantially alter the energy balance of the global atmosphere over shorter periods of time include volcanic eruptions (producing aerosols), changes in solar activity, and cosmic rays.

The onset of the last interglacial period, known as the Holocene, about 11,000 years ago, during which time global temperature oscillated by not more than 1°C (Marcott et al. 2013), enabled humans to establish agriculture and their first highly organized civilizations. At the beginning of Industrial Revolution, however, which is defined mainly by an exponential rise in human population, energy consumption, and mineral and other resource use, the world entered what many scientists call today the Anthropocene (Crutzen 2002). The use of fossil fuels over the last ca 250 years has led to a rapid increase in atmospheric CO_2 concentration ($[CO_2]$) from about 280 µmol mol^{-1} in 1850 to more than 400 µmol mol^{-1} today. In the past, CO_2 as a greenhouse gas acted as a feedback during climatic oscillations and enhanced both warming and cooling of the atmosphere (Scheffer et al. 2002). Consequently, rising $[CO_2]$ together with concentrations of such other greenhouse gases as CH_4 and N_2O are now dominant drivers of global warming, which is manifested as global climate change (GCC) (IPCC 2013). $[CO_2]$ was last as high as it is currently 15 to 10 million years ago (Tripati et al. 2009), and it is widely recognized that ongoing and expected unmitigated GCC will bring significant and often disruptive and irreversible impacts to natural ecosystems as well as human-made socio-economic systems (IPCC 2014a).

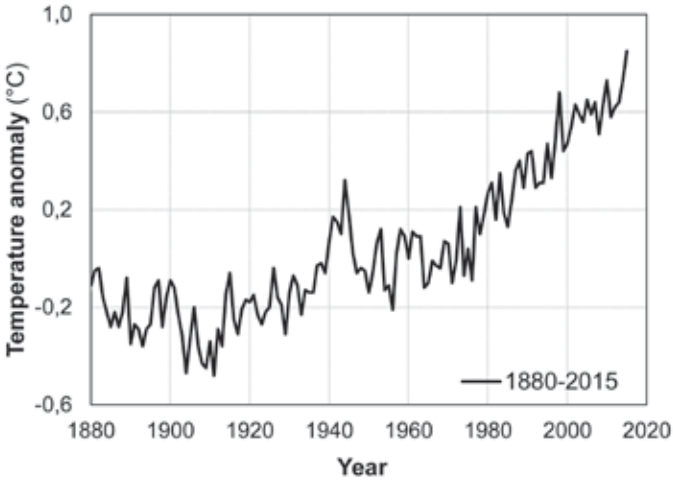

Fig. 1. *Global mean temperatures during 1880–2014 relative to 1951–1980 as calculated based on measurements from meteorological stations and ocean areas (https://www.ncdc.noaa.gov/cag/time-series/global). The current January–September period is hotter than the previous record in 2014 by about 0.1°C. Updated and adapted from Hansen et al. (2010).*

1.1. Observed selected impacts of climate change

In many ways, significant impacts of GCC can already be observed. One of the most visible signs of warming can be seen in the Arctic region, where a significant decline in summer Arctic ice cover has been detected. About 75% of the volume of Arctic ice has been lost since the 1980s (Overland & Wang 2013). Such a rapid decline in ice cover and volume is unprecedented during at least the past 1,450 years (Kinnard et al. 2011), and temperatures in some parts of the Arctic are their highest in at least 44,000 years (Miller et al. 2013). However, what happens in the Arctic does not stay in the Arctic. While specific consequences of declining ice cover on weather patterns are a matter of scientific discussion, an increasing amount of evidence points to more extreme weather at middle latitudes, such as more persistent dry and wet periods (Petoukhov et al. 2013). It has been hypothesized that this teleconnection is driven by enhanced warming of the Arctic, which affects the polar jet stream by slowing its west-to-east winds and promoting larger north–south meanders in its flow (Francis & Vavrus 2015). Irrespective of impacts outside the region, abrupt climate change with severe and often irreversible ecological consequences is already occurring in the Arctic (Duarte et al. 2012).

Ecological response to GCC is ultimately driven not by changes in average weather but by changes in weather extremes. It is not possible to attribute every weather event to GCC, but the rise in the probability of new weather records can be quantified. Fischer & Knutti (2015) estimated that about 75% of moderate temperature extremes and about 18% of moderate precipitation extremes over land areas are attributable to GCC. Moreover, the lower the probability of a given weather event, the higher is the GCC footprint. Stott et al. (2004) estimated that the likelihood of Europe's summer of 2003, which was the warmest in at least the previous 500 years and caused tens of thousands of premature deaths, almost doubled

as a result of GCC. Similarly, the probability of the present record-setting drought in California (which began in 2012 and continues as of late-2015) has been significantly aggravated by GCC (Diffenbaugh et al. 2015; Williams et al. 2015). While no significant decline in mean precipitation has been observed, increased mean temperature has led to a record decline in the Palmer drought severity index. It is generally more of a stretch to attribute precipitation extremes to GCC than it is for temperature extremes, but some of the heavier precipitation which is observed globally at approximately two-thirds of weather stations can be attributed to GCC (Min et al. 2011). Based on observations, the rate of increase in annual maximum daily rainfall intensity is estimated at 5.9–7.7% per °C of warming, with higher rates of increase in tropical regions (for a recent review, see Westra et al. 2014). Rising sea surface temperatures are also amplifying extreme precipitation (Meredith et al. 2015). In some coastal areas, where there is a combined effect of sea level rise, with an average rate of increase of 4–5 mm per year over the past 5 years, and stronger tropical cyclones, while floods which previously occurred once every 500 years are now occurring each 25 years (Reed et al. 2015). As previously predicted by climate models, real intensification of the water cycle at both extremes is thus well documented (O'Gorman 2015).

Forest ecosystems are also increasingly impacted by GCC. A recent global study has shown that longer fire seasons can be observed over almost 30 million km^2 and the burnable area of forest more than doubled from 1979 to 2013 together with the frequency of long fire seasons (Jolly et al. 2015). On a more local level, decreased burning of biomass, increased extinguishment of wildfires leading to higher forest densities, and increased drought and temperatures have led in the western USA to the largest "wildfire deficit" in at least 3,000 years (Marlon et al. 2012). Despite the increasing area of forests burned by wildfires in the USA, the wildfire deficit continues to grow. In interior Alaska, Kelly et al. (2013) have shown that the current fire regime exceeds the extent of boreal fires over the past 10,000 years, mainly as a result of increasing temperatures and drought conditions. Moreover, this increased fire activity has caused this ecosystem to lose about 12% of stored C from 1950 to 2006 (Kelly et al. 2015). Significantly increased fire activity has been detected also in neighbouring tundra ecosystems (Hu et al. 2015). The combination of higher temperatures and increased wildfires has also lead to higher tree mortality after fires (van Mantgem et al. 2013).

The rapidly shifting climate favours species with fast migration rates and which are highly adaptable. As a consequence, forests in general are increasingly affected negatively by outbreaks of pests (Zhang et al. 2014) and diseases, which are killing large swaths of forests. Kurz et al. (2008) reported that an outbreak of *Dendroctonus ponderosae* in managed pine forests in British Columbia was an order of magnitude larger than any known previous pest outbreak. During its worst year, the net source of CO_2 from the beetle outbreak was equivalent to ca 75% of C emissions from all forest fires in Canada over 40 years. It also appears that forest ecosystems are more sensitive to drought than was previously thought (Allen et al. 2010; Choat et al. 2012). This means increased tree mortality in the western USA (van Mantgem et al. 2009), Canada (Peng et al. 2011), and around the world (Anderegg et al. 2013). Consequently, there are records of reduced C-sink capacity of forests in western Canada (Ma et al. 2012; Chen & Luo 2015), the western USA (Schwalm et al. 2012), Asia (Liu et al. 2013), and the Amazon tropical forest over the past 30 years (Brienen et al. 2015).

Apart from forest ecosystems, GCC is already affecting food production in many places around the world and the global net effect is negative (IPCC 2014a). A slowdown has been observed in the rate of increase in yields of such crops as maize and wheat, leading to greater food insecurity. Even more worryingly, GCC has been found to have played an important role in triggering the civil war in Syria. That conflict was preceded

by an historic drought that was intensified by GCC and which led to migration of as many as 1.5 million farmers into rural areas and heightened ethnic tensions (Kelley et al. 2015). The link between violence and GCC is further supported by the evidence that interpersonal and intergroup violence has risen by 4% and 14%, respectively, for each standard deviation change in temperature (becoming warmer) or rainfall (becoming more extreme) (Hsiang et al. 2013).

1.2. Enhancing feedbacks of climate change

Without any additional climate feedbacks, a doubling of atmospheric [CO_2] would lead to 1.2ºC of warming (Wolff et al. 2015). The climate system is nevertheless interconnected with various feedback mechanisms which lead to either weakening or strengthening of the initial warming. The net effect of all feedbacks is expected significantly to strengthen the warming trend (IPCC 2013).

Two of the strongest and fastest negative feedbacks are ocean and land C sinks. Together these constantly absorb ca 55% of anthropogenic C emissions (Knorr 2009), which means that they have been increasing in strength over time (Ballantyne et al. 2012). Both observational and modelling evidence suggest, however, that the capacities of both ocean (Marsay et al. 2015) and land C sinks will diminish in future, although the magnitude of such change is uncertain (Friedlingstein 2015).

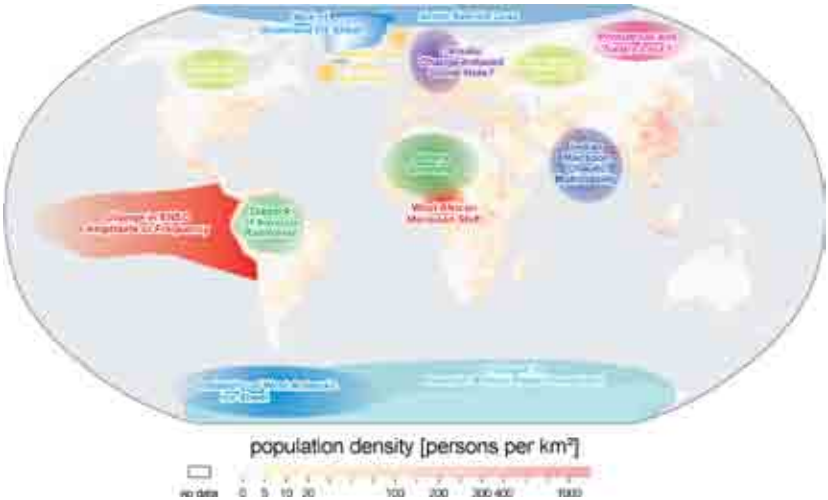

Fig. 2. *Important Earth ecosystems which may undergo significant abrupt changes in future with important implications for humans. Different levels of climate warming are required to trigger "tipping points". Adapted with permission from Lenton et al. (2008).*

Weakening of the terrestrial C sink capacity is expected to be the result mainly of disintegrating forests as they are affected by greater drought and temperature stress (Anderegg et al. 2013), extreme weather (Gu et al. 2008), pest outbreaks (Kurz et al. 2008), and forest fires (Jolly et al. 2015). A recent study stated that while terrestrial ecosystems may continue to absorb C, albeit at a slower rate, incorporating N and P limitation into the calculation meant that global land sinks would switch to become C sources by the middle of

this century (Wieder et al. 2015). An increasing number of studies have suggested that many forest ecosystems will become net C sources in coming decades (Williams et al. 2012; Anderegg et al. 2015). In fact, recent reviews have considered as a possible scenario large-scale disintegration and tipping-point crossing (see Figs. 2 and 3) for boreal (Gauthier et al. 2015), temperate (Millar & Stephenson 2015), and tropical (Lewis et al. 2015) forests.

Another potentially strong feedback is in the far North above the Arctic Circle. Permafrost that is already melting – and which seems to be melting faster than had been estimated by climate models – will continue to melt into the foreseeable future. The amount of stored C in the upper 3 m of permafrost is approximately double the amount of C in the atmosphere. According to expert assessments, about 10% of permafrost C, which is equivalent to 162–288 Pg C, could be released into the atmosphere by 2100 under the worst-case emission scenario (Schuur et al. 2013; for further description of emission scenarios see also chapters 2 and 11). This estimate is somewhat greater than model estimates of up to 112 Pg C (Koven et al. 2015). The latest research suggests that the release of C from terrestrial permafrost will occur gradually and over decades rather than abruptly and add 0.13–0.27°C to warming by 2100 (Schuur et al. 2015).

Yet another strong feedback is hidden under the sea beds in the form of frozen methane hydrates. Although the scenario of CH_4 or CO_2 escaping from the ocean floor has until recently been mainly theoretical, new and solid evidence from paleoclimate data make this now appear more real and likely. Westbrook et al. (2009) showed that gas bubbles escaping from the West Spitsbergen seabed at depths of 150 to 400 m may have been a result of the ocean's warming by 1°C over the previous 30 years. The amount of CH_4 is not yet large enough to enter the atmosphere, but this may change with further ocean warming. In addition, a study by Johnson et al. (2015) has documented methane plumes escaping from the ocean bed in the Cascadia margin at depths of 180 to 500 m. These observed methane anomalies may be the result of sea water warming in this region, although, again, the amount of CH_4 is not large enough to enter the atmosphere. CH_4 is escaping into the atmosphere from the East Siberian Arctic Shelf, however, probably due to degradation of submarine permafrost over thousands of years (Shakhova et al. 2013). Inasmuch as the Arctic region is expected to warm 2–3 times faster than the global mean, there is a certain potential for abrupt release of methane from the ocean shelf (Whiteman et al. 2013). A renewed increase in the global CH_4 level since about 2007 might be explained by some of the aforementioned processes, as well as by the recently described teleconnection between declining Arctic ice and increased CH_4 emission from northern wetlands (Parmentier et al. 2015).

Probably the best-known enhancing feedback, and which is rather easily predictable, is the Arctic ice albedo decline. Using direct satellite measurements, Pistone et al. (2014) estimated that reduced albedo has caused ca 6.4 W m^{-2} of radiative forcing since 1979. Such forcing is approximately double that of previous model estimates and is equivalent to as much as 25% of direct forcing caused by CO_2 emissions. Similarly, though not as strongly as in the case of Arctic ice, declining albedo is also speeding the melting of the Greenland ice sheet (GIS) (Box et al. 2012).

1.3. Expected impacts of climate change

Various Earth (eco)systems have different sensitivity to GCC and thus also different spatio-temporal responses. It is estimated that, given the long lifetime of [CO_2] and the long lagged responses of such factors as oceans, some GCC impacts will be irreversible over hundreds and possibly even thousands of years (Solomon et al. 2009). While the transition to "simplified" ecosystems (Lewis et al. 2015; Nagelkerken &

Connell 2015) may be gradual or abrupt, a commonly used term for the moment when significant simplification or disruption cannot be avoided is "tipping point" (Barnosky & Hadly 2015; Drijfhout et al. 2015). Recent evidence suggests that we may be closer to such tipping point elements in the Earth's system than had previously been thought (Lenton et al. 2008).

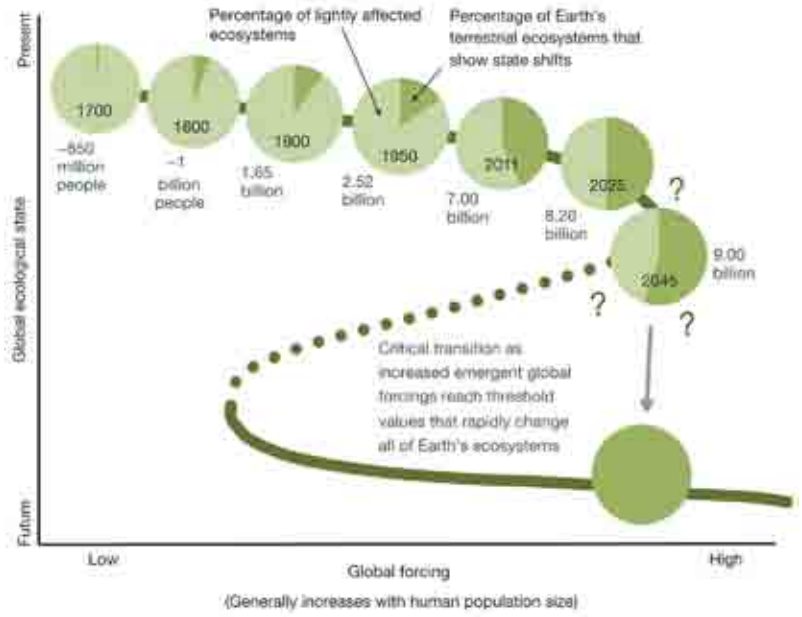

Fig. 3. *Schematic view of Earth's state shift forwards the tipping point when abrupt global change will become irreversible. Notice the increasing fraction of ecosystems that had underdone drastic changes by 2011. The global ecosystem may react to the disturbance in the same way as local ecosystems did in the past. Understanding feedback mechanisms that lead to abrupt transitions is critical for predicting the future. Adapted with permission from Barnosky et al. (2012).*

As mentioned above, Arctic ice is very sensitive to temperature change, with potentially strong strengthening feedback mechanisms. The current generation of climate models significantly underestimates the rate of Arctic ice decline (Stroeve et al. 2012). A recalibration of models with recent observations led to an estimation that further warming of about 2°C would lead to the disappearance of Arctic ice cover in September with profound implications for the broader region (Mahlstein & Knutti 2012). Linear extrapolations based on Arctic ice volume decline from 1996 onwards points to the disappearance of Arctic ice as early as 2016 (Maslowski et al. 2012). Were the Arctic ice to disappear in summer, however, it would be for the first time in 4 million years (Knies et al. 2014).

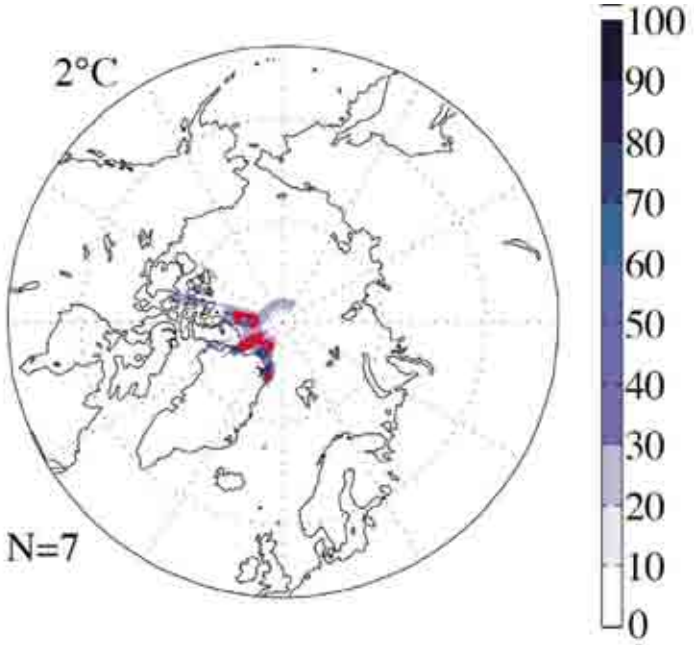

Fig. 4. *Arctic sea ice is predicted to disappear in coming years and decades with further warming of about 2°C. N shows the number of model simulations. Figure adapted from Mahlstein & Knutti (2012).*

Closely linked to the Arctic region are the surrounding vast areas of permafrost. As mentioned in section 1.2., thawing of the permafrost would add significantly to the GCC problem once significant areas of permafrost began to thaw irreversibly in coming decades. Recent evidence suggests that slight further warming of ca 0.5°C above present temperatures would be sufficient to trigger this process (Vaks et al. 2013). Climate sensitivity seems to be much higher than previously thought also for melting of large parts of the GIS and the West Antarctica ice sheet (WAIS). Large areas of the GIS are situated farther below sea level than was previously thought and are thus much more sensitive to ocean warming than is assumed by models (Morlighem et al. 2014). New paleoclimate evidence from the interglacial period 400,000 years ago shows that temperatures only ca 1°C warmer than today were sufficient to trigger irreversible thawing of large parts of the GIS (Reyes et al. 2014). In fact, no further warming is necessary to melt parts of the WAIS, which would lead to an irreversible sea level rise of ca 1–2 m in coming decades and centuries (Joughin et al. 2014; Rignot et al. 2014). With a further rise in global temperature of 1–2°C, a sea level rise of 6–13 m would be unavoidable (Dutton et al. 2015).

Marine ecosystems are also surprisingly sensitive to even small changes in global air temperature. The latest experimental and modelling evidence suggests that a rise of 0.5°C above present temperatures would be sufficient to cause significant or terminal damage to about 90% of the world's coral reefs and that even under the optimistic scenario of high coral adaptability and low greenhouse gas concentrations one-third of coral reefs would suffer long-term degradation (Frieler et al. 2013). Furthermore, the combination of

warmer oceans with reduced pH would lead to overall "simplified" oceans with reduced productivity and energy flows, thereby leaving little room in future for the rest of ocean biodiversity to acclimate successfully (Nagelkerken & Connell 2015). Similar trends towards simplification are expected in agricultural systems and food production (Bailey et al. 2015), forest ecosystems (Trumbore et al. 2015), and socio-economic systems (Turner 2014). Without GCC mitigation, moreover, mean global incomes could be reduced by ca 23% by 2100, according to Burke et al. (2015), who also state that current climate models severely underestimate economic losses. This situation has forced many researchers to conclude that even global warming limited to 2°C higher than preindustrial temperatures is "highly dangerous" (Hansen et al. 2015).

1.4. Future scenarios and mitigation of climate change

Policy makers' current focus regarding climate change mitigation is upon the critical temperature threshold of 2°C warmer than in the preindustrial period. This threshold has its origins in the summit of the United Nations Framework Convention on Climate Change at Rio de Janeiro in 1992, where global leaders agreed to "prevent dangerous anthropogenic interference with the climate system". Following intense scientific and policy discussions, the 2°C limit became widely accepted as desirable and potentially reachable given technological progress and practical economic tools. However, as a result of recent progress in our understanding of the climate sensitivity of various of the Earth's critical systems, as outlined above, more scientists and policy makers are calling for an even lower temperature limit of 1.5°C. That would require rapid reduction in fossil fuels emissions at the global level, and the window for this goal is "small and rapidly closing" (Rogelj et al. 2015). Currently, the world is tracking the highest emission scenarios projected by the Intergovernmental Panel on Climate Change, and there is observational evidence of a rapid and persistent rise in global C emissions with the exception of during global economic recessions (Friedlingstein et al. 2014). Therefore, some have implied that solving the problem of GCC (i.e. keeping the temperature rise below 2°C or 1.5°C) is impossible without giving up on the continuation of economic growth (Anderson & Bows 2012).

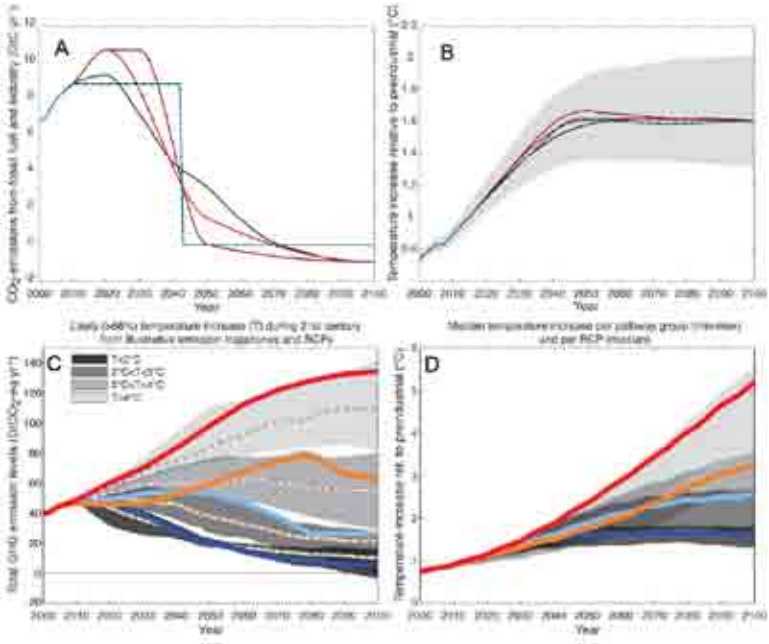

Fig. 5. *CO_2 emission scenarios from fossil fuel burning* (**a**) *compatible with limiting global mean temperature increase to 2°C* (**b**)*. Total emission of all anthropogenic greenhouse gases (GHGs) according to a range of Representative Concentration Pathway (RCP) scenarios (represented by different coloured lines)* (**c**)*, and respective rise in global mean temperature through 2100* (**d**)*. Grey areas show probability ranges of emission and temperature scenarios. Adapted from IPCC (2013; see the original IPCC report for a more detailed description of this figure).*

In order to achieve a 66% probability of avoiding a rise of 2°C, cumulative C emissions should not surpass 1,000 Gt CO_2 between 2011 and 2100 (IPCC 2014b). Over the first 4 years, and taking into account only emissions from energy production, more than 16% of this budget has already been spent (Global Carbon Project 2015). At this rate, our C budget would be surpassed well before 2040. Consequently, energy-related C emissions would need to decline increasingly until reaching 10% annual decrease by 2025 and then continue to decline at this rate until virtual elimination by 2050, which is 50 years sooner than had been suggested by the Intergovernmental Panel on Climate Change (Anderson 2015). In other words, about 33% of known oil reserves, 50% of known natural gas reserves, and more than 80% of known coal reserves should remain unused (McGlade & Ekins 2015).

2. CASE STUDY AT MOUNTAIN RESEARCH SITE

To confirm the manifestation of global change, and in particular an increase in air temperature, on a local scale, a case study was made based upon comprehensive analysis of a data set for daily mean air temperatures. The observations were performed at the Bílý Kříž experimental research site in the Beskydy Mountains (Czech Republic, 49°30′N, 18°32′E, 875 m a.s.l.). The research site, climate, and composition of the forest ecosystem are described in details in chapters 4, 5, 6, and 13 of this book and by Kratochvílová et al. (1989). At present, the experimental research site is a part of various international research networks and infrastructures, including CarboEurope-IP (http://www.carboeurope.org), ICOS (http://www.icos-infrastructure.eu), and AnaEE (http://www.anaee.com).

Table 1. *Mean daily air temperatures (Ta) during investigated time periods and p-value of the Kruskal–Wallis test. Statistically significant ($p < 0.01$) differences in comparison to the reference period 1989–1999 are indicated in bold.*

	Mean daily *Ta* (°C)	***p***
1989–1999	5.6	–
2000–2004	6.0	0.051
2005–2009	6.6	**<0.001**
2010–2014	7.0	**<0.001**

The experimental research site is equipped with a climatological station providing standardized observations of air temperature and precipitation in accordance with the methodologies of the Czech Hydrometeorological Institute and World Meteorological Organization. Observation at this station was initiated in 1988. Today, air temperature is measured automatically using an RHA1 temperature sensor (Delta-T Devices, Cambridge, UK). We analysed daily mean air temperatures for the 1989–2014 growing seasons and took the years 1989–1999 as reference period. The reference period was chosen in order not to comprise the studied years and yet to be as long as possible. Three 5-year periods (i.e. 2000–2004, 2005–2009, and 2010–2014) were analysed. The comparison examined daily mean air temperature (*T*a) during the investigated years (Table 1) and for individual months (Table 2).

Table 2. Daily mean air temperatures (°C) in individual months for investigated time periods.

	Jan	Feb	Mar	Apr	May	June	July	Aug	Sept	Oct	Nov	Dec
1989–1999	–2.96	–2.39	0.21	4.58	10.08	13.11	15.49	15.53	10.58	5.83	0.22	–3.35
2000–2004	–4.77	–2.56	0.43	5.33	12.05	14.11	15.22	16.55	9.91	6.81	2.29	–3.41
2005–2009	–2.98	–2.96	–0.23	7.20	11.48	14.82	17.34	15.32	11.97	6.87	1.88	–2.13
2010–2014	–3.40	–3.40	1.50	7.30	11.50	14.90	17.30	16.60	12.00	7.40	3.90	–2.10

Table 3. *p*-values of the Kruskal–Wallis test of the mean air temperatures in individual months for investigated time periods. Significant differences ($p < 0.01$) in comparison to the reference period 1989–1999 are indicated in bold.

	Jan	Feb	Mar	Apr	May	June	July	Aug	Sept	Oct	Nov	Dec
2000–2004	**<0.001**	0.580	0.560	0.140	**<0.001**	0.024	0.390	**0.008**	0.073	0.036	**<0.001**	0.710
2005–2009	0.820	0.220	0.680	**<0.001**	**0.010**	**<0.001**	**<0.001**	0.540	**<0.001**	**0.011**	**<0.001**	**0.001**
2010–2014	0.250	0.340	**0.003**	**<0.001**	**0.003**	**<0.001**	**<0.001**	0.032	**<0.001**	**0.001**	**<0.001**	**0.001**

Table 4. Comparison of the normal distribution functions of the mean air temperatures in individual months of investigated time periods in comparison to the 1989–1999 reference period. D+ (D–) = statistically significant increase (decrease) in air temperature.

	Jan	Feb	Mar	Apr	May	June	July	Aug	Sept	Oct	Nov	Dec
2000–2004	D–				D+			D+			D+	
2005–2009				D+	D+	D+	D+		D+	D+	D+	D+
2010–2014			D+	D+	D+	D+	D+		D+	D+	D+	D+

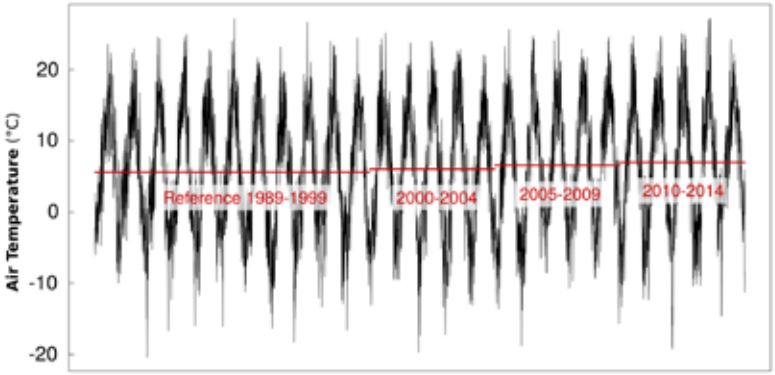

Fig. 6. *Seasonal courses of daily mean air temperature at the Bílý Kříž experimental research site during the reference period 1989–1999 and three examined periods 5 years long.*

According to the *p*-values of the non-parametric Kruskal–Wallis test, *T*a significantly increased in periods 2005–2009 and 2010–2014 as compared to the 1989–1999 reference period. In addition, the Kruskal–Wallis test revealed significantly different values of daily mean *T*a in individual months across the investigated periods (Table 3). Comparison of the normal distribution functions of the mean *T*a for individual months revealed significant increases in *T*a during the periods studied compared to 1989–1999 (Table 4). The analyses thus evidenced small and gradual, increase in daily mean *T*a at the Bílý Kříž experimental research site in comparison to 1989–1999 (Fig. 6). Increasing temperature has substantial effects on carbon capture within ecosystems, as detailed in chapters 6 and 12 of this book. Nevertheless studies investigating impacts of expected climate change, including impacts of global warming and heat waves, on mountain ecosystems are still rare.

3. CONCLUSIONS

Given the exponentially rising global population, and with most individuals struggling to achieve higher living standards and consequently greater energy consumption, anthropogenic pressures are increasingly detectable at the global scale. We do not know exactly where the "global" tipping point is or where the damage to our collective environment will become unbearable and surpass adaptation limits. In many parts of the world, environmental pressures are already too high and are forcing people to leave their homes permanently. We nevertheless do know that the status quo of global civilization is not sustainable. We either will face up to and address the challenges of the future or we will suffer the consequences of our inaction.

Acknowledgement

This work was supported by the Ministry of Education, Youth and Sports of the Czech Republic within the National Programme for Sustainability I, grant No. LO1415.

References

Allen, C.D., Macalady, A.K., Chenchouni, H. et al. (2010) A global overview of drought and heat-induced tree mortality reveals emerging climate change risks for forests. *Forest Ecology and Management*, **259**, 660–684.

Anderegg, W.R.L., Flint, A., Huang, C. et al. (2015) Tree mortality predicted from drought-induced vascular damage. *Nature Geoscience*, **8**, 367–371.

Anderegg, W.R.L., Kane, J.M. & Anderegg, L.D.L. (2013) Consequences of widespread tree mortality triggered by drought and temperature stress. *Nature Climate Change*, **3**, 30–36.

Anderson, K. (2015) Duality in climate science. *Nature Geoscience*, Early online publication.

Anderson, K. & Bows, A. (2012) A new paradigm for climate change. *Nature Climate Change*, **2**, 639–640.

Bailey, R., Benton, T.G., Challinor, A. et al. (2015) *Extreme Weather and Resilience of the Global Food System*. Final Project Report from the UK-US Taskforce on Extreme Weather and Global Food System Resilience, The Global Food Security Programme, UK.

Ballantyne, AP., Alden, C.B., Miller, J.B., Tans, P.P. & White, J.W.C. (2012) Increase in observed net carbon dioxide uptake by land and oceans during the past 50 years. *Nature*, **488**, 70–72.

Barnosky, A.D. & Hadly, E.A. (2015) *End Game: Tipping Point for Planet Earth?* HarperColllins, London.

Barnosky, A.D., Hadly, E.A., Bascompte, J. et al. (2012) Approaching a state shift in Earth's biosphere. *Nature*, **486**, 52–58.

Box, J.E., Fettweis, X., Stroeve, J.C., Tedesco, M., Hall, D.K. & Steffen, K. (2012) Greenland ice sheet albedo feedback: thermodynamics and atmospheric drivers. *The Cryosphere*, **6**, 821–839.

Brienen, R.J.W., Phillips, O.L., Feldpausch, T.R. et al. (2015) Long-term decline of the Amazon carbon sink. *Nature*, **519**, 344–348.

Burke, M., Hsiang, S.M. & Miguel, E. (2015) Global non-linear effect of temperature on economic production. *Nature*, Early online publication.

Crutzen, P.J. (2002) Geology of mankind. *Nature*, **415**, 23.

Diffenbaugh, N.S., Swain, D.L. & Touma, D. (2015) Anthropogenic warming has increased drought risk in California. *Proceedings of the National Academy of Sciences of the United States of America*, **112**, 3931–3936.

Drijfhout, S., Bathiany, S., Beaulieu, C. et al. (2015) Catalogue of abrupt shifts in Intergovernmental Panel on Climate Change climate models. *Proceedings of the National Academy of Sciences of the United States of America*, Early online publication.

Duarte, C.M., Lenton, T.M., Wadhams, P. & Wassmann, P. (2012) Abrupt climate change in the Arctic. *Nature Climate Change*, **2**, 60–62.

Dutton, A., Carlson, A., Long, A. et al. (2015) Sea-level rise due to polar ice-sheet mass loss during past warm periods. *Science*, **349**, 6244.

Fischer, E.M. & Knutti, R. (2015) Anthropogenic contribution to global occurrence of heavy-precipitation and high-temperature extremes. *Nature Climate Change*, **5**, 560–564.

Francis, J.A. & Vavrus, S.J. (2015) Evidence for a wavier jet stream in response to rapid Arctic warming. *Environmental Research Letters*, **10**, 014005.

Friedlingstein, P. (2015) Carbon cycle feedbacks and future climate change. *Philosophical Transactions of the Royal Society A: Mathematical, Physical and Engineering Sciences*, **373**, 20140421.

Friedlingstein, P., Andrew, R.M., Rogelj, J. et al. (2014) Persistent growth of CO_2 emissions and implications for reaching climate targets. *Nature Geoscience*, **7**, 709–715.

Frieler, K., Meinshausen, M., Golly, A. et al. (2013) Limiting global warming to 2°C is unlikely to save most coral reefs. *Nature Climate Change*, **3**, 165–170.

Gauthier, S., Bernier, P., Kuuluvainen, T., Shvidenko, A.Z. & Schepaschenko, D.G. (2015) Boreal forest health and global change. *Science*, **349**, 819–822.

Global Carbon Project (2015) The Global Carbon Project, Global Carbon Atlas Emissions. available online at: http://www.globalcarbonatlas.org/?q=en/emissions.

Gu, L., Hanson, P.J., Post, W. Mac et al. (2008) The 2007 Eastern US spring freeze: increased cold damage in a warming world. *Bioscience*, **58**, 253–262.

Hansen, J., Ruedy, R., Sato, M. & Lo, K. (2010) Global surface temperature change. *Reviews of Geophysics*, **48**, RG4004.

Hansen, J., Sato, M., Hearty, P. et al. (2015) Ice melt, sea level rise and superstorms: evidence from paleoclimate data, climate modeling, and modern observations that 2°C global warming is highly dangerous. *Atmospheric Chemistry and Physics Discussions*, **15**, 20059–20179.

Hsiang, S.M., Burke, M. & Miguel, E. (2013) Quantifying the influence of climate on human conflict. *Science*, **341**, 1235367.

Hu, F.S., Higuera, P.E., Duffy, P. et al. (2015) Arctic tundra fires: natural variability and responses to climate change. *Frontiers in Ecology and the Environment*, **13**, 369–377.

Chen, H.Y.H. & Luo, Y. (2015) Net aboveground biomass declines of four major forest types with forest ageing and climate change in western Canada's boreal forests. *Global Change Biology*, **21**, 3675–3684.

Choat, B., Jansen, S., Brodribb, T.J. et al. (2012) Global convergence in the vulnerability of forests to drought. *Nature*, **491**, 752–755.

IPCC (2013) Climate Change 2013: The Physical Science Basis. Contribution of Working Group I to the Fifth Assessment Report of the Intergovernmental Panel on Climate Change (eds T.F. Stocker, D. Qin, G.-K. Plattner, M. Tignor, S.K. Allen, J. Boschung, A. Nauels, Y. Xia, V. Bex & P.M. Midgley). Cambridge University Press, Cambridge, United Kingdom and New York, NY, USA.

IPCC (2014a) Climate Change 2014: Impacts, Adaptation, and Vulnerability. Part A: Global and Sectoral Aspects. Contribution of Working Group II to the Fifth Assessment Report of the Intergovernmental Panel on Climate Change (eds C.B. Field, V.R. Barros, D.J. Dokken, K.J. Mach, M.D. Mastrandrea, T.E. Bilir, M. Chatterjee, K.L. Ebi, Y.O. Estrada, R.C. Genova, B. Girma, E.S. Kissel, A.N. Levy, S. MacCracken, P.R. Mastrandrea & L.L. White). Cambridge University Press, Cambridge, United Kingdom and New York, NY, USA.

IPCC (2014b) Climate Change 2014: Synthesis Report. Contribution of Working Groups I, II and III to the Fifth Assessment Report of the Intergovernmental Panel on Climate Change (eds R.K. Pachauri & L.A. Meyer). IPCC, Geneva, Switzerland.

Johnson, H.P., Miller, U.K., Salmi, M.S. & Solomon, E.A. (2015) Analysis of bubble plume distributions to evaluate methane hydrate decomposition on the continental slope. *Geochemistry, Geophysics, Geosystems*, Early online publication.

Jolly, W.M., Cochrane, M.A., Freeborn, P.H. et al. (2015) Climate-induced variations in global wildfire danger from 1979 to 2013. *Nature Communications*, **6**, 7537.

Joughin, I., Smith, B.E. & Medley, B. (2014) Marine ice sheet collapse potentially under way for the Thwaites Glacier Basin, West Antarctica. *Science*, **344**, 735–738.

Kelley, C.P., Mohtadi, S., Cane, M.A., Seager, R. & Kushnir, Y. (2015) Climate change in the Fertile Crescent and implications of the recent Syrian drought. *Proceedings of the National Academy of Sciences of the United States of America*, **112**, 3241–3246.

Kelly, R., Genet, H., McGuire, A.D. & Hu, F.S. (2015) Palaeodata-informed modelling of large carbon losses from recent burning of boreal forests. *Nature Climate Change*, Early online publication.

Kelly, R., Chipman, M.L., Higuera, P.E., Stefanova, I., Brubaker, L.B. & Hu, F.S. (2013) Recent burning of boreal forests exceeds fire regime limits of the past 10,000 years. *Proceedings of the National Academy of Sciences of the United States of America*, **110**, 13055–13060.

Kinnard, C., Zdanowicz, C.M., Fisher, D.A., Isaksson, E., de Vernal, A. & Thompson, L.G. (2011) Reconstructed changes in Arctic sea ice over the past 1,450 years. *Nature*, **479**, 509–512.

Knies, J., Cabedo-Sanz, P., Belt, S.T., Baranwal, S., Fietz, S. & Rosell-Melé, A. (2014) The emergence of modern sea ice cover in the Arctic Ocean. *Nature Communications*, **5**, 5608.

Knorr, W. (2009) Is the airborne fraction of anthropogenic CO_2 emissions increasing? *Geophysical Research Letters*, **36**, L21710.

Koven, C.D., Schuur, E.A.G., Schädel, C. et al. (2015) A simplified , data-constrained approach to estimate the permafrost carbon – climate feedback Subject Areas : *Philosophical Transactions of the Royal Society A: Mathematical, Physical and Engineering Sciences*, **373**, 20140423.

Kratochvílová, I., Janouš, D., Marek, M., Barták, M. & Říha, L. (1989) Production activity of mountain cultivated Norway spruce stands under the impact of air pollution. I. General description of problems. *Ecology (CSSR)*, **8**, 407–419.

Kurz, W.A., Dymond, C.C., Stinson, G. et al. (2008) Mountain pine beetle and forest carbon feedback to climate change. *Nature*, **452**, 987–990.

Lenton, T.M., Held, H., Kriegler, E. et al. (2008) Tipping elements in the Earth's climate system. *Proceedings of the National Academy of Sciences of the United States of America*, **105**, 1786–1793.

Lewis, S.L., Edwards, D.P. & Galbraith, D. (2015) Increasing human dominance of tropical forests. *Science*, **349**, 827–832.

Liu, H., Park Williams, A., Allen, C.D. et al. (2013) Rapid warming accelerates tree growth decline in semi-arid forests of Inner Asia. *Global Change Biology*, **19**, 2500–2510.

Ma, Z., Peng, C., Zhu, Q. et al. (2012) Regional drought-induced reduction in the biomass carbon sink of Canada's boreal forests. *Proceedings of the National Academy of Sciences of the United States of America*, **109**, 2423–2427.

Mahlstein, I. & Knutti, R. (2012) September Arctic sea ice predicted to disappear near 2°C global warming above present. *Journal of Geophysical Research*, **117**, D06104.

van Mantgem, P.J., Nesmith, J.C.B., Keifer, M., Knapp, E.E., Flint, A. & Flint, L. (2013) Climatic stress increases forest fire severity across the western United States. *Ecology Letters*, **16**, 1151–1156.

van Mantgem, P.J., Stephenson, N.L., Byrne, J.C. et al. (2009) Widespread increase of tree mortality rates in the western United States. *Science*, **323**, 521–524.

Marcott, S.A., Shakun, J.D., Clark, P.U. & Mix, A.C. (2013) A Reconstruction of Regional and Global Temperature for the Past 11,300 Years. *Science*, **339**, 1198–1201.

Marlon, J.R., Bartlein, P.J., Gavin, D.G. et al. (2012) Long-term perspective on wildfires in the western USA. *Proceedings of the National Academy of Sciences of the United States of America*, **109**, E535–E543.

Marsay, C.M., Sanders, R.J., Henson, S.A., Pabortsava, K., Achterberg, E.P. & Lampitt, R.S. (2015) Attenuation of sinking particulate organic carbon flux through the mesopelagic ocean. *Proceedings of the National Academy of Sciences of the United States of America*, **112**, 1089–1094.

Maslowski, W., Clement Kinney, J., Higgins, M. & Roberts, A. (2012) The future of Arctic sea ice. *Annual Review of Earth and Planetary Sciences*, **40**, 625–654.

McGlade, C. & Ekins, P. (2015) The geographical distribution of fossil fuels unused when limiting global warming to 2°C. *Nature*, **517**, 187–190.

Meredith, E.P., Semenov, V.A., Maraun, D., Park, W. & Chernokulsky, A. V. (2015) Crucial role of Black Sea warming in amplifying the 2012 Krymsk precipitation extreme. *Nature Geoscience*, **8**, 615–619.

Milankovitch, M.M. (1941) Kanon der Erdbestrahlung und seine Anwendung auf des Eizeitenproblem. R. Serbian Acad. Spec. Publ. 132, Sect. Math. Nat. Sci., 33. Beograd: Köninglich Serbische Akademie. Reprinted in English: Canon of Insolation and the Ice-Age Problem. Zavod za udzbenikb i nastavna sredstva, Beograd (1998).

Millar, C.I. & Stephenson, N.L. (2015) Temperate forest health in an era of emerging megadisturbance. *Science*, **349**, 823–826.

Miller, G.H., Lehman, S.J., Refsnider, K. a., Southon, J.R. & Zhong, Y. (2013) Unprecedented recent summer warmth in Arctic Canada. *Geophysical Research Letters*, **40**, 5745–5751.

Min, S.-K., Zhang, X., Zwiers, F.W. & Hegerl, G.C. (2011) Human contribution to more-intense precipitation extremes. *Nature*, **470**, 378–381.

Morlighem, M., Rignot, E., Mouginot, J., Seroussi, H. & Larour, E. (2014) Deeply incised submarine glacial valleys beneath the Greenland ice sheet. *Nature Geoscience*, **7**, 418–422.

Nagelkerken, I. & Connell, S.D. (2015) Global alteration of ocean ecosystem functioning due to increasing human CO_2 emissions. *Proceedings of the National Academy of Sciences of the United States of America*, Early online publication.

O'Gorman, P.A. (2015) Precipitation Extremes Under Climate Change. *Current Climate Change Reports*, **1**, 49–59.

Overland, J.E. & Wang, M. (2013) When will the summer Arctic be nearly sea ice free? *Geophysical Research Letters*, **40**, 2097–2101.

Parmentier, F.-J.W., Zhang, W., Mi, Y. et al. (2015) Rising methane emissions from northern wetlands associated with sea ice decline. *Geophysical Research Letters*, **42**, 7214–7222.

Peng, C., Ma, Z., Lei, X. et al. (2011) A drought-induced pervasive increase in tree mortality across Canada's boreal forests. *Nature Climate Change*, **1**, 467–471.

Petoukhov, V., Rahmstorf, S., Petri, S. & Joachim, H. (2013) Quasiresonant amplification of planetary waves and recent Northern Hemisphere weather extremes. *Proceedings of the National Academy of Sciences of the United States of America*, **110**, 5331–5341.

Pistone, K., Eisenman, I. & Ramanathan, V. (2014) Observational determination of albedo decrease caused by vanishing Arctic sea ice. *Proceedings of the National Academy of Sciences of the United States of America*, **111**, 3322–3326.

Reed, A.J., Mann, M.E., Emanuel, K.A. et al. (2015) Increased threat of tropical cyclones and coastal flooding to New York City during the anthropogenic era. *Proceedings of the National Academy of Sciences of the United States of America*, Early online publication.

Reyes, A. V, Carlson, A.E., Beard, B.L. et al. (2014) South Greenland ice-sheet collapse during Marine Isotope Stage 11. *Nature*, **510**, 525–528.

Rignot, E., Mouginot, J., Morlighem, M., Seroussi, H. & Scheuchl, B. (2014) Widespread, rapid grounding line retreat of Pine Island, Thwaites, Smith, and Kohler glaciers, West Antarctica, from 1992 to 2011. *Geophysical Research Letters*, **41**, 3502–3509.

Rogelj, J., Luderer, G., Pietzcker, R.C. et al. (2015) Energy system transformations for limiting end-of-century warming to below 1.5°C. *Nature Climate Change*, **5**, 519–527.

Shakhova, N., Semiletov, I., Leifer, I. et al. (2013) Ebullition and storm-induced methane release from the East Siberian Arctic Shelf. *Nature Geoscience*, **7**, 64–70.

Scheffer, M., Brovkin, V., Cox, P.M. et al. (2002) Positive feedback between global warming and atmospheric CO_2 concentration inferred from past climate change. *Journal of Geophysical Research*, **33**, 1–22.

Schuur, E.A.G., Abbott, B.W., Bowden, W.B. et al. (2013) Expert assessment of vulnerability of permafrost carbon to climate change. *Climatic Change*, **119**, 359–374.

Schuur, E.A.G., McGuire, A.D., Grosse, G. et al. (2015) Climate change and the permafrost carbon feedback. *Nature*, **520**, 171–179.

Schwalm, C.R., Williams, C.A., Schaefer, K. et al. (2012) Reduction in carbon uptake during turn of the century drought in western North America. *Nature Geoscience*, **5**, 551–556.

Solomon, S., Plattner, G.-K., Knutti, R. & Friedlingstein, P. (2009) Irreversible climate change due to carbon dioxide emissions. *Proceedings of the National Academy of Sciences of the United States of America*, **106**, 1704–1709.

Stott, P.A., Stone, D.A. & Allen, M.R. (2004) Human contribution to the European heatwave of 2003. *Nature*, **432**, 610–614.

Stroeve, J.C., Kattsov, V., Barrett, A. et al. (2012) Trends in Arctic sea ice extent from CMIP5, CMIP3 and observations. *Geophysical Research Letters*, **39**, L16502.

Tripati, A.K., Roberts, C.D. & Eagle, R.A. (2009) Coupling of CO_2 and ice sheet stability over major climate transitions of the last 20 million years. *Science*, **326**, 1394–1397.

Trumbore, S., Brando, P. & Hartmann, H. (2015) Forest health and global change. *Science*, **349**, 814–818.

Turner, G.M. (2014) *Is Global Collapse Imminent? An Updated Comparison of The Limits to Growth with Historical Data*. Melbourne Sustainable Society Institute, The University of Melbourne.

Vaks, A., Gutareva, O.S., Breitenbach, S.F.M. et al. (2013) Speleothems reveal 500,000-year history of Siberian permafrost. *Science*, **340**, 183–186.

Westbrook, G.K., Thatcher, K.E., Rohling, E.J. et al. (2009) Escape of methane gas from the seabed along the West Spitsbergen continental margin. *Geophysical Research Letters*, **36**, L15608.

Westra, S., Fowler, H.J., Evans, J.P. et al. (2014) Future changes to the intensity and frequency of short-duration extreme rainfall. *Reviews of Geophysics*, **52**, 522–555.

Whiteman, G., Hope, C. & Wadhams, P. (2013) Vast costs of Arctic change. *Nature*, **499**, 401–403.

Wieder, W.R., Cleveland, C.C., Smith, W.K. & Todd-Brown, K. (2015) Future productivity and carbon storage limited by terrestrial nutrient availability. *Nature Geoscience*, **8**, 441–444.

Williams, P.A., Allen, C.D., Macalady, A.K. et al. (2012) Temperature as a potent driver of regional forest drought stress and tree mortality. *Nature Climate Change*, **3**, 292–297.

Williams, P.A., Seager, R., Abatzoglou, J.T., Cook, B.I., Smerdon, J.E. & Cook, E.R. (2015) Contribution of anthropogenic warming to California drought during 2012-2014. *Geophysical Research Letters*, **42**, 6819–6828.

Wolff, E.W., Shepherd, J.G., Shuckburgh, E. & Watson, A.J. (2015) Feedbacks on climate in the Earth system: introduction. *Philosophical Transactions of the Royal Society of London A: Mathematical, Physical and Engineering Sciences*, **373**, 20140428.

Zhang, X., Lei, Y., Ma, Z., Kneeshaw, D. & Peng, C. (2014) Insect-induced tree mortality of boreal forests in eastern Canada under a changing climate. *Ecology and Evolution*, **4**, 2384–2394.

Chapter 2

Climate change scenarios for Europe (with special attention to the Czech Republic) in terms of changes in temperature, precipitation, and drought conditions

Martin Dubrovský[1], Miroslav Trnka[2]

[1]*Department of Climate Variability and Climate Change Analysis, Global Change Research Centre, Czech Academy of Sciences, Bělidla 4a, CZ-60300 Brno, Czech Republic*

[2]*Department of Climate Change Impacts on Agroecosystems, Global Change Research Centre, Czech Academy of Sciences, Bělidla 4a, CZ-60300 Brno, Czech Republic*

1. INTRODUCTION

Climate change (CC) scenarios for use in CC impact studies are mostly based on simulations of future climate made using global climate models (GCMs) run with a given emission scenario. This chapter addresses some features (spatial structures and annual cycles of changes in temperature, precipitation, and drought risk) of CC scenarios derived from GCM simulations for use in CC impact experiments made by the Global Change Research Centre.

The CC scenarios were derived from the outputs of 40 GCM simulations* available from the Coupled Model Intercomparison Project Phase 5 (CMIP5) database (Taylor et al. 2012), which was used for the latest (fifth) Intergovernmental Panel on Climate Change (IPCC) Assessment Report (IPCC 2013). The CC scenarios shown in this chapter are based on GCM simulations driven by the RCP8.5 emission scenario. The maps are based on only those GCMs for which temperature and precipitation data were available for 1961–2100. Where multiple runs were available for a given GCM, we used only the first run for which data were available. The scenarios were defined in terms of changes (with respect to the 1961–1990 baseline) in climatic characteristics for two future periods: 2021–2050 and 2071–2100. Temperature changes were defined as the differences between future and reference values. Precipitation changes were defined in terms of percentage change with respect to baseline total precipitation. Changes in drought conditions are defined in terms of the relative Palmer drought severity index (rPDSI; Dubrovsky et al. 2009) for the entire year and its intermediate product, the relative Z-index, for individual seasons. Considering the high temporal persistency, the rPDSI is not a suitable indicator of drought risk changes for sub-annual periods because its changes are approximately identical for individual seasons.

2. DATA AND METHODOLOGY

Individual maps displaying changes in temperature, precipitation, and drought conditions show statistics derived from 40 values based on individual GCMs. Colours represent median values (MED), and the shape

* The 40 GCMs used to create the present CC scenarios are (using the official CMIP5 acronyms): ACCESS1-0, ACCESS1-3, bcc-csm1-1, bcc-csm1-1-m, BNU-ESM, CanESM2, CCSM4, CESM1-BGC, CESM1-CAM5, CESM1-WACCM, CMCC-CESM, CMCC-CM, CMCC-CMS, CNRM-CM5, CSIRO-Mk3-6-0, EC-EARTH, FGOALS-g2, FIO-ESM, GFDL-CM3, GFDL-ESM2G, GFDL-ESM2M, GISS-E2-H, GISS-E2-H-CC, GISS-E2-R, GISS-E2-R-CC, HadGEM2-AO, HadGEM2-CC, HadGEM2-ES, IPSL-CM5A-LR, IPSL-CM5A-MR, IPSL-CM5B-LR, MIROC5, MIROC-ESM, MIROC-ESM-CHEM, MPI-ESM-LR, MPI-ESM-MR, MRI-CGCM3, MRI-ESM1, NorESM1-M, and NorESM1-ME.

of the grid-specific symbols represents intermodel variability in terms of the STD/MED ratio (STD being the standard deviation): the lowest variability corresponding to the best agreement among GCMs is shown by squares and the highest variability is indicated by empty 4-point stars (i.e. the larger the symbol, the better the inter-model concordance).

Discussion as to the spatial structure of the CC scenarios found below focuses upon CC projected for the end of the 21st century while assuming the RCP8.5 emission scenario, which includes substantial increases in greenhouse gas (GHG) concentrations. This combination (a distant future period coupled with high emissions) implies the largest bias in the CC signal from noise (due to natural climate variability), which enables better identification of the characteristic features of the spatial pattern of CC.

Maps of multi-GCM scenarios for Europe are shown in Figs. 1–3. The same maps but for 2021–2050 are presented in Figs. 4–6 (RCP8.5 scenario) and Figs. 7–8 (RCP4.5 scenario). In the latter case (RCP4.5), changes in temperature and precipitation were derived from RCP8.5-based scenarios by applying the pattern scaling approach (Santer et al. 1990; Dubrovsky et al. 2005). This method is based on an assumption that changes in climatic characteristics will be proportional to changes in the global mean temperature. Specifically in our case, changes for the RCP4.5 emission scenario were obtained by multiplying the RCP8.5-based changes by k, which is defined according to the following equation:

$$k = [T_{glob}(\text{RCP4.5},2035) - T_{glob}(\text{RCP4.5},1975)] / [T_{glob}(\text{RCP8.5},2035) - T_{glob}(\text{RCP8.5},1975)],$$

where $T_{glob}(ES,Y)$ is the global mean temperature simulated by the Model for the Assessment of Greenhouse Gas Induced Climate Change (MAGICC) (Harvey et al. 1997; Hulme et al. 2000) for emission scenario ES and year Y. In our case, we obtain $k = 0.88$. The pattern scaling method and MAGICC were employed also in IPCC's aforementioned Fifth Assessment Report (IPCC 2013). The next section will focus on the spatial structure of changes in surface air temperature, precipitation, and drought indices for RCP8.5 emissions.

3. RESULTS AND DISCUSSION

3.1. Temperature changes

Changes in surface temperature (Fig. 1) in Europe exhibit increases in all seasons of the year. Increases in summer tend to be greater towards the south (temperatures in the south over land further from the sea are projected to increase by nearly 7°C, especially over the interiors of the Balkan and Iberian peninsulas). In winter, the spatial gradient of temperature increase has the opposite direction: it gets higher towards the north (nearly 9°C in north-eastern Scandinavia). We might also note that temperature increases in summer over land are much greater than are those over sea. In the Czech Republic, summer temperatures should increase by about 5°C and spring temperatures by about 4.5°C, while changes in autumn and winter should be between these two values. As for inter-model variability, which may be considered to be (partly) a result of the modelling uncertainty involved in GCM-based future climate projections, the square symbol (which occurs in the western Czech Republic in spring) indicates good concordance among GCMs: the STD(ΔT)/MED(ΔT) ratios, based on 40 values of ΔT, are less than 0.25 or within 0.25–0.5, which indicates good inter-model concordance.

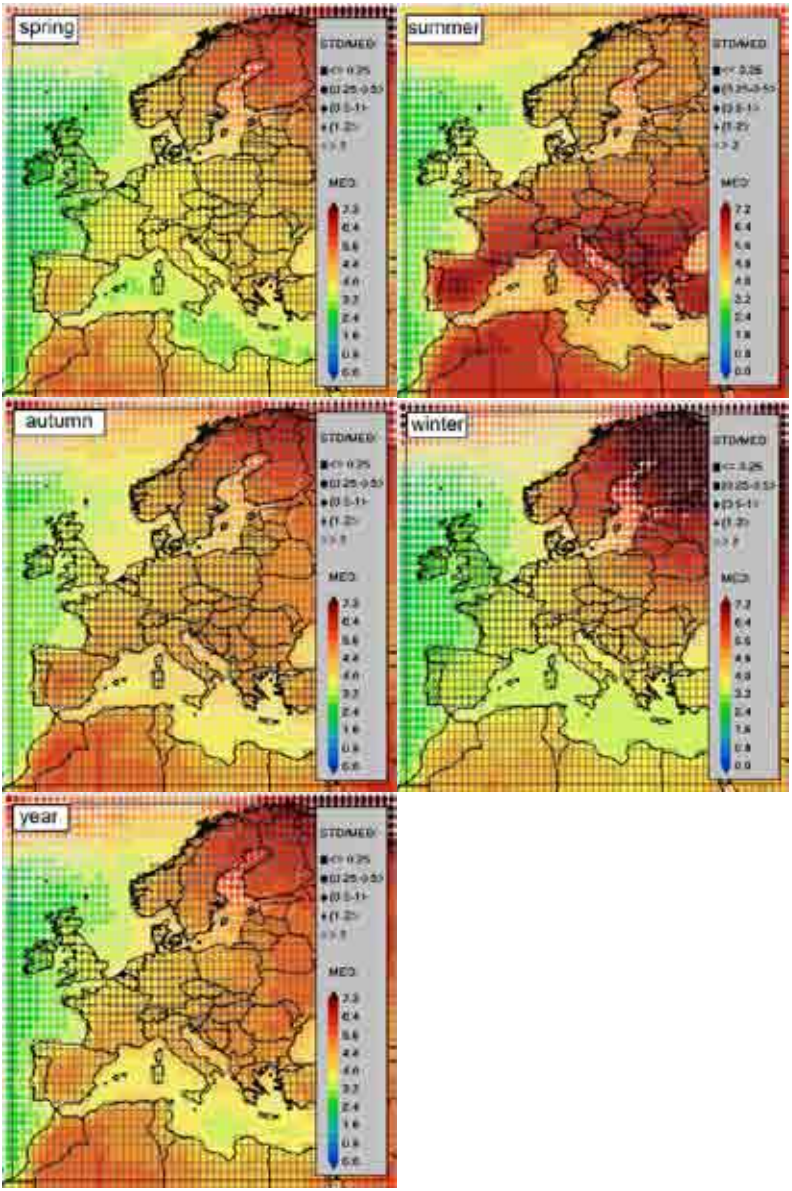

Fig. 1. *Temperature (°C) change scenarios based on 40 global climate model (GCM) simulations (CMIP5 database) for the RCP8.5 emission scenario for individual seasons and the year as a whole. Additive changes for 2071–2100 are expressed with respect to the 1961–1990 reference period. Colours represent the median value, and symbol shape expresses inter-GCM variability (standard deviation-to-median ratio [STD/MED]).*

3.2. Precipitation changes

The maps in Fig. 2 show that the south-to-north gradient can be detected also in precipitation changes, and it is substantially positive (changes are greater to the north) in all seasons of the year. Decreases in total precipitation in southern Europe give way to increases in northern Europe, resulting in a latitudinal band of insubstantial precipitation changes. This band moves throughout the year, with its northernmost position occurring in summer and its southernmost in winter. As a result of the spatial pattern of precipitation changes and its movement throughout the year, precipitation changes north of (approximately) the 62nd parallel will be positive in all seasons and those south of the 40th parallel always negative. In the Czech Republic, total precipitation will decrease in summer, increase in winter, increase less substantially in spring, and change insubstantially in autumn. The inter-model variability of precipitation changes is substantially greater than that of temperature changes, which is obvious especially in the band of insubstantial precipitation changes. As distance from this band increases, concordance among models improves. Specifically within the Czech Republic, the STD/MED ratio is within 0.5–1 in winter, within 1–2 in spring and summer, and > 2 in autumn. In terms of statistical significance, we could state that precipitation changes with STD/MED ratios higher than (approximately) 3 may be considered insignificant (95% confidence level). Therefore, considering the values shown in the maps together with the well-expressed spatial structure of the changes and its seasonal cycle, we feel safe stating that precipitation will increase in summer and decrease in winter.

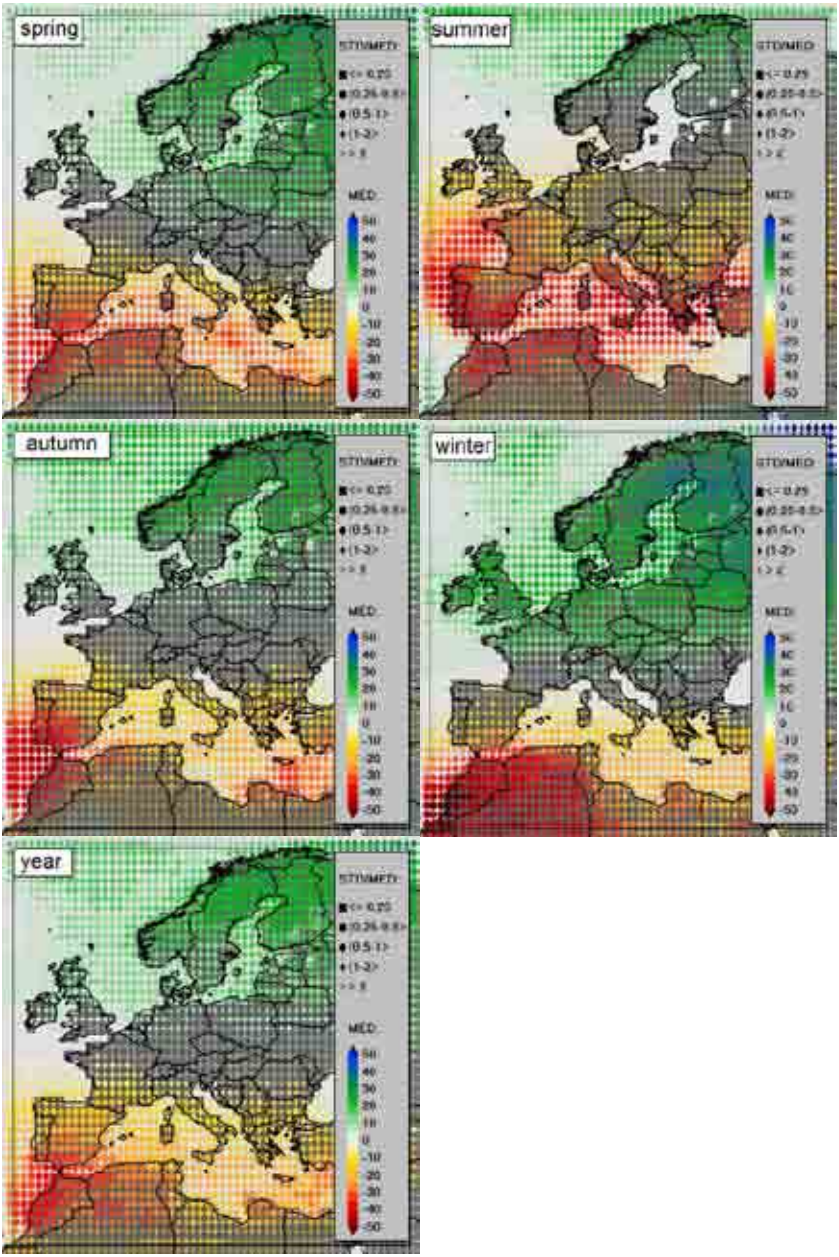

Fig. 2. *Scenarios for precipitation change. Multiplicative changes in precipitation (%) for 2071–2100 are expressed with respect to the 1961–1990 reference period. See Fig. 1 for more details on legend.*

3.3. Changes in drought risk

Considering the fact that drought risk increases with rising temperature (which is projected for all of Europe) and decreasing precipitation, the maps showing the changes in drought conditions (Fig. 3) only quantitatively supplement our expectations following from the spatial patterns of changes in temperature and precipitation (Figs. 1–2): drought risk will substantially increase in most of Europe, and especially so south of the band of insubstantial precipitation changes. The most substantial increase in drought risk in summer results from the substantial increase (the greatest across all seasons) in temperature coupled with the substantial decrease in summer precipitation. Drought risk is projected to increase also during other seasons in most of Europe, and the magnitude of that change correlates with the changes in temperature and precipitation. Drought risk will decrease only in areas and seasons where the negative (drought-suppressing) effect of increased precipitation will be larger than the positive (drought-elevating) effect of increased temperature. This in fact holds only for winter in Ireland and western Scandinavia, where an insubstantial decrease in winter drought risk may be expected. Mean rPDSI values (bottom map in Fig. 3) indicate that future mean annual conditions may be classified as extreme drought (with respect to present normal conditions) nearly everywhere in Europe. We should point out, however, that the rPDSI model used herein (Wells et al. 2004) utilizes the Thornthwait equation for potential evapotranspiration and that it is considered for warmer climate conditions to be less appropriate than is the Penman–Monteith equation. The latter equation was preferred by such authors as Burke et al. (2006), Hoerling et al. (2012), Dai (2013), and van der Schrier et al. (2013). On the other hand, we suggest that even the present version of rPDSI may be applied in warmer climate conditions if its outputs are suitably corrected: Dubrovsky et al. (2014) found that the two equations for evapotranspiration imply very similar spatial structures of PDSI changes, differing only in the multiplicative factor. Specifically, results from the Thornthwait equation for rPDSI values at the end of the 21st century are approximately twice as large as are the results from the Penman–Monteith equation. Consequently, if extreme drought in the present climate is indicated by rPDSI < -4, we may assume that extreme drought conditions in the warmer climate will be rather implied by rPDSI values < -8. For more on this, see also the Results in Chapter 11 of this book.

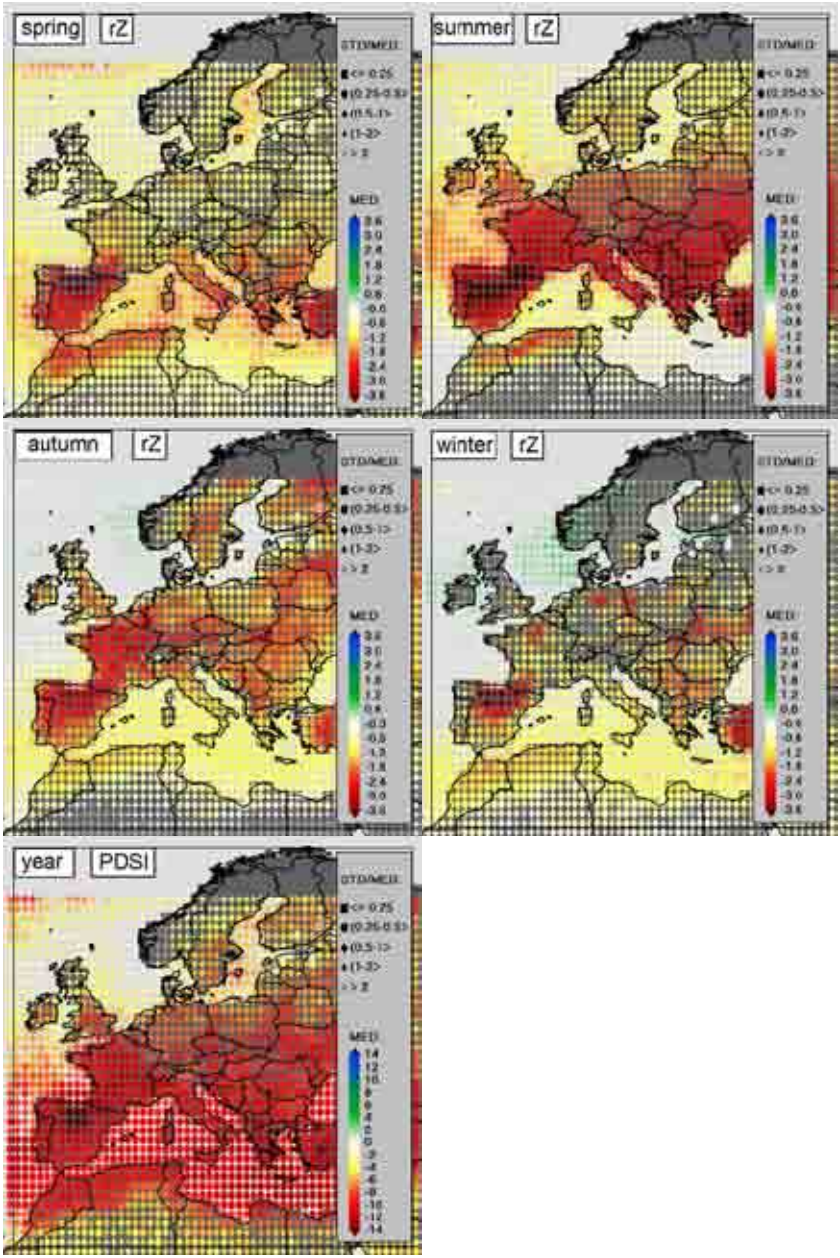

Fig. 3. *Scenarios for mean values of relative Z-index (rZ; related to seasons) and relative Palmer drought severity index (PDSI; for the whole year), determined using the PDSI model calibrated using reference 1961–1990 model-simulated monthly series and then applied to 2071–2100 model-simulated series. See Fig. 1 for more details on legend.*

3.4. Comparison of future climate projections based on CMIP3 and CMIP5 data sets

The present CC scenarios based on the GCMs included in the CMIP5 database are similar to those derived from the older CMIP3 models (Meehl et al. 2007), which were used for the IPCC's Fourth Assessment Report (IPCC 2007). In comparing the CC scenarios derived from the two data sets, it should be remembered that the new climate projections relate to emission scenarios which differ from those used previously. Bearing this in mind, we will now compare the present scenarios derived from 40 GCMs run using the RCP8.5 emissions scenario (which scenario assumes substantial increases in GHG concentrations implying high increases in global mean temperature) with CC scenarios derived by Dubrovsky et al. (2015) from 16 GCMs (CMIP3 database) run using the SRES-A2 emission scenario, which was considered to be one of the most extremely high emission scenarios within the CMIP3 database. We have chosen SRES-A2 because the number of GCM simulations for the even more extreme SRES-A1T emission scenario was much lower. As the SRES-A2 emission scenario assumes lower (as compared to RCP8.5) GHG emissions (and therefore smaller increases in global mean temperature), the old scenarios were adjusted using the pattern scaling approach: they were multiplied by the scale factor 1.27, which corresponds to the ratio of global temperature change (2071–2100 vs 1961–1990) simulated by MAGICC for the RCP8.5 vs the SRES-A2 emission scenarios. Only after making this adjustment may we effectively compare two characteristics of the CC scenarios: the spatial pattern of the changes and their annual cycle.

When comparing the CC scenarios based on the (adjusted) CMIP3 and CMIP5 data sets, we find that the CMIP5-based projection indicates smaller temperature increases. The larger increases in summer temperatures north of (approximately) the 50th parallel (which also imply a less substantial meridional gradient of temperature changes during this season) show an apparent deviation from this rule. The inter-model variability of the CMIP5-based scenarios is mostly slightly greater in comparison with that of the CMIP3-based scenarios. Again, different results are found in northern Europe, where the new CC scenarios show improved inter-model concordance. Concerning the Czech Republic, the new scenarios indicate larger temperature increases in summer and smaller increases in the rest of the year.

Precipitation changes derived from the CMIP5 and CMIP3 data sets show very similar spatial patterns, but the changes (both increases and decreases) based on CMIP5 are less substantial. Generally, the new scenarios show less substantial precipitation increases in northeast Europe in winter as well as less substantial precipitation decreases in southern Europe in spring and summer. Similarly to temperature changes, the inter-model variability of precipitation changes based on CMIP5 is somewhat greater. Within the Czech Republic, the precipitation change scenarios based on CMIP3 and CMIP5 are very similar in terms of both CC signal magnitude and inter-model variability. As a result of the aforementioned differences between CMIP3-based and CMIP5-based scenarios of temperature and precipitation changes, the CMIP5-based projections indicate less substantial increases in drought risk in all seasons of the year throughout Europe. Despite this finding, the CC-induced increase in drought risk (based on CMIP5) in the Czech Republic may be regarded as very substantial in all seasons. That is especially the case in summer, however, when the model projections based on CMIP3 and CMIP5 are approximately equal.

Regarding CC scenarios for 2021–2050, the maps shown in Figs. 4–8 exhibit the same spatial structure of changes as do the aforementioned scenarios for 2071–2100. In fact, the only difference consists in the changes' magnitude, which is proportional to the changes in global mean temperature for the given future and emission scenario (as mentioned above, the scenarios for RCP4.5 and 2021–2050 were created by scaling the changes for RCP8.5 and 2071–2100). Apart from that, we emphasise that changes in the near

future (2021–2050) are generally affected by larger inter-model uncertainty (compared to changes in the distant future of 2071–2100), which results from the lower ratio of CC signal to natural climate variability. This is apparent especially in precipitation changes, which bear much higher (compared to temperature changes) inter-model uncertainty. For example, the summer values of STD(ΔP)/MED(ΔP) for 2021–2050 in Central Europe (including the Czech Republic) are larger than 2 nearly everywhere, but this ratio falls below 2 (and below 1 in Poland) for 2071–2100. Because the STD/MED ratio does not change when we scale the CC scenarios by global temperature change, it appears that the pattern scaling approach for determining CC scenarios for the lower emission scenarios and/or less distant future is more advantageous than is using GCM-simulated data for a given target future and emissions. The reason lies in the fact that, in this case, CC scenarios determined using the pattern scaling approach are less affected by natural climate variability noise and thus better capture the CC signal.

4. CONCLUSION

This chapter presented CC scenarios derived from the GCM simulations available from the CMIP5 database. Emphasis was given to scenarios derived for the RCP8.5 emission scenario and 2071–2100. This combination was selected in order to obtain a strong CC signal from the GCM-simulated data, thereby enabling improved identification of the CC signal's spatial structure and annual cycle. Though the chapter presented CC scenarios only for temperature and precipitation for selected combinations of emission scenarios and future periods, it should be mentioned that we have available an elaborated methodology for creating CC scenarios also for other surface weather characteristics; for any future period, emission scenario, and climate sensitivity; and for any site on the globe. That means we may provide CC scenarios for a wide range of CC impact experiments. CC scenarios may be also linked with stochastic weather generators, thus enabling the creation of realistic time series for surface weather characteristics representing both present and future climatic conditions.

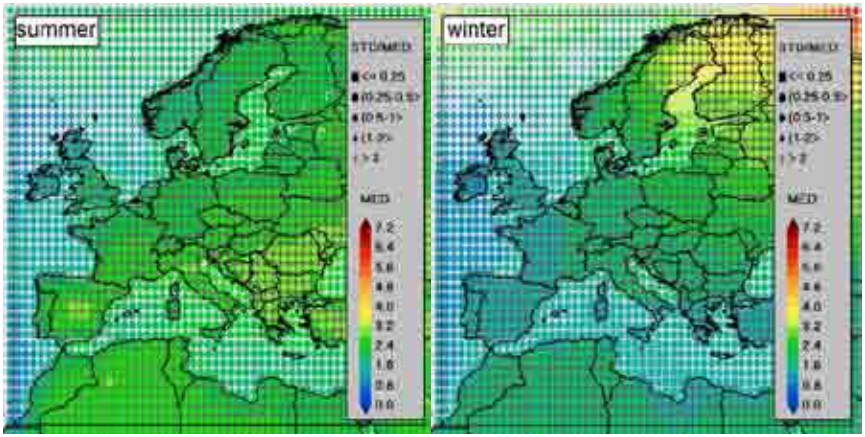

Fig. 4. *Temperature changes in summer and winter for 2021–2050 with respect to the 1961–1990 reference period. See Fig. 1 for more details on legend.*

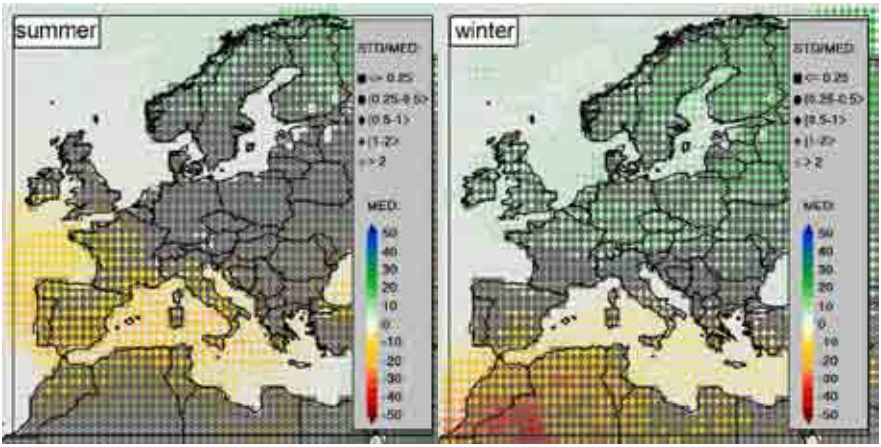

Fig. 5. *Precipitation changes in summer and winter for 2021–2050 with respect to the 1961–1990 reference period. See Fig. 1 for more details on legend.*

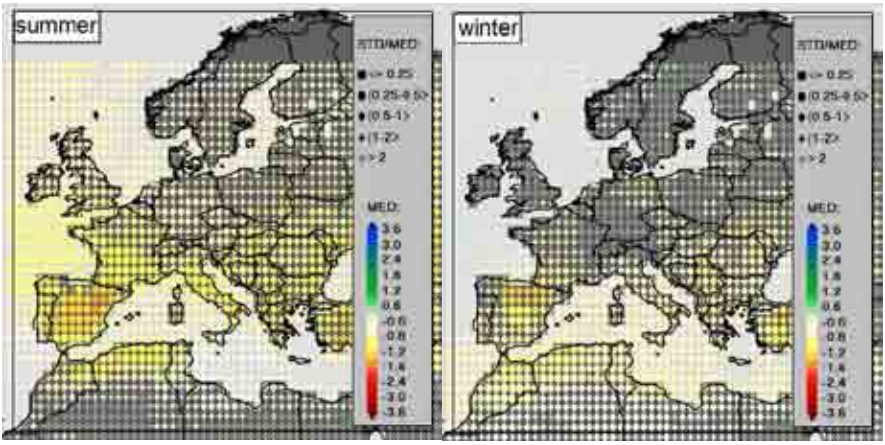

Fig. 6. *Same as Fig. 1 but for mean relative Z-index values in summer and winter for 2021–2050. See Fig. 1 for more details on legend.*

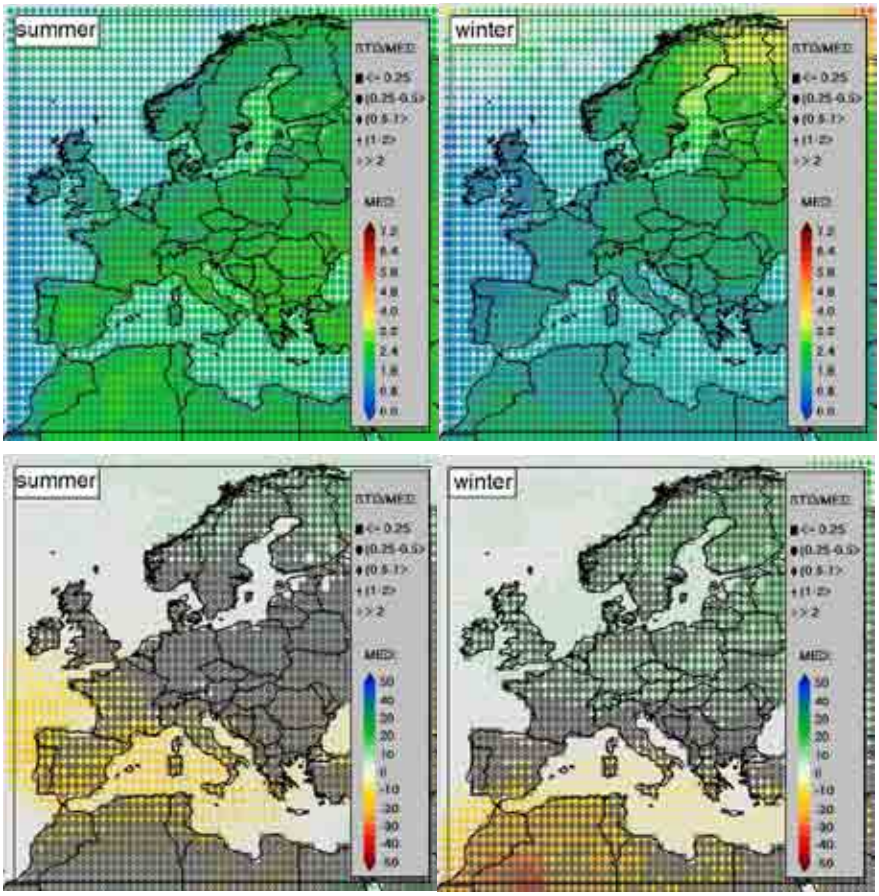

Fig. 7. *Changes in temperature (°C; upper half) and precipitation (%; lower half) during summer and winter for RCP4.5 emission scenario and 2021–2050. Scenarios were determined by applying the pattern scaling method to RCP8.5-based scenarios. See Fig. 1 for more details on legend.*

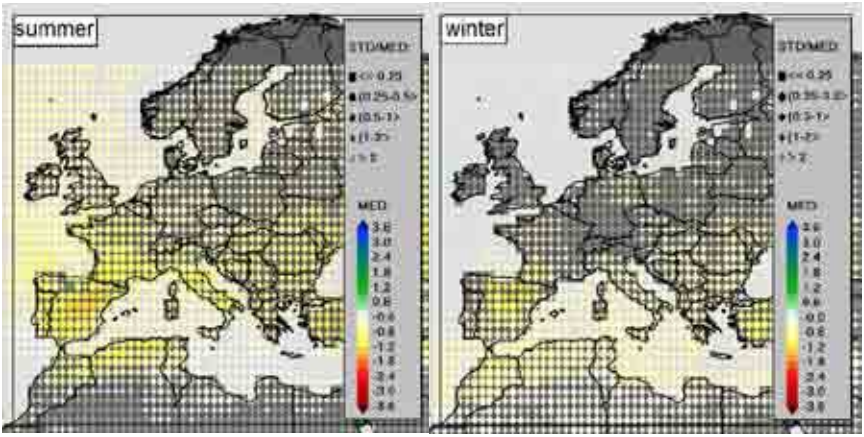

Fig. 8. *Mean relative Z-index values during summer and winter for RCP4.5 emission scenario and 2021–2050. Scenarios were determined by applying the pattern scaling method to RCP8.5-based scenarios. See Fig. 1 for more details on legend.*

Acknowledgement

This work was supported by the Ministry of Education, Youth and Sports of the Czech Republic within the National Programme for Sustainability I, grant No. LO1415.

References

Burke, E.J., Brown, S.J. & Christidis, N. (2006) Modeling the recent evolution of global drought and projections for the twenty-first century with the Hadley Centre climate model. *Journal of Hydrometeorology*, **7**, 1113–1125.

Dai, A. (2013) Increasing drought under global warming in observations and models. *Nature Climate Change*, **3**, 52–58.

Dubrovsky, M., Nemesova, I. & Kalvova, J. (2005) Uncertainties in climate change scenarios for the Czech Republic. *Climate Research*, **29**, 139–156.

Dubrovsky, M., Svoboda, M.D., Trnka, M. et al. (2009) Application of relative drought indices in assessing climate-change impacts on drought conditions in Czechia. *Theoretical and Applied Climatology*, **96**, 155–171.

Dubrovsky, M., Hayes, M., Duce, P., Trnka, M., Svoboda, M. & Zara P. (2014): Multi-GCM projections of future drought and climate variability indicators for the Mediterranean region. *Regional Environmental Change*, **14**, 1907–1919.

Dubrovsky, M., Trnka, M., Holman, I.P., Svobodova, E. & Harrison P.A. (2015) Developing a reduced-form ensemble of climate change scenarios for Europe and its application to selected impact indicators. *Climatic Change*, **128**, 169–186.

Harvey, L.D.D., Gregory, J., Hoffert, M. et al. (1997) *An introduction to simple climate models used in the IPCC Second Assessment Report*. IPCC Tech Paper 2, Intergovernmental Panel on Climate Change, Geneva.

Hoerling, M.P., Eischeid, J.K., Quan, X.W. et al. (2012) Is a transition to semipermanent drought conditions imminent in the U.S. Great Plains? *Journal of Climate*, **25**, 8380–8386.

Hulme, M., Wigley, T.M.L., Barrow, E.M. et al. (2000) *Using a climate scenario generator for vulnerability and adaptation assessments: MAGICC and SCENGEN Version 2.4 Workbook*. Climatic Research Unit, Norwich.

IPCC (2007) *Climate Change 2007: Synthesis Report. Contribution of Working Groups I, II and III to the Fourth Assessment Report of the Intergovernmental Panel on Climate Change* (eds Core Writing Team, R.K. Pachauri & A. Reisinger). IPCC, Geneva, Switzerland.

IPCC (2013) Summary for policymakers. *Climate Change 2013: The Physical Science Basis. Contribution of Working Group I to the Fifth Assessment Report of the Intergovernmental Panel on Climate Change* (eds T.F. Stocker, D. Qin, G.-K. Plattner et al.), pp. 3–29, Cambridge, UK and New York, NY, USA: Cambridge University Press.

Meehl, G.A., Covey, C., Delworth, T. et al. (2007) The WCRP CMIP3 Multimodel Dataset: A new era in climate change research. *Bulletin of the American Meteorological Society*, **88**, 1383–1394.

Santer, B.D., Wigley, T.M.L., Schlesinger, M.E. & Mitchell, J.F.B. (1990) *Developing climate scenarios from equilibrium GCM results. Report No.47.* Max Planck Institute für Meteorologie, Hamburg.

van der Schrier, G., Barichivich, J., Briffa, K.R. & Jones, P.D. (2013) A scPDSI-based global data set of dry and wet spells for 1901–2009. *Journal of Geophysical Research: Atmosphere*, **118**, 4025–4048.

Taylor, K.E., Stouffer, R.J. & Meehl, G.A. (2012) An overview of CMIP5 and the experiment design. *Bulletin of the American Meteorological Society*, **93**, 485–498.

Wells, N., Goddard, S. & Hayes, M.J. (2004) A self-calibrating Palmer Drought Severity Index. *Journal of Climate*, **17**, 2335–2351.

Chapter 3

Assessing Köppen–Geiger climate classification by individual regional climate models considering the influence of bias correction methods

Beáta Szabó-Takács, Aleš Farda, Petr Štěpánek, Petr Skalák, Pavel Zahradníček

Department of Climate Modelling, Global Change Research Centre, Czech Academy of Sciences, Bělidla 4a, CZ-60300 Brno, Czech Republic

1. INTRODUCTION

Global circulation models (GCMs) and regional climate models (RCMs) are designed to predict climate development based on direct physical modelling of the atmosphere, oceans, and other components of the climate system on both global and regional scales. The project ENSEMBLES within the European Commission's 6th Framework Programme applies a probabilistic approach to climate changes at a regional scale (Hewitt & Griggs 2004) by downscaling GCMs into higher-resolution RCMs (van der Linden & Mitchell 2009).

The Köppen–Geiger climate classification (Köppen 1900; Geiger 1954) is derived directly from eco-biological vegetation characteristics in individual regions of the Earth and so is suitable for assessing climate changes' impacts on ecosystems. Castro et al. (2007) and Gallardo et al. (2013) used the Köppen–Trewartha classification (Trewartha & Horn 1980) to estimate climate change in Europe with an ensemble mean of RCM simulations incorporating the uncertainty related to GCMs. RCM ensemble medians may fit observations in the case of temperature simulations (Teutschbein & Seibert 2013), but precipitation simulations are afflicted with biases specifically within Europe (Christensen et al. 2008; Piani et al. 2010; Dosio & Paruolo 2011). Errors come from such various sources as downscaling GCMs to RCMs, inadequately resolved surface properties, and numerical parameterizations (Allen et al. 2006; Fowler & Ekström 2009; Casper et al. 2012).

In our previous work, Köppen–Geiger classification had been applied as a diagnostic tool to six individual ENSEMBLES simulations as a representative selection of models with respect to GCMs and RCMs (Szabó-Takács et al. 2015). The simulations were implemented using the SRES A1B emissions scenario of the Intergovernmental Panel on Climate Change in near (2021–2050) and distant (2071–2100) future. The bias correction technique for empirical quantile mapping of precipitation and temperature was used to eliminate the uncertainties of ENSEMBLES using the E-OBS set of observed data (Haylock et. al. 2008) as a reference field.

Given the fact that choice of correction method is an additional source of uncertainty (Chen et al. 2011), the present study implemented several correction techniques to study their impacts on projected climate classification.

Table 1. *Selected regional climate models (RCMs) and their spatial horizontal resolution and driving global circulation models (GCMs).*

Institute/Reference	GCM	RCM	Resolution
Centre National de Recherches Météorologiques/Gibelin & Déqué (2003)	ARPÈGE	–	50 km
Danish Meteorological Institute/Christensen et al. (1996)	ARPÈGE	HIRHAM	25 km
Swedish Meteorological and Hydrological Institute/ Kjellström et al. (2005)	ECHAM5-r3	RCA	25 km
Abdus Salam International Centre for Theoretical Physics/Giorgi et al. (2004)	ECHAM5-r3	RegCM	25 km

2. DATA AND METHODS

Köppen and Geiger had classified the climate based on annual and monthly temperature and precipitation means. A key for calculating Köppen–Geiger climate classes is detailed in Kottek et al. (2006). Köppen–Geiger classification distinguishes five vegetation groups: the equatorial zone (A), the arid zone (B), the warm temperate zone (C), the snow zone (D), and the polar zone (E). These climate types are subdivided into subtypes. The polar zone is divided into tundra (ET) and frost (EF) climates. The arid zone is divided into wetter steppe (BS) and dryer desert (BW) climates. The third index (letter) of B subcategories indicates the temperature. If the annual mean temperature is above 18°C, the third letter is *h*, while if it is below 18°C, the third letter is *k*. The second index of the A, C, and D vegetation groups indicates the precipitation pattern: the letters *s*, *w*, and *f* mean dry summers, dry winters, and fully humid, respectively. The third index of the C and D groups indicates the degree of summer heat. The letter *a* means that the mean temperature of the warmest month is above 22°C with at least 4 months averaging above 10°C, *b* means that the mean temperature of the warmest month is below 22°C with at least 4 months averaging above 10°C, *c* indicates that fewer than 4 months have mean temperatures above 10°C and the mean temperature of the coldest month is above –38°C, while *d* is similar to c but the mean temperature of the coldest month is equal to or below –38°C.

Four individual ENSEMBLES models were chosen and are shown in Table 1. Large-scale processes were driven by the ARPÈGE GCM for the ARPÈGE and HIRHAM RCMs and by the ECHAM5-r3 GCM for the RegCM and RCA RCMs. The E-OBS gridded data set of daily station observations was utilized for bias correction as it is currently perhaps the best pan-European gridded data set with spatial resolution of 0.25° in longitude and latitude (or 0.22° on the rotated pole grid typical for many RCMs) covering the period from 1950.

The bias correction methods applied were local intensity scaling and power transformation of precipitation and variance scaling and empirical quantile mapping of temperature. Local intensity scaling corrects the mean as well as both the wet-days frequency and wet-day intensity of precipitation. The power transformation of precipitation can be used to correct precipitation's variance statistics. Correspondingly, the variance scaling of temperature corrects both the mean and variance of temperature. Empirical quantile mapping is used to correct the distribution function of simulated climate values. These methods' equations are detailed in Teutschbein & Seibert (2012). Bias corrections and Köppen–Geiger classification were implemented in Matlab using the MeteoLab and Weaclim toolboxes.

3. RESULTS AND DISCUSSION

3.1. Climate classification based on observation

Fig. 1 shows the Köppen–Geiger climate classes according to E-OBS observed precipitation and temperature data within the calibration time period of 1961–1990. The ET tundra climate occurred in Iceland, higher mountains, Scandinavia, and some regions of the North Sea coast. The Dfc snow climate was dominant in Scandinavia and north-eastern Europe. Owing to increasing temperature, the Dfb climate became predominant towards the south. The Cfb class was typical in Great Britain; in western, central, and partly south-eastern Europe; and along the Scandinavian coast. Primarily the Cs dry summer climate occurred in southern Europe (Italian Peninsula, Iberian Peninsula, Balkan Peninsula, and Turkey). Summers were hot near the Mediterranean coast, while summers were warm inland away from the sea. Steppe and arid climates occurred in southern eastern Europe where the temperature is cold (BSk, BWk).

Fig. 1. *Köppen–Geiger climate classification according to E-OBS observed temperature and precipitation during 1961–1990.*

3.2. Projected climate classifications according to bias corrections

3.2.1. Local intensity scaling of precipitation and empirical quantile mapping of temperature

Because local intensity scaling can be applied only to precipitation, it was combined with empirical quantile mapping of temperature to calculate Köppen–Geiger classification. Climate classifications in near future can be seen in Fig. 2. Differences among RCMs in the coverage of different climate types were negligible. In addition, the HIRHAM and RAC simulations produced very similar results. Scandinavia was predominantly covered by the Dfc and Dfa classes with scattered ET tundra climate. The Dfb class was predominant in eastern Europe, but the coverage of Dfa east of the Black Sea was larger in ARPÈGE. Great Britain and western and central Europe were characterized by the Cfb climate class. The Csa and Csb dry summer and BSk arid climate classes occurred in southern Europe. Differences in climate class proportions were larger among those RCMs driven by ARPÈGE than those driven by ECHAM5-r3. A larger area was covered by the hot summer climate classes (Dfa, Cfa, Csa) in the ARPÈGE than in the HIRHAM simulation. The Cfa climate class covered a larger area in western, south-eastern, and central Europe in distant future than in near future (Fig. 3). Moreover, the Dfa class shifted to the north in eastern Europe. These

changes were significant in each RCM. In each RCM, the predicted coverage of the ET and Dfc classes was smaller while that of the Cfa, Dfa and Dfb classes was markedly larger than that in Fig. 1.

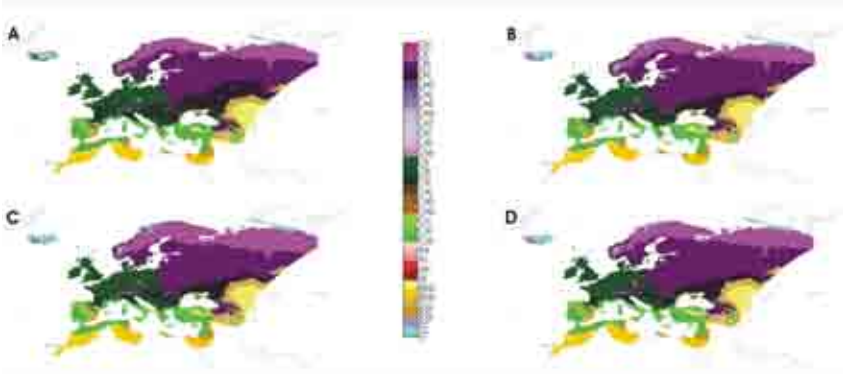

Fig. 2. *Projected Köppen–Geiger climate classification during 2021–2050 according to the ARPÈGE (***A***), HIRHAM (***B***), RegCM (***C***), and RCA (***D***) regional climate models taking into account empirical quantile mapping of temperature and local intensity scaling of precipitation.*

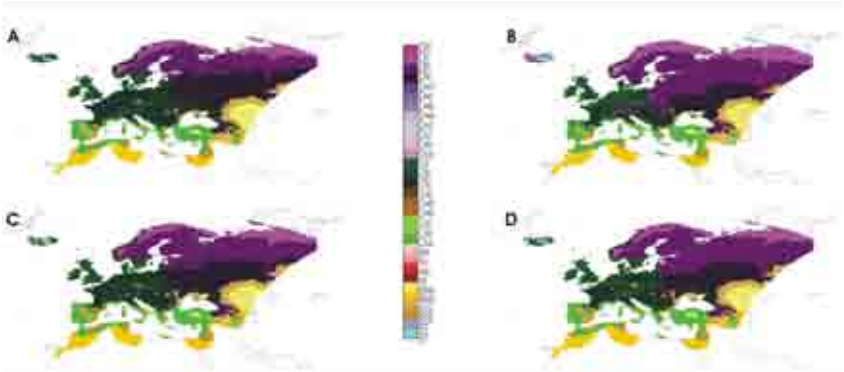

Fig. 3. *Projected Köppen–Geiger climate classification during 2071–2100 according to the ARPÈGE (***A***), HIRHAM (***B***), RegCM (***C***), and RCA (***D***) regional climate models while taking into account empirical quantile mapping of temperature and local intensity scaling of precipitation.*

3.2.2. Power transformation of precipitation and variance scaling of temperature

The power transformation of precipitation has previously been implemented in smaller domains: the Meuse River basin (Leander & Buishand 2007) and meso-scale catchments in Sweden (Teutschbein & Seibert 2012), where precipitation is significant. In our work, the power of precipitation was calculated using Brent's root-finding algorithm (Brent 1971). Mean precipitation might be near zero in summer within Europe due to dryer regions. This near-zero mean might have led to an invalid coefficient of variation of precipitation which stopped the root-finding algorithm. For the HIRHAM and RCA simulations, power values could be calculated only in January. In addition, Brent's algorithm returns a missing value if its

function value is below –0.28. These missing values caused lines in the maps (Fig. 4 and Fig. 5). Among RCMs, the power transformation of precipitation seemed to be the most stable for ARPÈGE. This model had power values near every point of domain from January to April. According to ARPÈGE, the Dfc class was predominant in Scandinavia. Toward the south, the Dfb and BSk climates extended into eastern Europe. In near future, the BS type became dominant in eastern, south-eastern, southern, and western Europe and in south-eastern Great Britain. In distant future, the ET climate disappeared in Scandinavia and the BS class shifted to the north and west in eastern Europe and to the east in western Europe. The HIRHAM and RCA models projected similar values in northern Scandinavia and northern eastern Europe. But a strange line boundary can be seen between the D*fc* and BW*k* climates toward the south, which seems to be unreliable.

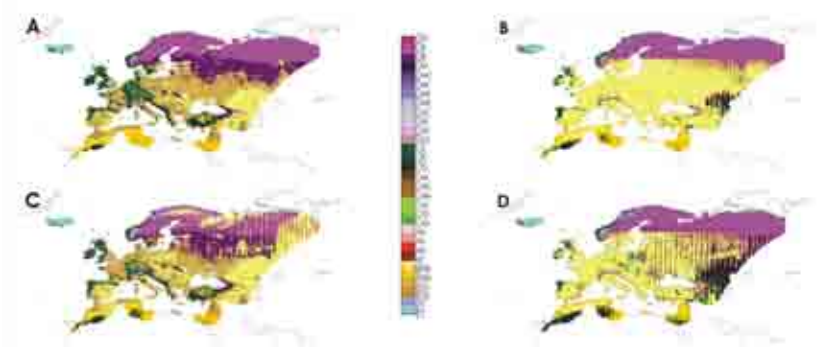

Fig. 4. *Projected Köppen–Geiger climate classification during 2021–2050 according to the ARPÈGE (***A***), HIRHAM (***B***), RegCM (***C***), and RCA (***D***) regional climate models while taking into account variance scaling of temperature and power transformation of precipitation.*

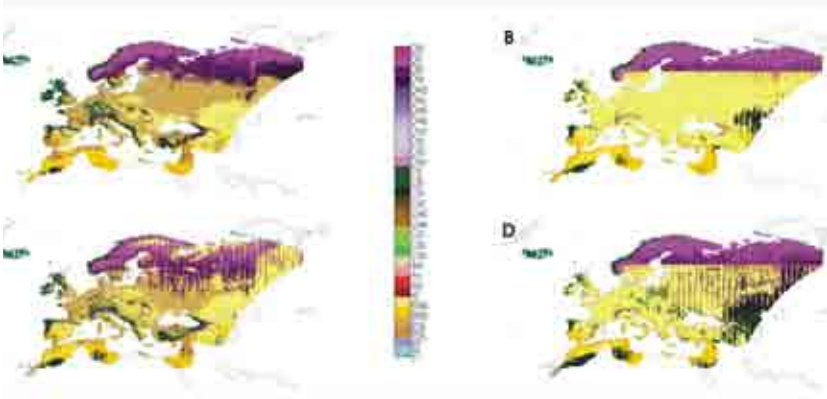

Fig. 5. *Projected Köppen–Geiger climate classification during 2071–2100 according to the ARPÈGE (***A***), HIRHAM (***B***), RegCM (***C***), and RCA (***D***) regional climate models while taking into account variance scaling of temperature and power transformation of precipitation.*

When local intensity scaling of precipitation and empirical quantile mapping of temperature were applied, the predicted climate classes were nearly the same in each RCM. These results confirm that bias correction of precipitation has a larger effect on climate predictions than does bias correction of temperature. The results of predicted climates also depended on model type. A statistical evaluation of these bias corrections within the calibration period has been published by Teutschbein & Seibert (2012) and Teutschbein & Seibert (2013). These authors found that the power transformation of precipitation had better performance than did local intensity scaling in five Swedish catchments. Although a given bias correction performing well with the calibration period does not guarantee its good performance within the projected time period, it is more likely to perform better for changed conditions than is a method which performs poorly in current conditions (Teutschbein & Seibert 2012). Although we did not analyse the performance of bias correction with the calibration period, based on our results the power transformation seemed to be poorer within Europe than was the other correction of precipitation.

4. CONCLUSION

We calculated predicted Köppen–Geiger climate classification using four individual RCMs from the ENSEMBLES project within Europe during 2021–2050 and 2071–2100. Projected precipitation and temperature data were corrected with the following bias corrections using E-OBS observed data: (i) empirical quantile mapping and (ii) variance scaling of temperature and (iii) local intensity scaling and (iv) power transformation of precipitation. The bias corrections had significant effects on climate projections, but the degree of their effects varied among RCMs. Bias correction of precipitation had a greater impact than did correction of temperature. Our results about the power transformation of precipitation differ from previous results in the literature where this correction was implemented in smaller catchments. Given this result, we conclude that bias corrections depend also on the chosen domain.

Acknowledgement

This work was supported by the Ministry of Education, Youth and Sports of the Czech Republic within the National Programme for Sustainability I, grant No. LO1415. We would like to thank Sixto Herrera García for his help with bias correction and MeteoLab.

References

Allen, M., Frame, D., Kettleborough, J. & Stainforth, D. (2006) Model error in weather and climate forecasting. Predictability of Weather and Climate (eds T. Palmer & R. Hagedorn), pp. 391–427. Cambridge University Press, United Kingdom.

Brent, R.P. (1971) An algorithm with guaranteed convergence for finding a zero of a function. *Computer Journal*, **14**, 422–425.

Casper, M.C., Grigoryan, G., Gronz, O. et al. (2012) Analysis of projected hydrological behavior of catchments based on signature indices. *Hydrology and Earth System Sciences*, **16**, 409–421.

Castro, M., Gallardo, C., Jylha, K. & Tuomenvirta, H. (2007) The use of climate-type classification for assessing climate change effect in Europe from an ensemble of nine regional climate models. *Climate Change*, **81**, 329–341.

Chen, J., Brissette, F.P. & Leconte, R. (2011) Uncertainty of downscaling method in quantifying the impact of climate change on hydrology. *Journal of Hydrology*, **401**, 190–202.

Christensen, J.H., Boberg, F., Christensen, O.B. & Lucas-Picher, P. (2008) On the need for bias correction of regional climate change projections of temperature and precipitation. *Geophysical Research Letters*, **35**, L20709.

Christensen, J.H., Christensen, O.B., Lopez, P., van Meijgaard, E. & Botzet, M. (1996) The HIRHAM4 regional atmospheric model. Scientific Report 96-4. The Danish Meteorological Institute, Copenhagen, Denmark.

Dosio, A. & Paruolo, P. (2011) Bias correction of the ENSEMBLES high resolution climate change projections for use by impact models: Evaluation on present climate. *Journal of Geophysical Research*, **116**, D16106.

Fowler, H.J. & Ekström, M. (2009) Multi-model ensemble estimates of climate change impacts on UK seasonal precipitation extremes. *International Journal of Climatology*, **29**, 385–416.

Gallardo, C., Gil, V., Hagel, E., Tejeda, C. & Castro, M. (2013) Assessment of climate change in Europe from an ensemble of regional climate models by the use Köppen-Trewartha classification. *International Journal of Climatology*, **33**, 2157–2166.

Geiger, R. (1954) Landolt-Börnstein – Zahlenwerte und Funktionen aus Physik, Chemie, Astronomie, Geophysik und Technik, alte Serie Vol. 3, Ch. Klassifikation def Klimate nach W. Köppen. Springer, Berlin. 603-607

Gibelin, A.-L. & Déqué, M. (2003) Anthropogenic climate change over the Mediterranean region simulated by a global variable resolution model. *Climate Dynamics*, **20**, 327–339.

Giorgi, F., Bi, X. & Pal, J. (2004): Mean, interannual variability and trends in regional climate change experiment over Europe. I. Present-day climate (1961–1990). *Climate Dynamics*, **22**, 733–756.

Haylock, M.R., Hofstra, N., Klein Tank, A.M.G., Klok, E.J., Jones, P.D. & New, M. (2008) A European daily high-resolution gridded data set of surface temperature and precipitation for 1950–2006. *Journal of Geophysical Research*, **113**, D20119.

Hewitt, C.D. & Griggs, D.J. (2004) Ensembles-based predictions of climate changes and their impacts. Eos, Transactions American Geophysical Union, 85, 566.

Kjellström, E., Bärring, L., Gollvik, S. et al. (2005) A 140-year simulation of European climate with the new version of Rossby Central regional atmospheric climate model (RCA3). SMHI Reports Meteorology and Climatology, 108, SMHI, SE-60176. Norrköping, Sweden.

Kottek, M., Grieser, J., Beck, C., Rudolf, B. & Rubel, F. (2006) World Map of the Köppen-Geiger climate classification updated. *Meteorologische Zeitschrift*, **15**, 259–263

Köppen, W. (1900) Versuch einer Klassifikation der Klimate, vorzugsweise nach ihren Beziehungen zur Pflanzenwelt. *Geographische Zeitschrift*, **6**, 593–611, 657–679.

Leander, R. & Buishand, T.A. (2007) Resampling of regional climate model output for simulation of extreme river flows. *Journal of Hydrology*, **332**, 487–496.

Piani, C., Haerter, J.O. & Coppola, E. (2010) Statistical bias correction for daily precipitation in regional climate models over Europe. *Theoretical and Applied Climatology*, **99**, 187–192.

Szabó-Takács, B., Farda, A., Zahradníček, P. & Štěpánek, P. (2015) Köppen-Geiger climate classification by different Regional Climate Models according to A1B SERES scenario in 21st century. Global Change: A Complex Challenge conference proceedings (eds O. Urban, M. Šprtová & K. Klem), pp. 18–21. Global Change Research Centre AS CR, v.v.i, Brno.

Teutschbein, C. & Seibert, J. (2012) Bias correction of regional climate model simulations for hydrological climate-change impact studies: Review and evaluation of different methods. *Journal of Hydrology*, **456–457**, 12–29.

Teutschbein, C. & Seibert, J. (2013) Is bias correction of regional climate model (RCM) simulations possible for non-stationary conditions? *Hydrology and Earth System Sciences*, **17**, 5061–5077.

Trewartha, G.T. & Horn, L.H. (1980) An Introduction to Climate (5th edition). McGraw-Hill, New York, NY.

van der Linden, P. & Mitchell, J.F.B. (2009) ENSEMBLES: Climate Change and its Impacts: Summary of research and results from the ENSEMBLES project. Met Office Hadley Centre, FitzRoy Road, Exeter EX1 3PB, United Kingdom.

Chapter 4

Temporal dynamics and spatial identification of growth increments

Radek Pokorný[1], Justyna Szatniewska[1], Dalibor Janouš[2]

[1] *Department of Biomass Production, Global Change Research Centre, Czech Academy of Sciences, Bělidla 4a, CZ-60300 Brno, Czech Republic*

[2] *Department of Matters and Energy Fluxes, Global Change Research Centre, Czech Academy of Sciences, Bělidla 4a, CZ-60300 Brno, Czech Republic*

1. INTRODUCTION

Terrestrial ecosystems – and especially forest ecosystems – are potential sinks for atmospheric carbon. Although terrestrial ecosystems are small carbon sinks in comparison to oceans, the annual exchange of carbon between terrestrial ecosystems and the atmosphere is comparable with the exchange between oceans and the atmosphere. In addition, it has been shown that at least 2% of carbon in atmospheric CO_2 is annually exchanged between the atmosphere and terrestrial biota (Wigley & Schimel 2000).

Photoautotrophic plants comprise a basic biotic component of ecosystems. Their metabolism is closely related to photosynthetic assimilation of atmospheric carbon. Photosynthesis thus forms a link between biotic and abiotic components of the carbon cycle. Carbon bound in photosynthetic processes is incorporated into the carbon-based organic compounds constituting biomass. A part of these compounds is immediately used in respiratory processes and carbon is thus again released into the atmosphere. Another part of the carbon is released through respiration associated with heterotrophic plant tissues and the activity of soil micro-organisms occurring in the ecosystem.

Ecosystems' carbon balance and its dynamics through a given vegetation season can be evaluated using the eddy covariance method (Aubinet et al. 2000; Kuglitsch et al. 2008; see also Chapters 5 and 6 in this book) and/or by measuring biomass increment dynamics. In contrast to the eddy covariance method, biomass increment analysis can be performed for much smaller stands and even individual trees or such of a stand's structural components as the age and height classes of trees growing within it. Many studies have focused on trees' allometric relationships, wood inventory, carbon sequestration, and expansion factors inasmuch as these are the first steps to assessing the carbon sinks of different ecosystems (e.g. Lehtonen et al. 2004; Teobaldelli et al. 2009). Identification and quantification of these terrestrial carbon sinks and the ecosystem's carbon balance on the one hand and quantification of CO_2 emissions on the other are currently in great demand (Penman et al. 2003).

Temperate forests have recently been identified as an important carbon sink (Janssens et al. 2003). This substantial sink is influenced, however, by ongoing environmental changes (increases in atmospheric CO_2 concentration, oscillations of air temperature, nitrogen deposition, etc.) as well as by the increasing proportion of managed forests consisting of young stands and short-rotation woody crops. Vetter et al. (2005) showed that these positive changes are especially evident in stands growing at higher altitudes (600–900 m a.s.l.).

Accurate quantification of different plant organs' biomass (fresh or dry) and their surface areas is very important not only in analysing the matter and energy fluxes between vegetation and the adjacent atmosphere but also for parameterizing ecosystem models. Determining the biomass and spatial distribution of individual tree components is also important for constructing mechanical models (most often used to assess tree and/or stand stability against wind, snow, etc.) and growth models.

Determination of a tree's biomass and its various parts (roots, trunk, branches, and assimilation apparatus) is based mostly on the application of allometric relationships describing the proportions of different plant organs. Most frequently used are relationships between easily measurable parameters of the trunk or crown and the biomass or surface area of other plant parts. The basic dendrometric parameters used for allometric relationships are stem diameter measured at breast height (i.e. 1.3 m; DBH) and tree height (*H*). The DBH increment depends on carbon assimilation efficiency and the tree's carbon balance, because carbon is first reallocated from needles or leaves to the branches and roots (Waring 1987). Less attention has been devoted to allometric relationships including crown parameters as these parameters are more difficult to obtain, even though crown dimensions are the main determinants of a stand's radiation regime (Kellomäki et al. 1984), canopy cover, crown core size (inner defoliation of the crown), and the so-called self-pruning effect (Mäkelä1997). Trees' biomass production is closely related to crown surface area, especially to its insolated, so-called effective part (Assmann 1968).

Because Norway spruce (*Picea abies*) is a dominant tree species in both the Czech Republic (55%) and Central Europe (35%) and naturally occupies middle and upper altitude zones (Ministry of Agriculture of the Czech Republic 2014), the present study focused on Norway spruce. Growth increment dynamics and spatial identification were studied over several growing seasons in a young spruce stand located at the Bílý Kříž experimental research site in the Beskydy Mountains. The main emphasis was placed on the effects of stand density and applied thinning.

2. MATERIALS AND METHODS

2.1. Site and stand description

All measurements were carried out on an evenly aged monoculture of Norway spruce (4-year-old seedlings planted in rows in 1981) located in the Beskydy Mountains (north-eastern Czech Republic; 49°30′N, 18°32′E) on a gently descending slope (12°, 820–908 m a.s.l.) oriented to the south–southwest. The climate conditions of the Bílý Kříž research area are detailed in chapters 5 and 6 of this book. Total stand area was 6.15 ha. Within this stand, two experimental plots measuring 50 x 50 m with different stand densities were established and were denoted sparse (FS) and dense (FD) (Table 1). In 2001, the FS plot underwent low–high thinning (20% intensity). In 2004, the FD plot underwent low–moderate thinning/negative selection (17% intensity). At other times, natural thinning occurred (with intensity varying from 3% to 8%).

2.2. Biomass estimation

Total biomass (TB) and the annual biomass increment (ΔTB) were obtained based on a stand inventory carried out at the end of each growing season. The inventory procedure consisted of measuring stem circumference at breast height (SC) and *H* of each tree located on the experimental plot. SC was

measured using a metal ruler (accuracy: 0.001 m) and *H* using a Forestor Vertex height-measuring instrument (Haglöf, Långsele, Sweden) with an accuracy of 0.1 m. Based on SC, the final DBH was calculated. Biomass of stems (SB), branches (BB), and foliage (LB) was obtained based on local site-specific allometric relationships with DBH (Pokorný 2002; Pokorný & Tomášková 2007). Root biomass (RB) was estimated using the allometric relationship between DBH and RB described by Drexhage & Gruber (1998). Therefore, the total biomass formed during one growing season was obtained as the sum of total above-ground biomass (TBA = SB + BB + LB) and total below-ground biomass (RB).

The total and/or individual tree organ biomass increment formed during a growing period was estimated as the difference between the present and previous year's SB (ΔSB), BB (ΔBB), LB (ΔLB), and RB (ΔRB). The dynamics of the biomass increments of individual parts of investigated trees were obtained based on observations of increments of i) DBH, ii) *H*, and iii) leaf area index (LAI). This process took into account that the DBH growth dynamic related to ΔSB and ΔRB, the *H* growth dynamic related to ΔBB, and the LAI dynamic related to ΔLB.

2.3. Temporal variation

LAI was measured with an LAI-2000 Plant Canopy Analyzer (Li-Cor, Lincoln, NE, USA) using a 1 x 1 m grid of measurement points (at a total of 49 points) located at representative parts of the investigated FD and FS plots. The method and measurement procedure used have been carefully described by Pokorný & Marek (2000) and Pokorný et al. (2008).

The seasonal dynamic of the DBH increment was measured using a set of dendrometer bands (accuracy: 0.01 cm) located 1.3 m above the ground on 30 sample trees. Each investigated stand (i.e. the FD and FS plots) contained 15 sample trees. *H* increment dynamics were observed on a set of 10 trees located near a meteorological mast. ΔSB and ΔRB dynamics were obtained from the DBH increment. ΔBB dynamics were obtained from the *H* increment. ΔLB dynamics were obtained from the LAI increment. Thus, the ΔTB of the distinctive time period of the growing season was obtained as the sum of actual ΔSB + ΔBB + ΔLB + ΔRB.

2.4. Spatial data distribution measurements

During harvest analysis of 37 trees in a sub-plot measuring 10 x 12 m (Pokorný & Marek 2000), 11 of the trees were analysed in detail along their vertical stems and crown profiles to estimate the spatial distribution of biomass and surface area of different above-ground tree organs and within three different needle/branch age classes. Mean *H* and DBH of sampled trees (± standard error) were 7.0 ± 0.2 m and 8.4 ± 0.4 cm in the year of harvest, respectively. Mean tree crown dimensions were: 6.5 ± 0.5 m in length and 2.5 ± 0.2 m maximum diameter. Mean crown projection area was 4.9 ± 0.6 m^2.

Branches were cut from sections defined by 1 m height lengths (i.e. strata, upward from the bottom of the canopy) for all trees. Sample branches were collected together from each section and dried (100°C for 48 h). A representative branch of average length was chosen from each section. The shoots of sampled branches were split into three age classes: c = current year shoots, c-1 = previous-year shoots, and r = rest (i.e. shoots older than 2 years). The following structural parameters were then assessed: specific leaf area (i.e. the ratio of dry weight to fresh projected needle area), specific branch area, dry LB and BB, projected needle area (LAp), and total branch surface area (BAt).

A Li-3000A Portable Area Meter (Li-Cor) was used to estimate fresh projected needle area. Needles were dried for 2 days at 100°C and weighed on a scale with a precision of 0.001 g (Sartorius, Göttingen,

Table 1. Chosen stand parameters of dense (FD) and sparse (FS) research plots and their development from 1997 to 2007.

Parameter	Plot	Unit	1997	1998	1999	2000	2001	2002	2003	2004	2005	2006	2007
Stand age		*years*	16	17	18	19	20	21	22	23	24	25	26
Total tree age		*years*	20	21	22	23	24	25	26	27	28	29	30
Stand density	**FD**	*trees* ha^{-1}	2,668	2,664	2,664	2,656	2,612	2,492	2,484	2,088	2,076	1,908	1,552
	FS	*trees* ha^{-1}	2,408	2,396	2,392	2,388	1,848	1,836	1,836	1,668	1,664	1,580	1,508
Median tree height	**FD**	*m*	6.6	7.4	8.0	8.6	9.2	9.9	10.5	11.3	12.0	13.0	13.4
	FS	*m*	5.7	6.4	7.0	7.6	8.5	9.3	9.9	10.6	11.3	12	12.4
Mean tree height	**FD**	*m*	4.7	5.2	5.8	6.6	7.3	7.8	8.4	9.1	9.8	10.4	11.2
	FS	*m*	5.6	6.3	6.9	7.5	8.4	9.1	9.8	10.5	11.2	11.8	12.2
Crown base height	**FD**	*m*	0.3	0.6	0.8	1.0	1.3	1.5	1.9	2.2	2.5	3.1	3.3
	FS	*m*	0.4	0.4	0.5	0.5	0.8	0.9	0.9	1.1	1.5	2.0	2.3
Mean stem diameter at 1.3 m	**FD**	*cm*	8.2	8.9	9.5	10.1	10.8	11.5	12.0	13.0	13.5	14.1	15.0
	FS	*cm*	7.1	7.8	8.5	9.1	10.2	11.0	11.7	12.6	13.3	14.0	14.6
Basal area	**FD**	$m^2\ ha^{-1}$	15.00	17.61	20.29	22.87	25.34	27.55	29.92	29.20	31.47	31.44	28.64
	FS	$m^2\ ha^{-1}$	10.33	12.36	14.50	16.62	16.01	18.29	20.60	21.69	24.09	25.29	26.11

Germany). Total needle surface area was established as LAp multiplied by the conversion coefficient of 2.57 (Waring 1987).

Branch surface area was calculated from the known lengths and diameters (in the middle parts) of all individual shoots detached from the sample branches. Projected branch area equalled BAt divided by π. Percentage proportions of individual age classes were calculated and subsequently used to determine the dry weight and surface area of given needle/shoot age classes within all of a section's branches. These accurate proportion data were used for biomass and surface area assessment of all sample trees except forked trees.

Stem volume as well as total stem surface area were obtained as the sum of individual stem sections' volumes and surface areas, during which time the stems were also divided into sections 1 m long. Thus, total stem volume and surface area were estimated from the known length and diameter measured in the middle part of each stem section. Cylindrical section shapes were assumed. SB was estimated based on stem volume and stem-wood density. For this purpose, seven small blocks of trunk in the shape of rollers were taken along five chosen tree stems and then dried and weighed.

2.5. Photosynthetic photon flux density measurements within a crown

Detailed spatial monitoring of the distribution of photosynthetic photon flux density (PPFD) within a tree crown was conducted using a special system of BPW-21 optical sensors (Siemens, Berlin, Germany) with fibre-optic cables (see also Chapter 6 of this book and Urban et al. 2007 for details). The sensors were placed on the branches' main axes at three different levels, in the four cardinal directions, and in the central part of the shoot length perpendicularly to its axis, in order to quantify most accurately incident PPFD on shoots from the selected crown part. Sensor placement was selected randomly but in accordance with shoots' morphological parameters as modified by the radiation regime (Pokorný et al. 2004). Thus, in co-dominant trees' crowns, the third whorl (counted downward from the tree's top) represented the sun-acclimated part of the crown, the sixth whorl the middle part, and the ninth whorl the shade-acclimated part.

3. RESULTS AND DISCUSSION

The above-ground biomass of the spruce forests was quantified based on annual measurements of the DBH increment and destructive studies determining a set of specific allometric relationships (Pokorný 2002; Pokorný & Tomášková 2007). To estimate below-ground biomass, an allometric relationship describing a similar spruce stand (Drexhage & Gruber 1998) was used. The effects of the two stand densities on spruce growth and physiology was investigated until 2006, because after the winter season of 2005/2006 there was a substantial reduction in the number of trees on the FD plot due to heavy snow and the densities on the studied plots converged. Nevertheless, due to the previous development of trees under different light conditions, a greater DBH increment persisted in trees growing on the FS plot (Fig. 1). This example is given to illustrate the importance of long-term monitoring of changes in stand density, stand development, and growth conditions. In the annual growth cycle of the young spruce forest, the DBH increment culminated on average on the 232nd (± 18) day of the year (DOY; average for 1998–2005 ± standard deviation). The largest growth rate from the beginning of the growing season and the earliest culmination was found for the *H* increment (204th ± 11 DOY; average for 2000–2003) and the LAI increment (207th ± 15 DOY; average for 1998–2005; Figs. 2 and 4).

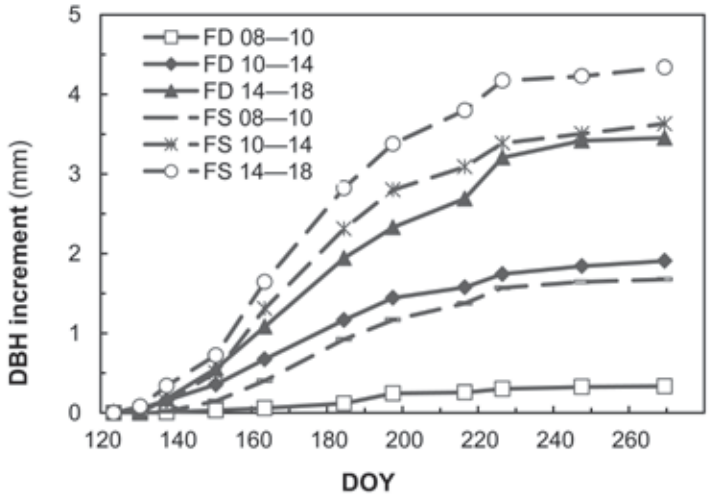

Fig. 1. *Cumulative increment of stem diameter at breast height (DBH) in dense (FD) and sparse (FS) spruce plots according to diameter classes in 2007. DBH classes correspond to the social status of individual trees in the stand: dominant trees = DBH 14.1–18.0 cm; co-dominant trees = DBH 10.1–14.0 cm; suppressed trees = DBH ≤ 10.0 cm. Means are presented; n = 50. DOY = day of the year. Basic parameters of FD and FS stands at the end of the 2007 growing season are described in Table 1.*

Differences in the dynamics of the increment of above-ground organs between the two studied stands prior to the winter of 2005/2006 (Fig. 2) increased in the vector: *H*, DBH, and LAI increments. The *H* increment dynamics were almost identical between the FD and FS plots. The DBH increment varied most, likely depending on water availability. After winter (in April and May), the soil was sufficiently saturated with water; then soil moisture decreased probably due to passive evaporation, first in the FS plot (in June). Increasing active evaporation (transpiration) and occurrence of drought (in August and September) caused a gradual decline in stem volumetric water content, to a greater extent in the FS plot (in 2003). During a precipitation-rich and balanced growth period (2002), the dynamics of DBH growth were similar on both plots. In 2003, there was an extremely dry and hot late summer (August–September), which was also reflected in substantial leaf fall. The LAI increment in the FD plot culminated earlier, and leaf fall also occurred earlier.

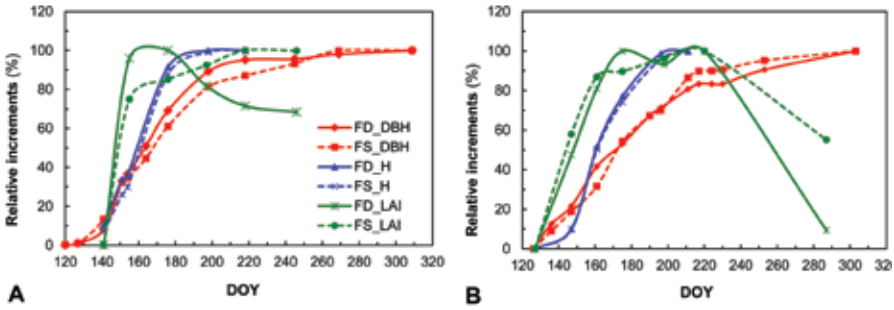

Fig. 2. *Relative increases in stem diameter at breast height (DBH), tree height (H), and leaf area index (LAI) in dense (FD) and sparse (FS) spruce plots during the 2002 (***A***) and 2003 (***B***) growing seasons. The total or maximum annual increase is indicated as 100%. The years 2002 and 2003 were chosen due to the dramatically increased LAI after thinning in 2002 (in FS) and non-standard weather conditions (drought) during the 2003 growing season.*

The biomass growth dynamics of individual above-ground organs can be derived as follows: ΔLB from the LAI dynamics, ΔBB from the *H* increment dynamics, and ΔSB from the DBH growth dynamics. The TBA growth dynamics can be adequately described by DBH growth alone (Pokorný & Tomášková 2007). The validity of this statement and the accuracy of the results will increase with stand age, as an increasing amount of biomass will be allocated to stems (Assmann 1968) and the ratio of LB to TBA will begin to decline.

The same conclusions also emerged from the destructive analyses conducted on spruce in the Beskydy Mountains. For example, the TBA of the 6-year-old spruce monoculture with density of ca 7,000 trees ha^{-1} consisted of 36% LB, 27% BB, and 37% SB. These proportions for the 16-year-old spruce monoculture with density of ca 3,100 trees ha^{-1} were 28% LB, 24% BB, and 48% SB. Ten years later, the same forest stand had substantially lower density (ca 1,400 trees ha^{-1}) due to the thinning intervention and TBA was 19% LB, 23% BB, and 58% SB.

The destructive analyses resulted in a set of allometric equations for estimating the biomass and surface area of trees' above-ground organs (Fig. 3). Based on the aforementioned results of phenometric studies and comparisons of stands with different densities, it is recommended to implement silvicultural treatments at an early stage of stand growth. In this way, trees maintain long crowns (a larger area of effective, efficient assimilation apparatus), which supports the biomass increment and eliminates defoliation due to extreme drought during the growing season. It probably also improves trees' mechanical stability against heavy snow, wind, etc.

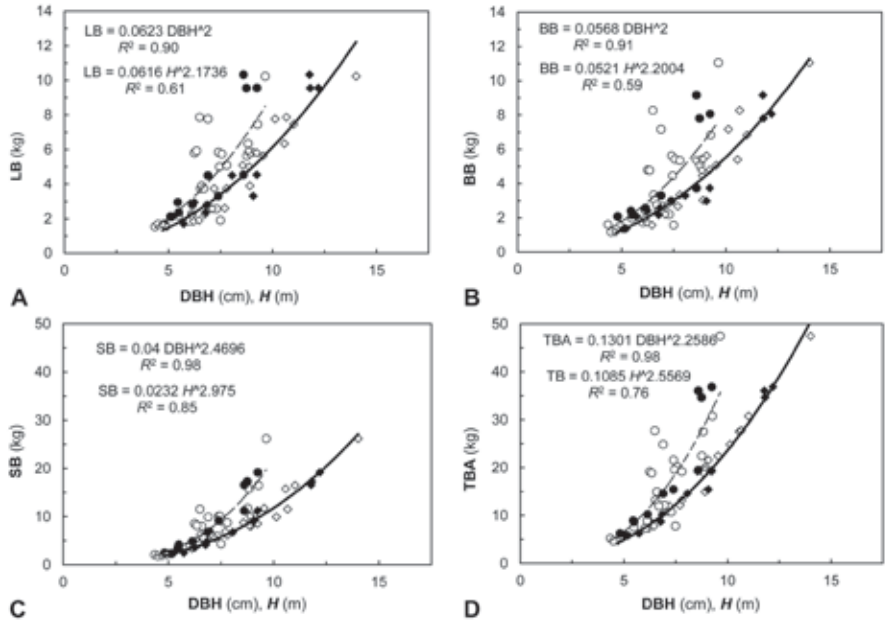

Fig. 3. *Allometric relationships between stem diameter at breast height (DBH) or tree height (H) and biomass of foliage (LB)* (**A**)*, branches (BB)* (**B**)*, and stems (SB)* (**C**) *and total aboveground biomass (TBA)* (**D**) *of spruce trees. Grey markers represent data from the destructive analysis conducted in 1997; black markers represent updated analyses of the allometric relationships carried out in 2007. Diamonds and black lines represent DBH relationships; circles and dashed lines represent H relationships. Adapted from Pokorný & Tomášková (2007).*

The dynamics of biomass increments for a stand's and individual trees' above-ground organs have a typical course. For example, the development of LB among conifers was typically intensive during the first half of the growing season and showed a gradual decline during the second half. Substantial decreases in TBA frequently occurred in winter, due to tree fall or damaged treetops caused by the destructive influence of heavy snow, ice, and wind. In addition to this "natural thinning" in winter, a major decline in TBA was caused by thinning interventions. Other factors affecting TBA and the new biomass increment include weather conditions during the growing season and the occurrence of biotic factors. Among basic microclimatic parameters, only rainfall in the first half of the growing season significantly affected seasonal increase in LAI on the FS plot ($r = -0.77$) (analysed for 1998–2005). On the FD plot, LAI was significantly affected by air temperature ($r = 0.82$). Similarly, the seasonal TBA increment on the FD plot (Fig. 4) was significantly affected by mean air temperature during May–July ($r = 0.72$). On the FS plot, the seasonal TBA increment was significantly correlated with the amount of rainfall in June ($r = -0.73$). The cumulative seasonal TBA increment culminated on the FD and FS plots similarly as occurred for the DBH increment, on average on the 232nd (± 18) DOY.

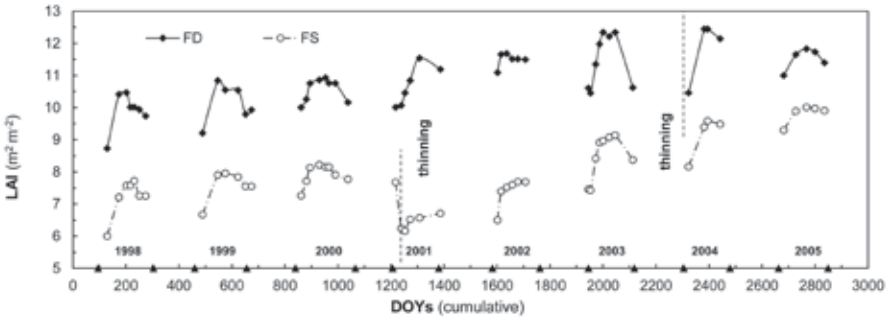

Fig. 4. *Long-term development of leaf area index (LAI; 1998–2005) in young spruce stands with different densities (FD = dense, FS = sparse). In 2001, high thinning was applied to the FS plot with an intensity of 20% of stand density. In 2004, low thinning was applied to the FD plot with an intensity of 17% of stand density. In winter 2005/2006, there was a significant natural reduction in stand density on both plots as a result of heavy snowfall. In 2007, the densities of the two plots converged. Adapted from Pokorný et al. (2008).*

The seasonal development of LAI during summer is affected by warming and reduced rainfall, although forests in such humid and cold regions as the Beskydy Mountains are less prone to changes in productivity and hydric regime than are forests in dry and warm regions. In the Beskydy Mountains, therefore, the LAI and TBA increments were more affected by microclimatic conditions during the first half of the growing season.

The distribution of the leaf area (LA) and biomass of individual above-ground organs of spruce trees changed across the crown's vertical profile depending on a tree's social status (Fig. 5). Dominant trees are highly irradiated and profit from light for biomass production efficiency (Assmann 1968).

The spatial distribution of foliage in a forest stand greatly depends upon the changing light environment during growth. The youngest needles (i.e. current and 1-year-old needles) are the most active physiologically (Marek et al. 1989 and Chapter 6 in this book). Older needles, particularly those in the low canopy, do not reach a positive carbon balance (most of the time they are exposed to PPFDs below so-called light compensation irradiance) and gradually fall. In those parts of the crown layer where the proportion of transmitted PPFD is <2% of incident PPFD, new needles are not created at all (Celniker 1978). This developmental trajectory reflects a functional proportion among individual needle age classes (Fig. 6).

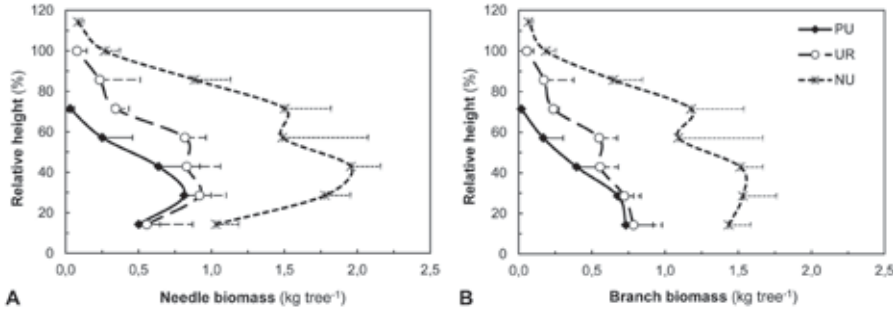

Fig. 5. *Vertical distribution of needle biomass* **(A)** *and branch biomass* **(B)** *of suppressed (PU), co-dominant (UR), and dominant (NU) trees within a stand. 100% = mean tree height. Means (points) and standard deviations (error bars) are presented; n = 11.*

In addition to the fact that foliage plays a key role in CO_2 assimilation, it is also important for biomass formation in young spruce forests. Based upon determination of the spatial distribution of LA and PPFD within a tree crown, so-called solar equivalent LA (SELA) can be determined as LA × PPFD (Čermák 1989). Based on SELA, it is possible to identify in more detail the production potential of the stand by crown layer. To calculate SELA (Fig. 7), we used the observed dependence of the LA distribution within the vertical profile of a selected individual tree with a representative social position (Fig. 5) and the specifically quantified LA of different needle age classes based on the allometric relationship.

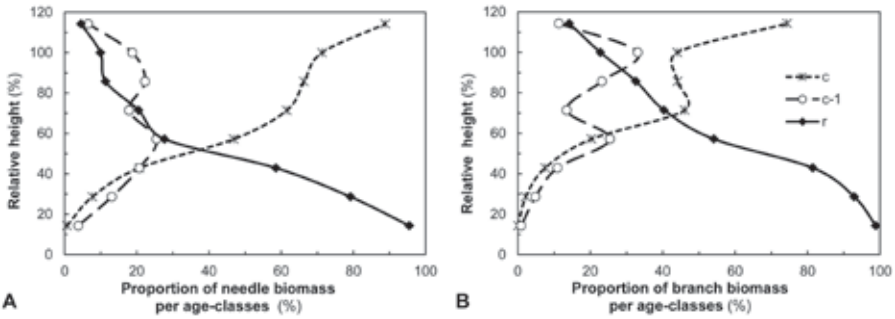

Fig. 6. *Proportions of needle* **(A)** *and branch* **(B)** *biomass of shoots within different age classes in the vertical profile of a forest canopy. 100% = mean tree height. c = current-year needles, c-1 = previous-year needles, r = all needles older than 2 years.*

The example of SELA calculated for clear and cloudy sky conditions (Fig. 7) showed that during cloudy skies the greatest carbon sink is located in the lower crown layers. This is in full agreement with the conclusion of direct physiological measurements of carbon uptake presented in Chapter 6 of this book. This

is related to different transmission of direct and diffuse radiation through the tree crown as well as to the specific LA distribution function in the stand's vertical profile (Fig. 5). Early in the morning, production potential is located in the upper canopy parts. Later, the major carbon sink moves to the middle part of the crown and remains there until late afternoon. Reduction in photosynthetic activity in the upper canopy layers is marked particularly during hot sunny days (Urban et al. 2012) when stomatal conductance to CO_2 diffusion is reduced. This phenomenon is sometimes referred to as afternoon depression in photosynthesis (see chapters 6 and 7 of this book for details).

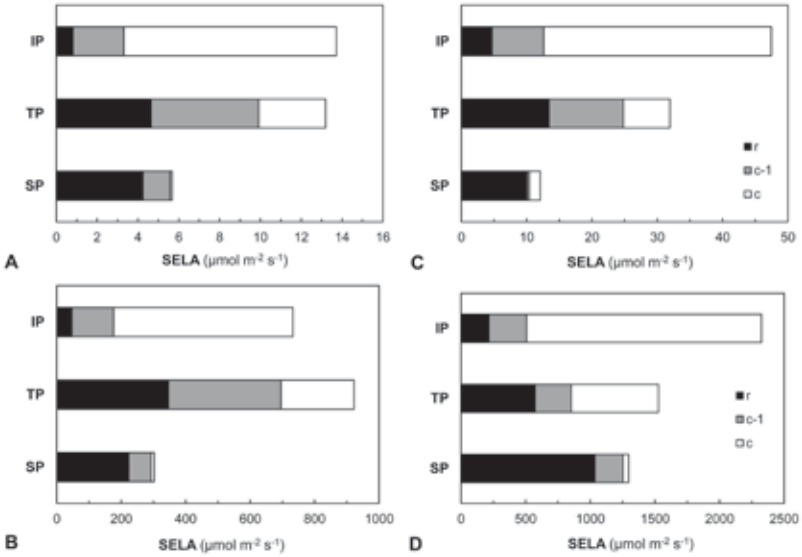

Fig. 7. *Solar equivalent leaf area (SELA) in three crown levels (IP = third whorl/sun-acclimated part, TP = sixth whorl/transitional part, and SP = ninth whorl/shade-acclimated part) of a co-dominant tree at 06:00 (***A***, ***C***) and at 12:00 (***B***, ***D***) during cloudy (***A***, ***B***) and clear sky conditions (***C***, ***D***). Proportions of individual shoot age classes are shown separately: c = current year shoots, c-1 = previous-year shoots, r = shoots older than 2 years.*

CONCLUSIONS

Although the two investigated stands with different densities induced by high thinning came close to having equal stand densities after several years (due to natural thinning in the dense stand, especially after winters with heavy snow), individual DBH increments and biomass production were nevertheless higher in the sparse stand. ΔSB played a key role in TBA production, and even more so with increasing stand age. At a stand age of 25 years, both investigated spruce monocultures reached not only similar stand densities but also similar LA, albeit with a higher proportion of the sun-adapted needle area in the artificially thinned stand. This higher LA efficiency related to higher production (Pokorný et al. 2008).

The highest production potential seems to have been located in the upper part of spruce crowns on sunny days. Nevertheless, in contrast to sunny days, production activity during cloudy sky conditions moves from the upper crown parts to the middle parts.

The present results confirm present silvicultural practice of early high thinning of Norway spruce stands, which can lead to a higher increment and biomass production of individual trees and increased stand stability, particularly in mountain areas.

Acknowledgement

This work was supported by the Ministry of Education, Youth and Sports of the Czech Republic within the National Programme for Sustainability I, grant No. LO1415.

References

Assmann, E. (1968) *Waldertragskunde*. BLV Verlagsgesellschaft, Munchen, Bonn, Wien.

Aubinet, M., Grelle, A., Ibrom, A. et al. (2000) Estimates of the annual net carbon and water exchange of forests: The EUROFLUX methodology. *Advances in Ecological Research*, **30**, 113–175.

Celniker, J.L. (1978) Fiziologičeskije osnovy tenevynoslivosti drevesnnych rastenij. *Nauka, Moskva*. [In Russian]

Čermák, J. (1989) Solar equivalent leaf area as the efficient biometrical parameter of individual leaves, trees and stands. *Tree Physiology*, **5**, 269–289.

Drexhage, M. & Gruber, F. (1998) Architecture of the skeletal root system of 40-year-old *Picea abies* on strongly acidified soils in the Hartz Mountains (Germany). *Canadian Journal of Forest Research,* **28**, 13–22.

Janssens, I.A., Freibauer, A., Ciais, P. et al. (2003). Europe's terrestrial biosphere absorbs 7 to 12% of European anthropogenic CO_2 emissions. *Science*, **300**, 1538–1542.

Kellomäki, S., Oker-Blom, P. & Kuuluvainen, T. (1984) The effect of crown and canopy structure on light interception and distribution in a tree stand. *Crop Physiology of Forest Trees* (eds P.M.A. Tigerstedt, P. Puttonen & V. Koski), pp. 107–115. Helsinki University Press, Helsinki.

Kuglitsch, F.G., Reichstein, M., Beer, C. et al. (2008) Characterisation of ecosystem water-use efficiency of European forests from eddy covariance measurements. *Biogeosciences Discussions*, **5**, 4481–4519.

Lehtonen, A, Mäkipää, R., Heikkinen, J., Sievänen, R. & Liski, J. (2004) Biomass expansion factors (BEFs) for Scots pine, Norway spruce and birch according to stand age for boreal forests. *Forest Ecology and Management*, **188**, 211–224.

Mäkelä, A. (1997) A carbon balance model of growth and self-pruning in trees based on structural relationships. *Forest Science*, **43**, 7–24.

Marek, M., Barták, M. & Pirochtová, M. (1989) Vertical topography of photosynthetic activity and crown structure in Norway spruce. *Acta Scientiarum Naturalium Brno*, **23**, 1–52.

Ministry of Agriculture of the Czech Republic (2014) *Annual Report about Forest Conditions and Forest Management of the Czech Republic*. Prague. [In Czech]

Penman, J., Gytarsky, M., Hiraishi, T. et al. (2003) Good Practice Guidance for Land Use, Land-Use Change and Forestry. Institute for Global Environmental Strategies (IGES) for The Intergovernmental Panel on Climate Change (IPCC), Hayama, Japan.

Pokorný, R. & Marek, M.V. (2000) Test of accuracy of LAI estimation by LAI-2000 under artificially changed leaf to wood area proportions. *Biologia Plantarum*, **43**, 537–544.

Pokorný, R (2002) Leaf area index in forest tree stands. Ph.D. Thesis, Mendel University in Brno, Brno. [In Czech]

Pokorný, R., Urban., O. & Marek, M.V. (2004) Effect of Norway spruce planting density on shoot morphological parameters. *Biologia Plantarum*, **48**, 137–139.

Pokorný, R. & Tomášková, I. (2007) Allometric relationships for surface area and dry mass of Norway spruce aboveground organs. *Journal of Forest Science*, **53**, 548–554.

Pokorný, R., Tomášková, I. & Havránková, K. (2008) Temporal variation and efficiency of LAI in young mountain Norway spruce stand. *European Journal of Forest Research,* **127**, 359–367.

Teobaldelli, M., Somogyi, Z., Migliavacca, M., & Usoltsev, V.A. (2009) Generalized functions of biomass expansion factors for conifers and broadleaved by stand age, growing stock and site index. *Forest Ecology and Management*, **257**, 1004–1013.

Urban, O., Janouš, D., Acosta, M. et al. (2007). Ecophysiological controls over the net ecosystem exchange of mountain spruce stand. Comparison of the response in direct vs. diffuse solar radiation. *Global Change Biology*, **13**, 157–168.

Urban, O., Klem, K., Ač, A. et al. (2012) Impact of clear and cloudy sky conditions on the vertical distribution of photosynthetic CO_2 uptake within a spruce canopy. *Functional Ecology*, **26**, 46–55.

Vetter, M., Wirth, Ch., Böttcher, H. et al. (2005) Partitioning direct and indirect human-induced effects on carbon sequestration of managed coniferous forests using model simulations and forest inventories. *Global Change Biology*, **11**, 810–827.

Waring, R.H. (1987) Characteristics of trees predisposed to die: stress causes distinctive changes in photosynthate allocation. *Bioscience*, **37**, 569–574.

Wigley, T.M.L. & Schimel, D.S. (2000) *The Carbon Cycle.* Cambridge University Press, Cambridge, United Kingdom.

Chapter 5

Ecosystem stations – a tool for global change observations

Kateřina Havránková, Ladislav Šigut, Lenka Macálková, Jiří Dušek, Pavel Sedlák, Marian Pavelka

Department of Matters and Energy Fluxes, Global Change Research Centre, Czech Academy of Sciences, Bělidla 4a, CZ-60300 Brno, Czech Republic

1. INTRODUCTION

Global change is one of the major problems facing humanity. Among other effects, changes are seen in climate, ecosystems, atmospheric chemistry, and landscape and ocean productivity (Millennium Ecosystem Assessment 2005; IPCC 2013). As summarized in chapters 1 and 2 of this book, climate change is caused by Earth's energy imbalance, occurring when the planet absorbs on average more energy than is radiated back into space. The result is a rise in global temperature. The main cause of this energy imbalance is the increasing concentration of greenhouse gases in the atmosphere (reviewed in Field et al. 2007). The impacts and feedbacks of climate change on key ecosystems are therefore of particular interest.

Ecosystem stations within the Czech Carbon Observation System (CzeCOS) serve for long-term observation of matter (especially greenhouse gases) and energy fluxes between ecosystems and the atmosphere in regional and international contexts. The method used for this purpose is eddy covariance, which is the most direct and accurate approach and relies on high frequency measurements of wind speed and direction as well as CO_2, H_2O, and CH_4 concentrations (Aubinet et al. 2012). Auxiliary measurements consist of meteorological parameters, soil characteristics, and biomass inventory. The services provided by CzeCOS also include monitoring and evaluation of the effectiveness of carbon sequestration as well as research on carbon sinks and sources in different regions. The goal is to understand the ecophysiological processes within the ecosystems in terms of the changing climate and find ways to reduce greenhouse gas emissions.

Proper interpretation of flux measurements is essential and depends on good knowledge of the instrumentation and measurement principles (Baldocchi 2003). First, the acquired raw data (20 Hz sampling frequency) should be corrected, converted to appropriate units, and controlled as to its quality by means of processing software. It is necessary to correct for errors caused by setup limitations (due to such factors as instrument tilt and separation) and physical principles (due to such factors as instrument heating). Each half-hourly flux measurement is assigned a quality code according to the instrument operability, turbulence intensity, and steady state conditions required by the method. Data not meeting the quality requirements are rejected and gap-filled (Aubinet et al. 2012).

Second, it is essential to analyse the study's footprint. The fetch should not extend beyond the ecosystem of interest. If this condition is not met, data from the extraneous areas should be flagged and excluded from further analysis.

Since the launch of regional and international tower networks, development in standardization of eddy-covariance data quality control has attracted more attention. Several authors have already proposed solutions for different parts of quality control schemes (e.g. Reichstein et al. 2005; Papale et al. 2006; Mauder

et al. 2013). In this study, we build on this research and present our methodology with a particular focus on data quality control and the results from footprint analysis.

2. MATERIAL AND METHODS

2.1. CzeCOS ecosystem stations

The ecosystem stations that form CzeCOS are located in mixed (floodplain), spruce, and beech forests; wetland; mountain grassland; and an agroecosystem. The studied ecosystems are typical for Central Europe, important for its greenhouse gas balance, and represent different climatic conditions (along an altitude gradient). Site characteristics are summarized in Table 1.

2.2 Flux measurement

Unified eddy covariance systems were installed for flux measurements at all investigated ecosystems. The systems were placed on meteorological towers above vegetation. They use an ultrasonic anemometer (R3 or HS-50, Gill Instruments, Hampshire, UK), a Li-7000 or Li-7200 fast-response infrared gas analyser (Li-Cor, Lincoln, NE, USA), and Windows Interface Software for the Li-7200 (Li-Cor). After post-processing using Open source software EddyPro® (Li-Cor; EddyPro is a registered mark of Li-Cor Biosciences company in the United States and other countries), half-hourly averages of fluxes are available for further analysis.

2.3 Micrometeorological measurements

Standardized measurements of the following parameters were made at each site: global radiation (pyranometer CM6B, Kipp & Zonen, Delft, Netherlands); radiation balance (Net Radiometer CRN 4, Kipp & Zonen); incident, reflected, and transmitted photosynthetic photon flux density (EMS 12, EMS, Brno, Czech Republic); air temperature and relative humidity in vertical profile (EMS 33, EMS); soil temperature in vertical profile (Pt1000, Sensit, Rožnov pod Radhoštěm, Czech Republic); soil moisture in vertical profile (CS-616, Campbell Scientific, Logan, UT, USA, or ML2 ThetaProbe, Delta-T Devices, Cambridge, UK); soil heat flux (HFP01SC self-calibrating heat flux sensor, Hukseflux Thermal Sensors, Delft, Netherlands); and precipitation (Precipitation Gauge 386C, Met One Instruments, Grants Pass, OR, USA).

2.4 Post-processing, quality control, and gap-filling

EddyPro was used to calculate half-hourly CO_2, latent heat, sensible heat, and momentum fluxes from the high frequency raw data. It applies the most recent methods for flux corrections, conversions, and quality control. This process contains several steps, of which the most important are the following: despiking and raw data statistical screening, axis rotation for tilt correction (planar fit, double rotation), detecting and compensating for time lags of signals from the ultrasonic anemometer and gas analyser, spectral correction (compensation for spectral loss), calculating corrected fluxes, basic quality control of turbulent fluxes (flux stationarity and integral turbulence characteristics tests), and footprint estimation. The software's default settings, termed Express Mode, needed to be adapted to each site depending on instrument setup, canopy height, and surface topography.

Further quality control was performed on the half-hourly EddyPro output similarly to as described by

Table 1. Characteristics of Czech Carbon Observation System ecosystem stations. T_a – mean annual temperature, Precipitation – annual total precipitation (long-term annual averages and totals: Bílý Kříž 1998–2012, Lanžhot 1961–2014, Štítná nad Vláří 2010–2012, Křešín u Pacova 1988–2014, Rájec 1975–2012, Třeboň 1977–2013).

Location	Ecosystem type	Elevation (m a.s.l.)	Prevailing species	Age (years)	T_a (°C)	Precipitation (mm)	Coordinates
Bílý Kříž	spruce forest	875	Norway spruce (*Picea abies*)	34	6.8	1,258	49°30′08″N 18°32′13″E
Bílý Kříž	grassland	860	matgrass (*Nardus stricta*), red fescue (*Festuca rubra*), creeping soft grass (*Holcus mollis*), common sorrel (*Rumex acetosa*), imperforate St John's wort (*Hypericum maculatum*), yarrow (*Achillea millefolium*)		6.8	1,258	49°29′40″N 18°32′34″E
Lanžhot	floodplain forest	150	narrow-leaved ash (*Fraxinus angustifolia*), English oak (*Quercus robur*), European white elm (*Ulmus laevis*), European hornbeam (*Carpinus betulus*), field maple (*Acer campestre*), small-leaved linden (*Tilia cordata*)	110	9.6	542	48°40′54″N 16°56′47″E
Štítná nad Vláří	beech forest	540	European beech (*Fagus sylvatica*)	112	8.4	770	49°02′09″N 17°58′12″E
Křešín u Pacova	agroecosystem	545	10-year crop rotation		8.0	650	49°34′24″N 15°04′44″E
Rájec	spruce forest	625	Norway spruce (*Picea abies*)	110	7.1	673	49°26′37″N 16°41′48″E
Třeboň	wetland	426	tall sedges (*Carex acuta*, *Carex vesicaria*), reed canary grass (*Phalaris arundinacea*)		7.6	614	49°01′29″N 14°46′13″E

Mauder et al. (2013). The quality control scheme consisted of checking for instrumentation and data sampling problems, missing raw data within a half hour (maximum 10% allowed), plausibility limits of the variables used, spike percentage within a half hour (maximum 1% allowed), a large mean vertical wind velocity after planar fit rotation (an indicator of vertical advection), and a large spectral correction factor (an indicator of large flux uncertainty). The quality flags obtained for each flux were combined and their interdependency due to conversions and corrections taken into account. To ensure that outliers did not affect gap-filling results, a robust outlier estimator based on the median of absolute deviations from the median (Sachs 1996) was applied. A directional footprint filter (5° resolution) ensured that the majority of flux contributions came from the desired area. Another filtering procedure, filtering friction velocity (u^*), assured the exclusion of CO_2 flux measurements not representative of the biotic flux. This filtering applied mostly to nighttime measurements when u^* decreased, a pattern often connected with night-time flux underestimation (Goulden et al. 1996). u^* filtering based on Reichstein et al. (2005) was applied to correct for this systematic bias. The flag system followed the agreement reached within CarboEurope IP (Mauder & Foken 2004): data were flagged as 0 (excellent quality, suitable for fundamental research and development of parametrization), 1 (good quality, suitable for general analysis and annual budgets), or 2 (bad quality, needing to be removed and gap-filled).

Missing or excluded data were gap-filled in order to create the continuous flux time series necessary to estimate annual budgets. The empirical method (marginal distribution sampling) described in Reichstein et al. (2005) was applied using the online service of the Max Planck Institute for Biogeochemistry (http://www.bgc-jena.mpg.de/~MDIwork/eddyproc/index.php). The same tool is used also to separate net ecosystem exchange into ecosystem respiration and gross primary productivity (Reichstein et al. 2005).

2.5. Footprint calculation

A flux measurement's footprint is that fraction of the upwind surface containing effective sources and sinks contributing to the measurement point. It defines the measurement's spatial context, which means the area of surface sources and sinks contributing to total measured flux. Each point or area source potentially contributes to the concentration or flux profile downwind to a degree that varies with distance from the instruments' locations, observation's elevation, characteristics of the turbulent boundary layer, and atmospheric stability (Schuepp et al. 1990).

Mathematically, the footprint can be defined as follows: consider a coordinate system such that the x-axis is pointing against the direction of the wind and the sensors are located at $(0,0,z_m)$, where z_m is measurement height. The footprint function $f(x,y,z)$ describes the flux at $(0,0,z)$ caused by a point source at $(x,y,0)$. Two approaches were used – the footprint function in EddyPro (Kormann & Meixner 2001) and a stochastic Lagrangian approach (Kljun et al. 2004).

The Kormann–Meixner model was used for extremely stable conditions. For other conditions, the Kljun model was used. The Kormann–Meixner model was not used for unstable and neutral conditions because it is computationally demanding in such conditions.

The mean distance from the tower at which cumulative contribution to turbulent fluxes is 70% was used for our visualization of flux footprints (angular resolution 5°). Footprints were further distinguished according to atmospheric stability into stable, neutral, and unstable conditions.

3. RESULTS AND DISCUSSION

3.1. Post-processing, quality control, and gap-filling

The selected 8-day period (8–15 June 2013) at the Rájec Norway spruce site demonstrates the effects of the applied quality control scheme (Fig. 1). Excellent and good quality data (flags 0 and 1) prevailed during the white day and nights with unstable atmospheric stratification and well-developed turbulence. In contrast, bad data (flag 2) occurred at times with instrumental problems (Fig. 1; 14–15 June), stationarity issues, or low turbulence intensity (more common at night). Gap-filled fluxes also show that failing to exclude bad quality data at night would lead to a strong underestimation of ecosystem respiration, as often described in the literature (Reichstein et al. 2005; Lasslop et al. 2010).

3.2. Footprint results

For each site, three footprint curves were computed according to atmospheric stability conditions. The distribution of stability conditions followed a daily course, with stable conditions occurring mostly at night and unstable conditions during the day. The proportions of stability conditions at each site are summarized in Table 2.

For all sites, the footprint curves for neutral and unstable conditions covered mostly only the studied ecosystem (dashed and dotted lines in Figs. 2 and 3). Under stable atmospheric conditions, the footprint curve extended beyond the studied ecosystem's border in certain wind directions (solid lines in Figs. 2 and 3).

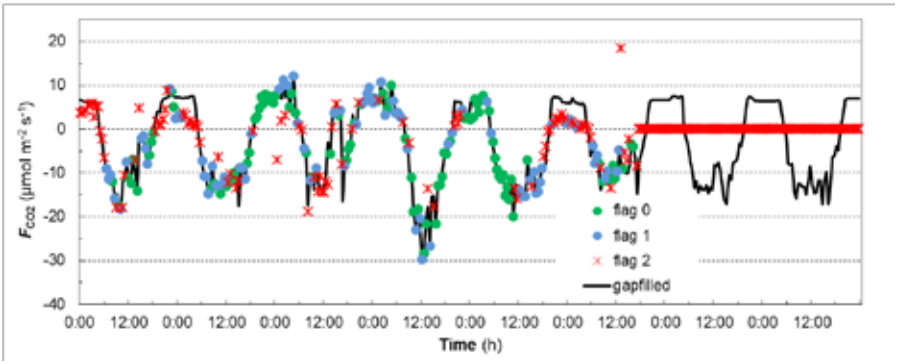

Fig. 1. *CO_2 flux (F_{CO2}) quality control results for Rájec spruce forest site (8–15 June 2013). Flux quality is marked as excellent (flag 0, green dots), good (flag 1, blue dots), and bad (flag 2, red stars). Excluded data (flag 2) are gap-filled (black line).*

Each investigated ecosystem site had different wind and turbulence characteristics (data not shown) associated with footprint features. Křešín u Pacova, Třeboň, and Lanžhot are situated in even terrain and their footprints were more or less circular (Fig. 2C,D and Fig. 3A). At Křešín u Pacova, there was a problematic grassy area in the south, south-east, and east of the footprint under stable conditions. The wind came relatively frequently (15% of cases under stable atmospheric conditions) from this area. The flux footprint reached the grass under unstable conditions under southerly winds in 8% of cases. Generally, winds from the south, south-east, and east should be treated with care when processing flux data from this site.

Třeboň had much lower wind speeds (mean 1.5 m s^{-1}) than did Křešín u Pacova (mean 4 m s^{-1}) and its footprint was smaller even though the eddy covariance system was placed at the same height above the ground (2.5 m). The wind most frequently came from the north-west (25% of all cases). A further 30% of flux came from the south–south-west, south, and south-east. No data from unstable and neutral conditions were excluded (62% of half hours under all atmospheric conditions). The footprint curves (Fig. 2D) show that the data acquired represented the studied ecosystem. Although the stable footprint included an area across the river and one must accordingly be attentive when processing flux data, wind from this direction occurred only infrequently (10% of stable conditions, i.e. 3.8% of all conditions).

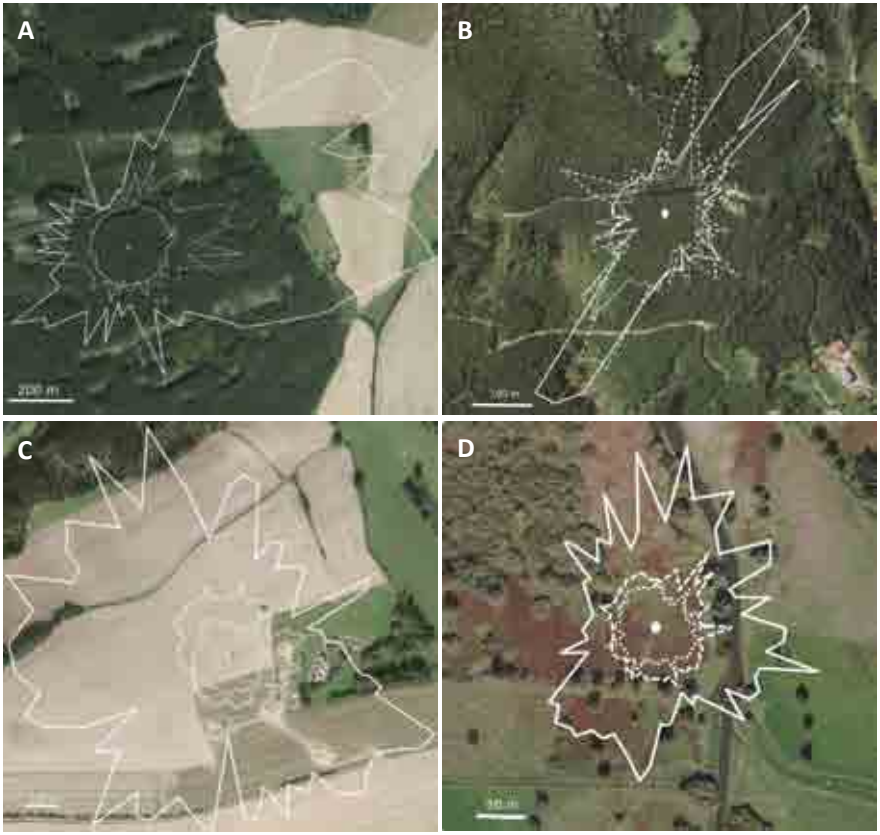

Fig. 2. *Footprint curves for ecosystem stations in Rájec – spruce forests(A), Bílý Kříž – spruce forest (B), Křešín u Pacova – agroecosystem (C), and Třeboň – wetland (D). Solid lines denote the flux footprint for stable conditions, dashed lines for neutral conditions, and dotted lines for unstable conditions. White dots represent tower locations. Data are presented for all of 2012.*

The footprint in Lanžhot (Fig. 3A) was circular. The majority (69%) of winds exceeded 2 m s^{-1} and winds came most frequently from the north and north-west (34.3%) and the south-east (17%). All data from

unstable and neutral conditions came from the floodplain forest. Under stable conditions (22% of all atmospheric conditions), the footprint covered a large area but still mostly covered the ecosystem except for the south-east and south–south-east.

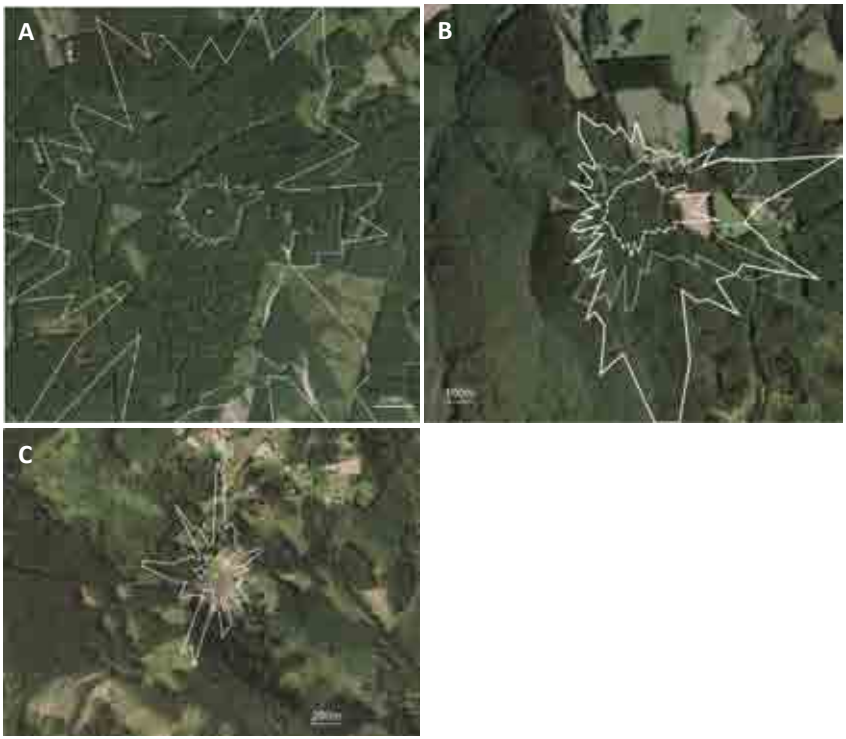

Fig. 3. *Footprint curves for ecosystem stations in Lanžhot – mixed forest (A), Štítná – beech forest (B), and Bílý Kříž – grassland (C). Solid lines denote the flux footprint for stable conditions, dashed lines for neutral conditions, and dotted lines for unstable conditions. Data are presented from January–June 2015 in Lanžhot, all of 2014 in Štítná, and all of 2012 in Bílý Kříž.*

Table 2. *Atmospheric stability conditions distribution at Czech Carbon Observation System sites.*

Locality	Height of measurement (m)	Unstable (%)	Neutral (%)	Stable (%)
Bílý Kříž forest	20.5	32	30	38
Bílý Kříž grassland*	1.5	22	49	27
Lanžhot*	44.0	33	35	22
Štítná nad Vláří*	44.0	33	30	35
Křešín u Pacova	2.6	28	52	20
Rájec	41.0	22	52	26
Třeboň	2.5	32	30	38

** Data with stability parameters outside the interval [−10,10] were excluded from analysis.*

Although Rájec (Fig. 2A) is situated on a modest slope and the landscape around the target forest stand is patchy with varying surface roughness, the footprint for unstable and neutral conditions nevertheless covered the studied mature spruce forest well. Under stable conditions (mostly at night), however, the footprint was elongated to the north-east and east. At such times, the measured data included an agriculture field and thus should be excluded from further flux analysis. The amount of such data was not crucial, as wind from these directions occurred only infrequently (14% of stable atmospheric conditions).

The footprint in Štítná (Fig. 3B) was affected by the site's position on a west–south-west slope. The footprint was prolonged to the south and east. Winds most frequently occurred from the south-east and south–south-east (30% of all atmospheric conditions) with high wind speeds (more than 75% of data). This area represents the studied ecosystem, although it should be checked for high turbulence. There is an agriculture field to the east and east–north-east (the source of 10% of all winds). Even under unstable conditions, the footprint reached this area and most data from this area should be excluded.

The Bílý Kříž forest (Fig. 2B) is situated on a slope near the top of a mountain ridge. Due to flow modification by terrain, southerly winds prevailed at the site (40% of all atmospheric conditions) and the southern fetch was also the longest under all atmospheric conditions. Data from northerly winds should be treated with care due to the effect of the ridge.

The Bílý Kříž grassland (Fig. 3C) represents a small area surrounded by forest. Although the eddy covariance system was placed only 1.5 m above the ground and 90% of winds were under 2 m s^{-1}, the footprint nevertheless extended away from the grassland. Under stable conditions, this extension was long and data within 40–180° should thus be excluded. Under neutral and unstable conditions, the north-eastern and southern areas should be treated with care.

It is well known that footprints' shape and extent change primarily due to surface roughness, atmospheric stability, and measurement height (Leclerc & Thurtell 1990; Foken & Leclerc 2004). Given this fact, we could expect measurements performed above short canopies (Bílý Kříž grassland, Křešín u Pacova, Třeboň) to have fetches considerably shorter than those at tall canopies (Bílý Kříž forest, Lanžhot, Štítná nad Vláří, Rájec; see Table 2 for measurement heights). For tall vegetation, however, it has been shown that canopy turbulence and source/sink levels inside the canopy have the greatest effects on footprint prediction (reviewed in Aubinet et al. 2012). The effects of high forest canopy roughness and observation level thus probably cancelled each other out and we saw a considerably smaller fetch only for the Třeboň wetland site.

It is also important to note that the footprints shown are probably simplifications of the real footprints due to several reasons which are beyond the scope of this chapter (Schmid 2002; Göckede et al. 2004). A better understanding is needed of the turbulence structure in forest canopies and the effects of horizontal inhomogeneities, forest edges and gaps on footprints.

Thorough footprint analyses coupled with data-quality assessments have been provided for the Bílý Kříž forest in Rebmann et al. (2005) and Göckede et al. (2008). Their results agree with our findings and conclude that more than 95% of fluxes come from the target land use type. Both studies also stated that footprint models tend to overestimate footprints (conservative footprint estimate). This was well demonstrated for the northerly and southerly wind fetch at Bílý Kříž under stable stratification and may have been the result of averaging across overestimated fetch distances.

Footprint models rely on certain assumptions about turbulent conditions, and nocturnal footprints are particularly prone to errors (Vesala et al. 2008). Therefore, improvements could probably be achieved by

performing analyses separately for day and night, using stricter conditions for data filtering (e.g. excluding half hours with stability parameters outside the interval [−1,1]), or applying more robust statistics (median instead of mean).

4. CONCLUSIONS

We aimed to show the ecosystem stations network to be a powerful tool for global climate change observations. We introduced CzeCOS study sites with the measurement technique and performed observations. The core of taking care of data includes proper treatment of the data and the area's footprint. Post-processing, quality control, and gap-filling are described as standardized procedures based on up-to-date knowledge of the eddy covariance method. Source areas were well covered for all studied ecosystems under unstable and neutral stability conditions. Footprints under stable conditions in certain cases extended beyond the studied ecosystems (the south-east of Křešín, east of Rájec, south-east of Lanžhot, and north to south-east of Bílý Kříž grassland) or could be difficult to interpret (northerly winds in Bílý Kříž forest, southerly winds in Štítná). Data from these conditions were generally night-time data that were already treated with special care due to night-time CO_2 flux underestimation. These data were typically excluded from flux analysis and gap-filled.

Acknowledgement

This work was supported by the Ministry of Education, Youth and Sports of the Czech Republic within the National Programme for Sustainability I, grant No. LO1415.

References

Aubinet, M., Vesala, T. & Papale, D. (2012) Eddy Covariance: A Practical Guide to Measurement and Data Analysis. Springer Atmospheric Sciences, Springer Verlag.

Baldocchi, D.D. (2003). Assessing the eddy covariance technique for evaluating carbon dioxide exchange rates of ecosystems: past, present and future. *Global Change Biology*, **9**, 479–492.

Field, C.B., Lobell, D.B., Peters, H.A. & Chiariello, N.R. (2007) Feedbacks of Terrestrial Ecosystems to Climate Change. *Annual Review of Environment and Resources*, **32**, 1–29.

Foken, T. & Leclerc, M.Y. (2004) Methods and limitations in validation of footprint models. *Agricultural and Forest Meteorology*, **127**, 223–234.

Göckede, M., Rebmann, C. & Foken, T. (2004) A combination of quality assessment tools for eddy covariance measurements with footprint modelling for the characterisation of complex sites. *Agricultural and Forest Meteorology*, **127**, 175–188.

Göckede, M., Foken, T., Aubinet, M. et al. (2008) Quality control of CarboEurope flux data – Part 1: Coupling footprint analyses with flux data quality assessment to evaluate sites in forest ecosystems. *Biogeosciences*, **5**, 433–450.

Goulden, M.L., Munger, J.W., Fan, S.-M., Daube, B.C., Wofsy, S.C. (1996) Measurements of carbon sequestration by long-term eddy covariance: methods and a critical evaluation of accuracy. *Global Change Biology,* **2**, 169–182.

IPCC (2013) Summary for policymakers. Climate Change 2013: The Physical Science Basis. Contribution of Working Group I to the Fifth Assessment Report of the Intergovernmental Panel on Climate Change (eds T.F. Stocker, D. Qin, G.-K. Plattner et al.), pp. 3–29, Cambridge, UK and New York, NY, USA: Cambridge University Press.

Kljun, N., Calanca, P., Rotach, M.W. & Schmid, H.P. (2004) A simple parameterization for flux footprint predictions. *Boundary-Layer Meteorology*, **112**, 503–523.

Kormann, R. & Meixner, F.X. (2001) An analytical footprint model for non-neutral stratification. *Boundary-Layer Meteorology*, **99**, 207–224.

Lasslop, G., Reichstein, M., Papale, D. et al. (2010) Separation of net ecosystem exchange into assimilation and respiration using a light response curve approach: critical issues and global evaluation. *Global Change Biology*, **16**, 187–208.

Leclerc, M.Y. & Thurtell, G.W. (1990) Footprint prediction of scalar fluxes using a Markovian analysis. *Boundary-Layer Meteorology*, **52**, 247–258.

Mauder, M., Cuntz, M., Druee, C. et al. (2013) A strategy for quality and uncertainty assessment of long-term eddy-covariance measurements. *Agricultural and Forest Meteorology*, **169**, 122–135.

Mauder, M. & Foken, T. (2004) Documentation and instruction manual of the eddy covariance software package TK2. University at Bayreuth, Abtailung Mikrometeorologie, Germany.

Millennium Ecosystem Assessment (MEA) (2005) Ecosystems and Human Well-Being: Scenarios. Island Press, Washington, DC.

Papale, D., Reichstein, M., Aubinet, M. et al. (2006) Towards a standardized processing of Net Ecosystem Exchange measured with eddy covariance technique: algorithms and uncertainty estimation. *Biogeosciences*, **3**, 571–583.

Rebmann, C., Göckede, M., Foken, T. et al. (2005) Quality analysis applied on eddy covariance measurements at complex forest sites using footprint modelling. *Theoretical and Applied Climatology*, **80**, 121–141.

Reichstein, M., Falge, E., Baldocchi, D. et al. (2005) On the separation of net ecosystem exchange into assimilation and ecosystem respiration: review and improved algorithm. *Global Change Biology*, **11**, 1424–1439.

Sachs, L. (1996) Angewandte Statistik: Anwendung Statistischer Methoden. Springer, Berlin.

Schmid, H.P. (2002) Footprint modeling for vegetation atmosphere Exchange studies: a review and perspective. *Agricultural and Forest Meteorology*, **113**, 159–183.

Schuepp, P.H., Leclerc, M., Macpherson, J.I. & Desjardins, R.L. (1990) Footprint prediction of scalar fluxes from analytical solutions of the diffusion equation. *Boundary-Layer Meteorology*, **50**, 355–373.

Vesala, T., Kljun, N., Rannik, Ü. et al. (2008) Flux and concentration footprint modelling: State of the art. *Environmental Pollution*, **152**, 653–666.

Chapter 6

Modification of carbon cycle in forest ecosystems by distinct sky conditions

Otmar Urban[1], Marian Pavelka[2], Karel Klem[3]

[1] *Laboratory of Plant Ecological Physiology, Global Change Research Centre, Czech Academy of Sciences, Bělidla 4a, CZ-60300 Brno, Czech Republic*

[2] *Department of Matters and Energy Fluxes, Global Change Research Centre, Czech Academy of Sciences, Bělidla 4a, CZ-60300 Brno, Czech Republic*

[3] *Department of Impact Studies, Global Change Research Centre, Czech Academy of Sciences, Bělidla 4a, CZ-60300 Brno, Czech Republic*

1. INTRODUCTION

Light is one of the key drivers of photosynthesis and primary production by plants. Light reaches the Earth's surface both as direct beams from the sun and in diffuse form (Fig. 1) after being scattered in the atmosphere by small molecules (Rayleigh scattering) and aerosols (Mie scattering). The diffuse index, defined as the ratio between diffuse and global radiation intensities, has undergone substantial variation in recent decades with trends described as global 'dimming' and 'brightening' (e.g. Wild 2009). These changes result particularly from stratospheric ozone depletion and its variability, cloudiness, and aerosol loading in the atmosphere. In addition, it is predicted that convective mixing between the lower and middle troposphere will dehydrate the low-cloud layer, particularly in the tropics and at middle latitudes (Chepfer et al. 2014; Sherwood et al. 2014), and this will thus have a substantial global effect on future sky conditions.

In general, cloud cover and aerosol loading in the atmosphere lead to reduced light intensity, increased proportions of diffuse radiation, changes in the spectral composition of solar radiation, and decreases in temperature and vapour pressure deficit (see Spitters et al. 1986; Campbell & Norman 1998; Navrátil et al. 2007; Urban et al. 2007a; Wild 2009). Thus, sky conditions, and not just light intensity, may influence ecosystems' photosynthesis and have the potential to cause substantial change in the global carbon cycle.

It has been reported that an eruption of Mount Pinatubo in 1991 stimulated biomass production in tropical forests and the allocation of an extra 2 Gt(C) per year, which consequently resulted in reduced allocation of CO_2 in the atmosphere during 1992–1993 (Farquhar & Roderick 2003; Gu et al. 2003). This stimulation of carbon uptake was attributed to a reduction in global temperature by 0.5°C and increased proportion of diffuse solar radiation by 50%. Many researchers have now observed enhanced canopy photosynthesis under cloudy as opposed to clear sky conditions (e.g. Hollinger et al. 1994; Law et al. 2001; Mercado et al. 2009; Dengel & Grace 2010; Pingintha et al. 2010). Nevertheless, the specific mechanisms whereby sky conditions and diffuse light stimulate ecosystem CO_2 uptake are still not well understood.

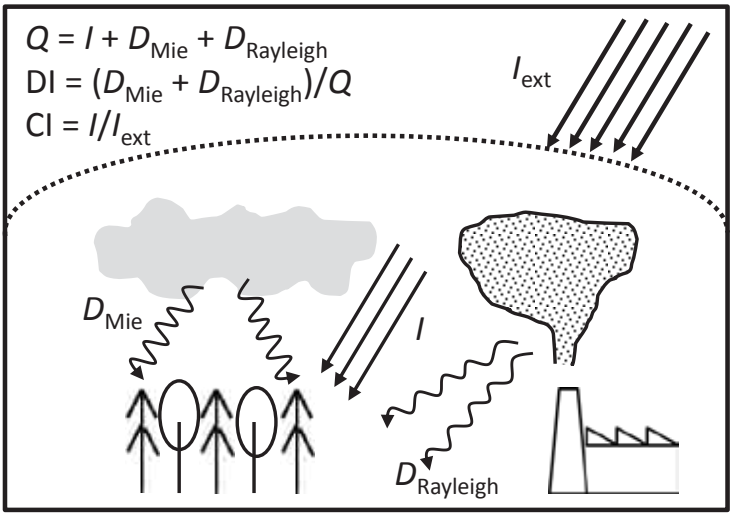

Fig. 1. *Simplified scheme of solar radiation components. I (direct irradiance) = intensity of parallel rays that come in a straight line from the direction of the sun; I_{ext} (extra-terrestrial irradiance) = intensity of solar irradiation directly outside the Earth's atmosphere on a horizontal surface; D = intensity of diffuse radiation after being scattered in the atmosphere by small molecules ($D_{Rayleigh}$) or aerosols (D_{Mie}). Q represents global radiation received by the Earth's surface. To quantify the amount of diffuse and direct radiation, diffuse (DI) and clearness (CI) indexes, respectively, are usually used.*

We investigated this problem on a Norway spruce canopy and compared the results during days with cloudy versus clear sky conditions. We tested whether more favourable microclimatic conditions (lower temperatures and vapour pressure deficits during cloudy periods) and increased penetration of light into the canopy lead to stimulation of CO_2 uptake.

2. MATERIALS AND METHODS

2.1. Site description

The investigated forest stand is located at the Bílý Kříž experimental research site (Beskydy Mountains, 49°30'N, 18°32'E, 875 m a.s.l.). From a climatic point of view, the region is moderately cold, wet, and rich in precipitation. During 1998–2012, mean annual air temperature was 6.8 ± 1.1°C, mean annual relative humidity was 84 ± 4%, and mean annual total precipitation was 1,258 ± 215 mm. The studied stand had been established in 1981 by row planting of 4-year-old seedlings of Norway spruce (Picea abies). Planting spacing had been 2 x 1 m and in a north–south row orientation. Stand height during this experiment was 13.4 m, tree density 1,428 trees ha^{-1}, and hemi-surface leaf area index 9.5 m^2 m^{-2}. A meteorological mast (36 m tall) equipped with a set of meteorological sensors (e.g. for air temperature, relative humidity, wind speed and direction, and air pressure) was placed within the studied stand (see Chapter 5 in this book for details about the meteorological sensors available). Mean stand slope is 12.5° and it is exposed to the south. The soil types in the stand are modal podzol and modal kryptozol. The soil is moderately deep to shallow, from loamy-sand to sandy-loam with high soil skeleton content in the lower layers. Maximum soil depth is 60–80 cm.

Interpretation of the carbon assimilation data was based on the incident photosynthetic photon flux density (PPFD) measured by quantum sensors (Li-190; Li-Cor, Lincoln, NE, USA) located above the stand canopy. In addition, a laboratory-made canopy fibre optic system (CANFIB; see Urban et al. 2007a for detailed description) was used to measure PPFD within the tree canopy. The CANFIB sensors were located at four levels perpendicularly to a shoot axis representing the upper canopy (5th whorl; 1-year-old shoots), middle canopy (8th and 10th whorl; 2-year-old shoots), and lower canopy (15th whorl; > 2-year-old shoots). See Chapter 4 in this book for details about the sensors placement.

2.2. Canopy and shoot-level measurement of CO_2 assimilation

An eddy covariance system, described in detail in Chapter 5 of this book, was used to measure CO_2 and water vapour fluxes between the forest and atmosphere. Half-hourly averaged H_2O and CO_2 flux values were evaluated for data quality and correlated with selected microclimatic factors.

Shoot-level physiological measurements were carried out on representative trees situated within the flux footprint. Shoots representing the upper, middle, and lower canopies were investigated. Daily courses of CO_2 assimilation rate (A) and stomatal conductance were measured on intact shoots using a Li-6400 gas exchange system (Li-Cor) under conditions of ambient CO_2 concentration and natural irradiance, leaf temperature, and vapour pressure deficit. See Urban et al. (2012) for details.

2.3. Modelling of light response curve and carbon gain

Instantaneous rates of CO_2 assimilation (A) at both canopy and shoot levels, the socalled light-response curve, were modelled as a general non-rectangular hyperbolic function of incident PPFD (Q):

$$\Phi A^2 - (\alpha Q + A_{max})A + \alpha Q A_{max} = 0, \quad (1)$$

where α is the apparent quantum yield (AQY; mol mol^{-1}), Φ is a number between 0 and 1 determining the shape of the light-response curve, and A_{max} is the light-saturated value of A.

Carbon gain of individual shoots and whorls over 24 h was calculated based on the derived parameters of the light-response curve and instantaneous PPFD measured by CANFIB sensors. The amount of respired CO_2 during night periods (PPFD = 0 μmol m^{-2} s^{-1}) was estimated based on the relationship between nighttime respiration rate and shoot temperature (see Chapter 12 in this book). Leaf areas of individual whorls, estimated by allometric equations, were used to scale up CO_2 assimilation rates from shoot to whorl level.

3. RESULTS AND DISCUSSION

3.1. Microclimate conditions

The periods selected for the study were characterized by highly distinctive patterns of microclimatic conditions. In addition to reduced PPFD, cloudy sky conditions also resulted in a significantly higher diffuse index than that during clear sky conditions (Table 1). It is known, however, that the greatest instantaneous solar irradiances may occur during partly cloudy days due to reflection and scattering from cumulus clouds (e.g. Segal & Davis 1992). Diffuse radiation penetrated to lower depths of the canopy more efficiently than did direct radiation. Extinction coefficients, describing an attenuation of solar radiation passing through a canopy, were ca 0.33 and 0.48 for the whole tree canopy when measured under cloudy and

clear sky conditions, respectively. On clear-sky days, temperatures and vapour pressure deficits showed typical daily courses characterized by their maximum and minimum values, but they remained more or less constant under cloudy skies (Table 1).

In addition to changes in PPFD, the relative proportion of the blue–green wavelengths of incident PPFD is higher under cloudy sky conditions in comparison with clear skies (Campbell & Norman 1998; Navrátil et al. 2007), particularly at low elevation angles. In contrast, the contribution of red wavelengths to total incident *I* (direct irradiance) is reduced under cloudy sky conditions and thus leads to an increase in the ratio of blue to red light. The preferential scattering of blue light to the radiation path-length through the atmosphere is thus documented. This could have a number of physiological consequences inasmuch as it is known that blue light influences such processes directly connected with photosynthetic carbon uptake as leaf and chloroplast movement, enzyme activation, and stomata opening.

Table 1. *Means of photosynthetic photon flux density (PPFD; µmol m^{-2} s^{-1}), the diffuse index (DI; dimensionless), and the extinction coefficient (Ec; dimensionless), as well as minima (min) and maxima (max) of air temperature (T_{air}; °C) and vapour pressure deficit (VPD; kPa) during investigated cloudy- and clear-sky days.*

	PPFD	DI	Ec	T_{air}		VPD	
				min	max	min	max
Cloudy sky	650	0.73	0.33	11.7	18.7	0.3	1.0
Clear sky	1,250	0.31	0.48	18.8	25.1	0.9	2.5

3.2. Effects on canopy level

At corresponding irradiances, we found significantly higher CO_2 net ecosystem exchange (NEE) during cloudy sky conditions particularly when compared with clear sky conditions in afternoon hours (Fig. 2). Cloudy sky conditions resulted in lower compensation irradiance (by 38–51%), lower saturating irradiance (by 24–34%), and higher AQY (by 77–121%) as compared with clear-sky days, while night-time respiration remained almost unchanged (Table 1).

It is noteworthy that an afternoon depression of NEE in response to PPFD was often observed during clear-sky days but not during cloudy-sky days. This depression was associated with decreases in AQY and increases in lower compensation irradiance, and it leads to a hysteresis response of daytime NEE (Pingintha et al. 2010; Urban et al. 2012), particularly during drought periods. Afternoon depressions in NEE are caused in particular by substantial reduction in stomatal conductance, which is associated with high vapour pressure deficits on those days (Wong et al. 1979; Grace et al. 1995; Panek & Goldstein 2001; Urban et al. 2007a). The stomata were partly closed to minimize water loses. This situation occurred due to the trees' insufficient water supplies, as water consumption through leaf transpiration was greater than water supply by roots and water reserves in stems were depleted. Reduced stomatal conductance leads, however, to a parallel reduction in CO_2 diffusion into the intercellular space of leaves or needles, and its biochemical fixation in the reactions of the Calvin cycle is thus decreased.

Because CO_2 NEE represents the balance between fluxes associated with photosynthetic assimilation and effluxes from respiratory processes, the downward shift of the NEE–PPFD relationship during clear-sky days (Fig. 2) could have been caused by increased ecosystem respiration during hot, clear days. It is well known that respiratory CO_2 efflux from all parts of the ecosystem (e.g. soil, stem, leaves) correlates exponentially with temperature (see also Chapter 12 in this book). Soil is the dominant source of ecosystem CO_2

efflux, and its CO_2 dynamic is usually smaller than is the dynamic of CO_2 fluxes from other ecosystem components (e.g. stems and leaves). This is particularly the case in dense forest stands (Campbell & Norman 1998; Law et al. 2001; Urban et al. 2007a). In this case study, ecosystem respiration was greater by only ca 20–30% during clear-sky days compared with cloudy days. It is therefore insufficient to explain the differences of ca 80–140% in NEE on cloudy- versus clear-sky days.

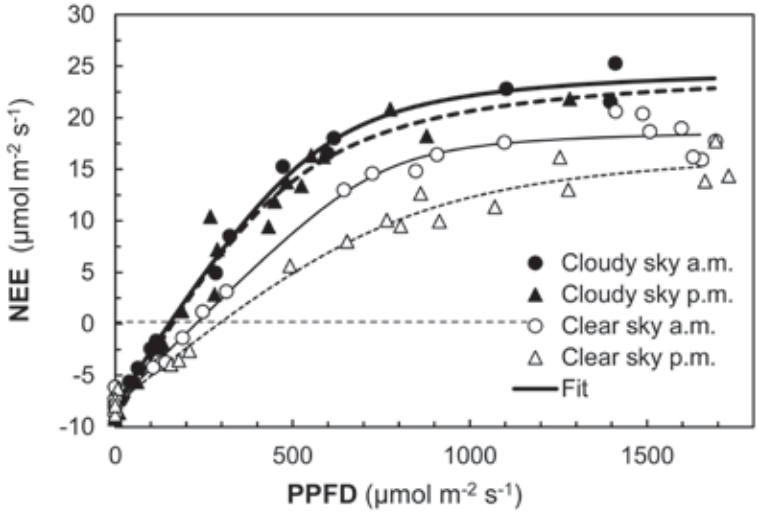

Fig. 2. *Relationship between photosynthetic photon flux density (PPFD) and canopy CO_2 net ecosystem exchange (NEE) during clear (open symbols) and cloudy (closed symbols) sky conditions. Morning (circles) and afternoon (triangles) NEE data were analysed separately. Adapted from Urban et al. (2012).*

3.2. Effects on shoot level

Exponential attenuation of solar radiation passing through a canopy leads to distinct differences in light intensity across the vertical canopy profile (Spitters et al. 1986; Urban et al. 2012). Shoots acclimate to their light environments through (i) modulation of leaf morphology, anatomy, and chloroplast ultrastructure; and (ii) changes in their chemical composition, including in particular reallocation of N between photosynthetic components associated with light capture, thylakoid membrane composition, and CO_2 assimilation (Boardman 1977; Kubiske & Pregitzer 1997; Lichtenthaler et al. 2007; Rajsnerová et al. 2015). While upper shoots have higher rates of light-saturated CO_2 assimilation which are associated with higher N and Rubisco contents and stomatal conductance, lower leaves more effectively utilize low light intensities (Sims & Pearcy 1994; Urban et al. 2007b). It remains unclear, however, how individual canopy layers contribute to the entire ecosystem's CO_2 exchange.

Table 2. *Mean values ± standard deviations of selected parameters of CO_2 assimilation light-response curves at canopy and shoot levels: R_D = dark (night-time) respiration rate; A_{max} = light-saturated rate of CO_2 assimilation; AQY = apparent quantum yield. These photosynthetic parameters are expressed per unit ground area (at canopy level) or per unit leaf area (at shoot level). PLA is the projected leaf area of investigated whorls within the canopy profile. Carbon gain is the amount of CO_2 assimilated per day (24 h) per whorl studied.*

	R_D	A_{max}	AQY	PLA	Carbon gain
	$\mu mol\ m^{-2}\ s^{-1}$	$\mu mol\ m^{-2}\ s^{-1}$	$mmol\ mol^{-1}$	m^2	$gCO_2\ whorl^{-1}\ day^{-1}$
Canopy level					
Clear sky a.m.	7.9 ± 0.4	26.8 ± 0.9	35 ± 3	–	–
Clear sky p.m.	7.8 ± 0.6	25.6 ± 2.6	28 ± 4		
Cloudy sky a.m.	7.9 ± 0.4	33.1 ± 1.4	53 ± 4	–	–
Cloudy sky p.m.	7.3 ± 0.7	34.4 ± 3.8	61 ± 9		
Shoot level					
Whorl 5					
Clear sky a.m.	1.3 ± 0.4	8.3 ± 0.7	49 ± 9	4.00	74 ± 5.0.
Clear sky p.m.	1.1 ± 0.2	14.0 ± 1.8	16 ± 2		
Cloudy sky a.m.	1.1 ± 0.2	9.6 ± 0.5	42 ± 9	4.00	69 ± 5.1.
Cloudy sky p.m.	1.7 ± 0.3	9.9 ± 0.6	37 ± 3		
Whorl 8					
Clear sky a.m.	0.9 ± 0.1	8.3 ± 0.7	31 ± 4	6.85	24 ± 2.0
Clear sky p.m.	0.9 ± 0.1	10.3 ± 1.0	20 ± 3		
Cloudy sky a.m.	1.1 ± 0.5	10.2 ± 1.8	38 ± 5	6.85	59 ± 3.0.
Cloudy sky p.m.	1.7 ± 0.2	11.7 ± 1.1	32 ± 5		
Whorl 10					
Clear sky	0.6 ± 0.1	6.0 ± 0.2	24 ± 2	7.80	3 ± 1.7.
Cloudy sky	0.4 ± 0.1	4.7 ± 0.4	32 ± 5	7.80	16 ± 2.7.
Whorl 15					
Clear sky	0.3 ± 0.1	1.1 ± 2.7	35 ± 16	19.7	–2 ± 2.2·
Cloudy sky	0.3 ± 0.1	1.8 ± 0.2	60 ± 8	19.7	21 ± 1.6.

Parameters of the *A*–PPFD response curves at shoot-level (Table 2), which were derived from daily courses of *A* at different vertical positions, reflected typical differences between shoots in upper (whorl 5th) and in lower (whorls 10th and 15th) canopy and demonstrate distinct acclimation to the light environment within the canopy.

Similarly to the case at canopy level, there was an afternoon depression of *A* in response to PPFD in shoots from the upper canopy layer. However, the afternoon depression was usually not observed in shaded shoots within the lower canopy. Reduced intercellular CO_2 concentration due to stomatal conductance reduced by high vapour pressure deficits and low leaf water potentials (Wong et al. 1979; Panek & Goldstein 2001; Hu et al. 2009) as well as stimulated photorespiration (Zhang et al. 2009;Urban et al. 2012) have been identified as the main reasons for reduced CO_2 uptake during afternoon hours. It has also been reported that an accumulation of zeaxanthin (Zeiger & Zhu 1998) and specific primary metabolites (Lu et al. 1997) in the guard cells of stomata may result in closure of the stomatal aperture and thus contribute to reduced CO_2 uptake.

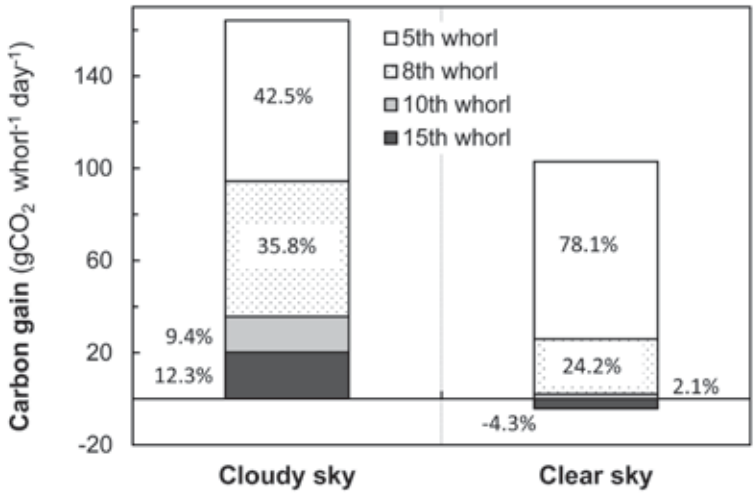

Fig. 3. *Carbon gain over 24 h calculated for individual spruce canopy whorls during typical cloudy and clear sky conditions. The light-response curve parameters presented in Table 2 were used for the modelling. Percentages denote individual whorls' contributions to total carbon uptake.*

Blue-light enrichment under cloudy sky conditions has been hypothesized by many researchers as stimulating photosynthetic CO_2 uptake through its effect on stomatal conductance (Zeiger & Zhu 1998), hydraulic conductance of leaf blades (Sellin et al. 2011), activation of photosynthetic processes (Košvancová-Zitová et al. 2009), and effective chloroplast movement (Briggs & Christie 2002). Detailed analyses conducted by Urban et al. (2012), however, identified a relatively minor effect of blue-light enrichment on photosynthesis stimulation. In contrast, it has been shown that stomatal conductance closely correlates with the intensity of the diffuse fraction of incident light irrespective of sky conditions. It is likely that anisotropic diffuse light better illuminates the abaxial leaf side where the stomata are usually located (Leverenz & Jarvis 1979) and thus stimulates the diffusion of CO_2 into the leaf/shoot interior.

3.4. Within-canopy variation of carbon gain

Carbon gain, defined as total fixed CO_2 over 24 h and including night-time respiration carbon losses, of the investigated whorls was calculated for cloudy and sunny days based on measurements of PPFD at the

levels of individual whorls; the light-response curves of *A,* including the possibility of an afternoon depression in *A*; and measurements of night-time respiration rates and with respect to the vertical distribution of leaf area (Table 2). Total assimilated CO_2 was within 154–170 g per whorl per day during cloudy sky conditions, while that range was only 89–108 g per whorl per day during clear-sky days.

Although shoots located even in the lowest part of the canopy (10th and 15th whorls) attained markedly positive carbon balances during cloudy-sky days, only marginal or even negative carbon balances were achieved by this part of the canopy during clear-sky days (Fig. 3). Except for the uppermost part of the canopy, the carbon gains estimated for individual whorls were generally higher on cloudy days than on clear days. The within-canopy variation of carbon gain was thus reduced under cloudy sky conditions (Table 2). These results support the previous theoretical modelling of net CO_2 exchange in forest stands by Still et al. (2009). These authors found shade-leaf cumulative photosynthetic fluxes to be less than half of sun-leaf fluxes on sunny days but equal to or even greater than sun-leaf fluxes on partly cloudy and cloudy days.

Effective penetration of anisotropic diffuse radiation into the canopy causes more even distribution of light among leaves across the vertical canopy profile. Lower whorls thus receive more radiation and so become significant contributors to canopy photosynthesis during cloudy days. Figure 4 depicts the advantage of an evenly illuminated canopy for obtaining high photosynthetic CO_2 uptake. Sunlit leaves are often brightly illuminated and photosynthesize at saturating rates, whereas shaded leaves are in deep shade. As whole-canopy photosynthesis includes the contribution of photosynthesis from sunlit and shaded leaves, the assimilation rates of shaded leaves may be enhanced by additional diffuse radiation reaching the lower parts of the canopy (Gu et al. 2003; Still et al. 2009).

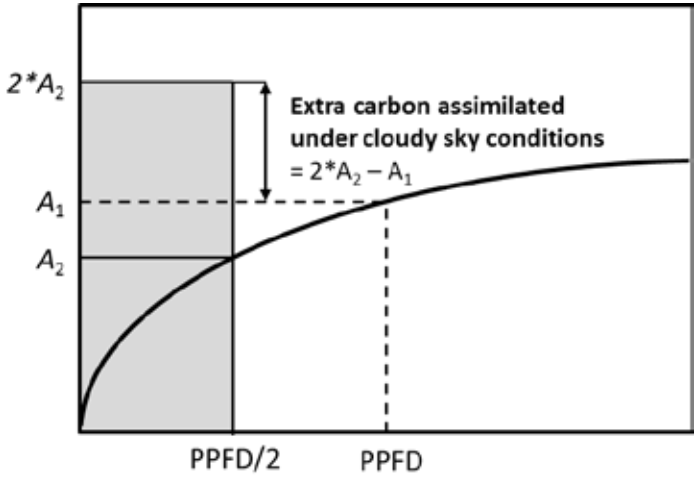

Fig. 4. *Relationship between photosynthetic photon flux density (PPFD) and CO_2 assimilation rate (A). Equal illumination of two leaves by diffuse light (indicated by grey-shaded area) results in higher CO_2 uptake than if one leaf is over-illuminated and the second is in deep shade (no photosynthesis). The non-linear response between A and PPFD is responsible for the photosynthetic advantages of diffuse radiation over direct beam radiation at canopy level. Adapted from Gu et al. (2003).*

The reported reduction by 25–35% in the extinction coefficient on cloudy days in comparison to clear sky conditions (Table 1; Campbell & Norman 1998) thus leads to larger solar equivalent leaf area (= leaf area × PPFD; Čermák 1998 and Chapter 4 of this book). The solar equivalent leaf area of the entire spruce canopy was 37% greater during cloudy days (1,090 µmol s^{-1}) than it was during sunny days (800 µmol s^{-1}).

4. CONCLUSIONS

Cloudy sky conditions resulted in significantly greater ecosystem carbon uptake than was found at corresponding incident light intensities on clear-sky days. Shoot-level data showed that shoots from deep within the canopy substantially contributed to the overall carbon balance during cloudy days when enhanced diffuse radiation effectively penetrated into the lower parts of the canopy. In addition, convenient microclimatic conditions (i.e. lower vapour pressure deficits and temperatures) also contributed to higher ecosystem carbon uptake under cloudy sky conditions. Sky conditions thus have important direct effects on the productivity and structure of vegetation. Increased penetration of diffuse light may explain how forests with high leaf area indexes can maintain positive carbon balance despite a high degree of self-shading by individual shoots (Roderick et al. 2001).

Acknowledgement

This work was supported by the Ministry of Education, Youth and Sports of the Czech Republic within the National Programme for Sustainability I, grant No. LO1415.

References

Boardman, N. (1977) Comparative photosynthesis of sun and shade plants. *Annual Reviews in Plant Physiology*, **28**, 355–377.

Briggs, W.R. & Christie, J.M. (2002) Phototropins 1 and 2: versatile plant blue-light receptors. *Trends in Plant Science*, **7**, 204–210.

Campbell, G.S. & Norman, J.M. (1998) *An Introduction to Environmental Biophysics.* Springer, Berlin.

Čermák, J. (1998) Leaf distribution in large trees and stands of the floodplain forest in southern Moravia. *Tree Physiology*, **18**, 727–737.

Chepfer, H., Noel, V., Winker, D. & Chiriaco, M. (2014) Where and when will we observe cloud changes due to climate warming? *Geophysical Research Letters*, **41**, 8387–8395.

Dengel, S. & Grace, J. (2010) Carbon dioxide exchange and canopy conductance of two coniferous forests under various sky conditions. *Oecologia*, **164**, 797–808.

Farquhar, G.D. & Roderick, M.L. (2003) Atmospheric science: Pinatubo, diffuse light, and the carbon cycle. *Science*, **299**, 1997–1998.

Grace J, Lloyd J, McIntyre J et al. (1995) Fluxes of carbon dioxide and water vapour over an undistributed tropical forest in south-west Amazonia. *Global Change Biology*, **1**, 1–12.

Gu, L.H., Baldocchi, D.D., Wofsy, S.C. et al. (2003) Response of a deciduous forest to the Mount Pinatubo eruption: enhanced photosynthesis. *Science*, **299**, 2035–2038.

Hollinger, D.Y., Kelliher, F.M., Byers, J.N. et al. (1994) Carbon-dioxide exchange between an undisturbed old growth temperate forest and the atmosphere. *Ecology*, **75**, 134–150.

Hu, M.J., Guo, Y.P., Shen, Y.G., Guo, D.P. & Li, D.Y. (2009) Midday depression of photosynthesis and effects of mist spray in citrus. *Annals of Applied Biology*, **154**, 143–155.

Košvancová-Zitová, M., Urban, O., Navrátil, M., Špunda, V., Robson, T.M. & Marek, M.V. (2009) Blue radiation stimulates photosynthetic induction in *Fagus sylvatica* L. *Photosynthetica*, **47**, 388–398.

Kubiske, M.E. & Pregitzer, K.S. (1997) Ecophysiological responses to simulated canopy gaps of two tree species of contrasting shade tolerance in elevated CO_2. *Functional Ecology*, **11**, 24–32.

Law, B.E., Kelliher, F.M., Baldocchi, D.D. et al. (2001) Spatial and temporal variation in respiration in a young ponderosa pine forest during a summer drought. *Agricultural and Forest Meteorology*, **110**, 27–43.

Lichtenthaler, H.K., Ač, A., Marek, M.V., Kalina, J. & Urban O. (2007) Differences in pigment composition, photosynthetic rates and chlorophyll fluorescence images of sun and shade leaves of four tree species. *Plant Physiology and Biochemistry*, **45**, 577–588.

Leverenz, J.W. & Jarvis, P.G. (1979) Photosynthesis in Sitka spruce. 8. Effects of light-flux density and direction on the rate of net photosynthesis and the stomatal conductance of needles. *Journal of Applied Ecology*, **16**, 919–932.

Lu, P., Outlaw, W.H., Smith, B.G. & Freed, G.A. (1997) A new mechanism for the regulation of stomatal aperture size in intact leaves: accumulation of mesophyll-derived sucrose in the guard-cell wall of *Vicia faba*. *Plant Physiology*, **114**, 109–118.

Mercado, L.M., Bellouin, N., Sitch, S. et al. (2009) Impact of changes in diffuse radiation on the global land carbon sink. *Nature*, **458**, 1014–1017.

Navrátil, M., Špunda, V., Marková, I. & Janouš, D. (2007) Spectral composition of photosynthetically active radiation penetrating into a Norway spruce canopy: the opposite dynamics of the blue/red spectral ratio during clear and overcast days. *Trees*, **21**, 311–320

Panek, J.A. & Goldstein, A.H. (2001) Response of stomatal conductance to drought in ponderosa pine: implications for carbon and ozone uptake. *Tree Physiology*, **21**, 337–344.

Pingintha, N., Leclerc, M.Y., Beasley, J.P. et al. (2010) Hysteresis response of daytime net ecosystem exchange during drought. *Biogeosciences*, **7**, 1159–1170.

Rajsnerová, P., Klem, K., Holub, P. et al. (2015) Morphological, biochemical and physiological traits of upper and lower canopy leaves of European beech tend to converge with increasing altitude. *Tree Physiology*, **35**, 47–60.

Roderick, M.L., Farquhar, G.D., Berry, S.L. & Noble, I.R. (2001) On the direct effect of clouds and atmospheric particles on the productivity and structure of vegetation. *Oecologia*, **129**, 21–30.

Segal, M. & Davis, J. (1992) The impact of deep cumulus reflection on the ground-level global irradiance. *Journal of Applied Meteorology*, **31**, 217–222.

Sellin, A., Sack, L., Ounapuu, E. & Karusion, A. (2011) Impact of light quality on leaf and shoot hydraulic properties: a case study in silver birch (*Betula pendula*). *Plant, Cell and Environment*, **34**, 1079–1087.

Sherwood, S.C., Bony, S. & Dufresne, J.-L. (2014) Spread in model climate sensitivity traced to atmospheric convective mixing. Nature, 505, 37–42.

Sims, D.A. & Pearcy, R.W. (1994) Scaling sun and shade photosynthetic acclimation to whole plant performance. I Carbon balance and allocation at different daily photon flux densities. Plant, Cell and Environment, 17, 881–887.

Spitters, C.J.T., Toussaint, H.A.J.M. & Goudriaan, J. (1986) Separating the diffuse and direct component of global radiation and its amplification for modelling canopy photosynthesis. 1. Components of incoming radiation. Agricultural and Forest Meteorology, 38, 217–229.

Still, C.J., Riley, W.J., Biraud, S.C. et al. (2009) Influence of clouds and diffuse radiation on ecosystem–atmosphere CO_2 and (COO)-O-18 exchanges. *Journal of Geophysical Research-Biogeosciences*, **114**, 17.

Urban, O., Janouš, D., Acosta, M. et al. (2007a) Ecophysiological controls over the net ecosystem exchange of mountain spruce stand. Comparison of the response in direct vs. diffuse solar radiation. *Global Change Biology*, **13**, 157–168.

Urban, O., Košvancová, M., Marek, M.V. & Lichtenthaler, H.K. (2007b) Induction of photosynthesis and importance of limitations during the induction phase in sun and shade leaves of five ecologically contrasting tree species from the temperate zone. *Tree Physiology*, **27**, 1207–1215.

Urban, O., Klem, K., Ač, A. et al. (2012) Impact of clear and cloudy sky conditions on the vertical distribution of photosynthetic CO_2 uptake within a spruce canopy. *Functional Ecology*, **26**, 46–55.

Wild, M. (2009) Global dimming and brightening: a review. *Journal of Geophysical Research-Atmospheres*, **114**, D00D16.

Wong, S.C., Cowan, I.R. & Farquhar, G.D. (1979) Stomatal conductance correlates with photosynthetic capacity. *Nature*, **282**, 424–426.

Zeiger, E. & Zhu J. (1998) Role of zeaxanthin in blue light photoreception and the modulation of light-CO_2 interactions in guard cells. *Journal of Experimental Botany*, **49**, 433–442.

Zhang, J.-L., Meng, L.-Z. & Cao, K.-F. (2009) Sustained diurnal photosynthetic depression in uppermost-canopy leaves of four dipterocarp species in the rainy and dry seasons: does photorespiration play a role in photoprotection? *Tree Physiology*, **29**, 217–228.

Chapter 7

Effect of elevated CO_2 concentration: Acclimation of Rubisco

Otmar Urban, Mirka Šprtová

Laboratory of Plant Ecological Physiology, Global Change Research Centre, Czech Academy of Sciences, Bělidla 4a, CZ-60300 Brno, Czech Republic

1. INTRODUCTION

There is clear evidence that such anthropogenic activities as fossil fuel burning, deforestation, land use change, and cement production have led to an increase in concentrations of CO_2 and other greenhouse gases in the lower atmosphere (IPCC 2013). The Representative Concentration Pathways (RCPs) predict atmospheric CO_2-equivalent concentrations between 420 (RCP2.6) and 1,200 µmol mol^{-1} (RCP8.5) by the end of the 21st century. The most likely scenario, RCP6.0, predicts a gradual increase in atmospheric CO_2 concentration ($[CO_2]$) and global temperature by as much as 700 µmol mol^{-1} and 2.2°C, respectively, by 2100 (IPCC 2013). See also Chapter 1 of this book for details. Whether rising $[CO_2]$ will cause faster growth and higher photosynthetic C storage in C_3 plants remains an open question.

CO_2 has two direct physiological effects on plants. It is (1) an activator of Rubisco (Enzyme Commission number 4.1.1.39; ribulose-1,5-bisphosphate carboxylase/oxygenase) activity, and (2) the substrate of the Calvin cycle. Inactive, dark-adapted Rubisco is activated by a CO_2 molecule in a slow reversible reaction followed by a rapid reversible reaction of a $Rubisco_{inactive}$-CO_2 complex with an Mg^{2+} ion (the process of carbamylation). Subsequently, CO_2 acts as the substrate for an enzymatic reaction with the second carbon of the primary acceptor RuBP (ribulose-1,5-bisphosphate). In the first step, CO_2 is bound to the active site of Rubisco. In the second step, the reaction of a $Rubisco_{active}$-CO_2 complex with RuBP leads to the formation of triose phosphate (the process of carboxylation).

Theoretically, there are at least two reasons why under sufficient light intensity elevated $[CO_2]$ should lead to increased photosynthetic CO_2 uptake in C_3 plants: (1) it can be expected that photorespiration (Rubisco oxygenase activity) will be depressed, and (2) it can be expected that the substrate binding of Rubisco, the primary C-fixing enzyme in C_3 plants, will be enhanced (Farquhar et al. 1980; Eamus & Jarvis 1989).

Although initial exposure of C_3 plants to elevated $[CO_2]$ leads to increases in their CO_2 assimilation rates, longer periods (ranging from weeks to years) of CO_2 treatment may lead to substantial reductions in $[CO_2]$-enhanced photosynthesis known as acclimation or down-regulation (Eamus & Jarvis 1989; Urban 2003; Körner et al. 2005; Way et al. 2015). When measured at ambient $[CO_2]$, which means at concentrations where photosynthesis is limited by Rubisco carboxylation activity, acclimation usually manifests in lower CO_2 assimilation rates in plants grown at elevated $[CO_2]$ than is found in plants grown at ambient $[CO_2]$ (Farquhar et al. 1980; Bernacchi et al. 2001).

Fig. 1. *Glass domes with adjustable windows at the Bílý Kříž experimental research site. The domes measure 10 x 10 x 7 m and are primarily used to simulate the long-term impacts of elevated CO_2 concentration on small stands of tree saplings or juvenile trees. See Urban et al. (2001) for technical details.*

Over time, plants may develop photosynthetic acclimation to elevated [CO_2]. There exist several causes for this. The following hypotheses (reviewed in Urban 2003; Ainsworth & Rogers 2007; Leakey et al. 2009) have been formulated to explain photosynthetic acclimation to elevated [CO_2]: (1) Increased accumulation of phosphorylated sugar intermediates in the sucrose synthesis pathway, occurring within minutes, can lead to a shortage of inorganic phosphate in the chloroplast for ATP synthesis and subsequently to RuBP regeneration. (2) Increased contents of specific saccharides (e.g. glucose, sucrose) may repress the expression of genes transcribing for Rubisco or other photosynthetic enzymes (D1 and D2 proteins, cytochrome *f*, Rubisco activase, and carbonic anhydrase) over a time scale of hours to days. Moreover, a reported local phosphorus deficiency may lead to Rubisco decarboxylation owing to reduced Rubisco activase activity. In addition, a decrease in carbonic anhydrase activity controlling the ratio between CO_2 and HCO_3^- has the potential to reduce Rubisco activity via carbamylation. Contrariwise, genes for saccharide utilization (e.g. genes coding for ADP-glucose pyrophosphorylase) may be up-regulated if the assimilates exceeded their utilization rates (van Oosten & Besford 1995; Leakey et al. 2009). (3) Dilution and/or redistribution of N at organ and whole-plant levels results in larger downward acclimation of photosynthesis, which is preferably observed in low-N environments as compared to high-N environments. The correlation between a reduction in leaf N and the activity of photosynthetic enzymes is obvious inasmuch as Rubisco alone comprises 25–50% of leaf N. In addition, a decrease in chlorophyll synthesis is one of the main symptoms of N deficiency. (4) Over days to weeks, photosynthesis and growth responses to elevated [CO_2] depend on the

plant's ability to develop new sinks or expand existing sinks' storage capacity or growth rate. A new sink–source status alters the production and utilization rates of photosynthetic products and through feedback affects C metabolism and gene expression at the leaf or chloroplast scale. Therefore, source–sink interactions are key determinants of photosynthetic acclimation to elevated [CO_2] at both the whole-plant and ecosystem scales (Luo et al. 1999). Thus, acclimation to elevated [CO_2] accelerates in older tissues/plants and with the progress of the growth season as a result of the lack of active basal meristems.

Downward acclimation of photosynthesis limited by Rubisco under elevated [CO_2] is frequently accompanied by decreased Rubisco activity (Bowes 1991; Cen & Sage 2005; Ainsworth & Rogers 2007; Urban et al. 2012). Although higher plants contain six different forms of Rubisco, just two of these are photosynthetically active (von Caemmerer & Quick 2000). Potential causes of decreased Rubisco activity thus include (1) a decline in Rubisco protein content, (2) inhibition of the carbamylated enzyme, and (3) an increased proportion of inactive non-carbamylated forms of Rubisco. Currently, however, there are few studies that have investigated Rubisco content together with its activity or seasonal courses in Rubisco activity and/or content in relation to CO_2 treatment.

Therefore, to understand the mechanism and dynamics of Rubisco acclimation to elevated [CO_2], we comprehensively studied Rubisco adjustment in European beech (*Fagus sylvatica*), a broadleaved tree species dominant in the Czech Republic, using electrophoretic (Rubisco content), spectrophotometric (*in vitro* Rubisco activity), and gas-exchange (*in vivo* Rubisco carboxylation activity) techniques.

2. MATERIALS AND METHODS

2.1 Site description

The experiment was carried out in glass domes at the Bílý Kříž experimental research site in the Beskydy Mountains, Czech Republic (49°30′N, 18°32′E; 908 m a.s.l.). A detailed description of climatic conditions there is provided in Chapter 6 of this book. In the present study, we investigated 6- to 8-year-old European beech saplings. The saplings were planted and then grown in their native soil at ambient (385 μmol mol^{-1}; AC) and elevated (700 μmol mol^{-1}; EC) atmospheric [CO_2] for at least 4 years using glass dome facilities (Fig. 1). CO_2 enrichment under the glass domes was continuous from April to November each year. Environmental air conditions inside the domes were maintained using an air-conditioning device together with an adjustable window system, which also enabled throughput of incident rainfall. In case of differences in soil moisture outside and inside the domes, an automatic system provided irrigation. A detailed description of the glass dome microclimate can be found in Urban et al. (2001, 2014).

2.2. Estimation of Rubisco content

Leaf samples (approximately 0.3 g) were homogenized in a chilled mortar with inert sand and extraction buffer containing 62 mM Tris, 2% (w/v) sodium dodecyl sulphate, 65 mM DTT, and 10% (v/v) glycerol, all at pH 6.8. The homogenate was centrifuged at 10,000 g for 2 min. The mixture of supernatant and sample buffer was subsequently incubated for 5 min at 100°C. Rubisco content ($R_{content}$) was determined by sodium dodecyl sulphate polyacrylamide gel electrophoresis using a Mini-PROTEAN 3 system (Bio-Rad, Hercules, CA, USA) with purified Rubisco protein (Sigma–Aldrich, St. Louis, MO, USA) as a standard. See Hrstka et al. (2008) for more details.

2.3. Estimation of in vitro Rubisco activity

Approximately 0.3 g of leaf tissue was homogenized in a chilled mortar with inert sand, liquid nitrogen, and 10 cm^3 extraction buffer (50 mM HEPES, 25 mM^3 $KHCO_3$, 5 mM $MgCl_2$, 0.2 mM Na2EDTA, 5 mM dithiothreitol, and 0.1 g insoluble polyvinylpolypyrrolidone) at pH 8.0. The homogenate was filtered and the filtrate was assayed for Rubisco activity. Initial ($RA_{initial}$) and total (RA_{total}) *in vitro* Rubisco activities were assayed spectrophotometrically by the continuous measurement of 3-phosphoglycerate-dependent NADH oxidation in a coupled enzyme system. Changes in absorbance were measured at 340 nm using a spectrophotometer. $RA_{initial}$ was assayed immediately after the extract was added to an activation solution (25 mM $KHCO_3$ and 20 mM $MgCl_2$). For RA_{total}, an aliquot of the extract was incubated for 15 min at room temperature in the activation solution. See Hrstka et al. (2008) for details.

Rubisco activation state (AS) and Rubisco specific activity ($RA_{specific}$) *in vitro* were subsequently calculated as:

$$AS = RA_{initial} / RA_{total}, \text{ and} \quad (1)$$

$$RA_{specific} = RA_{total} / R_{content}. \quad (2)$$

2.4. Estimation of in vivo Rubisco activity

Maximum *in vivo* Rubisco carboxylation rates (V_{Cmax}, µmol m^{-2} s^{-1}) were derived from the relationship between CO_2 assimilation rate (A) and intercellular [CO_2] (C_i) at saturating irradiance. The assimilation rate at low C_i (50–250 µmol mol^{-1}) is limited by Rubisco maximum carboxylation rate (W_C) and is modelled based on Farquhar's theoretical model of photosynthesis (Farquhar et al. 1980) as:

$$W_C = \frac{V_{Cmax} \cdot C_i}{C_i + k_C(1 + O_i/k_O)}, \quad (3)$$

where O_i is an intercellular O_2 concentration (209 mmol mol^{-1}) and k_C and k_O represent the Michaelis–Menten constants for carboxylation (µmol mol^{-1}) and oxygenation (mmol mol^{-1}), respectively. The temperature dependences of the Michaelis–Menten constants, which are key parameters in Farquhar's photosynthetic model, were calculated as

$$Parameter = \exp(c - \Delta Ha/(R \times T_{leaf})), \quad (4)$$

where R is the molar gas constant (8.314 J mol^{-1} K^{-1}), c represents a scaling constant (38.05 for k_C and 20.30 for k_O), T_{leaf} is leaf temperature (K), and ΔHa is activation energy (79.43 for k_C and 36.38 kJ mol^{-1} for k_O) as suggested by Bernacchi et al. (2001).

3. RESULTS AND DISCUSSION

3.1. Seasonal changes in Rubisco content and activity

The EC treatment reduced RA_{total} only in young expanding leaves at the beginning of the vegetation season (May), whereas this activity was stimulated over most of the vegetation season (Fig. 2A). The decrease in RA_{total} observed in May might have been caused by several mechanisms: (1) a decrease in AS through inhibition of the carbamylated enzyme, (2) a reduction in total $R_{content}$, and/or (3) an increase in the proportion of inactive noncarbamylated forms of Rubisco (Bowes 1991; von Caemmerer & Quick 2000; Yamori & von Caemmerer 2009; Urban et al. 2012).

While AS remained unchanged over the vegetation season in AC plants, the EC treatment led to a slight increase in AS over the vegetation season in beech leaves (Fig. 2B). Such variability in AS response has also been observed in 1-year-old spruce needles (Urban et al. 2012) and may partially result from the dependence of Rubisco AS on temperature (e.g. Yamori et al. 2006) and ultimately from the thermal properties of Rubisco activase (Hozain et al. 2010) and the thermal properties of Rubisco itself (Fig. 4). Changes in $R_{content}$ depended particularly on EC treatment duration. While $R_{content}$ remained unaffected or slightly increased after a short EC treatment at the beginning of the vegetation season (May), it was substantially reduced during the vegetation season (June–September; Fig. 2C). Similar trends have been reported for Norway spruce, particularly in 1-year-old needles (Urban et al. 2012). Although substantial differences among functional groups of C_3 species have been observed, Košvancová et al. (2009) and Sallas et al. (2003) reported decreases in $R_{content}$ of 28% in *F. sylvatica* and 12% in *Picea abies*.

The EC treatment tended to reduce $RA_{specific}$ at the beginning of the vegetation season, whereas the treatment led to increases in $RA_{specific}$ over the vegetation season as a whole (Fig. 2D). Similar results have been reported for *P. abies* (Sallas et al. 2003; Urban et al. 2012) and *Pinus sylvestris* (Sallas et al. 2003). In comparison to AC plants, EC plants thus have lower amounts of Rubisco but higher proportions of Rubisco in its active form.

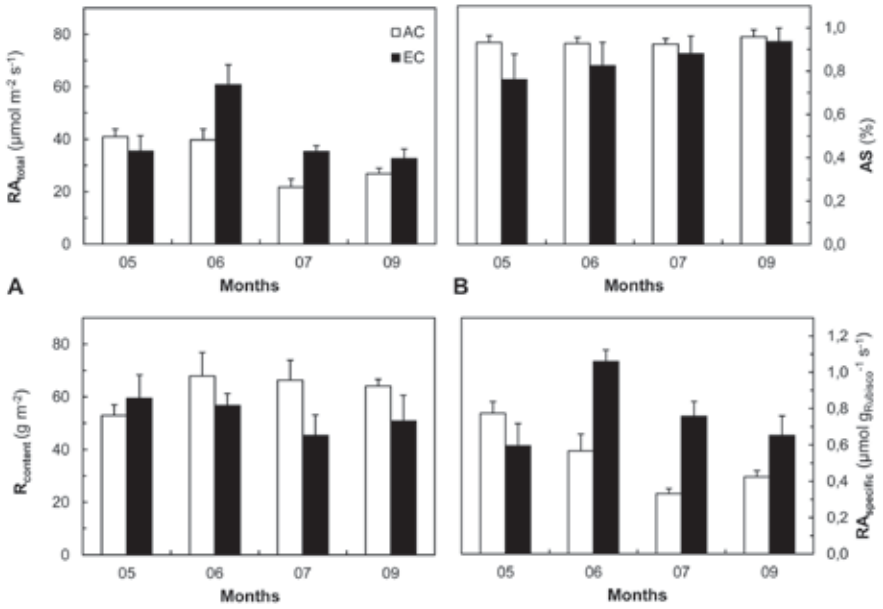

Fig. 2. *Seasonal courses (5 May–9 September) of total in vitro Rubisco activity (RA_{total};* **A***), Rubisco activation state (AS;* **B***), Rubisco content per unit leaf area ($R_{content}$;* **C***), and Rubisco specific activity ($RA_{specific}$;* **D***) estimated in Fagus sylvatica leaves cultivated under ambient (AC; white columns) and elevated (EC; black columns) CO_2 concentrations. Leaves were exposed to natural saturating irradiance (>1300 µmol m^{-2} s^{-1}) before sampling. Means (columns) and standard deviations (bars) are presented (n = 10–12).*

3.2. Daily courses of in vivo Rubisco activity

In contrast to RA_{total}, a substantial decrease in V_{Cmax} induced by the EC treatment was found under actual (see Urban et al. 2014) as well as normalized (to 25°C) temperatures ($V_{Cmax,25}$; Fig. 3). This decrease in V_{Cmax} documents a downward acclimation of the photosynthetic machinery under EC conditions. Moreover, a substantial interaction effect between atmospheric [CO_2] and sky conditions (discussed in detail in Chapter 6) was observed on the level of V_{Cmax}. While $V_{Cmax,25}$ values reached daily maxima of ca 45 µmol m^{-2} s^{-1} in AC plants irrespective of sky condition, $V_{Cmax,25}$ for EC plants was considerably lower under cloudy-sky conditions (ca 19 µmol m^{-2} s^{-1}) than under clear-sky conditions (ca 32 µmol m^{-2} s^{-1}; Fig. 3A,B).

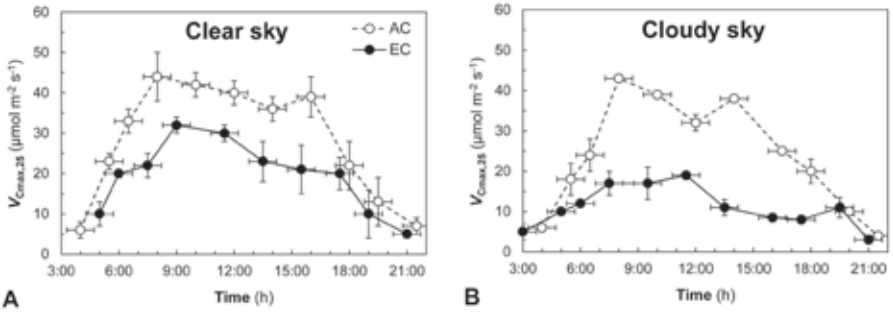

Fig. 3. *Diurnal courses of maximum in vivo Rubisco carboxylation rates corrected to the leaf temperature of 25°C ($V_{Cmax,25}$) during clear (***A***) and cloudy (***B***) sky conditions. Measurements were taken on sun-adapted beech leaves cultivated under ambient (AC; open circles) and elevated (EC; filled circles) CO_2 concentrations. Means (points) and standard deviations (error bars) are presented (n = 3).*

Relatively low morning and evening total activity values indicate a binding of such nocturnal inhibitors as 2-carboxy-D-arabinitol-1-phosphate (Berry et al. 1987) or RuBP (Portis 1995). Our data show also a slight decrease in $V_{Cmax,25}$ at noon and in the early afternoon hours (Fig. 3). Such changes in Rubisco activity can be explained by the presence of various daily inhibitors that can tightly bind to the active site of Rubisco and thus reduce its AS. Potential daily inhibitors include in particular D-xylulose-1,5-bisphosphate and 3-keto-D-arabinitol-1,5-bisphosphate (Portis 1995; von Caemmerer & Quick 2000). In addition, Rubisco activity may decrease within several minutes due to insufficient contents of RuBP and inorganic phosphate and/or reduced activity of Rubisco activase (Zhang & Portis 1999). The activity of this latter enzyme is controlled by the ATP/ADP ratio (Parry et al. 2008), which ratio is modified particularly by irradiance and atmospheric [CO_2]. It seems that the relative contribution of each mechanism to Rubisco activity regulation is species specific and varies with the duration of the CO_2 treatment and the progress of the vegetation season.

3.3. Thermal properties of Rubisco activity

Inasmuch as plants growing under EC often have reduced stomatal conductance and subsequently increased leaf temperature (Eamus & Jarvis 1989; Leakey et al. 2009), it has been hypothesized that long-lasting EC treatment increases the photosynthetic apparatus's thermostability. Indeed, EC instantaneously

increases temperature optima of light-saturated rates of photosynthesis, which is primarily caused by reduced photorespiration and prevailing limitation of photosynthesis by RuBP regeneration instead of Rubisco limitation (Bernacchi et al. 2001; Hikosaka et al. 2006). This increase disappears, however, when plants are exposed to identical [CO_2] (Šigut et al. 2015). Nevertheless, temperature response curves of V_{Cmax} (Fig. 4) show a substantial shift in temperature optima for Rubisco carboxylation rate by ca 3.5°C for EC saplings compared to their AC counterparts. This shift indicates a certain temperature acclimation of Rubisco's kinetic properties induced by EC.

The following mechanisms may contribute to the reduction in Rubisco activity at temperatures >35°C: (1) an increase in mesophyll resistance to CO_2 diffusion followed by Rubisco decarbamylation (Bernacchi et al. 2001), (2) a reduction in Rubisco AS due to Rubisco activase constraint (Crafts-Brandner & Salvucci 2000), (3) increased synthesis of the Rubisco inhibitor xylulose-1,5-bisphosphate (Newman & Gutteridge 1994), and (4) insufficient inorganic phosphate in chloroplast stroma followed by a limitation to ATP production (June et al. 2004). Previous studies on EC have shown that high intercellular [CO_2] in EC plants protects Rubisco against decarbamylation (Košvancová et al. 2009; Urban et al. 2012) and maintains a higher proportion of Rubisco in its active form than is found in AC plants. In contrast, the often reported inaccessibility of inorganic phosphate in EC plants may reduce the ATP/ADP ratio and subsequently lead to reduced Rubisco activase activity (Crafts-Brandner & Salvucci 2000). Such contrasting [CO_2]-dependent mechanisms of Rubisco regulation may consequently lead to the reported species-specific and seasonal variability in V_{Cmax} temperature dependence (Ziska 2000; Urban et al. 2012; Crous et al. 2013).

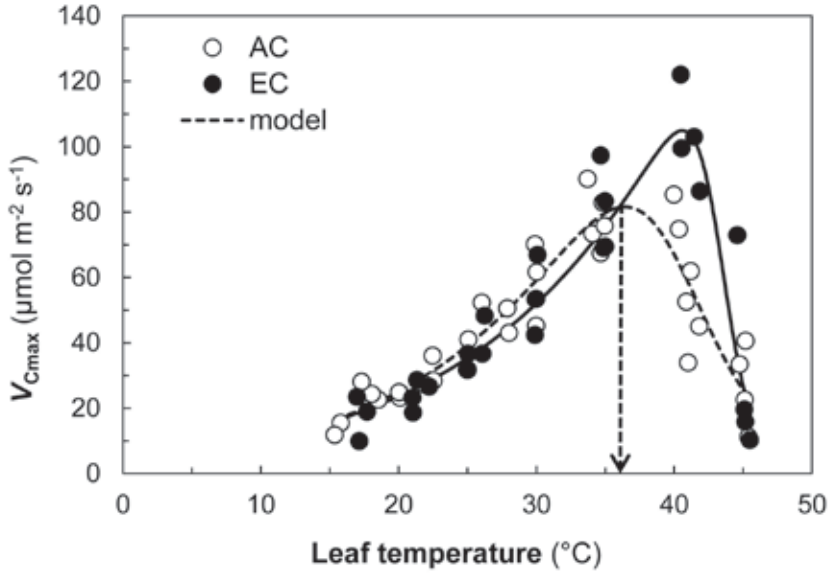

Fig. 4. *Dependence of light-saturated Rubisco carboxylation rate (V_{Cmax}) on leaf temperature in Fagus sylvatica grown at ambient (AC) and elevated (EC) atmospheric CO_2 concentrations. Arrows indicate temperature optima for V_{Cmax} in plants grown under AC (dashed line) and EC (solid line) conditions. Rearranged from Šigut et al. (2015).*

4. CONCLUSIONS

Inasmuch as the Rubisco active site exists in at least six forms but only two of these are catalytically active, there is no simple correlation between Rubisco content and activity. It is therefore necessary to apply different methodological approaches to study the acclimation of this key enzyme of photosynthetic CO_2 uptake to elevated atmospheric [CO_2]. We have shown that long-term Rubisco acclimation includes reduction of its content while its specific activity increases (i.e. a higher proportion of Rubisco is present in its active form in EC plants than in AC plants). Plants' great capacity to tune Rubisco activity is thus demonstrated.

Acknowledgement

This work was supported by the Ministry of Education, Youth and Sports of the Czech Republic within the National Programme for Sustainability I, grant No. LO1415.

References

Ainsworth, E.A. & Rogers, A. (2007) The response of photosynthesis and stomatal conductance to rising [CO_2]: mechanisms and environmental interactions. *Plant, Cell and Environment*, **30**, 258–270.

Bernacchi, C.J., Singsaas, E.L., Pimentel, C., Portis, A.R. & Long, S.P. (2001) Improved temperature response functions for models of Rubisco-limited photosynthesis. *Plant, Cell and Environment*, **24**, 253–259.

Berry, J.A., Lorimer, G.H., Pierce, J., Seemann, J.R., Meek, J. & Freas S. (1987) Isolation, identification, and synthesis of 2-carboxyarabinitol 1-phosphate, a diurnal regulator of ribulose-bisphosphate carboxylase activity. *Botany*, **84**, 734–738.

Bowes, G. (1991) Growth at elevated CO_2: photosynthetic responses mediated through Rubisco. *Plant, Cell and Environment*, **14**, 795–806.

Cen, Y.-P. & Sage, R.F. (2005) The regulation of Rubisco activity in response to variation in temperature and atmospheric CO_2 partial pressure in sweet potato. *Plant Physiology*, **139**, 979–990.

Crafts-Brandner, S.J. & Salvucci, M.E. (2000) Rubisco activase constrains the photosynthetic potential of leaves at high temperature and CO_2. *Proceedings of the National Academy of Sciences of the United States of America*, **97**, 13430–13435.

Crous, K.Y., Quentin, A.G., Lin, Y.S. et al. (2013) Photosynthesis of temperate *Eucalyptus globulus* trees outside their native range has limited adjustment to elevated CO_2 and climate warming. *Global Change Biology*, **19**, 3790–3807.

Eamus, D. & Jarvis, P.G. (1989) The direct effects of increase in the global atmospheric CO_2 concentration on natural and commercial temperate trees and forests. *Advances in Ecological Research* (eds M. Begon, A.H. Fitter, E.D. Ford & A. MacFadyen), pp. 1–55. Academic Press, London – Tokyo – Toronto.

Farquhar, G.D., von Caemmerer, S. & Berry, J.A. (1980) A biochemical model of photosynthetic CO_2 assimilation in leaves of C3 species. *Planta*, **149**, 78–90.

Hikosaka, K., Ishikawa, K., Borjigidai, A., Muller, O. & Onoda, Y. (2006) Temperature acclimation of photosynthesis: mechanisms involved in the changes in temperature dependence of photosynthetic rate. *Journal of Experimental Botany*, **57**, 291–302.

Hozain, M.I., Salvucci, M.E., Fokar, M. & Holaday, A.S. (2010) The differential response of photosynthesis to high temperature for a boreal and temperate *Populus* species relates to differences in Rubisco activation and Rubisco activase properties. *Tree Physiology*, **30**, 32–44.

Hrstka, M., Zachová, L., Urban, O. & Košvancová, M. (2008) Seasonal changes of Rubisco activity and its content in Norway spruce exposed to ambient and elevated CO_2 concentration. *Chemické Listy*, **102**, 657–659.

IPCC (2013) Summary for policymakers. *Climate Change 2013: The Physical Science Basis. Contribution of Working Group I to the Fifth Assessment Report of the Intergovernmental Panel on Climate Change* (eds T.F. Stocker, D. Qin, G.-K. Plattner et al.), pp. 3–29, Cambridge, UK and New York, NY, USA: Cambridge University Press.

June, T., Evans, J.R. & Farquhar, G.D. (2004) A simple new equation for the reversible temperature dependence of photosynthetic electron transport: a study on soybean leaf. *Functional Plant Biology*, **31**, 275–283.

Košvancová, M., Urban, O., Šprtová, M., Hrstka, M., Kalina, J., Tomášková, I., Špunda, V. & Marek, M.V. (2009) Photosynthetic induction in broadleaved *Fagus sylvatica* and coniferous *Picea abies* cultivated under ambient and elevated CO_2 concentrations. *Plant Science*, **177**, 123–130.

Körner, C., Asshoff, R., Bignucolo, O. et al. (2005) Carbon flux and growth in mature deciduous forest trees exposed to elevated CO_2. *Science*, **309**, 1360–1362.

Leakey, A.D.B., Ainsworth, E.A., Bernacchi, C.J., Rogers, A., Long, S.P. & Ort, D.R. (2009) Elevated CO_2 effects on plant carbon, nitrogen, and water relations: six important lessons from FACE. *Journal of Experimental Botany*, **60**, 2859–2876.

Luo, Y., Reynolds, J., Wang, Y. & Wolfe, D. (1999) A search for predictive understanding of plant responses to elevated [CO_2]. *Global Change Biology*, **5**, 143–156.

Newman, J. & Gutteridge, S. (1994) Structure of an effector-induced inactivated state of ribulose 1,5-bisphosphate carboxylase/oxygenase: the binary complex between enzyme and xylulose 1,5-bisphosphate. *Structure*, **2**, 495–502.

Parry, M.A.J., Keys, A.J., Madgwick, P.J., Carmo-Silva, A.E. & Andralojc, P.J. (2008) Rubisco regulation: a role for inhibitors. *Journal of Experimental Botany*, **59**, 1569–580.

Portis, A.R. (1995) The regulation of Rubisco by Rubisco activase. *Journal of Experimental Botany*, **46**, 1285–1291.

Sallas, L., Luomala, E.M., Utriainen, J., Kainulainen, P. & Holopainen, J.K. (2003) Contrasting effects of elevated carbon dioxide concentration and temperature on Rubisco activity, chlorophyll fluorescence, needle ultrastructure and secondary metabolites in conifer seedlings. *Tree Physiology*, **23**, 97–108.

Šigut, L., Holišová, P., Klem, K. et al. (2015) Does long-term cultivation of saplings under elevated CO_2 concentration influence their photosynthetic response to temperature? *Annals of Botany*, **116**, 929–939.

Urban, O. (2003) Physiological impacts of elevated CO_2 concentration ranging from molecular to whole plant responses. *Photosynthetica,* **41**, 9–20.

Urban, O., Janouš, D., Pokorný, R. et al. (2001) Glass domes with adjustable windows: a novel technique for exposing juvenile forest stands to elevated CO_2 concentration. *Photosynthetica*, **39**, 395–401.

Urban, O., Hrstka, M., Zitová, M. et al. (2012) Effect of season, needle age and elevated CO_2 concentration on photosynthesis and Rubisco acclimation in *Picea abies*. *Plant Physiology and Biochemistry*, **58**, 135–141.

Urban, O., Klem, K , Holišová P. et al. (2014) Impact of elevated CO_2 concentration on dynamics of leaf photosynthesis in *Fagus sylvatica* is modulated by sky conditions. *Environmental Pollution*, **185**, 271–280.

van Oosten, J.-J. & Besford, R.T. (1995) Some relationships between the gas exchange, biochemistry and molecular biology of photosynthesis during leaf development of tomato plants after transfer to different carbon dioxide concentrations. *Plant, Cell and Environment*, **18**, 1253–1266.

von Caemmerer, S. & Quick, W.P. (2000) Rubisco: physiology in vivo. Photosynthesis: Physiology and Metabolism (eds R.C. Leegood, T.D. Sharkey & S. von Caemmerer), pp. 85–113, Kluwer Academic Publishers, Dordrecht, Boston, London.

Way, D.A., Oren, R. & Kroner, Y. (2015) The space-time continuum: the effects of elevated CO_2 and temperature on trees and the importance of scaling. *Plant, Cell and Environment*, **38**, 991–1007.

Yamori, W. & von Caemmerer, S. (2009) Effect of Rubisco activase deficiency on the temperature response of CO_2 assimilation rate and Rubisco activation state: insights from transgenic tobacco with reduced amounts of Rubisco activase. *Plant Physiology,* **151**, 2073–2082.

Yamori, W. Suzuki, K. Noguchi, K. Nakai, M. & Terashima, I. (2006) Effects of Rubisco kinetics and Rubisco activation state on the temperature dependence of the photosynthetic rate in spinach leaves from contrasting growth temperatures. *Plant, Cell and Environment*, **29**, 1659–1670.

Zhang, N. & Portis, A.R. (1999) Mechanism of light regulation of Rubisco: A specific role for the larger Rubisco activase isoform involving reductive activation by thioredoxin-f. *Proceedings of the National Academy of Sciences of the United States of America*, **96**, 9438–9443.

Ziska, L.H. (2000) The impact of elevated CO_2 on yield loss from a C3 and C4 weed in field-grown soybean. *Global Change Biology*, **6**, 899–905.

Chapter 8

Effect of elevated CO_2 concentration: Tree morphology and biomass production

Radek Pokorný, Justýna Szatniewska, Jan Krejza

Department of Biomass Production, Global Change Research Centre, Czech Academy of Sciences, Bělidla 4a, CZ-60300 Brno, Czech Republic

1. INTRODUCTION

Plants respond to increasing atmospheric CO_2 concentration ($[CO_2]$) by acclimation or adaptation at physiological and morphological levels (Luo et al. 1999; Urban 2003). Regarding temporal onset, physiological responses may be categorized as short-term and morphological responses as long-term. In other words, as a consequence of elevated atmospheric $[CO_2]$, all of plants' physiological, anatomical, and morphological properties can be modified directly and/or indirectly (Pritchard et al. 1999; Urban 2003; Körner 2006). The direct physiological effects are based on the functionality of CO_2 as an activator of Rubisco activity (see Chapter 7 for details) and as substrate for the carboxylation reactions of the Calvin cycle. In addition, CO_2 affects photorespiration, dark mitochondrial respiration, and stomata number and openness. Such secondary physiological responses as the accumulation and translocation of photosynthetic products (e.g. sucrose and starch) and changes in plants' water status have crucial effects on plant growth, plant tissue anatomy, and whole plant morphology. Hypothetically, the entire architecture of a tree or other plant can change substantially as plant organs respond differently to elevated $[CO_2]$.

Increased biomass under elevated $[CO_2]$ is reported for 66% of tree species that have been studied (Pritchard et al. 1999). Under multi-competitive conditions, however, elevated $[CO_2]$ does not lead to a stimulating effect upon biomass growth, which could indicate a reduction in soil N availability (Hättenschwiler & Körner 1997). In terms of biomass allocation, the root system often shows the highest growth increment among all tree organs (Eamus & Jarvis 1989). The root-to-shoot ratio is significantly affected by growing period duration because of the primary investment into such short-term longevity tissues as fine roots and needles (Gielen et al. 2005).

Globally elevated $[CO_2]$ is accompanied by generally higher air temperatures. Temperature is regarded as an important environmental factor inducing plant growth, manifesting itself in bud flushing and shoot development (Hannerz 1999). Not only temperature (Linkosalo et al. 2000), however, but also such other environmental factors as global radiation, total precipitation (e.g. Bigras & D'Aoust 1993; Häkkinen 1999), and fertilization may act as stimulators of plant growth (Roberntz 1999). Recently, earlier flowering and an extended period of active plant growth across much of the Northern Hemisphere have been interpreted as responses to global climate change (Cleland et al. 2006). Schwartz et al. (2006) showed an earlier onset of spring across the Northern Hemisphere.

In the present study of juvenile Norway spruce (*Picea abies*) trees grown under elevated $[CO_2]$ conditions inside glass domes for 8 years, we summarize our findings for phenological response (budding and growth), stem dendrometric and crown-architecture parameters, above-ground tree organ biomass and secondary branching (with respect to the effect of thinning), root structure and morphology, and functional relationship between above- and below-ground biomass and/or surface areas.

2. MATERIALS AND METHODS

2.1. Site and stand description

Norway spruce trees were cultivated under two different [CO_2] environments: ambient (AC, 375 µmol mol^{-1}) and elevated (EC, 700 µmol mol^{-1}) [CO_2] inside two glass domes (GDs) with adjustable windows located at the Bílý Kříž experimental research site (Beskydy Mountains, Czech Republic). This location's characteristics are described in detail in chapters 5 and 6 of this book.

The GDs have a square base measuring 9 x 9 m with a height of 7 m at the central part. A detailed technical description of the GDs was presented by Urban et al. (2001). In the autumn of 1996, 11-year-old saplings were planted in triangular spacing at two densities (the dense sub-treatment at 10,000 trees ha^{-1} and the sparse sub-treatment at 5,000 trees ha^{-1}) inside each GD. Saplings were grown in their native soil (see Formánek 2000 for detailed soil characteristics). Trees were selected for planting based on their phenotype and having identical bud-break phenology and were obtained from samplings of the same origin located in an artificially established plot close to Bílý Kříž. At the time of planting, 54 trees had the following dimensions (mean ± standard deviation): trees in the AC GD had tree height of 1.45 ± 0.02 m and stem diameter 0.3 m above the ground of 22.6 ± 0.5 mm, and those in the EC GD measured 1.42 ± 0.03 m and 21.6 ± 0.6, respectively. [CO_2] treatment began in the early spring of 1997. In the following spring, all trees were fertilized with Silvamix-forte (N+P_2O_5+K_2O+MgO, 17 g m^{-2}) and Ureaform (urea-formaldehyde condensate, 21 g m^{-2}) to avoid continuous needle yellowing, as the nitrogen content within the current needles was found nearly under the nutrition sufficiency limit (1.3%; Pokorný et al. 2010). Both treatments received the same fertilizer at the same application rate. Schematically chosen trees were first harvested in summer 2002. The final harvest took place in autumn 2004, and root systems were excavated in early spring 2005.

2.2. Bud phenology observation

The methodology of Murray et al. (1994) was used to identify five phenological phases of spring bud development: 0 = dormant bud, 1 = slight swelling, 2 = swollen bud, 3 = green needle/leaf clearly showing through the bud scales, and 4 = leaf/needle elongation. Shoot elongation growth was observed continuously. Five trees per subtreatment were continuously monitored. On each tree, we observed terminal, lateral, and apical buds/shoots that were as similar to one another as possible in terms of position and age. Needle samples from five shoots were used to estimate N content monthly (for details see Pokorný et al. 2010).

2.3. Morphological parameter measurements

Needle parameters were measured in both sun-exposed and shaded parts of tree crowns. All chosen whorls were cut and separated into the following shoot age classes: current (c), 1 year old (c-1), 2 years old (c-2), etc. Needles were removed from the sample shoots and scanned (Astra 1220 P, UMAX, Taiwan). The following set of needle parameters was analysed using ACC software (Sofo Brno, Czech Republic): (1) projected leaf area, (2) needle shape factor, (3) needle length, and (4) number of needles per shoot. See Pokorný et al. (2011) for details.

Harvested trees were also used to conduct dendrometric analyses. The following dendrometric parameters were measured on each sampled tree: tree height, stem diameter, branching frequency (number of branches per whorl), and whorl branch length and inclination angle. Each stem-thickness measurement

was taken in two perpendicular directions using callipers (Mitutoyo, Takatsu-ku, Japan) at 1/10 of tree height and 0.3 m above the ground (Pokorný et al. 2012).

2.4. Biomass allocation

The effect of EC on biomass production was studied using annual measurement of tree height and stem diameters in each sub-treatment. Sample trees were cut into whorl sections, separated into needles and woody parts (stem and branches), oven-dried at 80°C for 48 h, and then weighed. Root systems of 10 trees per [CO_2] treatment were excavated in 2005 (i.e. after 8 years of [CO_2] treatment). A 150/90 Air-Spade (Concept Engineering Group, Verona, PA, USA) was used for root excavation (Pokorný et al. 2013). Root systems were structurally analysed by separating roots according to type (secondary vs. primary) and thickness class as well as the location of secondary roots. Separated and washed roots were oven-dried (80°C, 48 h) and weighed. Roots were scanned, and their length and root surface area were measured using ACC software. Specific root area was calculated as the ratio of root surface to root dry mass and specific root length as the ratio of root length to root dry mass. Root parameters were compared between [CO_2] treatments. Biomass allocation to trees' above- and below-ground organs was calculated.

3. RESULTS AND DISCUSSION

3.1. Phenology

Bud phenology and consecutive shoot elongation growth were monitored during several growing periods (1997–2002; Pokorný et al. 2001, 2010). This revealed that air temperature is the main driving force inducing bud flushing and that EC only slightly accelerated subsequent bud germinating phases (insignificantly, by about 3–7 days). The buds of trees in the EC GD fully developed about 1 week sooner than did those of trees in the AC GD. EC substantially induced shoot elongation growth, in particular that of sun-exposed shoots in the lower-density stand. However, this accelerated growth lasted only 1–3 weeks after full bud development, and at the end of shoot elongation growth there were no significant differences in total shoot length between investigated treatments. We supposed that limiting needles' N supply would slow subsequent shoot elongation growth in the EC treatment. Nevertheless, faster shoot growth in EC conditions can enhance the carbon sink in spruce and delay its acclimation depression (Urban 2003).

In terms of growth phenology, at the beginning of experiment under EC the stem diameter increment was slightly more positively stimulated in the dense sub-variant than it was in the sparse sub-variant (though this difference was not significant), but after 2 years the opposite trend began to manifest. Then, sparse tree spacing, enhanced especially after schematic thinning (25% intensity), acted as an increased stimulus for stem growth (Pokorný et al. 2012). In contrast, the tree height increment was still slightly higher in the dense sub-treatment under EC than in the dense sub-treatment under AC (Fig. 1).

After 6 years of tree cultivation (i.e. in 2002), EC had no significant effect on tree height growth. Trees were even taller in both AC subtreatments than were those in the EC GD (by 8% for the sparse sub-treatment and 3% for the dense). Then, 2 years after thinning (i.e. in 2004), EC trees were found to be taller than AC trees by an average of about 14% for the sparse sub-treatment and about 8% for the dense (Pokorný et al. 2012).

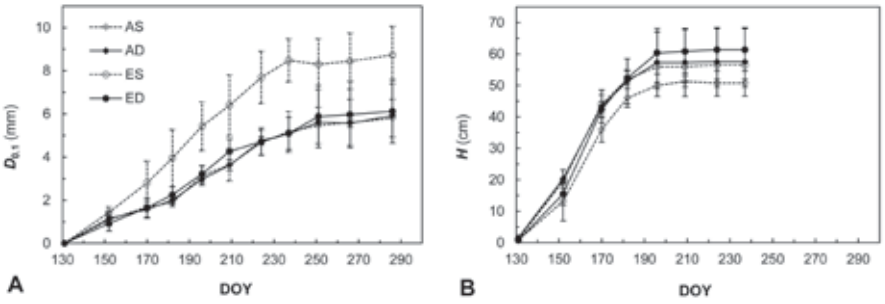

Fig. 1. *Stem diameter increment ($D_{0.1}$, measured 0.1 m above the ground;* **A***) and tree height (H) increment (***B***) during the third year (i.e. in 1999) of elevated CO_2 concentration ([CO_2]). DOY = day of the year. The first letter in the abbreviation legend describes treatment (A = ambient [CO_2], E = elevated [CO_2]) and the second letter describes sub-variant (S = sparse [i.e. 5,000 trees ha^{-1}], D = dense [i.e. 10,000 trees ha^{-1}]). Means (points) and standard deviations (bars) are presented (n = 25).*

3.2. Needle, branch, and crown morphology

To avoid a possible effect from replanting shock on the tree morphology results, needle and shoot parameters were first analysed 1–2 years after the experimental plots were established. In terms of needle and shoot morphology, in 1998 current shoots displayed no significant differences between AC and EC treatments or subtreatments except for differences in the coefficients of shoot shape (i.e. the ratio between shoot length and maximum width) and cross-sectional shoot shape (i.e. the ratio between shoot cross-section circumference and its diameter in the middle section). At that time, the needle and shoot parameters of trees in the EC treatments were found to be rather of shade type (i.e. flat and short; Pokorný & Šalanská 1999; Pokorný et al. 2001). Mean shoot length also did not significantly differ between sparse AC and EC sub-treatments at the end of the experiment (i.e. in 2004). Shoots in the EC dense sub-treatment were negligibly about 4% shorter than those in the AC subtreatment. Nevertheless, the total length of all shoots (i.e. the sum) within the crown differed as the number of shoots in the EC dense sub-treatment was about 42% higher (this difference was significant) and the number of shoots in the EC sparse subtreatment was about 10% lower (this difference was not significant) than the numbers in the respective AC sub-treatments.

The specific leaf area of EC needles was greater than that of AC needles from the first months of [CO_2] treatment.

Annual analyses performed after several years (from 2002 to 2004) revealed higher values for needle length (especially for current needles, up to 18% longer) and projected needle area (up to 13% greater) accompanied by lower values for specific needle area (as much as 15% lower, as quantified by the ratio of needle mass to projected area) in the EC treatment than were found in the AC treatment. There were significant differences in most of the investigated morphological parameters for young needles in the well-irradiated, sun-adapted crown parts, and particularly so under water-limiting soil conditions in 2003 (Pokorný et al. 2011). This likely resulted from different water relationships in EC trees than existed in AC trees investigated under temperate water stress (Kupper et al. 2006). In this case, needle length and shape factor were identified as the parameters most sensitive to drought. Furthermore, EC trees had much larger absorbing-root area (Pokorný et al. 2013), which modified and enhanced the root-to-shoot ratio as well as

the root-to-conductive-stem-area ratio. These hydraulic properties and early-seasonal stimulation of photosynthesis forced advanced needle development in EC trees, particularly under limited soil water conditions. The number of needles per unit shoot length was found to be unaffected by EC.

Branch length was similar across sub-treatments, with differences not exceeding 5%. Thinning had a positive effect on branch length only in the dense sub-treatment where the branches were about 10% longer in the EC GD than they were in the AC GD. Prior to thinning, EC stimulated branching frequency. Compared to the AC subtreatments, mean branching frequency was about 3% and about 20% higher in the EC sparse and dense sub-treatments, respectively, and these differences were significant. After thinning, branching frequency increased in the sparse sub-treatment by about 13% but decreased in the dense sub-treatment by about 7%. Our results on branching frequency were quite inconsistent, and thinning probably did not influence new bud formation (Pokorný et al. 2012).

In both [CO_2] variants, trees from the dense sub-variants showed lower branch inclination angles and slimmer crowns than did trees from the sparse sub-variants due to limited growing space. Branch inclination angle ranged mostly from 70° to 75° for all treatments, and there were no significant differences. There were no shifts in branch inclinations after thinning.

There was a higher frequency of secondary shoots on branches as well as on the stem and more 1-year-old secondary shoots as well as older secondary shoots in the EC treatment, and particularly so in the dense sub-treatment. This indicates a possible early alternative carbon sink for assimilates formatted under EC. After thinning, secondary shoots production decreased under EC (Pokorný et al. 2012).

3.3. Growth increment and above-ground biomass production

EC had no effect on tree height in either sub-treatment. After 6 years of treatment, tree heights were similar. In 2002, trees in the AC sparse and dense sub-treatments were taller than were those in the EC subtreatments by about 10% and 3%, respectively. Nevertheless, 2 years after thinning tree height in the EC subtreatments was enhanced by about 14% and 8%.

Although trees under EC started to be slightly stimulated also in stem diameter increment after 3 years of treatment, there were no significant differences in stem diameter between AC and EC treatments (± 5%). After thinning in 2002, stem diameter showed a relatively similar increment in the AC and EC dense sub-variants, and these sub-treatments did not differ prior to or after thinning. In contrast, stem diameter increased by about 22% in the EC sparse sub-treatment as compared to the AC sparse subtreatment. Under EC conditions, stem diameter increased relatively more than did height. This indicates that EC affects the apical meristem and cambium differently.

After 6 years of the experiment (in 2002), there was a slight stimulation of the above-ground biomass increment in the EC dense sub-treatment but there was no stimulation effect in the EC sparse sub-treatment. Total above-ground biomass (TBA) was greater by about 9% in the AC sparse sub-treatment than in the EC one. Following the trajectory of biomass allocation to above-ground tree organs, more biomass was allocated to branches than to stems. The lowest amount of biomass was invested into leaf biomass, particularly in the sparse sub-treatment. There were no significant differences between AC and EC sub-treatments, except for significantly lower leaf biomass in the AC dense sub-treatment than in the AC sparse sub-treatment. Two years after thinning, TBA was greatly increased in both EC sub-treatments, particularly in the sparse one. In comparison to the AC treatment at that time, trees from both EC sub-treatments invested more biomass into stems (up to 39% in the sparse subtreatment) and branches (up to 29%, though this

difference was not significant) than into leaves (Pokorný et al. 2012). Stem and branch biomass increments greatly stimulated by thinning under EC resulted in higher TBA for both investigated spacing densities (by about 22%; Fig. 2). The increased TBA of the trees grown in the EC dense sub-treatment can be supported by studies showing a high relative effect of [CO_2] enrichment under low light, most likely because of a reduction (shift to lower light intensities) in the light-compensation point (Körner et al. 2003). In contrast, as irradiances above 250 µmol m^{-2} s^{-1} significantly enhance the daily courses of net CO_2 assimilation for EC trees in comparison to AC trees (Špunda et al. 2005), thinning can have a high stimulating effect on growth under EC. This is supported by the present results where thinning greatly stimulated growth of the primary branch structure and the biomass increments of branches and stems. As is known, TBA increment is a function of stem diameter, although this allometric function may change under the influence of EC (Fig. 3). An overview of the temporal development of stand density, stand basal area, and leaf area index by sub-treatment was presented also by Pokorný et al. (2012).

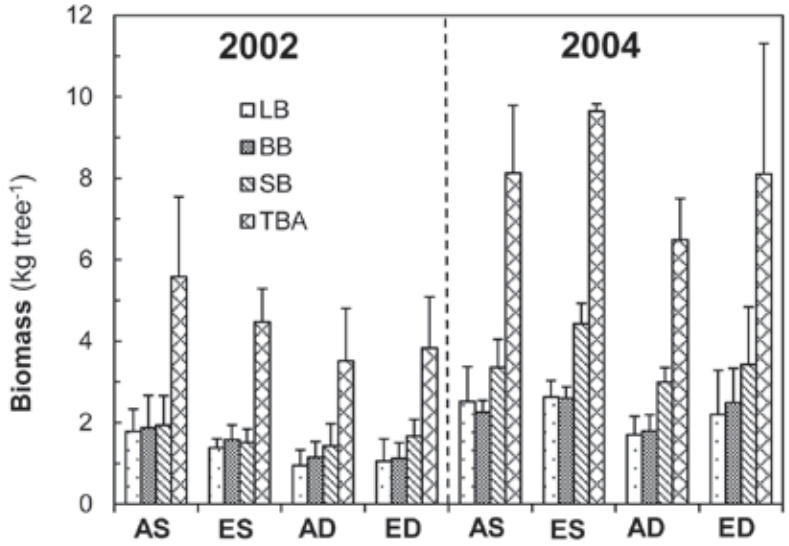

Fig. 2. *Biomass characteristics of Norway spruce trees after 6 (in 2002) and 8 years (in 2004) of cultivation under ambient (A, the first letter in abbreviations) and elevated (E) CO_2 concentrations. The second letter in abbreviations represents sparse (S) and dense (D) sub-treatments. Schematic thinning at 25% intensity relative to stand density was carried out in 2002. LB = leaf biomass, BB = branch biomass, SB = stem biomass, TBA = total above-ground biomass. Means (columns) and standard deviations (bars) are presented; n = 14 in 2002 and n = 19 in 2004.*

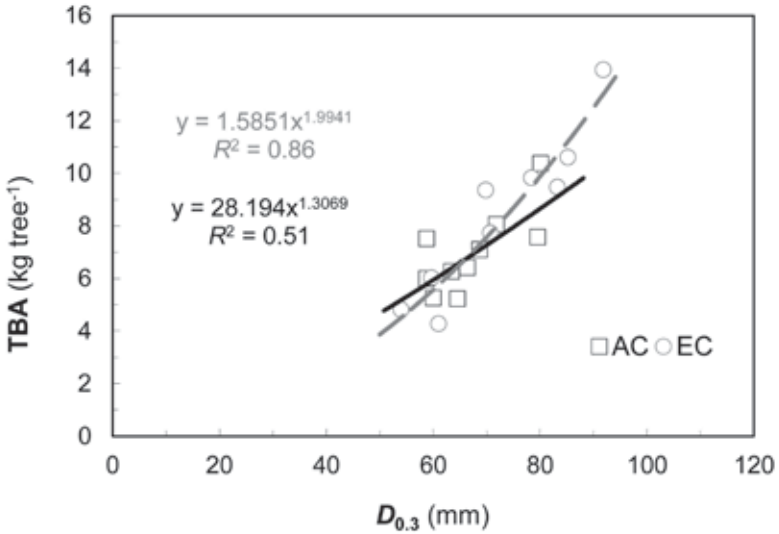

Fig. 3. *Allometric relationships between stem diameter 0.3 m above the ground ($D_{0.3}$) and total above-ground biomass (TBA). Empty grey circles represent trees from plots with elevated CO_2 concentration (EC) and empty black squares represent trees from plots with ambient CO_2 concentration (AC).*

3.4. Root system morphology and below-ground biomass production

After 8 years of treatment, an average EC tree exhibited about 37% more belowground biomass than did an average AC tree. Primary root structure growth was unaffected by EC, but the biomass of secondary roots growing on the primary root structure and in particular the biomass of secondary roots growing in the zone between the soil surface and the first primary root ramification were significantly higher under EC than they were under AC by about 58% and 70%, respectively (Fig. 3). The finest roots' (diameters < 1 mm) biomass as well as the length and surface area of both primary and secondary root structures showed the greatest differences between treatments, with values on average 43% higher under EC than under AC (Pokorný et al. 2013). Therefore, Norway spruce trees cultivated under well-watered and nitrogen-rather-poor soil conditions responded to the EC environment by enhancing their secondary root structure increments, enlarging their root length and absorbing-root area, and altering their ratio of roots to above-ground organ biomass. Higher root-to-leaf and root-to-stem-basal-area ratios could be beneficial for Norway spruce trees to survive periods with limited soil water availability.

During tree development, root biomass increased less proportionally to above-ground biomass of tree organs (except for branch biomass) in the EC treatment than it did in the AC treatment. In the EC GD, the 37% increase in below-ground biomass was accompanied by a mere 12% increase in TBA after 8 years of treatment. Therefore, there was a higher root-to-shoot ratio in EC trees (0.18) than in AC trees (0.16). Needle biomass accounted for 25% and 23% of total tree biomass in the EC and AC treatments, respectively, branch biomass 26% and 24%, stem biomass 34% and 42%, and root biomass 15% and 11%. The root-biomass increment was accompanied by a similar branch-biomass increment per tree.

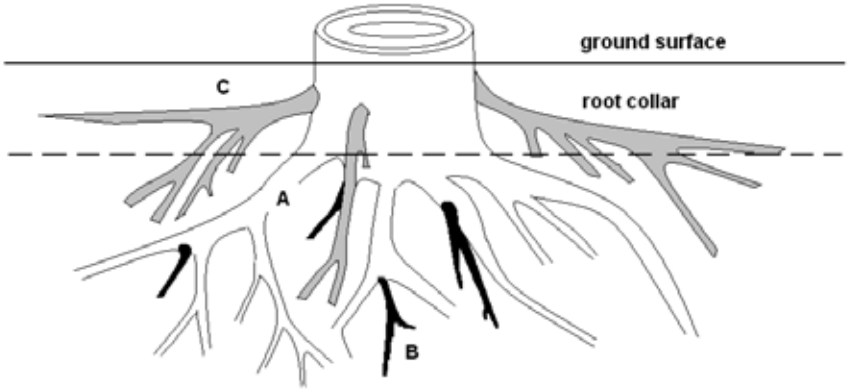

Fig. 4. *Root type schematic: A = primary roots, B = secondary roots growing on primary roots, and C = secondary roots growing in the zone between the soil surface and the first primary root ramification.*

4. CONCLUSIONS

The response to EC of Norway spruce saplings cultivated in GDs over eight growing seasons often included no significant effects at the organ level for individual trees as indicated by growth dynamic, anatomy, or morphology, but at a whole-tree level these small changes led to significant differences in such parameters as total biomass production and functionality.

Bud break is controlled mainly by temperature. Therefore, as global climate change is presumed to increase air temperature as well as plant-tissue temperature (due to restricted transpiration), more frequent earlier bud germination and then expansive shoot and foliage extension should be expected in future spring periods, particularly in sparsely spaced Norway spruce stands with sufficient nutrient availability. Rapidly formed new shoots in spring served also as the nearest growth sink for produced assimilates.

As our experimental design may be considered a pseudoreplication, we suggest that most of the stem dendrometric and crown morphological parameters of Norway spruce trees grown in different tree-spacing treatments were not significantly affected by EC. Nevertheless, based on the present results, the growth stimuli or forcing preferences of biomass allocation to different above-ground tree organs changed rapidly as young trees developed in temporal onset and particularly after the effects of thinning. Thinning forced growth in stems' dendrometric parameters, stem biomass, and the primary branch structure as described by increased branching frequency of whorl branches and biomass increment of all branches.

Total below-ground biomass was about 37% greater and TBA about 12% greater in the EC treatment than in the AC treatment, which implies an unbalanced relationship between below- and above-ground biomass allocation. The biomass increment of the primary root structure was slightly stimulated (by ca 10%) in the EC treatment compared to the AC treatment, but the biomass of the secondary root structures was significantly stimulated (by more than 58%). This reflects the fact that secondary roots growing in the zone between the soil surface and the first primary root ramification were stimulated more than were secondary roots growing on the primary root structure. In particular, the finest roots showed high positive growth stimulation under EC conditions and this led to increased absorbing-root area per tree. Therefore,

the hydraulic properties in the roots–stem–leaves continuum also shifted. In EC trees, higher proportions between absorbing and conductive (about 29%) and absorbing and evaporative (about 7%) surface areas supported the results of better water supply by trees under EC. Increased biomass of thin conducting roots confirmed the hypothesis of shifts in biomass allocation from leaves to fine roots for plants grown under EC, thereby resulting in better water and nutrition availability but also improved fitness to survive dry periods.

Stimulation of the growth dynamic of primary shoots, development of secondary shoots on stems and branches, and in particular secondary roots development prior to thinning were identified and termed as the "alternative sink" for enhancing assimilates production under atmospheric EC. Tree spacing and thinning modified this "sink strategy", as, for example, the amount of secondary shoots decreased and growth of the primary branching structure, stem size, and biomass increment showed high positive consecutive stimulation under EC.

Acknowledgement

This work was supported by the Ministry of Education, Youth and Sports of the Czech Republic within the National Programme for Sustainability I, grant No. LO1415.

References

Bigras, F.J. & D'Aoust, A. (1993) Influence of photoperiod on shoot and root frost tolerance and bud phenology of white spruce seedlings (*Picea glauca*). *Canadian Journal of Forest Research*, **23**, 219–228.

Cleland, E.E., Chiariello, N.R., Loarie, S.R., Mooney, H.A. & Field C.B. (2006) Diverse responses of phenology to global changes in a grassland ecosystem. *Proceedings of the National Academy of Sciences of the United States of America*, **103**, 13740–13744.

Eamus, D. & Jarvis, P.G. (1989) The direct effects of increase in the global atmospheric CO_2 concentration on natural and commercial temperate trees and forests. *Advances in Ecological Research* (eds M. Begon, A.H. Fitter, E.D. Ford & A. MacFadyen), pp. 1–55. Academic Press, London – Tokyo – Toronto.

Formánek, P. (2000) *Transformace dusíku v antropogenně ovlivněných smrkových ekosystémech Moravskoslezských Beskyd*. PhD thesis. Mendel University in Brno, Brno.

Gielen, B., Calfapietra, C., Lukac, M. (2005) Net carbon storage in a poplar plantation (POPFACE) after three years of free-air CO_2 enrichment. *Tree Physiology*, **25**, 1399–1408.

Hannerz, M. (1999) Evaluation of temperature models for predicting bud burst in Norway spruce. *Canadian Journal of Forest Research*, **29**, 9–19.

Häkkinen, R. (1999) Statistical evaluation of bud development theories: application to bud burst of *Betula pendula* leaves. *Tree Physiology*, **19**, 613–618.

Hättenschwiler, S. & Körner, C. (1997) Biomass allocation and canopy development in spruce model ecosystems under elevated CO_2 and increased N deposition. *Oecologia*, **113**, 104–114.

Körner, C. (2006) Plant CO_2 responses: an issue of definition, time and resource supply. *New Phytologist*, **172**, 393–411.

Körner, C. (2003) Ecological impacts of atmospheric CO_2 enrichment on terrestrial ecosystems. *Philosophical Transactions of the Royal Society of London A*, **361**, 2023–2041.

Kupper, P., Sellin, A., Klimankova, Z., Pokorny, R. & Puertolas, J. (2006) Water relations in Norway spruce trees growing at ambient and elevated CO_2 concentrations. *Biologia Plantarum*, **50**, 603–609.

Linkosalo, T., Carter, T.R., Häkkinen, R. & Hari, P. (2000) Predicting spring phenology and frost damage risk of *Betula* spp. under climatic warming: a comparison of two models. *Tree Physiology*, **20**, 1175–1182.

Luo, Y.Q., Reynolds, J., Wang, Y.P. & Wolfe, D. (1999) A search for predictive understanding of plant responses to elevated CO_2. *Global Change Biology*, **5**, 143–156.

Murray, M.B., Smith, R.I., Leith, I.D. et al. (1994) Effects of elevated CO_2, nutrition and climatic warming on bud phenology in Sitka spruce (*Picea sitchensis*) and their impact on the risk of frost damage. *Tree Physiology*, **14**: 691–706.

Pokorný, R. & Šalanská, P. (1999) Vliv hnojení dusíkem na asimilační aparát a přírůst smrku rostoucího v různých hustotách sponu. *Zpravodaj Beskydy*, **12**, 29–34.

Pokorný, R., Šalanská, P. & Janouš, D. (2001) Growth and transpiration of Norway spruce trees in atmosphere with elevated CO_2 concentration. *Ekológia (Bratislava)*, **20**, 14–28.

Pokorný, R., Tomášková, I., Drápelová, I., Kulhavý, J. & Marek, M.V. (2010) Long term effects of [CO_2] enrichment on bud phenology and shoot growth patterns of Norway spruce juvenile trees. *Journal of Forest Science*, **56**, 251–257.

Pokorný, R., Tomášková, I. & Marek, M.V. (2011) The effects of elevated atmospheric [CO_2] on Norway spruce needle parameters. *Acta Physiologiae Plantarum*, **33**, 2269–2277.

Pokorný, R., Tomášková, I. & Marek, M.V. (2013) Response of Norway spruce root system to elevated atmospheric CO_2 concentration. *Acta Physiologiae Plantarum,* **35**, 1807–1816.

Pokorný, R., Tomášková, I. & Slípková, R. (2012) The effect of air elevated [CO_2] on Norway spruce crown architecture and aboveground biomass. *Baltic Forestry*, **18**, 2–11.

Pritchard, S.G., Rogers, H.H., Prior, S.A. & Peterson, C.M. (1999) Elevated CO_2 and plant structure: a review. *Global Change Biology*, **5**, 807–837.

Roberntz, P. (1999) Effects of long-term CO_2 enrichment and nutrient availability in Norway spruce I. Phenology and morphology of branches. *Trees*, **13**, 188–198.

Schwartz, M.D., Ahas, R. & Aasa A. (2006) Onset of spring starting earlier across the Northern Hemisphere. *Global Change Biology*, **12**, 343–351.

Špunda, V., Kalina, J, Urban, O. et al. (2005) Diurnal dynamics of photosynthetic parameters of Norway spruce trees cultivated under ambient and elevated CO_2: the reasons of midday depression in CO_2 assimilation. *Plant Science*, **168**, 1371–1381.

Urban, O., Janouš, D., Pokorný, R. et al. (2001) Glass domes with adjustable windows: A novel technique for exposing juvenile forest stands to elevated CO_2 concentration. *Photosynthetica*, **39**, 395–401.

Urban, O. (2003) Physiological impacts of elevated CO_2 concentration ranging from molecular to whole plant responses. *Photosynthetica*, **41**, 9–20.

Chapter 9

Interactive effects of ultraviolet and photosynthetically active radiation on photosynthesis, growth, and photoprotective mechanisms

Karel Klem[1], Otmar Urban[2]

[1] *Department of Impact Studies, Global Change Research Centre, Czech Academy of Sciences, Bělidla 4a, CZ-60300 Brno, Czech Republic*

[2] *Laboratory of Plant Ecological Physiology, Global Change Research Centre, Czech Academy of Sciences, Bělidla 4a, CZ-60300 Brno, Czech Republic*

1. INTRODUCTION

Ultraviolet (UV) radiation is an important environmental factor influencing the processes of photosynthesis, plant growth, and development and thus the primary production of terrestrial ecosystems and carbon cycling. Depending on the timing, duration, wavelength, and dose of UV radiation, responses can range from no effect or slight stimulation to severe damage. Alteration of growth and morphology can also lead to changes in competitive balance among species and a subsequent change in ecosystems' species composition (reviewed by Robson et al. 2015). With regard to the range of possible interactions between exposure to UV radiation and other factors accompanying global change such as elevated CO_2 concentration, drought stress, and increased temperature, the anticipated impacts of global change on ecosystems should be always considered in relation to UV radiation intensity. For example, changes in plants' chemical composition due to enhanced UV radiation are often reported and can modulate plants' photoprotective ability (Klem et al. 2015) and sensitivity to such other environmental stresses as drought (Petropoulou et al. 1995). Enhanced UV radiation also usually reduces the stimulation effect of elevated CO_2 concentration as the two factors' effects are counteractive (reviewed by Caldwell et al. 2003).

Changes in the intensity of UV-B radiation ($\lambda = 280–320$ nm) are closely related to stratospheric ozone depletion. Even if the concentration of ozone-depleting substances in the atmosphere is now decreasing as a result of the Montreal Protocol, ozone depletion continues to develop, and particularly so in Antarctica and Arctic (EEAP Report 2006). The changes in ozone depletion can be attributed also to changes in atmospheric circulation, indicating a linkage to climate change. Nevertheless, future changes in the stratospheric ozone layer remain uncertain. Current chemical models predict that ozone will recover at mid-latitudes by mid-century (EEAP Report 2006).

Elevated UV (particularly UV-B) radiation has pleiotropic effects on plant development, morphology, physiology, and biochemistry, as summarized in Fig. 1. The final effect of UV radiation is strongly modulated by environmental conditions that result in plant responses ranging from positive (regulatory) to negative (stress). Morphological consequences include reduced growth (height), leaf thickening and curling, increased axillary branching, and a higher root-to-shoot ratio. Higher UV doses or lower UV doses combined with adverse environmental conditions are accompanied by reduced biomass and leaf area (reviewed in Jansen 2002).

Higher UV doses also can negatively affect photosynthetic capacity (Jansen et al. 2010). The most vulnerable

target of UV-B is considered to be photosystem II (PS II) (e.g. Tyystjärvi 2008) due to degradation of the D1 protein. CO_2 assimilation rate may be further reduced due to decreases in chlorophyll content, disruption of thylakoid membrane, and degradation or reduced activity of Rubisco (reviewed in Takeuchi et al. 2002). Reduction in CO_2 assimilation rate can be also caused by UV regulation of stomatal conductance (Jansen & van den Noort 2000; Urban et al. 2006).

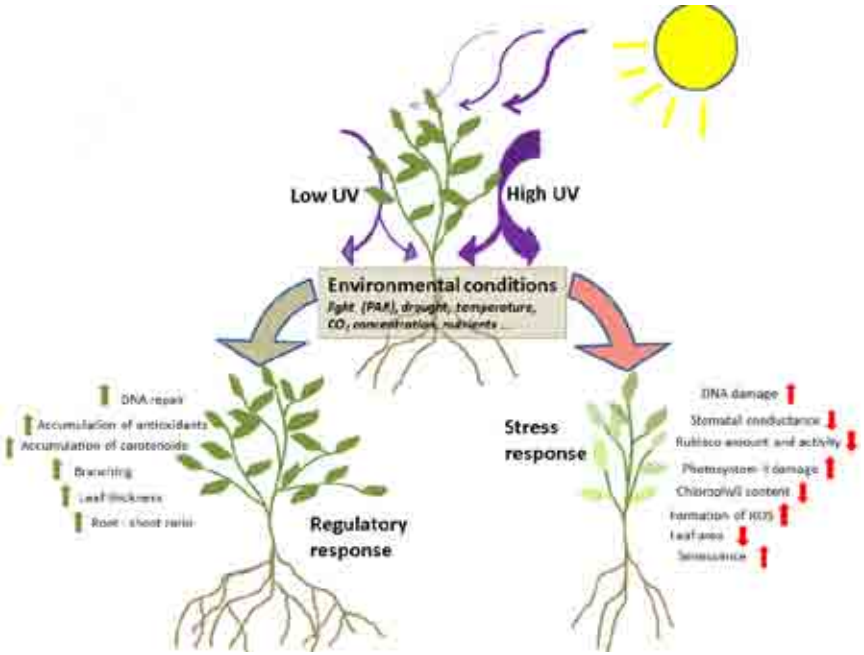

Fig. 1. *Schematic representation of plant responses to ultraviolet (UV) radiation, which is determined by the interaction of dose and other environmental conditions. Plant responses may therefore be either regulatory or stress responses, with many intermediate stages occurring between these two boundary responses. Red arrows represent negative (stress) responses and green arrows positive (regulatory) responses. ROS = reactive oxygen species, PAR = photosynthetically active radiation.*

DNA is obviously one of the key targets for UV-induced damage in plants. Absorption of UV-B causes DNA phototransformations which disable reading of DNA and RNA polymerases through the photoproducts formed (Britt & May 2003). Plants have developed a complex set of repair mechanisms (including photoreactivation, excision, and recombination repair) to avoid cytotoxic effects following DNA damage (reviewed by Frohnmeyer & Staiger 2003).

Similarly, high UV doses accompanied by adverse environmental conditions induce the formation of reactive oxygen species (ROS) that result in oxidative damage, whereas low doses can induce biosynthesis of compounds with UV absorbing, antioxidative, or energy-quenching features. Such compounds include in particular flavonoids and hydroxycinnamate esters accumulated in vacuoles of epidermal cells and xanthophyll

cycle carotenoids. Flavonoids play important roles as stress protecting agents (e.g. as antioxidants), attractants, and feeding deterrents as well as, in general, a significant role in plant resistance (Hernández et al. 2004; Treutter 2006). Flavonoids are also the main group of phenolics providing protection from UV radiation. These compounds have absorption maxima predominantly in the range of 240–390 nm (Cerovic et al. 2002) and so act as sunscreens in the leaf epidermis to protect inner cells from potentially harmful short-wavelength radiation (Bassman et al. 2002) while photosynthetically active radiation (PAR) is transmitted to mesophyll cells. In addition to constitutive production of flavonoids, their biosynthesis is induced by a wide range of environmental stimuli, including light intensity and its spectral composition (Götz et al. 2010; Agati et al. 2011), drought (Hernández et al. 2004), nitrogen and/or phosphorus deficiency (Stewart et al. 2001), pathogen attack (Dixon & Paiva 1995), and low temperature (Leyva et al. 1995). Flavonoid accumulation and the expression of chalcone synthase and other flavonoid biosynthesis genes are strongly affected by light quality. For example, Götz et al. (2010) reported that accumulation of flavonoids induced by UV-B is modulated by PAR. However, UV radiation and PAR act differently on specific flavonoids. It seems that light quality (UV-B, UV-A/blue and red/far-red) affects flavonoid induction, and thus different photoreceptors are involved in this process (Barnes et al. 1996; Ballaré et al. 2011).

Furthermore, flavonoid accumulation is affected by leaf age and leaf position on the plant (Klem et al. 2012). Morales et al. (2011) have shown that epidermal UV-screening responded differently to UV treatment depending on leaf position. Young leaves quickly adjusted UV-screening in their epidermis according to the UV they received and these adjustments were affected by previous UV-A and UV-B exposure.

Plants have evolved different mechanisms to dissipate excess energy before and after it reaches the photosynthetic electron transport chain (e.g. by photoprotective pigments, antioxidants, chloroplast movements). Hernández & van Breusegem (2010) hypothesized that flavonoid accumulation might act as an excess energy escape valve by consuming triose phosphate, ATP, and NADPH and also act as a sink for reduced carbon. Therefore, flavonoid biosynthesis is strongly related to variation in CO_2 assimilation rate and excess light (Tattini et al. 2004). The synthesis of flavonoids consumes more energy and photoassimilates than does that of simple phenylpropanoids, which may make flavonoids a more efficient excess energy outlet (Grace & Logan 2000). The carotenoids of the xanthophyll cycle and their role in non-photochemical energy dissipation are believed to be the major photoprotective mechanism by which excessive light energy is dissipated as heat (Demmig-Adams & Adams 2006). On the other hand, flavonoids represent a group of compounds with such diverse protective functions as epidermal UV-screening and scavenging of free radicals and reactive oxygen species (antioxidants). However, some flavonoids (e.g. anthocyanins) are able to absorb high-energy quanta of visible light and protect chloroplasts from the photoinhibitory and photooxidative effects (Gould 2004). In contrast to flavonoids, the xanthophyll cycle pigments seem to be mainly relevant to the protection of photosynthesis against sudden increases in light intensity.

The following hypotheses were tested in our model field experiment utilizing two barley varieties: (1) PAR contributes to the accumulation of photoprotective phenolic compounds in a similar way as does UV radiation, (2) PAR is involved in both physiological photosynthetic acclimation and leaf morphological acclimation to enhanced UV-B, (3) acclimation to UV-B radiation is modified by leaf age and barley genotype with contrast sensitivity to photo-oxidative stress, and (4) barley plants respond to high light stress differently depending on whether their photoprotective phenolic compounds were induced by PAR or by UV radiation.

2. MATERIALS AND METHODS

2.1. Plant material

The experiment was conducted during August 2010 in a field trial in the garden of the Global Change Research Centre of the Czech Academy of Sciences (Brno, Czech Republic). Two barley varieties differing in their sensitivity to light-induced oxidative stress (Wu and von Tiedemann, 2004) were studied: Barke (sensitive) and Bonus (tolerant). Barley plants were grown in small pots (for details see Klem et al. 2012) in 16 replicates for each UV/PAR treatment.

The plants were pre-treated under conditions of low PAR intensities and UV-A and UV-B exclusion. 0.6ND neutral density filters (Lee Filters, Hampshire, UK) were used to reduce PAR intensity to 25% of natural sunlight. Lee U.V. 226 clear plastic filters (Lee Filters) were used for UV-A and UV-B exclusion. After 14 days (when the first leaf had fully developed), the barley plants were transferred to individual UV or PAR treatments.

2.2. UV and PAR treatments

Barley plants were grown under four treatments representing combinations of excluded [UV-] or enhanced [UV+] UV radiation and reduced [PAR-] or ambient [PAR+] PAR, hereafter reported as [UV-PAR-], [UV+PAR+], [UV-PAR+], and [UV+PAR-]. Barley plants were exposed to individual treatments for 7 days. The treatments were arranged using open-sided chambers covered by UV and PAR filters. Lee U.V. 226 and 0.6ND filters (Lee Filters) were used to exclude UV radiation and reduce PAR intensity to 25% of natural sunlight, respectively. A modulated illumination system with a design similar to that of Šprtová et al. (1999) was used to achieve enhanced UV radiation. The system consisted of two UV-A (TL 20W/10 SLV, Philips, Amsterdam, Netherlands) and three UV-B (TL 20W/12 RS SLV, Philips) fluorescent lamps (for details see Klem et al. 2012). A feedback-and-amplification circuit (Konel, Zlín, Czech Republic) was used to adjust lamp output to ensure total UV irradiance of 200% of incident UV.

2.3. Physiological and morphological measurements

In vivo epidermal flavonol contents were determined using the Flav index of a Dualex 4 instrument (Force-A, Orsay, France). A Li-6400 open gas-exchange system (Li-Cor, Lincoln, NE, USA) was used to estimate light-saturated (1,200 μmol m^{-2} s^{-1}) CO_2 assimilation rate (A_{max}) and stomatal conductance. All measurements were conducted on the intact leaves of five plants per treatment under constant microclimatic conditions. At the same time, a FluorPen FP 100 (PSI, Brno, Czech Republic) was used to measure maximum quantum yield of the PS II (F_V/F_M) of dark adapted leaves.

After 7 days of treatment, five plants from each treatment were used for destructive morphological analyses of above-ground biomass. Leaf area was estimated using a portable leaf area meter (Li-3000A, Li-Cor).

2.4. Short-term high radiation stress

After 7 days of acclimation to UV/PAR treatments, the plants were transferred into darkness for 12 h. Following dark adaptation, half of the samples were used for subsequent analyses of UV-screening compounds, photosynthetic pigments, and xanthophyll cycle pigments. The remaining plants were placed into controlled conditions within a Bio-Line HB 1014 growth chamber (Vötsch Industrietechnik, Balingen-Frommern, Germany) equipped with additional UV-B fluorescent lamps (TL 20W/12 RS SLV, Philips)

and exposed to high radiation stress (HRS) defined by continuous high intensities of PAR (1,000 µmol m^{-2} s^{-1}), UV-A (10 W m^{-2}) and UV-B (2 W m^{-2}) for 4 h. A constant air temperature of 25°C and 65% relative humidity were maintained during the HRS treatment.

2.5. Analysis of xanthophyll cycle pigments

To assess the effect of acclimation to different UV/PAR treatments, dark-adapted leaves (12 h) were used for the quantification of xanthophyll cycle pigments (violaxanthin, antheraxanthin, zeaxanthin; VAZ). The contents of individual carotenoids, including the pool of xanthophyll cycle pigments (VAZ) expressed on a Chl *a+b* basis was estimated using a gradient reversed-phase high-performance liquid chromatography instrument (TSP Analytical, Santa Clara, CA, USA) according to Štroch et al. (2008).

3. RESULTS AND DISCUSSION

3.1. Effects of UV/PAR treatments on photosynthetic parameters

Changes in A_{max} in leaves of different age classes caused by UV/PAR treatments are shown in Fig. 2. A_{max} values gradually decreased with increasing leaf age irrespective of treatment and barley variety. After 7 days of the [UV+PAR-] treatment, there was a statistically significant reduction in A_{max} for both Barke (44–71%) and Bonus (32–54%) plants as compared to the [UV-PAR-] treatment. There were negligible differences in A_{max} between [UV-PAR-] and [UV-PAR+] treatments for both barley varieties and all leaf age classes. In addition, there were no significant changes in A_{max} between [UV+PAR+] and [UV-PAR+] treatments, irrespective of leaf age and variety. In contrast, significantly lower A_{max} values were present in plants exposed to [UV+PAR-] as compared to [UV-PAR-] conditions, in particular for the variety Barke.

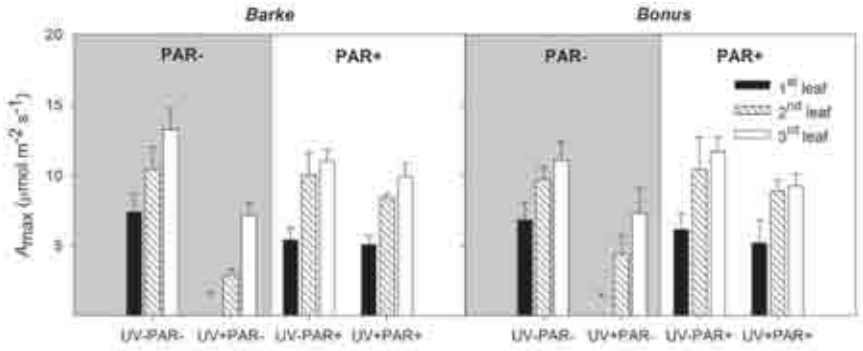

Fig. 2. *Changes in light-saturated rate of CO_2 assimilation (A_{max}) after 7-day acclimation to individual UV/PAR treatments. Measurements were conducted on old (1st – black column), middle (2nd – shaded column), and young (3rd – white column) leaves of two barley varieties – Barke and Bonus. Means (columns) and standard deviations (error bars) are presented (n = 5). Asterisks denote damaged leaves which were not measurable. Adapted from Klem et al. (2012).*

It is commonly acknowledged that high PAR intensities can alleviate the negative effects of enhanced UV-B radiation, although the evidence in the literature for this hypothesis is contradictory (Pfündel et al.

1992; Sullivan et al. 2003; Jansen et al. 2010). The acclimation of CO_2 assimilation rate to combined UV/PAR treatments operates on several structural levels encompassing changes in chlorophyll content and in stomatal function (reviewed in Caldwell et al. 2007; Jansen et al. 2010; Ballaré et al. 2011). Significant genotypic variability in UV-B responsiveness has similarly been reported in other barley varieties (Hideg et al. 2006), as well as cowpea (e.g. Singh et al. 2008), soybeans (e.g. Koti et al. 2007), and rice (e.g. Mohammed & Tarpley 2011).

Although the effects of UV/PAR treatments on F_V/F_M values were similar to trends for A_{max} (Fig. 3), the changes were less pronounced and not always statistically significant. Exposure to [UV+PAR-] for 7 days led to a decrease in F_V/F_M as compared to [UV-PAR-] by 29% for the second leaf and 7% for the third in the variety Barke, while for the variety Bonus it was by 19% and 4%, respectively. Similarly to the case with A_{max}, most changes in F_V/F_M due to enhanced UV were not statistically significant under [PAR+] treatments.

In vitro studies have shown that simultaneous PAR and UV-B illumination impairs PS II activity to a lesser extent than what is expected during independent illumination (e.g. Tyystjärvi 2008). This protective effect was pronounced only at low PAR irradiances and became negligible at high irradiances.

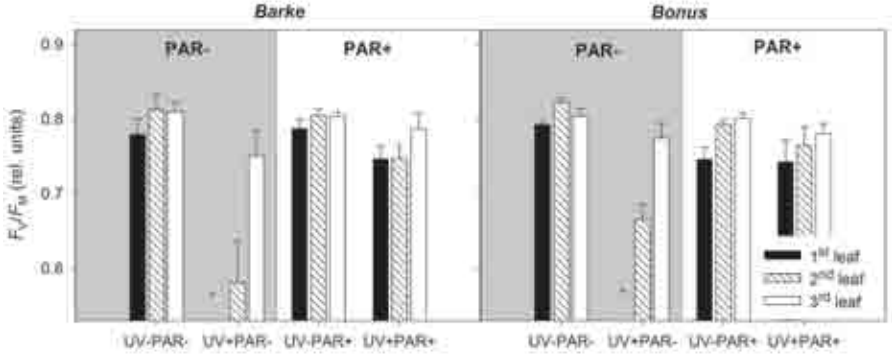

Fig. 3. *Changes in maximum quantum yield of photosystem II (F_V/F_M) after 7-day acclimation to individual UV/PAR treatments. Measurements were conducted on old (1st – black column), middle (2nd – shaded column), and young (3rd – white column) leaves of two barley varieties – Barke and Bonus. Means (columns) and standard deviations (error bars) are presented (n = 5). Asterisks denote damaged leaves which were not measurable. Adapted from Klem et al. (2012).*

3.2. Growth responses to UV/PAR treatments

After 7 days of acclimation, leaf area was significantly affected by UV/PAR treatment, although the effect of UV-B was modified by leaf age and genotype (Fig. 4). PAR intensity (comparing [UV-PAR-] and [UV-PAR+]) had no significant effect on leaf area development. The [UV+PAR-] treatment led to a significant reduction in leaf area as compared to [UV-PAR], primarily as a result of reduced leaf width (data not shown), in all leaf age classes and in both varieties studied (by 45–65% in Barke and by 26–48% in Bonus). The UV effect on leaf area was most pronounced in young (3rd) leaves and in the variety Barke. Comparing [UV-PAR+] and [UV+PAR+] treatments, a statistically significant reduction in leaf area was only present for the young (3rd) leaves of the variety Barke (by 32%).

Of the UV effects on morphology, growth inhibition (decreased elongation due to photooxidative

destruction of the indole acetic acid), leaf thickening activation, and axillary branching are regarded as typical UV-induced responses (Jansen et al. 1998; Jansen 2002). There is general agreement that high PAR intensities may compensate for UV radiation's negative effects on plant morphology (e.g. Krizek 2004). Both PAR and UV-B may lead to increased leaf thickening, which can contribute to reducing UV-B radiation's penetration into the interior of leaves (Burchard et al. 2000) and thus protect photosynthetically active mesophyll cells (Meijkamp et al. 2001).

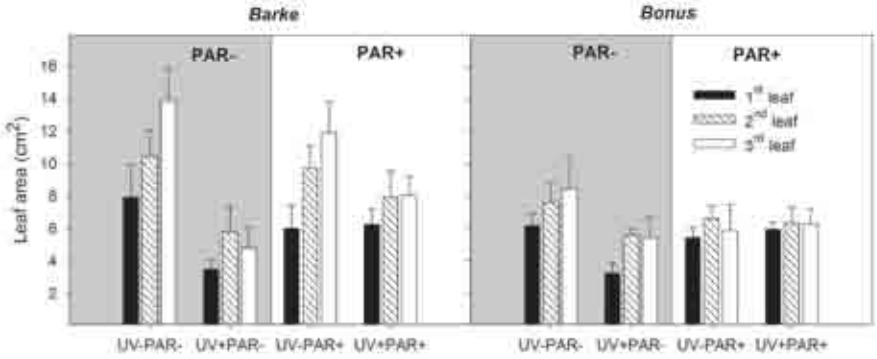

Fig. 4. *Leaf area after 7-day exposure to UV/PAR treatments. Measurements were conducted on old (1st – black column), middle (2nd – shaded column), and young (3rd – white column) leaves of two barley varieties – Barke and Bonus. Means (columns) and standard deviations (error bars) are presented (n = 5). Adapted from Klem et al. (2012).*

3.3. Accumulation of epidermal UV screening compounds

UV- and PAR-induced accumulation of UV-screening compounds in leaves was investigated in old (1st), middle (2nd), and young (3rd) leaves acclimated previously to [UV-PAR-] conditions. This enabled us to distinguish the effect of ontogenesis from the influence of UV-B or PAR on flavonol accumulation. There were similar trends in flavonol accumulation in individual leaf age classes determined during UV/PAR treatments in both varieties – Barke and Bonus (Fig. 5). Under the [UV-PAR-] treatment, flavonol content remained low and only increased in young (3rd) leaves. In comparison to old (1st) leaves, flavonol content was higher by 6–9% in middle (2nd) leaves and by 73–82% in young (3rd) leaves. The constitutive accumulation of flavonols under the [UV-PAR-] treatment was higher by 13–77% in the variety Bonus as compared to Barke.

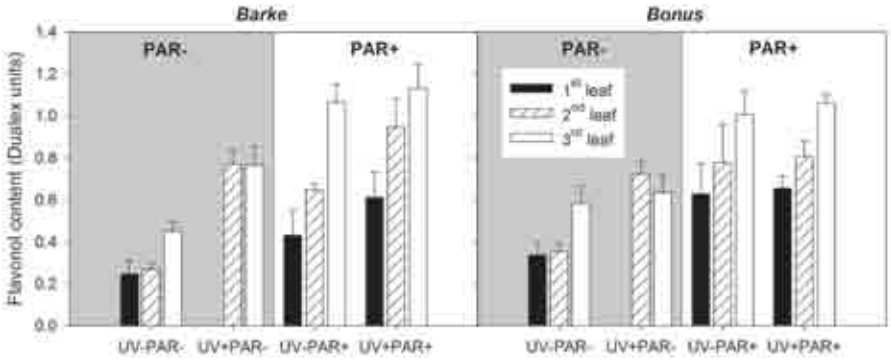

Fig. 5. *Flavonol content measured in vivo using UV screening technique (Dualex instrument) after 7-day exposure to UV/PAR treatments. Measurements were conducted on old (1st – black column), middle (2nd – shaded column), and young (3rd – white column) leaves of two barley varieties – Barke and Bonus. Means (columns) and standard deviations (error bars) are presented (n = 5).*

The [UV-PAR+] treatment mainly increased flavonol content in young leaves (by 137% in Barke and 73% in Bonus), whereas the [UV+PAR-] treatment tended to increase flavonol content more in older leaves. Thus the [UV+PAR+] treatment increased flavonol accumulation in all leaf age classes, particularly in middle (2nd) leaves (by 252% in Barke and 127% in Bonus), as compared to the [UV-PAR-] treatment. We showed that high PAR irradiances can induce flavonol accumulation in barley leaves irrespective of UV treatment. While high PAR irradiances mainly stimulated flavonol biosynthesis in young leaves, enhanced UV radiation stimulated flavonol accumulation in old leaves.

Likewise, Götz et al. (2010) showed that high PAR irradiances can trigger biosynthesis of flavonoids, in particular quercetin, in *Arabidopsis* plants exposed to low biologically effective UV irradiances (25 mW m^{-2}). The combination of high UV and PAR irradiances leads to further increases in both the quantity (Meijkamp et al. 2001; Götz et al. 2010) and quality (e.g. an increased ratio of quercetin to kaempferol) of UV-screening metabolites (Rozema et al. 2002; Jansen et al. 2008).

In general, epidermally located flavonoids and hydroxycinnamic acid esters prevent short solar wavelengths (280–450 nm) from penetrating into leaves (DeLucia et al. 1992; Burchard et al. 2000). However, Agati et al. (2009) demonstrated that acclimation to contrasting UV and PAR irradiances also leads to changes in flavonoid distribution within mesophyll and epidermal cells. Accumulation of quercetin and luteolin derivatives in mesophyll cells in the absence of UV wavelengths leads to the hypothesis that flavonoids, and particularly UV-inducible quercetin (Rozema et al. 2002), also play a key role in countering light-induced oxidative stress (Jansen et al. 2008; Agati et al. 2009).

3.4. Response of photosynthetic parameters to short-term HRS

Changes in light-saturated CO_2 assimilation rate (A_{max}) and maximum quantum yield of PS II (F_V/F_M) following exposure to short-term HRS are presented in Fig. 6. The greatest reduction in A_{max}, which was statistically significant, was in plants acclimated to [UV-PAR-] conditions and occurred for both barley varieties (66% for Bonus and 74% for Barke). When plants had been acclimated to the [UV-PAR+] treatment, there was a significant reduction only in A_{max} in the sensitive variety Barke (43%). Changes in A_{max} were not

statistically significant for [UV+PAR+]-acclimated plants, irrespective of variety. The effects of HRS on F_V/F_M were similar to those on A_{max}, although they were relatively less pronounced.

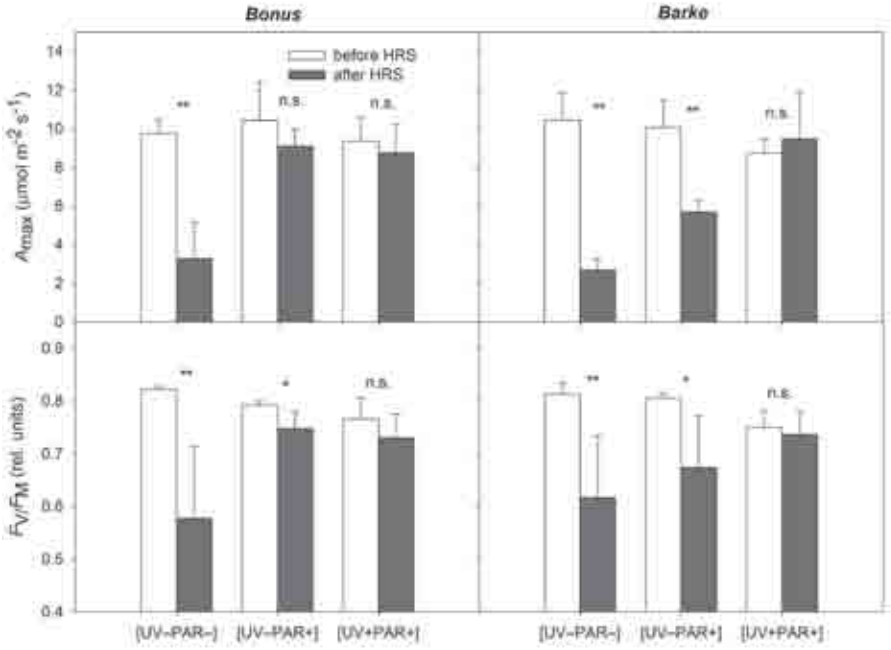

Fig. 6. *Changes in the light-saturated rate of CO_2 assimilation (A_{max}) and maximum quantum yield of photosystem II photochemistry (F_V/F_M) before (clear columns) and after (opaque columns) the application of short-term (4 h) high radiation stress (HRS). The barley varieties Bonus and Barke were acclimated for 7 days to individual UV/PAR treatments before HRS was applied. Means (columns) and standard deviations (error bars) are presented ($n \geq 5$). Significant differences between means before and after HRS were tested using a paired Student's t-test for independent samples (* significant at $p \leq 0.05$; ** significant at $p \leq 0.01$; n.s. non-significant). Adapted from Klem et al. (2015).*

The relative reductions in A_{max} and F_V/F_M following HRS application were inversely proportional to the contents of flavonols and xanthophyll cycle pigments (Fig. 7) accumulated in leaves. There was a consistent linear increase in leaf flavonols associated with a smaller reduction in both A_{max} and F_V/F_M for both varieties due to HRS. Although all relationships had high coefficients of determination ($p \leq 0.01$), the reduction in F_V/F_M was rather gradual. Similarly as with flavonols, there were positive relationships between VAZ and protection of both F_V/F_M and A_{max}. It is therefore appealing to consider some form of coupling between these protective mechanisms, be that at the level of receptors, signalling pathways, or even metabolite biosynthesis.

The results show that both PAR and UV radiation are important ecological factors that control plants' photoprotective capacity. This result agrees with previous findings that UV may induce enhanced photoprotection against high light stress or long-wave UV radiation (e.g. Hakala-Yatkin et al. 2010). The general role of optical screening by epidermal UV-absorbing pigments, presumably flavonoids, in photoprotection has been confirmed (e.g. Adamse & Britz 1996; Kataria et al. 2014).

Our study also highlights the importance of genotype in determining photoprotective capacity and inducible response. In barley plants acclimated to the [UV-PAR+] treatment, reductions in F_V/F_M and A_{max} were minor in the resistant variety Bonus, whereas the effect of short-term radiation stress was pronounced in the sensitive variety Barke. On the other hand, there was almost no difference between the two varieties in the reduction of photosynthetic activity when acclimated to [UV+PAR+] conditions. Thus, inducible protective mechanisms can compensate for differences in constitutive protection between barley genotypes under these conditions.

The published literature yields equivocal information concerning the effects of UV radiation on VAZ size and xanthophyll cycle activity, as there have been reports of both significant increases in VAZ size (Choo et al. 2005; Láposi et al. 2009) and decreases together with impairment of violaxanthin de-epoxidation (Pfündel et al. 1992; Lidon & Ramalho 2011). Nevertheless, the latter response is usually a result of acute oxidative stress induced by high UV-B irradiance (Lidon et al. 2012). In contrast, successful acclimation to UV-A and UV-B appears to be associated with enhanced VAZ size and unaffected xanthophyll cycle activity (Láposi et al. 2009). VAZ accumulation together with a slight increase in Chl *a/b* indicate that in our experiment UV-radiation mainly induced accumulation of xanthophyll cycle pigments that were not bound to pigment protein complexes (i.e. an effective acclimation response). Induction of VAZ by PAR/UV acclimation treatments broadly correlates with flavonol induction. Although this may be an effective protection response whereby two pathways leading to antioxidative protection are induced simultaneously, more research is required to determine whether these protective responses are truly linked or if they are separate but co-occurring phenomena.

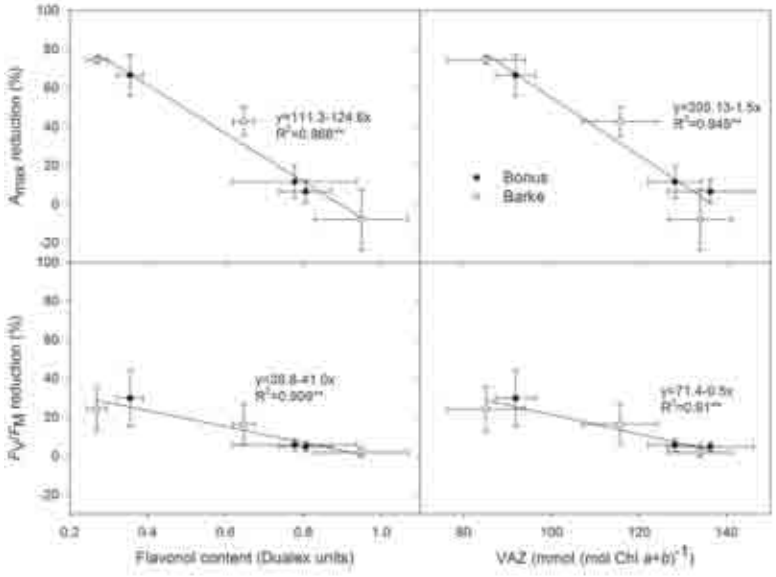

Fig. 7. *Relationships between in vivo flavonol content, total content of xanthophyll cycle pigments (VAZ), and relative reductions in photosynthetic parameters: light-saturated CO_2 assimilation rate (A_{max}) and maximum quantum yield of photosystem II photochemistry (F_V/F_M) after the application of short-term high radiation stress. The data show close relationships ($p \leq 0.01$) irrespective of barley variety. Means (points) and standard deviations (vertical and horizontal error bars) are presented ($n \geq 5$). Adapted from Klem et al. (2015).*

4. CONCLUSIONS

The [UV+PAR-] treatment significantly reduced the photosynthetic activity of barley leaves. This reduction was more pronounced in old than in young leaves and greater in the sensitive variety Barke than in the variety Bonus.

The [PAR+] treatment triggered photoprotective mechanisms which partially ameliorated UV effects on photochemistry and carbon assimilation. The [PAR+] treatment also induced flavonol accumulation, mainly in young leaves, while UV-induced accumulation was more pronounced in old leaves. Enhanced UV radiation reduced the final leaf area, particularly in [PAR-] plants, in young leaves, and in the variety Barke, but [PAR+] mitigated the morphological effects induced by the [UV+] treatment.

Acclimation to PAR and UV radiation substantially increased the photoprotective capacities of barley plants, especially for the variety Barke. As a consequence, subsequent high radiation events caused less photooxidative damage, with decreased harmful effects on both stages of photosynthesis associated with photochemical quantum yield and CO_2 assimilation.

Our results reveal that the accumulation of xanthophyll cycle pigments and flavonoids (mainly flavonols) during acclimation to PAR and/or UV correlated with protection against photoinhibitory damage to the photosynthetic apparatus. While high PAR intensity itself induced sufficient photoprotective capacity against HRS in the variety Bonus, additional acclimation to UV is necessary to induce adequate protection in the sensitive variety Barke.

These data demonstrate the importance of UV-acclimation, showing that UV exposure can contribute to the induction of tolerance to HRS in barley.

Acknowledgement

This work was supported by the Ministry of Education, Youth and Sports of the Czech Republic within the National Programme for Sustainability I, grant No. LO1415.

References

Adamse, P. & Britz, S.J. (1996) Rapid fluence-dependent responses to ultraviolet-B radiation in cucumber leaves: The role of UV-absorbing pigments in damage protection. *Journal of Plant Physiology*, **148**, 57–62.

Agati, G., Stefano, G., Biricolti, S. & Tattini, M. (2009) Mesophyll distribution of 'antioxidant' flavonoid glycosides in *Ligustrum vulgare* leaves under contrasting sunlight irradiance. *Annals of Botany*, **104**, 853–861.

Agati, G., Cerovic, Z. G., Pinelli, P., & Tattini, M. (2011) Light-induced accumulation of ortho-dihydroxylated flavonoids as non-destructively monitored by chlorophyll fluorescence excitation techniques. *Environmental and Experimental Botany*, ***73***, 3-9.

Ballaré, C.L., Caldwell, M.M., Flint, S.D., Robinson, A. & Bornman, J.F. (2011) Effects of solar ultraviolet radiation on terrestrial ecosystems. Patterns, mechanisms, and interactions with climate change. *Photochemical and Photobiological Sciences,* **10**, 226–241.

Bassman, J.H., Edwards, G.E. & Robberecht, R. (2002) Long-term exposure to enhanced UV-B radiation is not detrimental to growth and photosynthesis in Douglas-fir. *New Phytologist*, **154**, 107–120.

Barnes, P.W., Ballaré, C.L. & Caldwell, M.M. (1996) Photomorphogenic effects of UV-B radiation on plants: consequences for light competition. *Journal of Plant Physiology*, **148**, 15–20.

Britt, A.B. & May, G.D. (2003) Re-engineering plant gene targeting. *Trends in Plant Science*, **8**, 90–95.

Burchard, P., Bilger, W. & Weissenbock, G. (2000) Contribution of hydroxycinnamates and flavonoids to epidermal

shielding of UV-A and UV-B radiation in developing rye primary leaves as assessed by ultraviolet-induced chlorophyll fluorescence measurements. *Plant, Cell and Environment,* **23**, 1373–1380.

Caldwell, M.M., Ballaré, C.L., Bornman, J.F. et al. (2003) Terrestrial ecosystems, increased solar ultraviolet radiation and interactions with other climatic change factors. *Photochemical and Photobiological Sciences*, **2**, 29–38.

Caldwell, M.M., Bornman, J.F., Ballaré, C.L., Flint, S.D. & Kulandaivelu, G. (2007) Terrestrial ecosystems, increased solar ultraviolet radiation, and interactions with other climate change factors. *Photochemical and Photobiological Sciences*, **6**, 252–266.

Cerovic, Z.G., Ounis, A., Cartelat, A. et al. (2002) The use of chlorophyll fluorescence excitation spectra for the non-destructive in situ assessment of UV-absorbing compounds in leaves. *Plant, Cell and Environment*, **25**, 1663–1676.

Choo, K. S., Nilsson, J., Pedersen, M., & Snoeijs, P. (2005) Photosynthesis, carbon uptake and antioxidant defence in two coexisting filamentous green algae under different stress conditions. *Marine Ecolology-Progress Series*, **292**, 127–138.

DeLucia, E.H., Day, T.A. & Vögelmann, T.C. (1992) Ultraviolet-B and visible-light penetration into needles of 2 species of sub-alpine conifers during foliar development. *Plant, Cell and Environment*, **15**, 921–929.

Demmig-Adams, B. & Adams, W.W. (2006) Photoprotection in an ecological context: the remarkable complexity of thermal energy dissipation. *New Phytologist*, **172**, 11–21.

Dixon, R. A. & Paiva, N. L. (1995). Stress-induced phenylpropanoid metabolism. *Plant Cell*, **7**, 1085.

EEAP Report (2006) Environmental Effects of Ozone Depletion and its Interactions with Climate Change: 2006 Assessment. United Nations Environment Programme (UNEP), Nairobi, Kenya.

Frohnmeyer, H. & Staiger, D. (2003) Ultraviolet-B radiation-mediated responses in plants. Balancing damage and protection. *Plant Physiology*, **133**, 1420–1428.

Götz, M., Albert, A., Stich, S. et al. (2010) PAR modulation of the UV-dependent levels of flavonoid metabolites in *Arabidopsis thaliana* (L.) Heynh. leaf rosettes: cumulative effects after a whole vegetative growth period. *Protoplasma*, **243**, 95–103.

Gould, K.S. (2004) Nature's Swiss army knife: The diverse protective roles of anthocyanins in leaves. *Journal of Biomedicine and Biotechnology*, **2004**, 314–320.

Grace, S.C. & Logan, B.A. (2000) Energy dissipation and radical scavenging by the plant phenylpropanoid pathway. *Philosophical Transactions of the Royal Society of London Series B-Biological Sciences*, **355**, 1499–1510.

Hakala-Yatkin, M., Mäntysaari, M., Mattila, H. & Tyystjärvi, E. (2010) Contributions of visible and ultraviolet parts of sunlight to photoinhibition. *Plant and Cell Physiology*, **51**, 1745–1753.

Hernández, I., Alegre, L. & Munné-Bosch, S. (2004) Drought-induced changes in flavonoids and other low molecular weight antioxidants in *Cistus clusii* grown under Mediterranean field conditions. *Tree Physiology*, **24**, 1303–1311.

Hernández, I. & van Breusegem, F. (2010) Opinion on the possible role of flavonoids as energy escape valves: Novel tools for nature's Swiss army knife? *Plant Science*, **179**, 297–301.

Hideg, E., Rosenqvist, E., Varadi, G., Bornman, J.F. & Vincze, E. (2006) A comparison of UV-B induced stress responses in three barley cultivars. *Functional Plant Biology*, **33**, 77–90.

Jansen, M.A.K. (2002) Ultraviolet-B radiation effects on plants: induction of morphogenic responses. *Physiologia Plantarum*, **116**, 423–429.

Jansen, M.A.K., Gaba, V. & Greenberg, B.M. (1998) Higher plants and UV-B radiation: Balancing damage, repair and acclimation. *Trends in Plant Science*, **3**, 131–135.

Jansen, M.A.K., Hectors, K., O'Brien, N.M., Guisez, Y. & Potters, G. (2008) Plant stress and human health: Do human consumers benefit from UV-B acclimated crops? *Plant Science*, **175**, 449–458.

Jansen, M.A.K., Le Martret, B. & Koornneef, M. (2010) Variations in constitutive and inducible UV-B tolerance; dissecting photosystem II protection in *Arabidopsis thaliana* accessions. *Physiologia Plantarum*, **138**, 22–34.

Jansen, M.A., & van den Noort, R. E. (2000) Ultraviolet-B radiation induces complex alterations in stomatal behaviour. *Physiologia Plantarum,* **110**, 189–194.

Kataria, S., Jajoo, A. & Guruprasad, K.N. (2014) Impact of increasing Ultraviolet-B (UV-B) radiation on photosynthetic processes. *Journal of Photochemistry and Photobiology B-Biology*, **137**, 55–66.

Klem, K., Ač, A., Holub, P. et al. (2012) Interactive effects of PAR and UV radiation on the physiology, morphology and leaf optical properties of two barley varieties. *Environmental and Experimental Botany*, **75**, 52–64.

Klem, K., Holub, P., Štroch, M. et al. (2015) Ultraviolet and photosynthetically active radiation can both induce photoprotective capacity allowing barley to overcome high radiation stress. *Plant Physiology and Biochemistry,* **93**, 74–83.

Koti, S., Reddy, K.R., Kakani, V.G., Zhao, D. & Gao, W. (2007) Effects of carbon dioxide, temperature and ultraviolet-B radiation and their interactions on soybean (*Glycine max* L.) growth and development. *Environmental and Experimental Botany*, **60**, 1–10.

Krizek, D.T. (2004) Influence of PAR and UV-A in determining plant sensitivity and photomorphogenic responses to UV-B radiation. *Photochemistry and Photobiology,* **79**, 307–315.

Láposi, R., Veres, S., Lakatos, G., Oláh, V., Fieldsend, A. & Meszáros, I. (2009) Responses of leaf traits of European beech (*Fagus sylvatica* L.) saplings to supplemental UV-B radiation UV-B exclusion. *Agricultural and Forest Meteorology*, **149**, 745–755.

Leyva, A., Jarillo, J.A., Salinas, J. & Martinez-Zapater, J.M. (1995) Low temperature induces the accumulation of phenylalanine ammonia-lyase and chalcone synthase mRNAs of *Arabidopsis thaliana* in a light-dependent manner. *Plant Physiology*, **108**, 39–46.

Lidon, F.J.C. & Ramalho, J.C. (2011) Impact of UV-B- radiation on photosynthetic performance and chloroplast membrane components in *Oryza sativa* L. *Journal of Photochemistry and Photobiology B-Biology*, **104**, 457–466.

Lidon, F.J.C., Texeira, M. & Ramalho, J.C. (2012) Decay of the chloroplast pool of ascorbate switches on the oxidative burst in UV-B irradiated rice. *Journal of Agronomy and Crop Science*, **198**, 130–144.

Meijkamp, B.B., Doodeman, G. & Rozema, J. (2001) The response of *Vicia faba* to enhanced UV-B radiation under low and near ambient PAR levels. *Plant Ecology*, **154**, 135–146.

Mohammed, A.R. & Tarpley, L. (2011) Differential response of southern US rice (*Oryza sativa* L.) cultivars to ultraviolet-B radiation. *Journal of Agronomy and Crop Science*, **196**, 286–295.

Morales, L.O., Tegelberg, R., Brosché, M., Lindfors, A., Siipola, S. & Aphalo, P.J. (2011) Temporal variation in epidermal flavonoids due to altered solar UV radiation is moderated by the leaf position in *Betula pendula*. *Physiologia Plantarum*, **143**, 261–270.

Petropoulou, Y., Kyparissis, A., Nikolopoulos, D. & Manetas, Y. (1995) Enhanced UV-B radiation alleviates the adverse effects of summer drought in two Mediterranean pines under field conditions. *Physiologia Plantarum*, **94**, 37–44.

Pfündel, E.E., Pan, R.S. & Dilley, A. (1992) Inhibition of violaxanthin deepoxidation by ultraviolet-B radiation in isolated chloroplasts and intact leaves, *Plant Physiology*, **98**, 1372–1380.

Robson, T.M., Klem, K., Urban, O. & Jansen, M.A.K. (2015) Re-interpreting plant morphological responses to UV-B radiation. *Plant, Cell and Environment*, ***38*****,** 856–866.

Rozema, J., Björn, L.O., Bornman, J.F. et al. (2002) The role of UV-B radiation in aquatic and terrestrial ecosystems - an experimental and functional analysis of the evolution of UV-absorbing compounds. *Journal of Photochemistry and Photobiology B-Biology*, **66**, 2–12.

Singh, S.K., Surabhi, G.K., Gao, W. & Reddy, K.R. (2008) Assessing genotypic variability of cowpea (*Vigna unguiculata* [L.] Walp.) to current and projected ultraviolet-B radiation. *Journal of Photochemistry and Photobiology B-Biology*, **93**, 71–81.

Šprtová, M., Marek, M.V., Nedbal, L., Prášil, O. & Kalina, J. (1999) Seasonal changes of photosynthetic assimilation of Norway spruce under the impact of enhanced UV-B radiation. *Plant Science*, **142**, 37–45.

Stewart, A.J., Chapman, W., Jenkins, G.I., Graham, I., Martin, T. & Crozier, A. (2001) The effect of nitrogen and phosphorus deficiency on flavonol accumulation in plant tissues. *Plant, Cell and Environment*, **24**, 1189–1197.

Štroch, M., Lenk, S., Navrátil, M., Špunda, V. & Buschmann, C. (2008) Epidermal UV-shielding and photosystem II adjustment in wild type and chlorina f2 mutant of barley during exposure to increased PAR and UV radiation. *Environmental and Experimental Botany*, **64**, 271–278.

Sullivan, J.H., Gitz, D.C., Peek, M.S. & McElrone, A.J. (2003) Response of three eastern tree species to supplemental UV-B radiation: chemistry and gas exchange. *Agricultural and Forest Meteorol*ogy, **120**, 219–228.

Takeuchi, A., Yamaguchi, T., Hidema, J., Strid, A. & Kumagai, T. (2002) Changes in synthesis and degradation of Rubisco and LHCII with leaf age in rice (*Oryza sativa* L.) growing under supplementary UV-B radiation. *Plant, Cell and Environment*, **25**, 695–706.

Tattini, M., Galardi, C., Pinelli, P., Massai, R., Remorini, D. & Agati, G. (2004) Differential accumulation of flavonoids and hydroxycinnamates in leaves of *Ligustrum vulgare* under excess light and drought stress. *New Phytologist*, **163**, 547–561.

Tyystjärvi, E. (2008) Photoinhibition of Photosystem II and photodamage of the oxygen evolving manganese cluster. *Coordination Chemistry Reviews*, **252**, 361–376.

Treutter, D. (2006) Significance of flavonoids in plant resistance: a review. *Environmental Chemistry Letters*, **4**, 147–157.

Urban, O., Tůma, I., Holub, P. & Marek, M.V. (2006) Photosynthesis and growth response of *Calamagrostis arundinacea* and *C. villosa* to enhanced UV-B radiation. *Photosynthetica*, **44**, 215–220.

Wu, Y.X. & von Tiedemann, A. (2004) Light-dependent oxidative stress determines physiological leaf spot formation in barley. *Phytopathology*, **94**, 584–592.

Chapter 10

Drought and biomass production in natural grassland ecosystems

Petr Holub

Laboratory of Plant Ecological Physiology, Global Change Research Centre, Czech Academy of Sciences, Bělidla 4a, CZ-60300 Brno, Czech Republic

1. INTRODUCTION

Predicted scenarios of global change, discussed in detail by Ač & Marek in Chapter 1 of this book, include an increase in drought during the growing season and higher frequencies of extreme rainfall events (Cook et al. 2015). Such events will affect many soil, plant, and ecosystem properties of natural grasslands and then also their biomass productivity and plant diversity (Knapp et al. 2002; Fay et al. 2008; Kreyling et al. 2008b). Climate models predict greater variability in precipitation patterns between and within years, and there is increasing evidence that precipitation regimes during growing seasons have become more extreme around the world (e.g. Groisman & Knight 2008). Similar changes in the pattern of precipitation variability are predicted for the Czech Republic (see Chapter 2 of this book by Dubrovský & Trnka for details). The terrestrial water cycle and climate change impacts are very important for both agricultural and natural ecosystems. From an agricultural viewpoint, changes in composition and productivity in response to altered precipitation are important because they influence the grasslands' ability to support livestock production. From a conservation perspective, moreover, grassland ecosystem responses to altered precipitation may have important implications for regional diversity patterns (Fay et al. 2000).

Above-ground productivity (AP) in grasslands has been examined in many studies with a view to regional precipitation gradients (e.g. Epstein et al. 2002; Yang et al. 2009) and to variability in precipitation among years at a given location (Silvertown et al. 1994; Nippert et al. 2006). Plant species have adapted to moisture conditions at a given site through various functional and structural characteristics, such as plant size and architecture, ecophysiological characteristics, and growth strategy (Paruelo et al. 1999; Knapp & Smith 2001; Meinzer 2003; McCulley et al. 2005). Some experiments have shown that natural and simulated droughts have led to reductions in AP (Peñuelas et al. 2004; Ciais et al. 2005). On the other hand, other authors observed no significant effects from locally severe drought manipulations (Fay et al. 2000; Kreyling et al. 2008a). Generally, increased variability in precipitation within a growing season can affect AP more than changes in total precipitation (Knapp et al. 2002). In addition, Swemmer et al. (2007) noted various effects from precipitation distribution. They deduced that while precipitation event size is more significant at the driest sites, event spacing is more important at mesic sites (Swemmer et al. 2007).

Below-ground biomass and the rhizosphere comprise grassland ecosystems' main pool of organic matter and geobioelements (Stanton 1988; Hui & Jackson 2006). Because grassland ecosystems store up to 30% of the world's below-ground carbon, it is essential to know how changes in different climate drivers affect soil carbon pools and fluxes as well as how carbon cycling might be influenced by altered precipitation (Risch et al. 2007). New root growth is often found during periods of favourable soil water conditions, while drought periods correspond with reductions in root biomass (e.g. Titlyanova et al. 1999; Weltzin et

al. 2003; Weisshuhn et al. 2010). In contrast, Bakker et al. (2006) concluded that biomass and fine root length increased significantly at dry sites compared to humid sites, which is in accordance with studies by Ibrahim et al. (1997), Qaderi et al. (2006), and Wedderburn et al. (2010).

Not much is known regarding how differing amounts of precipitation affect changes in the proportion of below-ground plant matter within total plant production or the values of the ratio between root and shoot biomass (the R/S ratio). Nevertheless, Hui & Jackson (2006) summarized the collection of field biomass measurements and found that the proportion of below-ground net biomass production in total net primary production was negatively correlated with means of annual temperature and precipitation across locations. Werger (1983) summarized and discussed several examples from various climatic regions in an attempt to demonstrate the suitability of the R/S ratio as a characterization of plant strategy. According to that author, the characterization of a plants' strategy expressing its essential ecological responses is simple, but the literature on this subject shows a great deal of contradictory evidence. Werger (1983) estimated R/S values ranging from 3.0 to 6.0 for dry grassland, 7.0 to 12.5 for wet meadows, 1.7 to 3.7 for mountains, and 3.5 to 4.5 for alpine meadows. Comparing the estimated values is rather difficult because of the low decomposition rate and accumulation of undecomposed dead roots in both wet and dry habitats. Although decreased soil moisture and drought reduce the decomposition rate of dead plant matter in many ecosystems (e.g. van Oorschot et al. 2000; Fischer et al. 2006; Arriaga & Maya 2007; Teklay 2007), it is also the case that large amounts of precipitation or soil moisture can greatly impede dead root decomposition (Yang et al. 2002).

It remains unclear how much impact climate change will have on terrestrial carbon sequestration and cycling, and so it is necessary to collect additional data regarding geographic and interannual variability in below-ground biomass components (Hui & Jackson 2006). In addition, Beier et al. (2012) summarized that the climate change and ecosystem research communities would benefit greatly from a systematic and holistic approach to investigating how soil and plant community characteristics change as precipitation regimes change as well as to explorations of the subsequent effects on ecosystem processes and functioning. Those authors emphasized that experiments should specifically examine how ecosystem resilience and acclimation are affected by changes in precipitation that lead to the exceedance of biological thresholds.

We therefore investigated the effects of various recurrent precipitation intensities (reduced and increased rainfall) on biomass allocation to above- and below-ground plant parts in different grassland communities. Given that dry and warm conditions may lead to reductions in root growth, we expected to observe: (1) smaller root production and lower R/S ratios in water-shortage treatments in all grasslands studied, (2) more intensive reductions in root growth in drier and warmer lowland grasslands in contrast to wet and cool highlands and mountain grasslands, and (3) a cumulative decreasing trend in R/S ratios due to reduced root growth in dry conditions over the 5-year experiment.

2. MATERIALS AND METHODS

2.1. Site description

This study was conducted over 5 years (2006–2010) at three different grassland ecosystems (see Fig. 1). The experimental locations were established in grasslands occurring at (1) a lowland site (Podyjí National Park near the village of Havraníky, Znojmo District, in southern Moravian lowlands – lowland grasslands), (2) a highland site (Moravian–Bohemian Highlands near Kameničky, southeast of Hlinsko – highland

grasslands), and (3) a mountain site (Beskydy Mountains near Bílý Kříž – mountain grasslands). The lowland grassland site is covered with dry, acidophilous, short-grass vegetation. The highland site is a species-rich stand of wet *Cirsium* meadow, and the mountain site is a *Nardus* grassland. Table 1 provides a more detailed description of the grasslands' climate, vegetation, and soil characteristics.

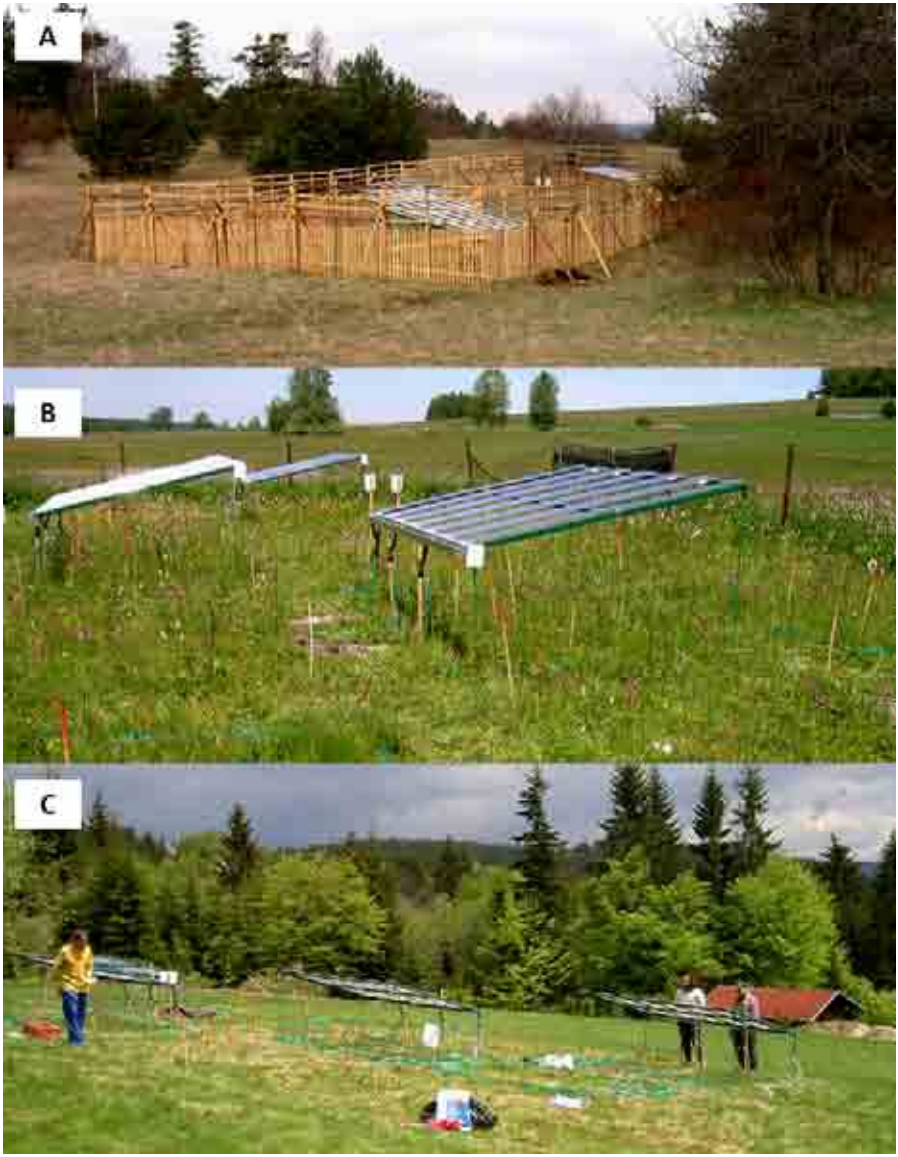

Fig. 1. *Lowland (***A***), highland (***B***), and mountain (***C***) grasslands studied using experimental rainout shelters.*

Table 1. *Key vegetation, soil, and climate characteristics of three grasslands. MAP = mean annual precipitation; MAT = mean annual temperature. Adapted from Holub et al. (2015).*

Characteristic	Lowland	Highland	Mountain
Climate and vegetation			
Latitude	48°49´N	49°43´N	49°30´N
Longitude	16°00´E	15°58´E	18°32´E
Elevation (m a.s.l.)	320	530	860
MAP (mm)	529	762	1,258
MAT (°C)	9.6	7.0	6.8
Plant community	*Potentillo arenariae-Agrostietum vinealis*	*Polygono-Cirsietum palustris*	*Nardo-Callunetea*
Dominant plant species	*Festuca ovina, Achillea collina*	*Sanguisorba officinalis, Cirsium palustre*	*Nardus stricta, Festuca rubra*
Land use history	*Grazed by sheep or goats*	*Mown three times per year*	*Mown once per year*
Soil characteristics			
pH (H_2O)	5.4	5.3	4.8
pH (KCl)	4.4	4.2	3.6
Organic matter (%)	8.3	16.3	13.1
N_{total} (%)	0.32	0.43	0.40
P (mg kg^{-1})	31.0	18.0	2.0
K (mg kg^{-1})	309	116	134
Ca (mg kg^{-1})	1,079	1,543	339
Mg (mg kg^{-1})	155	160	63
Pedon classification	Ranker type	Brown acid gleyed	Spodo-dystric cambisol

The precipitation records in lowlands and highlands show that the third experimental growing season of 2008 was the driest while the 2009 and 2010 growing seasons were wetter than previous years. Finally, substantially more precipitation was measured at the mountain site during the final growing season of 2010 in contrast to previous years, when marked drought periods had been observed during the summer months (Fig. 2). During 2006, the lowest amount of precipitation (168 mm) was recorded in the lowland site during the first part of the growing season (Fig. 2). In comparison with 2006, the total precipitation measured in 2007 was lower in the lowlands by 141 mm and in the highlands by 75 mm. The decreased precipitation from the end of May to the middle of July at the highland site was partly compensated by a higher underground water table lasting for the first several months due to the melting of a large amount of snow. More detailed data are given in Fiala et al. (2012).

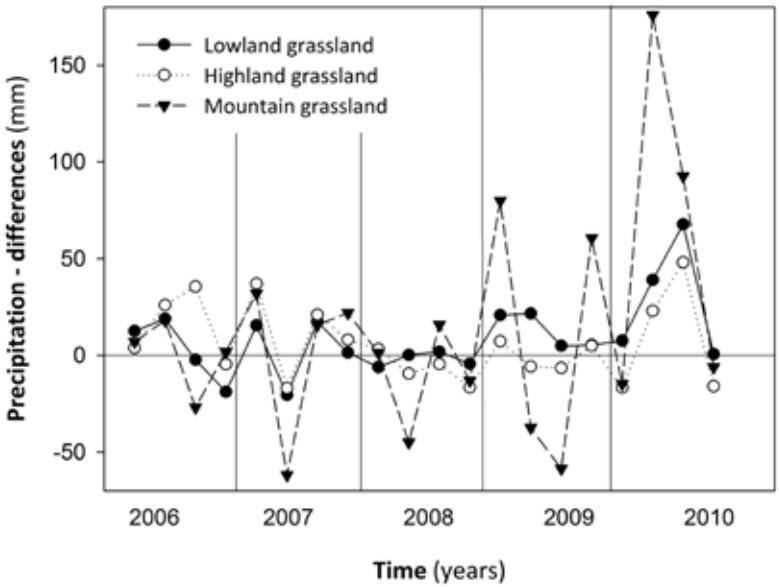

Fig. 2. *Differences from long-term means (1961–1990) in the amounts of precipitation recorded at meteorological stations in Kuchařovice (lowlands), Svratouch (highlands), and Lysá hora (mountains). The stations are ca 9, 4, and 8 km from the studied sites, respectively, and calculated for quarters of 2006–2010. Adapted from Fiala et al. (2012).*

2.2. Experimental design

Dedicated field experiments were set up in order to determine grasslands' responsiveness to different rainfall regimes. Twelve 2 x 3 m plots were laid out in an area of relatively homogeneous grasslands at each of the 3 locations. The locations were chosen along the altitudinal gradient and increased ambient precipitation. Four replications of each variant were made in a block design. Rainout shelters constructed above the grass stand canopies and a gravity irrigation system simulated three scenarios: (1) rainfall reduced by 50% (dry treatment), (2) rainfall enhanced by 50% (wet treatment), and (3) the full natural rainfall of the given growing season (ambient treatment). The rainout shelters constructed over the experimental plots consisted of a steel frame supporting plastic transparent strips (small troughs, see Yahdjian & Sala 2002) covering 50% of the plots. For a more detailed description see Fiala et al. (2012). Rainwater intercepted by the strips in the dry treatment was collected and piped as gravity irrigation into the corresponding wet treatment plots (see Fiala et al. 2012).

2.3. Plant biomass analyses

AP was determined annually by harvesting all above-ground biomass at the times of peak above-ground biomass during the 2006–2010 growing seasons. Four replicates of 0.2 × 0.4 m rectangles were harvested within each plot in the three grassland types. Plant samples were dried to a constant weight (at 60°C) and weighed. For more details see Fiala et al. (2009). In addition, total below-ground plant biomass (TBB) was studied in all treatments using the coring method. Eight soil cores (9.4 cm in diameter, 15 cm deep, n = 8) were collected at the end of each growing season. Collected samples were washed in nylon bags and

on sieves of 0.5 mm mesh size and dried to constant weight. TBB was separated into biomass of total roots (RB) and biomass of rhizomes with shoot bases.

2.4. Data analyses

The data were evaluated by analysis of variance using the STATISTICA 12 statistical package (StatSoft, Tulsa, OK, USA). Tukey's post-hoc test was used to compare means. Whether the mean of a single variable differed from a constant was tested using one-sample *t*-tests. Regression analysis was performed between below-ground biomass and precipitation to determine whether these parameters were related. Means from 2006–2010 were used in Fig. 4. All data were tested for normality and confirmed to be normally distributed.

3. RESULTS AND DISCUSSION

3.1. Effect of rainfall input on above- and below-ground plant parts

Plants are able to acclimate successfully to abiotic stress and reveal phenotypic plasticity in response to environmental variability. Here, the largest effect of precipitation on AP was observed in the dry lowland grassland. At this site, AP was 42–113% higher in the wet than in the dry treatment, except in 2009 (Table 2). In contrast, precipitation had no significant effect on AP in the highland and mountain grasslands. In the highland grasslands, only a cumulative effect of reduced precipitation was visible during the final 2 years of the experiment (Table 2).

Table 2. *Mean values (± standard deviation) of above-ground productivity (g m^{-2} $year^{-1}$) under different amounts of precipitation (dry, ambient [Amb], and wet treatments) recorded over 5 years (2006–2010). Results of Tukey's post-hoc HSD test for precipitation treatment and year comparison was used. Different letters denote significantly different values at $p \leq 0.05$ separately within each grassland site. Adapted from Holub et al. (2015).*

Lowland grasslands			Highland grasslands			Mountain grasslands		
Dry	**Amb**	**Wet**	**Dry**	**Amb**	**Wet**	**Dry**	**Amb**	**Wet**
2006								
273 ±21^{ab}	287 ±42^{abc}	389 ±126^{bcd}	665 ±199^{f}	492 ±112^{abcde}	581 ±113^{cdef}	396 ±115^{abcd}	419 ±31^{abcde}	472 ±165^{bcdef}
2007								
191 ±53^{a}	330 ±127^{abcd}	406 ±134^{bcd}	623 ±139^{ef}	593 ±122^{def}	587 ±11^{cdef}	553 ±162^{def}	571 ±39f	544 ±186ef
2008								
372 ±62^{bcd}	450 ±79^{d}	607 ±291^{d}	449 ±106^{abcd}	505 ±101^{abcdef}	419 ±90^{abc}	374 ±72^{abc}	396 ±46^{abcd}	422 ±74^{abcdef}
2009								
421 ±42^{c}	453 ±49^{d}	434 ±49^{c}	386 ±113^{ab}	394 ±142^{ab}	472 ±86^{abcde}	450 ±62^{bcdef}	520 ±128^{bcdef}	506 ±198^{cdef}
2010								
257 ±14^{ab}	372 ±59^{bcd}	425 ±77^{c}	355 ±51^{a}	423 ±111^{abc}	536 ±134^{bcdef}	282 ±67^{a}	368 ±121^{ab}	355 ±118^{ab}

In contrast, we found a reducing effect of decreased precipitation on growth of below-ground parts in all grasslands studied, although this effect was significant only in highland grasslands (Fig. 3). At this grassland site, the effect of altered precipitation resulted in TBB 26–80% lower for dry treatments than for wet treatments during the 5-year experiment. Our first hypothesis was therefore partly confirmed. On the other hand, the second hypothesis that more intensive reduction in root growth would be found in the drier and warmer lowland grasslands was not confirmed, as altered precipitation had the greatest effect in the wet highland grasslands.

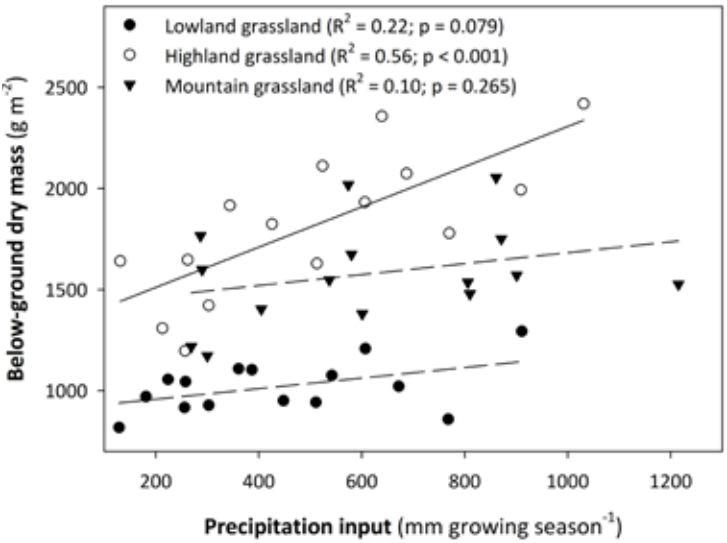

Fig. 3. *Relationships between total below-ground plant biomass and precipitation input along the experimental precipitation gradient in three grasslands. Each point indicates an annual mean. Solid and dash lines show significant and not significant fitted curves, respectively. Adapted from Fiala et al. (2012).*

Several studies have shown that plant species were negatively affected by drought with respect to biomass production and consistently allocated fewer resources to roots (e.g. Weisshuhn et al. 2010). In contrast, other authors have mentioned that water deficits led to significant increase in fine root length density and slight increase in fine root dry weight (Rodrigues et al. 1995; Walter et al. 2011). Harrach & Kunzmann (1983) compared the R/S ratios of various plant communities in different habitats and deduced that RB increased along the sites' increasing moisture gradient. This fact is in accordance with the results recorded in our three grasslands inasmuch as TBB was the highest in the wet *Cirsium* meadow. In addition, root turnover rates can increase exponentially with mean annual temperature for fine roots of grasslands (Gill & Jackson 2000). In the present study, the results recorded in the dry lowland grasslands indicate higher root turnover and lower RB/AP ratios (Fig. 4). Furthermore, summer droughts can lead to increased root mortality, thereby reducing root biomass (see Fiala 2010). Both living and dead root biomass can increase with a decrease in site fertility. All these influences may be reflected in TBB (Holub et al. 2015).

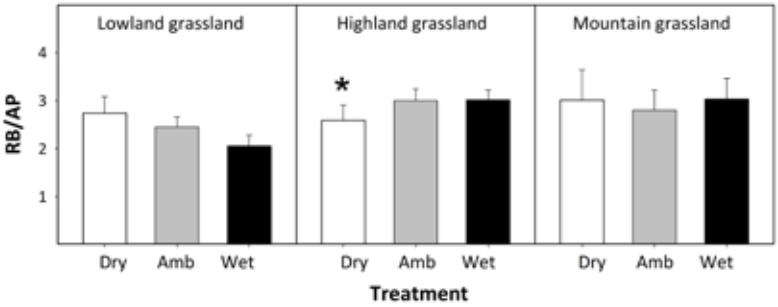

Fig. 4. *Mean values of ratios between root biomass and above-ground productivity under different amounts of precipitation (dry, ambient, and wet treatments) recorded in 5 years (means from 2006–2010) in lowland, highland, and mountain grasslands. * indicates a significantly different value at $p \leq 0.05$ in comparison with other precipitation treatments within the grassland site (Tukey's 2-tailed HSD test after ANOVA). Redrawn according to Holub et al. (2015).*

3.2. Root/shoot ratios and their interannual variations

Lesser amounts of precipitation can often cause reductions in below-ground production in different types of grasslands (Fiala et al. 2012). Accordingly, we had expected to find cumulative decreases in root proportion and lower biomass allocation to below-ground plant parts in drier conditions of the grasslands studied over the 5-year experiment. However, the interannual variability in annual ambient precipitation led to AP and TBB variability. This may have contributed to the substantial interannual variability in R/S ratios. In the present study, R/S ratios increased for some treatments in highland and mountain grasslands in later years. At these locations, increasing RB/AP ratios may have been caused by decreasing AP. Walter et al. (2011) reported that the effect of drought can increase RB in subsequent years and ratios can both decrease and increase. Thus, our third hypothesis that root growth would be reduced over the years as a response to pronounced drought stress was confirmed only in part at the dry lowland grassland site, where the ambient precipitation was the lowest.

4. CONCLUSIONS

Our findings indicate that water availability regulates grassland responses to accumulation of below-ground biomass, which can affect the global carbon cycle. Our results also show a substantial effect of decreased precipitation in reducing root dry mass. These data also confirmed our previous finding that wet highland grasslands, occurring often in Central Europe, were the most sensitive to altered precipitation. Decreases in below-ground dry mass can contribute to destabilization of grassland ecosystems. The thresholds and turning points of the mentioned phenomena require further study, inasmuch as intensification of weather extremes is emerging as one of the most important aspects of climate change. We suggest that long-term experiments studying the effects of such extreme events could provide new and useful insights for science and society.

Acknowledgement

This work was supported by the Ministry of Education, Youth and Sports of the Czech Republic within the National Programme for Sustainability I, grant No. LO1415.

References

Arriaga, L. & Maya, Y. (2007) Spatial variability in decomposition rates in a desert scrub of Northwestern Mexico. *Plant Ecology*, **189**, 213–225.

Bakker, M.R., Augusto, L. & Achat, D.L. (2006) Fine root distribution of trees and understory in mature stands of marine pine (*Pinus pinaster*) on dry and humid sites. *Plant and Soil*, **286**, 37–51.

Beier, C., Beierkuhnlein, C., Wohlgemuth, T. et al. (2012) Precipitation manipulation experiments – challenges and recommendations for the future. *Ecology Letters*, **15**, 899–911.

Ciais, P., Reichstein, M., Viovy, N. et al. (2005) Europe-wide reduction in primary productivity caused by the heat and drought in 2003. *Nature*, **437**, 529–533.

Cook, B.I., Ault, T.R. & Smerdon, J.E. (2015) Unprecedented 21st-century drought risk in the American Southwest and Central Plains. *Science Advances*, **1**, e1400082, doi:10.1126/sciadv.1400082.

Epstein, H.E., Burke, I.C. & Lauenroth, W.K. (2002) Regional patterns of decomposition and primary production rates in the U.S. Great Plains. *Ecology*, **83**, 320–327.

Fay, P.A., Carlisle, J.D., Knapp, A.K., Blair, J.M. & Collins, S.L. (2000) Altering rainfall timing and quantity in a mesic grassland ecosystems: Design and performance of rainfall manipulation shelters. *Ecosystems*, **3**, 308–319.

Fay, P.A., Kaufman, D.M., Nippert, J.B., Carlisle, J.D. & Harper, C.W. (2008) Changes in grassland ecosystem function due to extreme rainfall events: implications for responses to climate change. *Global Change Biology*, **14**, 1600–1608.

Fiala, K. (2010) Belowground plant biomass of grassland ecosystems and its variation according to ecological factors. *Ekologia Bratislava*, **29**, 182–206.

Fiala, K., Tůma, I. & Holub, P. (2009) Effect of manipulated rainfall on root production and plant belowground dry mass of different grassland ecosystems. *Ecosystems*, **12**, 906–914.

Fiala, K., Tůma, I. & Holub, P. (2012) Interannual variation in root production in grasslands affected by artificially modified amount of rainfall. *Scientific World Journal*, ID 805298.

Fischer, Z., Niewinna, M. & Yasulbutaeva, I. (2006) Intensity of organic matter decomposition in various landscapes of Caucasus (Daghestan). *Polish Journal of Ecology*, **54**, 105–116.

Gill, R.A. & Jackson, R.B. (2000) Global patterns of root turnover for terrestrial ecosystems. *New Phytologist*, **147**, 13–31.

Groisman, P.Y. & Knight, R.W. (2008) Prolonged dry episodes over the conterminous united states: New tendencies emerging during the last 40 years. *Journal of Climate*, **21**, 1850–1862.

Harrach, T. & Kunzmann, G. (1983) Wurzelverteilung von Gründlandgesselschaften in vershieden Böden untershiedlichen ökologischen Feuchtengrades. *Root ecology and its practical application* (eds W. Böhm, L. Kutschera & L. Lichtenegger), pp. 335–342. Int. Symp. Gumpenstein, Irdning.

Holub, P., Tůma, I., Záhora, J. & Fiala, K. (2015) Biomass production of different grassland communities under artificially modified amount of rainfall. *Polish Journal of Ecology*, **63**, 291–303.

Hui, D. & Jackson, R.B. (2006) Geographical and interannual variability in biomass partitioning in grassland ecosystems: a synthesis of field data. *New Phytologist*, **169**, 58–93.

Ibrahim, L., Proe, M.F. & Cameron, A.D. (1997) Main effects of nitrogen supply and drought stress upon whole-plant carbon allocation in poplar. *Canadian Journal of Forest Research*, **27**, 1413–1419.

Knapp, A.K., Fay, P.A., Blair, J.M., et al. (2002) Rainfall variability, carbon cycling, and plant species diversity in a mesic grassland. *Science*, **298**, 2202–2205.

Knapp, A.K. & Smith, M.D. (2001) Variation among biomes in temporal dynamics of aboveground primary production. *Science*, **291**, 481–484.

Kreyling, J., Ellis, L., Beierkuhnlein, C. & Jentsch, A. (2008a) Biotic resistance and fluctuating resources are additive in determining invasibility of grassland and heath communities exposed to extreme weather events. *Oikos*, **117**, 1524–1554.

Kreyling, J., Wenigmann, M., Beierkuhnlein, C. & Jentsch, A. (2008b) Effects of extreme weather events on plant productivity and tissue die-back are modified by community composition. *Ecosystems*, **11**, 752–763.

McCulley, R.L., Burke, I.C., Nelson, J.A., Lauenroth, W.K., Knapp, A.K. & Kelly, E.F. (2005) Regional patterns in carbon cycling across the Great Plains of North America. *Ecosystems*, **8**, 106–121.

Meinzer, F.C. 2003. Functional convergence in plant response to the environment. *Oecologia*, **134**, 1–11.

Nippert, J.B., Knapp, A.K. & Briggs, J.M. (2006) Intra-annual rainfall variability and grassland productivity: can the past predict the future? *Plant Ecology*, **184**, 65–74.

Paruelo, J.M., Lauenroth, W.K., Burke, I.C. & Sala, O.E. (1999) Grassland precipitation-use efficiency varies across a resource gradient. *Ecosystems*, **2**, 64–68.

Peñuelas, J., Gordon, C., Llorens, L., Nielsen, T., Tietema, A., Beier, C., Bruna, P., Emmet, B., Estiarte, M. & Gorissen, A. (2004). Nonintrusive field experiments show different plant responses to warming and drought among sites, seasons, and species in a north-south European gradient. *Ecosystems*, **7**, 598–612.

Qaderi, M.M., Kurepin, L.V. & Reid, D.M. (2006) Growth and physiological responses of canola (*Brassica napus*) to three components of global climate changes: Temperature, carbon dioxide and drought. *Physiologia Plantarum*, **128**, 710–721.

Risch, A.C., Jurgensen, M.F. & Frank, D.A. (2007) Effects of grazing and soil micro-climate on decomposition rates in a spatio-temporally heterogeneous grassland. *Plant and Soil*, **10**, 191–201.

Rodrigues, M.L., Pacheco, C.M.A. & Chaves, M.M. (1995) Soil-plant water relation, root distribution and biomass partitioning in *Lupinus albus* L. *Journal of Experimental Botany*, **48**, 947–959.

Silvertown, J., Dodd, M., McConway, K., Potts, J. & Crawley, M. (1994) Rainfall, biomass variation, and community composition in the park grass experiment. *Ecology*, **75**, 2430–2437.

Stanton, N.L. (1988) The underground in grasslands. *Annual Review of Ecology and Systematics*, **19**, 573–589.

Swemmer, A.M., Knapp, A.K. & Snyman, H.A. (2007) Intra-seasonal precipitation patterns and above-ground productivity in three perennial grasslands. *Journal of Ecology*, **95**, 780–788.

Teklay, T. (2007) Decomposition and nutrient release from pruning residues of two indigenous agroforestry species during the wet and dry seasons. *Nutrient Cycling in Agroecosystems*, **77**, 115–126.

Titlyanova, A.A., Romanova, I.P., Kosykh, N.P. & Mironycheva-Tokareva, N.P. (1999) Pattern and process in above-ground and below-ground components of grassland ecosystems. *Journal of Vegetation Science*, **10**, 307–320.

van Oorschot, M., van Gaalen, N., Maltby, E., Mockler, N., Spink, A. & Verhoeven, J.T.A. (2000) Experimental manipulation of water levels in two French reiverine grassland soils. *Acta Oecologica - International Journal of Ecology*, **21**, 49–62.

Walter, J., Nagy, L., Hein, R., Rascher, U., Beierkuhnlein, C., Willner, E. & Jentsch, A. (2011) Do plants remember drought? Hints towards a drought-memory in grasses. *Environmental and Experimental Botany*, **71**, 34–40.

Wedderburn, M.E. Crush, J.R., Pengelly, W.J. et al. (2010) Root growth patterns of perennial ryegrasses under well-watered and drought conditions. *New Zealand Journal of Agriculture Research*, **53**, 377–388.

Weisshuhn, K., Auge, H. & Prati, D. (2010) Geographic variation in the response to drought in nine grassland species. *Basic and Applied Ecology*, **12**, 21–28.

Weltzin, J.F., Loik, M.E., Schwinning, S. et al. (2003) Assessing the response of terrestrial ecosystems to potential changes in precipitation. *Bioscience*, **53**, 941–952.

Werger, M.J.A. (1983) Wurzel/Spross - Verhältnis als Merkmal der Pflanzenstrategie. Root ecology and its practical application (eds W. Böhm, L. Kutschera & L. Lichtenegger), pp. 323–334. Int. Symp. Gumpenstein, Irdning.

Yahdjian, L. & Sala, O.E. (2002) A rainout shelter design for intercepting different amounts of rainfall. *Oecologia*, **133**, 95–101.

Yang, X., Wang, M.X., Huang, Y. & Wang, Y. (2002) A one-compartment model to study soil carbon decomposition rate at equilibrium situation. *Ecological Modelling*, **151**, 63–73.

Yang, Y.H., Fang, J.Y., Pan, Y.D. & Ji, C.J. (2009) Aboveground biomass in Tibetan grasslands. *Journal of Arid Environments*, **73**, 91–95.

Chapter 11

Changing risk of agricultural drought in the Czech Republic

Miroslav Trnka[1], Jan Balek[1], Martin Dubrovský[2], Daniela Semerádová[1]

[1] *Department of Climate Change Impacts on Agroecosystems, Global Change Research Centre, Czech Academy of Sciences, Bělidla 4a, CZ-60300 Brno, Czech Republic*

[2] *Department of Climate Variability and Climate Change Analysis, Global Change Research Centre, Czech Academy of Sciences, Bělidla 4a, CZ-60300 Brno, Czech Republic*

1. INTRODUCTION

After floods, droughts are the most disastrous natural events occurring in the Czech Republic (Brázdil et al. 2007). While the severe droughts of the 19th century occurred in a relatively cooler climate and were caused by a lack of precipitation, more recent droughts in the Czech Republic have been driven primarily by increasing reference evapotranspiration (i.e. potential water requirements) rather than by any substantial decrease in precipitation totals (Brázdil et al. 2012). There are strong concerns that the increase in drought frequency may neutralize the expected positive effects of a longer growing season (e.g. Trnka et al. 2011), decrease the productivity of ecosystems (e.g. Ciais et al. 2005), or change the conditions for key soil processes (Trnka et al. 2013). These concerns were heightened recently by Trnka et al. (2015), who confirmed substantial shifts in drought severity during 1961–2012 within the Czech Republic using newly available high-resolution climate data sets. Although no statistically significant trends in precipitation were noted during 1961–2012 (Brázdil et al. 2012), statistically significant trends toward lower soil moisture content were observed, most notably during May–June. The study also indicated that the probability of drought in April–June increased by 50% when comparing its frequency during 2001–2012 with that from 1961–1980. Additionally, the probability of extreme drought (expressed as soil moisture anomalies more than 3 or even 5 standard deviations from the mean) increased markedly.

These trends have many potential implications. First, they may decrease the effectiveness of typical "drought mitigation strategies" (e.g. attempts to shorten the growing cycle to escape drought conditions later in the season). Second, they would inevitably affect the production of all major crops. The depletion of soil moisture early in the growing season would lead to changes in energy fluxes, which could increase the potential risk of heat waves (e.g. Mueller & Seneviratne 2012). A study by Trnka et al. (2015) added to increasing concerns related to the potentially higher severity and impact of future drought events in Central Europe due to expected climate change (e.g. Dubrovský et al. 2009). While that study relied on the soil moisture model, so-called drought indices also are used frequently to assess the risk of agricultural drought (e.g. Brázdil et al. 2009; Hlavinka et al. 2009; Brázdil et al. 2012). The current study explores likely changes in drought intensity as described by the soil moisture model for the Czech Republic for two periods in which observed data could be used (i.e. 1961–1990 and 1991–2014) as well as expected changes in drought intensity using a range of climate change scenarios. Section 2 describes the data, methods, and definitions. Section 3 examines the outlook for drought intensity and discusses how drought trends compare with changes in snow cover and growing season duration. Section 4 presents the study's conclusions.

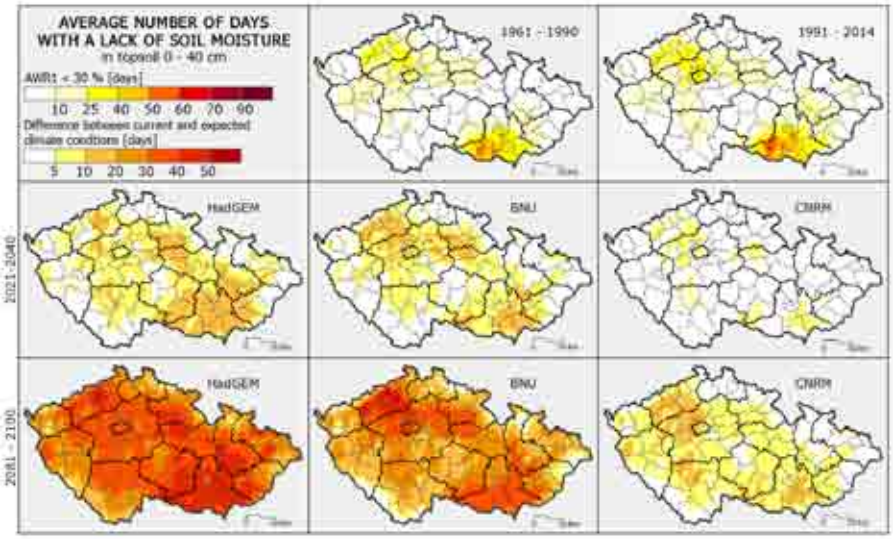

Fig. 1. *Number of days with substantial water stress in the topsoil (0–40 cm) expressed as the median per grid and evaluated period. Maps representing 1961–1990 and 1991–2014 are based on observed data while the six maps for future climate are from three global climate models and the RCP8.5 emissions scenario. AWR1 = relative saturation of the topsoil.*

2. DATA AND METHODS

2.1. Meteorological data

The meteorological data used in this study was produced as a result of joint projects by the Czech Hydrometeorological Institute, the Global Change Research Centre, and Mendel University in Brno. Climate data include daily minimum and maximum temperatures, total global radiation (combining directly measured shortwave radiation and hours of sunshine duration), precipitation totals, mean wind speed, and air humidity. These data were homogenized and assessed for consistency using AnClim and ProClim software packages (Štěpánek et al. 2009, 2011). To calculate areal means on a daily time step, maps were obtained using universal linear kriging interpolation while considering the effect of altitude on climate variables (see Šercl & Lett 2002 for details). Local linear regression was applied over a diameter of 40 km for climatological stations (e.g. for air temperature) and over a diameter of 20 km for rain gauge stations (for precipitation). Finally, data were interpolated into 5 km grids.

2.2. Climate change scenarios

The climate projections were developed for new emission scenarios referred to as Representative Concentration Pathways (RCPs) (van Vuuren et al. 2011) which represent a larger set of mitigation scenarios compared to those in the Special Report on Emissions Scenarios used in the Fourth Assessment Report of the Intergovernmental Panel on Climate Change. Different RCPs have different targets in terms of radiative forcing for 2100 which vary from 2.6 to 8.5 W m^{-2} (see also Chapter 1 of this book for details).

All these should be considered plausible and no probabilities have been attached to them. These RCPs were developed using different integrated assessment models that include economic, demographic, energy, and simple climate components. Two RCPs were integrated into our analysis: RCP8.5, which represents a pathway of rising radiative forcing leading to 8.5 W m^{-2} in 2100, and RCP4.5, which represents a pathway of stabilization without overshooting and leading to 4.5 W m^{-2} radiative forcing at stabilization in 2100. Corresponding CO_2 concentrations (μmol mol^{-1}) in 2100 for RCP4.5 and RCP8.5 are 533 μmol mol^{-1} and 845 μmol mol^{-1}, respectively. In our study, we used climate projections from three global climate models (GCMs) with very different climate sensitivities (HadGEM2-ES, BNU-ESM, and CNRM-CM5) as well as two RCPs (RCP4.5 and RCP8.5) and three future time slices (2021–2040, 2041–2060, and 2081–2100). HadGEM2-ES projections for 2080–2100 are nearly the hottest and driest (during summer) projections for both northern (latitude 48–75°N; longitude 10°W–40°E) and southern (latitude 30–48°N; longitude 10°W–40°E) Europe. CNRM-CM5 projections are nearly the coolest projections and include a suggested overall increase in precipitation.

2.3. Method of analysis

The principal method used to determine drought (described in detail by Trnka et al. 2015) relies on an analysis of daily soil moisture content in the root zone (as much as 1.0 m deep or the maximum rooting depth). This value was calculated for each grid using the SoilClim model, which had been based on the Allen et al. (1998) model, and which was further modified in part by Hlavinka et al. (2011). SoilClim applies the Penman–Monteith method to estimate reference evapotranspiration. In this study, we accounted for other factors that affect soil moisture, phenophase development, root growth, and snow cover accumulation or melting for winter wheat as the cover crop. In order to simplify the calculation procedure, the soil was considered to have a soil water holding capacity of 170 mm per m depth (with 1 m also set as the maximum rooting depth). Unlike Trnka et al. (2015), we did not consider horizon obstruction, slope, aspect, or differing land cover. As an indicator of drought, we considered the number of days when the relative saturation of the topsoil (0–40 cm; AWR1) was less than 30% of the maximum water holding capacity of the topsoil, where most roots are concentrated. This relative saturation value was considered to be the threshold below which soil water uptake is reduced substantially through decreased soil water potential preventing plants from obtaining the required amount of water.

In order to assess the factors contributing to drought, we included an analysis of snow cover duration (i.e. the number of days with snow cover > 3 cm of freshly fallen snow) and the number of tropical days (i.e. days with maximum daily temperature > 30°C). Snow cover was estimated based on daily maximum and minimum temperatures and precipitation totals using the SnowMAUS model, which was validated for the Central European region by Trnka et al. (2010). When calculating evapotranspiration, an adjustment for the atmospheric CO_2 concentration (533 μmol mol^{-1} for RCP4.5 and 845 μmol mol^{-1} for RCP8.5) was made by reducing the reference evapotranspiration using a scaling factor (Kruijt et al. 2008). The scaling factors for the 2090s were estimated to be 0.94 (RCP4.5) and 0.88 (RCP8.5) of baseline values.

3. RESULTS AND DISCUSSION

We found that the frequency of AWR1 < 30% substantially increased during the period of observed records (i.e. 1961–2014). As seen in Fig. 1, there was a clear increase in the number of such days between 1961–1990 and 1991–2014. While during 1961–1990 the median for the entire Czech Republic was close to 6.9

days per year, it increased to 8.1 days per year during 1991–2014 (Table 1). An even more pronounced difference could be seen at altitudes <400 m a.s.l., where the increase was from 11.4 to 12.9 days.

Changes (2081–2100 versus 1961–1990) in drought risk shown in Fig. 1 and Table 1 and measured in terms of the number of days with drought stress are quite substantial. Projected changes for the 21st century obviously differ according to the RCP and GCM used, but a step-change in drought intensity is to be expected for the Czech Republic regardless of the scenario considered. Even the most favourable scenarios project almost twice as many days with water stress during 2021–2040 than were recorded during 1961–1990 (Table 1).

Table 1. *Medians of days with water stress in the soil surface layer (0–40 cm) for two RCP scenarios and three future time slices. Values for 1961–1990 and 1991–2014 are based on observed data.*

RCP4.5					
Median for the entire Czech Republic					
	1961–1990	1991–2014	2021–2040	2041–2060	2081–2100
HadGEM2-ES			14.05	17.00	22.65
BNU-ESM	6.87	8.13	12.80	14.10	18.00
CNRM-CM5			10.45	11.00	12.40
Median for that part of the Czech Republic below 400 m a.s.l.					
HadGEM2-ES			21.20	24.20	31.05
BNU-ESM	11.37	12.92	20.05	21.35	27.50
CNRM-CM5			16.00	15.65	18.30
RCP8.5					
Median for the entire Czech Republic					
	1961–1990	1991–2014	2021–2040	2041–2060	2081–2100
HadGEM2-ES			14.90	20.95	40.90
BNU-ESM	6.87	8.13	13.20	16.45	28.85
CNRM-CM5			10.70	11.70	14.70
Median for that part of the Czech Republic below 400 m a.s.l.					
HadGEM2-ES			22.05	28.50	50.05
BNU-ESM	11.37	12.88	20.85	24.80	40.25
CNRM-CM5			16.35	16.70	20.30

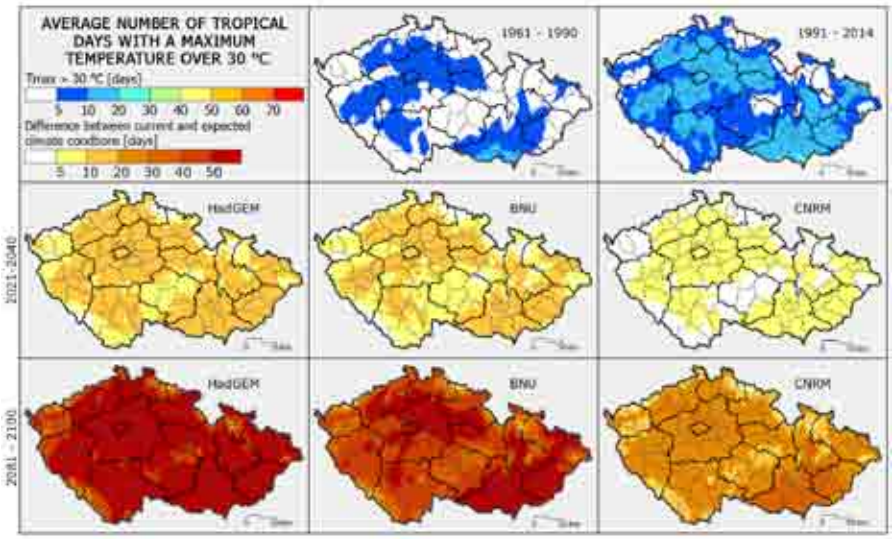

Fig. 2. *Number of days with daily maximum temperature (Tmax) > 30°C expressed as the median per grid and evaluated period. Maps representing 1961–1990 and 1991–2014 are based on observed data while the six maps for future climate represent three global climate models and the RCP8.5 emissions scenario.*

The maps in Fig. 1 show a substantial increase in drought risk, which is a logical consequence of increases in temperature, global radiation, and water vapour pressure deficit with relatively small changes in precipitation. The displayed changes exhibit relatively high inter-GCM agreement in terms of the trend's character (though not its magnitude) and should be considered in relationship with the RCP used. In particular, the results for RCP8.5 and the end of the 21st century, which look rather extreme, are worthy of discussion. First, this projection relates to the end of the 21st century and the RCP8.5 emission scenario, which is considered among the most extreme emission scenarios. As a consequence, drought conditions for the near future as well as those for less extreme emissions are less severe (Table 1). Nonetheless, the risk of drought under future climate conditions should be of major concern. This is also because Figs. 2 and 3 showed quite a marked increase in the number of tropical days (which will be made worse by the drying soil profile) together with a major decrease in the amount of winter snow. These shifts will inevitably lead to a decrease in the soil moisture reserve available at the beginning of the growing season, make growing winter crops more difficult (as the probability of frost damage will increase), and increase the exposure of whatever crop is grown to drought later in the season. These results are consistent with the findings from such recent studies as those of Brázdil et al. (2015) for the Czech Republic, Dubrovský et al. (2014) for Central Europe, and Dai (2013) for the entire world.

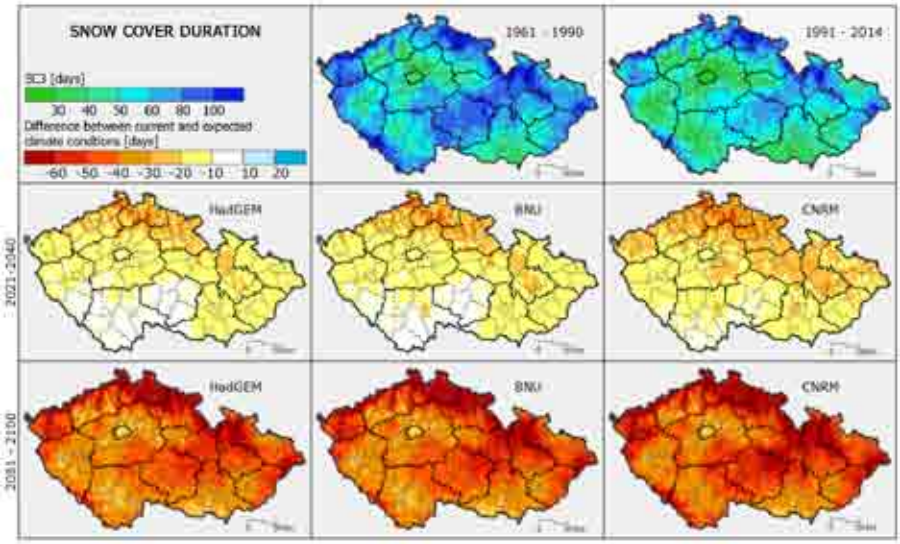

Fig. 3. *Number of days with snow cover > 3 cm (SC3) expressed as the median per grid and evaluated period. Maps representing 1961–1990 and 1991–2014 are based on observed data while the six maps for future climate represent three global climate models and the RCP8.5 emissions scenario.*

4. CONCLUSIONS

During 1961–2014, a period for which observed data were available, we noted a trend toward increased drought occurrence at most stations. These tendencies were followed also by an increase in the number of tropical days and a decrease in snow cover duration. The projections used for climate change in the Czech Republic indicate a risk of prolonged and intense drought episodes and a marked increase in the number of days that could be characterized as extremely dry. This would have a major impact on the agriculture, forestry, and water management sectors. It would adversely influence the stability of agricultural production, wood increments, and river flows and consequently water provisioning. With increased drought episode extremity (and its apparent coupling with increased numbers of tropical days), it is very likely that extreme impacts (e.g. large and substantial declines in agricultural and forest production, extensive forest fires, and regional water resource scarcities) will become a reality.

Acknowledgement

This work was supported by the Ministry of Education, Youth and Sports of the Czech Republic within the National Programme for Sustainability I, grant No. LO1415.

References

Allen, R.G., Pereira, L.S., Raes, D. & Smith, M. (1998) *Crop evapotranspiration (guidelines for computing crop water requirements)*. FAO Irrigation and Drainage Paper No. 56. Food and Agriculture Organization of the United Nations, Rome.

Brázdil, R., Kirchner, K., Březina, L. et al. (2007) *Selected Natural Extremes and their Impacts in Moravia and Silesia*

(in Czech). Masarykova univerzita, Český hydrometeorologický ústav, Ústav Geoniky Akademie věd České republiky, v.v.i., Brno, Praha, Ostrava.

Brázdil, R., Trnka, M. et al. (2015) *Drought in the Czechlands, past, present and future* (in Czech). Global Change Research Centre, Brno.

Brázdil, R., Trnka, M., Dobrovolný, P., Chromá, K., Hlavinka, P. & Žalud, Z. (2009) Variability of droughts in the Czech Republic, 1881–2006. *Theoretical and Applied Climatology*, **97**, 297–315.

Brázdil, R., Zahradníček, P., Pišoft, P., Štěpánek, P., Bělínová, M. & Dobrovolný, P. (2012) Temperature and precipitation fluctuations in the Czech Republic during the period of instrumental measurements. *Theoretical and Applied Climatology*, **110**, 17–34.

Ciais, P., Reichstein, M., Viovy, N. et al. (2005). Europe-wide reduction in primary productivity caused by the heat and drought in 2003. *Nature*, **437**, 529–533.

Dai, A. (2013) Increasing drought under global warming in observations and models. *Nature Climate Change*, **3**, 52–58

Dubrovský, M., Hayes, M., Duce, P., Trnka, M., Svoboda, M., & Zara, P. (2014) Multi-GCM projections of future drought and climate variability indicators for the Mediterranean region. Regional Environmental Change, 14, 1907–1919.

Dubrovský, M., Svoboda, M.D., Trnka, M. et al. (2009) Application of relative drought indices in assessing climate-change impacts on drought conditions in Czechia. *Theoretical and Applied Climatology*, **96**, 155–171.

Hlavinka, P., Trnka, M., Balek, J. et al. (2011) Development and evaluation of the SoilClim model for water balance and soil climate estimates. *Agriculture and Water Management*, **98**, 1249–1261.

Hlavinka, P., Trnka, M., Semerádová, D., Dubrovský, M., Žalud, Z. & Možný, M. (2009) Effect of drought on yield variability of key crops in Czech Republic. *Agricultural and Forest Meteorology*, **149**, 431–442.

Kruijt, B., Witte, J.-P.M., Jacobs, C.M.J. & Kroon, T. (2008) Effects of rising atmospheric CO_2 on evapotranspiration and soil moisture: A practical approach for the Netherlands. *Journal of Hydrol*ogy, **349**, 257–267.

Mueller, B. & Seneviratne, S.I. (2012) Hot days induced by precipitation deficits at the global scale. *Proceedings of the National Academy of Sciences of the United States of America*, **109**, 12398–12403.

Šercl, P. & Lett, P. (2002) *Calculation of precipitation grids in GIS – with use of ArvView Spatial Analyst* (in Czech). Uživatelská příručka verze 2.0.1, ČHMÚ, OPV, Praha.

Štěpánek, P., Zahradníček, P., Brázdil, R. & Tolasz, R. (2011) *Methodology of Data Quality Control and Homogenization of Time Series in Climatology* (in Czech). ČHMÚ, Praha.

Štěpánek, P., Zahradníček, P. & Skalák P. (2009) Data quality control and homogenization of air temperature and precipitation series in the area of the Czech Republic in the period 1961–2007. *Advances in Science and Research*, **3**, 23–26.

Trnka, M., Brázdil, R., Možný, M. et al. (2015). Soil moisture trends in the Czech Republic between 1961 and 2012. *International Journal of Climatology*, **35**, 3733–3747

Trnka, M., Eitzinger, J., Semerádová, D. et al. (2011) Expected changes in agroclimatic conditions in Central Europe. *Climatic Change*, **108**, 261–289.

Trnka, M., Kersebaum, K.C., Eitzinger, J. et al. (2013) Consequences of climate change for the soil climate in Central Europe and the central plains of the United States. *Climatic Change*, **120**, 405–418.

Trnka, M., Kocmánková, E., Balek, J. et al. (2010) Simple snow cover model for agrometeorological applications. *Agricultural and Forest Meteorology*, **150,** 1115–1127.

van Vuuren DP, Edmonds, J., Kainuma, M. et al. (2011) The representative concentration pathways: an overview. *Climatic Change*, **109**, 5–31.

Chapter 12

How does temperature affect carbon dioxide emissions?

Eva Dařenová, Manuel Acosta

Department of Matters and Energy Fluxes, Global Change Research Centre, Czech Academy of Sciences, Bělidla 4a, CZ-60300 Brno, Czech Republic

1. INTRODUCTION

Respiration is a series of metabolic processes in a cell that catabolize organic molecules to liberate energy, water, and CO_2. Most living organisms, including plants, animals, and microorganisms, share similar pathways of respiration to obtain energy while releasing CO_2. The energy is then used for growth, maintenance of existing structures and functions, transport of metabolites and ions, protein regeneration, and repair processes. Measurements of respiration are often quantified as the rate of CO_2 efflux into the atmosphere.

Ecosystem respiration returns a large portion of the CO_2 assimilated by photosynthesis, and the balance between these two carbon fluxes determines whether ecosystems represent CO_2 sinks or sources (see also Chapter 6 of this book for details).

CO_2 efflux from the ecosystem can be divided into the efflux from the soil and the efflux from above-ground plants. CO_2 efflux from the soil results from autotrophic respiration by live roots and heterotrophic respiration mainly by micro-organisms (Kuzyakov et al. 2005). The above-ground CO_2 efflux in forest ecosystems can be divided into CO_2 efflux from stems, branches, and leaves (Acosta et al. 2008).

Each component described above is affected by such common factors as temperature, water and substrate availability, as well as a few specific factors. Specific factors for soil include soil structure (Arrouays et al. 2001), amount and quality of litter (Buchmann 2000), and root amount (Craine & Wedin 2002). Woody tissue CO_2 efflux, on the other hand, can be influenced by growth or sap flow (Teskey & McGuire 2002; Gruber et al. 2009).

In most cases, the most important factor for all components of ecosystem CO_2 efflux is temperature. Temperature affects enzyme activity; substrate, O_2, and CO_2 diffusion; and CO_2 solubility in water. CO_2 efflux generally increases up to its maximum at a temperature of about 40°C and then declines (Atkin & Tjoelker 2003). CO_2 efflux at low temperatures is controlled in particular by enzyme activity, while at high temperatures it is most influenced by substrate supply (Atkin & Tjoelker 2003). In many ecosystems, the temperature of respiring cells does not reach values high enough to limit CO_2 efflux, and so the relationship between CO_2 efflux and temperature is often described as exponential (Lloyd & Taylor 1994). To determine the sensitivity of CO_2 efflux to temperature, the Q_{10} factor (that factor by which CO_2 efflux is multiplied when temperature increases by 10°C) has been widely used (Davidson et al. 2006).

In this study, we investigated the relationship between temperature and CO_2 efflux from different ecosystem components of a spruce forest and a wetland. In addition, we also examined factors that disturbed this relationship.

2. MATERIALS AND METHODS

2.1. Site description

For this study, we selected a 30-year-old Norway spruce (*Picea abies*) forest and a wetland ecosystem. The forest stand is located at the Bílý Kříž experimental research site (Beskydy Mountains, 49°30′N, 18°32′E, 875 m a.s.l.). This area has a cool (mean annual air temperature 6.8°C) and humid (annual mean relative humidity 80%) climate with high annual precipitation (the mean for 1998–2012 was 1,258 mm). The soil is classified as Haplic Podzol. For details see Acosta et al. (2013) and Chapter 5 of this book.

The wetland ecosystem is a sedge–grass marsh located near Třeboň, South Bohemia, Czech Republic (49°01′N, 14°46′E; 426 m a.s.l.). The site is characterized by mean annual air temperature of 7.6°C and mean annual precipitation of 614 mm (means for 1977–2013). The soil is classified as histosoil with a high amount of organic matter in the upper soil layers. Vegetation consists mainly of tall sedges (*Carex acuta, Carex vesicaria*) and hygrophytic grasses (especially *Calamagrostis canescens*). For more details see Dusek et al. (2012) and Chapter 5 of this book.

2.2. Measurements

CO_2 efflux was measured using closed gasometrical (non-steady-state through-flow) systems. Soil CO_2 efflux in the forest was determined using an automated system for continuous measurements with eight chambers (cylindrical shape, diameter 30 cm, height 20 cm) (Fig. 1). The system measured soil CO_2 efflux sequentially across the eight chambers at 10 min intervals. Therefore, the CO_2 efflux rate for each chamber was available every 80 min. Spruce tree stem CO_2 efflux was determined by applying a system similar to that for the soil component. It included eight chambers placed on the stem at breast height (semi-cylindrical shape, diameter 20 cm, height 20 cm) (Fig. 1). The system measured stem CO_2 efflux sequentially across the eight chambers at 10 min intervals, and the CO_2 efflux rate for each chamber was available every 120 min. For more details, see Pavelka et al. (2004).

Sap flow was measured on six trees using a SF 300 sap flow system (Greenspan Technology, Milperra, Australia) based on the heat pulse velocity method (Köstner et al. 1998).

Fig. 1. *Automated chambers for measurements of soil (left) and stem (right) CO_2 efflux. (Photo by Marian Pavelka.)*

Night-time measurements of CO_2 efflux from needles were carried out when conditions were completely dark (from 21:30 until 23:00) on three representative trees among the forest canopy using a Li-6400 gas exchange system (Li-Cor, Lincoln, NE, USA). Two shoots per tree and whorls oriented to the south–south-west were investigated in the upper canopy (5th whorl, 1-year-old shoots), middle canopy (8th and 10th whorls, 2-year-old shoots), and lower canopy (15th whorl, shoots ≥2 years old).

On the wetland, an automated system with one chamber (cylindrical shape, diameter 30 cm, height 20 cm) was used. This system measured soil CO_2 efflux at 15 min intervals.

All CO_2 efflux measurements were accompanied by temperature measurements: at a soil depth of 1.5 cm or in the cambium of tree stems using PT-100 thermometers (Treston, Částkov, Czech Republic).

Q_{10} was calculated according to the equation:

$$Q_{10} = e^{10\alpha}, \tag{1}$$

where a is the regression coefficient obtained from the exponential relationship between temperature (T) and CO_2 efflux (R). CO_2 efflux was then normalized for a temperature of 10°C (R_{10}) using the equation:

$$R_{10} = \frac{R}{Q_{10}^{\frac{T-10}{10}}}, \tag{2}$$

Data from the forest soil were analysed for the 2010 growing season and from stems for the 2010 and 2011 growing seasons. Data from the wetland were collected during one measurement campaign from 20 September to 27 September 2011. Night-time measurements from the needles were taken during one night after a sunny day and during one night after a cloudy day in summer 2006.

3. RESULTS AND DISCUSSION

3.1. Spruce forest soil

We found that CO_2 efflux was positively correlated with soil temperature. However, the mean regression coefficient (R^2) calculated from the eight chambers over the entire measurement period in 2010 was just 0.57. Darenova et al. (2014) had found even lower values (0.48 and 0.49) for the same site in 2008 and 2009, respectively. This indicates that other factors besides soil temperature affect CO_2 efflux.

We found that water availability had a substantial effect on soil CO_2 efflux rate and its temperature sensitivity. CO_2 efflux rate had a tendency to increase after rain events. A particularly obvious response was observed after a period without precipitation, when the soil was dry. After a rain event, soil CO_2 efflux became significantly greater than it had been, despite similar or even lower soil temperatures. Fig. 2 shows an example of how soil CO_2 efflux responded to a rain event. It shows CO_2 efflux from 3 to 8 July 2010. On 6 July, there occurred 39 mm of rain, and prior to this date there had been 1 week with no precipitation. Increased soil water content substantially enhanced soil CO_2 efflux. Moreover, temperature sensitivity increased from $Q_{10} = 1.20$ to $Q_{10} = 2.22$.

We can conclude from our results that soil temperature is the driving factor for CO_2 efflux from the experimental forest floor, but this relationship also depends strongly on soil water content. This was most evident during periods without rain events, when soil became dry, resulting in slower diffusion of substrates

to microbes (Stark & Firestone 1995) and lower enzyme activity (Steinweg et al. 2012). When soil water content drops below a certain threshold (about 10%) and is under drought stress, soil even can show a complete lack of dependence on temperature (Xu & Qi 2001).

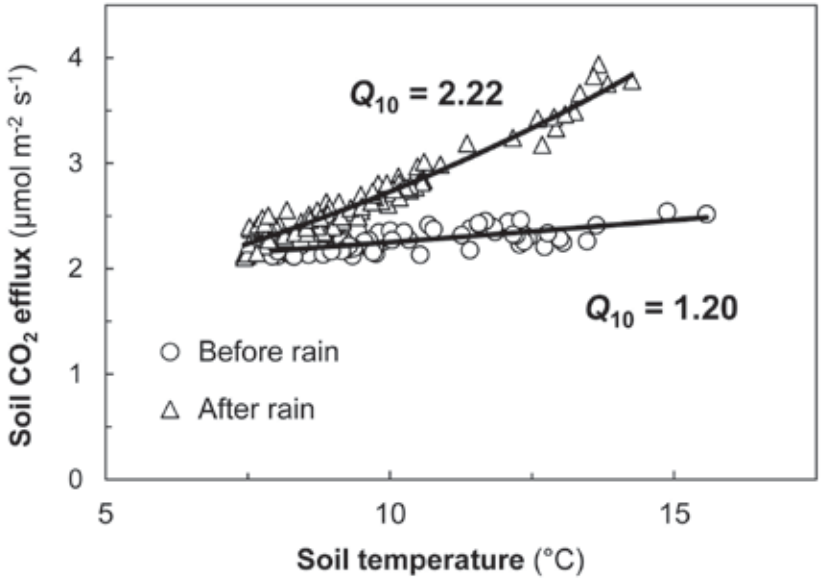

Fig. 2. *Soil CO_2 efflux response to soil temperature in spruce forest during 3–8 July 2010. Circles represent data from prior to 6 July, upon which date 39 mm of precipitation occurred, and triangles represent data from after this date. Q_{10} indicates the temperature sensitivity of soil CO_2 efflux.*

3.2. Wetland soil

At the wetland site, we began measurements when the water table was around 0 cm. The water table gradually decreased to 8.2 cm below the soil surface on 25 September. During this period, soil CO_2 efflux followed a daily pattern of changes in soil temperature with maxima in early afternoon and minima at night (Fig. 3). However, the relationship between temperature and soil CO_2 efflux was not strong ($R^2 = 0.59$). This can be attributed to the gradually decreasing water table accompanied by the increasing trend of CO_2 efflux. After a heavy rain event and rapid increase in the water table, soil CO_2 efflux dropped rapidly to approximately 0.2 µmol m^{-2} s^{-1}, despite temperature's remaining around the same level as it had been.

Unlike the forest soil, the wetland soil was not limited by water supply. On the contrary, large amounts of soil water, typical for wetland ecosystems, reduced the soil's oxygen content. This resulted in anoxic conditions within the soil and suppression of aerobic decomposition of organic matter, which alternated with slower anaerobic decomposition as described by Santruckova et al. (2004). This led to the development of CH_4 and its release into the atmosphere (Knorr et al. 2008).

These results show that soil temperature in wetland ecosystems drives soil CO_2 efflux only when the water table drops below the soil surface. Even under these conditions, however, CO_2 efflux is significantly affected by changes in soil water content. With a high water table, soil CO_2 efflux is suppressed by the lack of oxygen and so soil water content becomes the driving factor for soil CO_2 efflux.

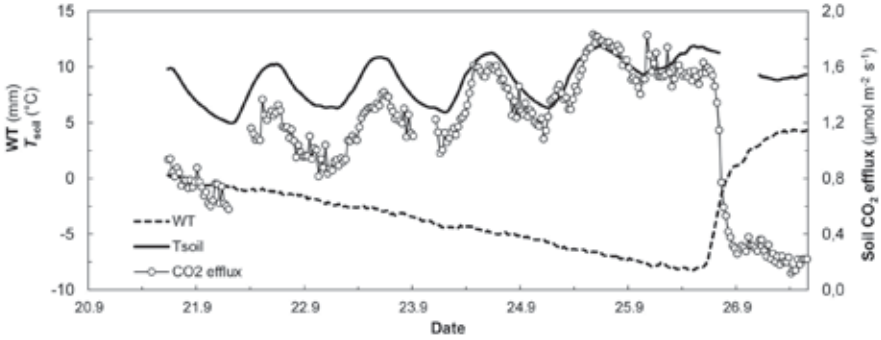

Fig. 3. *Diurnal courses of water table level (WT), soil temperature (T_{soil}), and soil CO_2 efflux at the wetland site during 20–26 September 2011.*

3.3. Spruce tree stems

Stem CO_2 efflux was highly correlated with soil temperature for the entire growing season (May–October; R^2 = 0.87 in 2010 and 0.81 in 2011). In our conditions, we determined two factors which affected this relationship.

The first was stem growth, which resulted in CO_2 efflux rates higher than were estimated using just temperature. The greatest stem growth at this site usually occurred in June and July, and during this time the activated dividing cells of the cambium, and consequent cell differentiation, have extra respiratory requirements (so-called growth respiration; Gruber et al. 2009).

Moreover, as shown in Fig. 4, during 2010 we observed a mild suppression of CO_2 efflux at midday. This figure displays sap flow rate and stem CO_2 efflux normalized to a temperature of 10°C (we thus excluded CO_2 efflux fluctuations resulting from stem temperature fluctuations; Buzkova et al. 2015). Sap flow reached its maxima at midday, when normalized CO_2 efflux reached its minima. Teskey & McGuire (2007) had explained such midday decline in stem CO_2 efflux as a result of increased transport of newly produced CO_2 by xylem up along the stem. As stem temperature was the driving factor, this suppression was not clear without normalization of stem CO_2 efflux.

In addition, we found that stem CO_2 efflux correlated with sap flow rate during days with low soil moisture in 2010 and during days with normal (above 12%) soil moisture in 2011. This indicates that sap flow may also regulate the dependency of stem CO_2 efflux on temperature over longer time periods. Nevertheless, this effect is probably more complex and involves additional environmental and physiological factors.

From our results, we can conclude that stem temperature was indisputably the driving factor for stem CO_2 efflux in a young spruce forest. The strength of this relationship may have been slightly disturbed by higher respiration during stem growth or by sap flow rate.

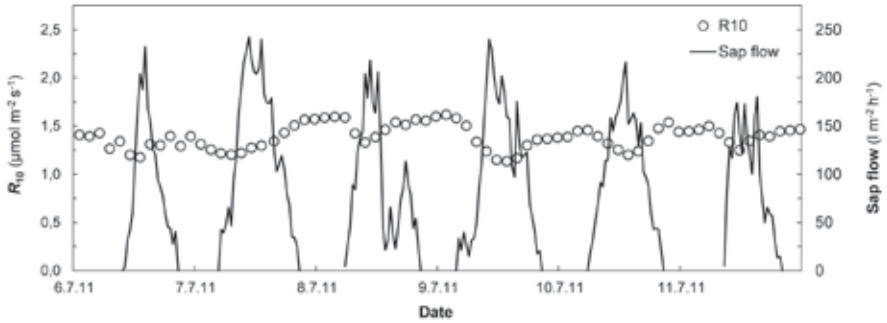

Fig. 4. *Diurnal courses of stem CO_2 efflux, normalized to a temperature of 10°C (R_{10}) (2 h time step), and sap flow (30 min time step) for Norway spruce during 6–11 July 2011.*

3.4. Spruce needles

In general, shoot CO_2 efflux during the night is affected by temperature. Moreover, this effect also presents a gradient difference depending upon the position of the whorl. There were substantial differences in measured shoot CO_2 efflux between the upper (5th) and lower (15th) whorls. The mean values of needle CO_2 efflux (night-time measurements) measured after sunny and cloudy days at different whorls are presented in Table 1. Mean shoot CO_2 efflux for the upper and lower whorls were 1.4 and 0.3 µmol m^{-2} s^{-1}, respectively. This difference is most likely related to canopy closure and the location of the shoot and/or whorl within the canopy. It is also possible that the forest canopy presents a spatial pattern that is responsible for a specific solar radiation regime (Urban et al. 2007) driving temperature differences among whorls. The relationship between temperature and needle CO_2 efflux is influenced by water availability in the soil, however, thus leading to a decrease in CO_2 efflux under water stress conditions (Muraoka et al. 2000). Moreover, Urban et al. (2007), in a study of the same investigated forest stand, had demonstrated that needle CO_2 efflux during night-time had a gradient difference that may have been connected to cloudy and sunny days during the photoperiod. This means that previous irradiation conditions during the day also influenced night-time needle CO_2 efflux.

Table 1. *Means (± standard deviations) of needle CO_2 efflux from dark respiration at different whorls (the 5th whorl is an upper whorl, the 15th whorl is a bottom whorl) in a spruce forest stand at the Bílý Kříž experimental site.*

Whorl	Needle CO_2 efflux (µmol m^{-2} s^{-1})
5th	1.3 (± 0.3)
8th	1.2 (± 0.3)
10th	0.5 (± 0.2)
15th	0.3 (± 0.1)

4. CONCLUSIONS

CO_2 efflux from different ecosystem components is driven by temperature. The strength of the temperature effect can be reduced by other, component-specific factors. The relationship between temperature and soil CO_2 efflux is affected by water stress through slower diffusion of substrates to microbes and lower enzyme activity or, in contrast, by high soil water content due to a lack of oxygen. The relationship between temperature and stem CO_2 efflux is affected by stem growth and sap flow rate. Finally, the relationship between temperature and needle CO_2 efflux can be affected by water stress and previous photoperiod type (sunny versus cloudy days).

Acknowledgement

This work was supported by the Ministry of Education, Youth and Sports of the Czech Republic within the National Programme for Sustainability I, grant No. LO1415. The authors wish to thank Dr. Ryan Patrick McGloin, Ph.D. for assistance with the language of this chapter.

References

Acosta, M., Pavelka, M., Montagnani, L. et al. (2013) Soil surface CO_2 efflux measurements in Norway spruce forests: Comparison between four different sites across Europe — from boreal to alpine forest. *Geoderma*, **192**, 295–313.

Acosta, M., Pavelka, M., Pokorny, R., Janous, D. & Marek, M.V. (2008) Seasonal variation in CO_2 efflux of stems and branches of Norway spruce trees. *Annals of Botany*, **101**, 469–477.

Arrouays, D., Deslais, W. & Badeau, V. (2001) The carbon content of topsoil and its geographical distribution in France. *Soil Use and Management*, **17**, 7–11.

Atkin, O.K. & Tjoelker, M.G. (2003) Thermal acclimation and the dynamic response of plant respiration to temperature. *Trends in Plant Science*, **8**, 343–351.

Buchmann, N. (2000) Biotic and abiotic factors controlling soil respiration rates in *Picea abies* stands. *Soil Biology & Biochemistry*, **32**, 1625–1635.

Buzkova, R., Acosta M., Darenova, E., Pokorny, R. & Pavelka, M. (2015) Environmental factors influencing the relationship between stem CO_2 efflux and sap flow. *Trees-Structure and Function*, **29**, 333–343.

Craine, J. M. & Wedin D.A. (2002). Determinants of growing season soil CO_2 flux in a Minnesota grassland. *Biogeochemistry*, **59**, 303–313.

Darenova, E., Pavelka, M. & Acosta, M. (2014) Diurnal deviations in the relationship between CO_2 efflux and temperature: A case study. *Catena*, **123**, 263–269.

Davidson, E.A., Janssens, I.A. & Luo, Y.Q. (2006) On the variability of respiration in terrestrial ecosystems: moving beyond Q_{10}. *Global Change Biology*, **12**, 154–164.

Dusek, J., Cizkova, H., Stellner, S., Czerny, R. & Kvet, J. (2012) Fluctuating water table affects gross ecosystem production and gross radiation use efficiency in a sedge-grass marsh. *Hydrobiologia*, **692**, 57–66.

Gruber, A., Wieser, G. & Oberhuber, W. (2009) Intra-annual dynamics of stem CO_2 efflux in relation to cambial activity and xylem development in *Pinus cembra*. *Tree Physiology*, **29**, 641–649.

Knorr, K.H., Oosterwoud, M.R. & Blodau, C. (2008) Experimental drought alters rates of soil respiration and methanogenesis but not carbon exchange in soil of a temperate fen. *Soil Biology & Biochemistry*, **40**, 1781–1791.

Köstner, B., Granier, A. & Cermak, J. (1998) Sapflow measurements in forest stands: methods and uncertainties. *Annals of Forest Science*, **55**, 13–27.

Kuzyakov, Y. (2005) Theoretical background for partitioning of root and rhizomicrobial respiration by delta C-13 of microbial biomass. *European Journal of Soil Biology*, **41**, 1–9.

Lloyd, J. & Taylor, J.A. (1994) On the Temperature-Dependence of Soil Respiration. *Functional Ecology*, **8**, 315–323.

Muraoka, H., Tang, Y.H., Terashima, I., Koizumi, H. & Washitani, I. (2000) Contributions of diffusional limitation, photoinhibition and photorespiration to midday depression of photosynthesis in *Arisaema heterophyllum* in natural high light. *Plant, Cell and Environment,* **23**, 235–250.

Pavelka, M., Acosta, M. & Janous, D. (2004) A new device for continuous CO_2 flux measurement in forest stand. *Ecology (Bratislava)*, **23**, 88–100.

Santruckova, H., Picek, T., Tykva, R., Simek, M. & Pavlu, B. (2004) Short-term partitioning of C-14-[U]-glucose in the soil microbial pool under varied aeration status. *Biology and Fertility of Soils*, **40**, 386–392.

Stark, J.M. & Firestone, M.K. (1995) Mechanisms for soil-moisture effects on activity of nitrifying bacteria. *Applied and Environmental Microbiology*, **61**, 218–221.

Steinweg, J.M., Dukes, J.S. & Wallenstein, M.D. (2012) Modeling the effects of temperature and moisture on soil enzyme activity: Linking laboratory assays to continuous field data. *Soil Biology & Biochemistry*, **55**, 85–92.

Teskey, R.O. & McGuire, M.A. (2002) Carbon dioxide transport in xylem causes errors in estimation of rates of respiration in stems and branches of trees. *Plant Cell and Environment*, **25**, 1571–1577.

Teskey, R.O. & McGuire, M.A. (2007) Measurement of stem respiration of sycamore (*Platanus occidentalis* L.) trees involves internal and external fluxes of CO_2 and possible transport of CO_2 from roots. *Plant Cell and Environment*, **30**, 570–579.

Urban O., Janouš D., Acosta M. et al. (2007) Ecophysiological controls over the net ecosystem exchange of mountain spruce stand. Comparison of the response in direct vs. diffuse solar radiation. *Global Change Biology*, **13**, 157–168.

Xu, M. & Qi, Y. (2001) Spatial and seasonal variations of Q_{10} determined by soil respiration measurements at a Sierra Nevadan forest. *Global Biogeochemical Cycles*, **15**, 687–696.

Chapter13

Effect of ozone concentration on net ecosystem production: A case study in a Norway spruce forest

Miloš Zapletal[1], Magda Edwards-Jonášová[1], Stanislav Juráň[2], Otmar Urban[2], Radek Pokorný[3], Marian Pavelka[4], Dalibor Janouš[4], Pavel Cudlín[1]

[1] *Department of Landscape Carbon Storage, Global Change Research Centre, Czech Academy of Sciences, Lipová 9, CZ-37005 České Budějovice, Czech Republic*

[2] *Laboratory of Plant Ecological Physiology, Global Change Research Centre, Czech Academy of Sciences, Bělidla 4a, CZ-60300 Brno, Czech Republic*

[3] *Department of Biomass Allocation, Global Change Research Centre, Czech Academy of Sciences, Bělidla 4a, CZ-60300 Brno, Czech Republic*

[4] *Department of Matters and Energy Fluxes, Global Change Research Centre, Czech Academy of Sciences, Bělidla 4a, CZ-60300 Brno, Czech Republic*

1. INTRODUCTION

Tropospheric ozone is one of the most important phytotoxic air pollutants (Paoletti et al. 2007). There is evidence that ambient ozone concentrations and stomatal fluxes cause detrimental effects in European forests, including visible leaf injuries, growth reduction, and altered sensitivity to biotic and abiotic stresses (Karlsson et al. 2003; UNECE 2005). Three processes are responsible for tropospheric ozone regulation: atmospheric transport, chemical destruction/production, and absorption into dry surfaces. Atmospheric turbulence transports ozone to vegetation cover, where it is taken up by plant stomata or chemical reactions. Global models, driven by observed ecosystem fluxes, suggest net removal by dry deposition onto vegetation cover to be 1,000 ± 200 Tg of ozone per year (Stevenson et al. 2006). Thus, ozone exposure regulation is related to the interplay between mixing from higher levels of the atmosphere and dry deposition of ozone onto surface layers. A highly reactive gas, ozone is simply deposited onto plant surfaces through oxidation. Many studies have shown that the main deposition occurs through plant stomata, which are usually open during daylight hours. Non-stomatal uptake, measured directly when stomata are treated to be closed or indirectly by subtracting stomatal uptake from total flux, is represented by incanopy chemistry, senescent vegetation (Potier et al. 2015), and reactions with soil and water surfaces (Fares et al. 2013a).

A long-term experiment with ozone treatment of Norway spruce (*Picea abies*) trees has demonstrated a change in biomass allocation patterns. Norway spruce invests more into the upper canopy parts and so is more vulnerable to a broad range of disturbances (Pretzsch et al. 2010). Detrimental effects of ozone result in substantial economic losses. Growth reductions derived from a long-term data set have been quantified for deciduous and coniferous trees, respectively, as 18.5% and 6.6% (Braun et al. 2014). Background atmospheric concentrations in northern latitudes have increased since preindustrial times, and it is estimated that for the near future stomatal ozone fluxes will not decrease to non-critical levels (Klingberg et al. 2014). Moreover, comparison of modelling studies indicate that tropospheric ozone load in the 1850s was 30% lower than it is at present (Young et al. 2013). Atmospheric ozone can be removed by deposition onto soil and plant surfaces, stomatal uptake, or various within-canopy reactions dominated by aging of

nitrogen oxides and removal of biogenic volatile organic compounds. Damage to the photosystem apparatus in plants causes reductions in net ecosystem production (NEP), thus slashing the terrestrial ecosystem's capacity to capture atmospheric CO_2. As forest ecosystems represent >50% of terrestrial NEP, the global impact is serious (Paoletti et al. 2010; Cudlín et al. 2013).

Various indices have been established to quantify ozone exposure. Accumulated amount of ozone over the threshold value of 40 nmol mol^{-1} (AOT40) is related to ambient ozone concentration. For better understanding of the real ozone stomatal flux, the flux-based POD_Y index (phytotoxic ozone dose above the flux threshold of Y nmol m^{-2} s^{-1}) has been established. This index takes into account solar radiation, temperature, water vapour pressure deficit, soil water potential, atmospheric ozone concentration, and plant phenology stage (Pleijel et al. 2007). Some studies have suggested linear and non-linear correlations between AOT40 and real flux depending on climate, canopy position, and tree age, among other factors (Matyssek et al. 2004). Moreover, it is worthwhile to use real-world measurements and modelling approaches to establish critical levels of various indices for specific vegetation covers together with their effects (Sicard et al. 2016).

The aims of this study were to (a) measure daily cycles of ozone deposition velocities and fluxes above a Norway spruce forest in the Czech Republic, (b) compare deposition velocities calculated using the gradient method with results from the multiple resistance model, (c) support EU environmental protection policy and risk assessment by calculating micrometeorological indices for accumulated stomatal ozone uptake, and (d) test whether elevated stomatal ozone uptake implies a reduction in NEP.

2. MATERIALS AND METHODS

2.1. Site description

The forest stand selected for this study is located at the Bílý Kříž experimental research site (Beskydy Mountains, 49°30′N, 18°32′E, north-eastern Czech Republic, 875 m a.s.l.) and it forms a part of the CarboEurope-IP (http://www.carboeurope.org) and ICOS (https://www.icos-ri.eu/) networks. The stand (6.2 ha) consists of Norway spruce (99%) and European silver fir (*Abies alba*; 1%) planted on a slope (11–16°) oriented to the south–southwest. The studied stand had been established in 1981 by row planting of 4-year-old seedlings. Planting spacing had been 2 x 1 m and in a north–south row orientation. For a detail description of the location and forest stand, see chapters 4–6 of this book and Urban et al. (2007).

2.2. Meteorological and environmental measurements

Meteorological (air temperature, air relative humidity, global radiation, wind speed) and environmental (ozone concentration) parameters were measured on an experimental tower 36 m tall placed in the forest during the 2007–2009 vegetation periods. In addition, CO_2 exchange was monitored using the eddy covariance method and NEP was calculated. Meteorological, environmental, and ozone concentration measurements at Bílý Kříž have been described in detail by Zapletal et al. (2011, 2012).

2.3. Gradient method and eddy covariance measurements

Total calculated ozone flux and deposition velocity were determined using the gradient method (Fowler & Duyzer 1989; Hummelshoj 1994) from ozone concentrations measured at 5, 15, and 25 m above the ground using $O_3$41M ozone analysers (Environment SA, Paris, France) from July to August 2008 and

from May to September 2009. We added a correction function for temperature to the traditional Monin–Obukhov stability function in accordance with Mölder et al. (1999). An eddy covariance system, described in detail in Chapter 5 of this book, was used to measure friction velocity as well as CO_2 and water vapour fluxes between the forest and atmosphere. Half-hourly averaged water vapour and CO_2 flux values were evaluated for data quality and correlated with micrometeorological measurements.

2.4. Ozone deposition flux model

Modelled deposition velocity for ozone (V_{dmod}) was calculated according to Hicks et al. (1987) using a resistance analogy. Ozone stomatal uptake was calculated according to Emberson et al. (2000). Stomatal ozone flux (F_{sto}) was then calculated according to Cieslik (2004) and Gerosa et al. (2009). Total modelled ozone flux (F_{mod}) was estimated from measured ozone concentration gradients multiplied by the corresponding deposition velocities derived from the resistance analogy. Non-stomatal uptake was calculated as the difference between total ozone flux and stomatal ozone flux. Modelling of total and stomatal ozone flux to the Norway spruce forest stand during the 2008 growing season had been described in detail by Zapletal et al. (2011).

2.5. Ozone dose and exposure

Exposure was calculated as AOT40 for daylight hours only (Fuhrer et al. 1997). Accumulated stomatal flux with no threshold (POD_0) and that above an hourly threshold of 1 nmol m^{-2} s^{-1} (POD_1) were calculated for the 2007, 2008, and 2009 vegetation periods (ICP Vegetation 2009).

2.6. Statistical analysis

The effects of ozone (expressed as concentration and stomatal flux), radiation, temperature, and humidity on NEP were tested using general regression models applied to data from the 2009 growing period. Photosynthetically active radiation intensity, air temperature, and humidity were used as covariates. The forward stepwise method was used for selection of predictors with significant effects at a probability level of 0.05. First, all predictors were tested in a linear form. Then, those models with predictors in the form of a second-degree polynomial and with interactions between ozone and climatic factors were tested. The data for NEP, radiation, humidity, and stomatal flux were square root transformed to obtain normality of the working data. The best model for each form of ozone was selected, and NEP predictions were made using these models.

3. RESULTS AND DISCUSSION

3.1. Ozone deposition velocity

The mean daily cycle of measured and modelled deposition velocities varied approximately from 0.2 to 0.5 cm s^{-1} from July to August 2008 and from 0.35 to 0.75 cm s^{-1} from May to September 2009. The cycle clearly differed from the mean daily course of ozone concentration (Fig. 1). The hourly means of measured and modelled deposition velocity were correlated ($R^2 = 0.45$, $p = 0.01$).

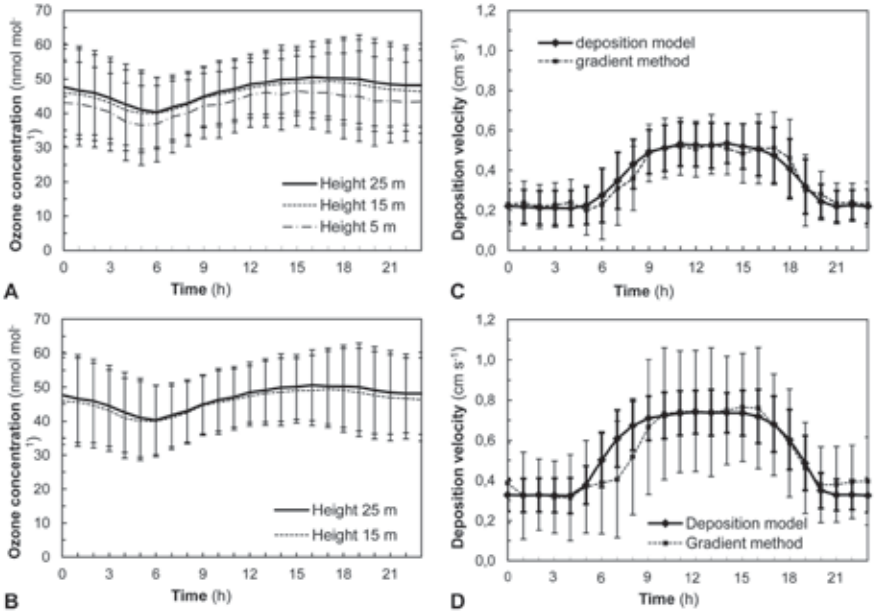

Fig. 1. *Mean daily courses of ozone concentrations (***A**,**B***) and ozone deposition velocities (***C**,**D***) for July–August 2008 (***A**,**C***) and May–September 2009 (***B**,**D***). Ozone concentrations were measured at 5, 15, and 25 m above the ground. Deposition velocities calculated based on gradient measurements (dotted line) and those modelled using the deposition model (solid line) for the Norway spruce stand are shown in panels* **C** *(2008) and* **D** *(2009). Means (points) and standard deviations (error bars) are presented.*

The daily courses of ozone concentrations and fluxes were not identical. Ozone fluxes and deposition velocities peaked around noon while ozone concentrations reached their highest values in the afternoon. This is in agreement with a report of non-linear correlation between the indices by Matyssek et al. (2004). The deposition velocities calculated using the resistance analogy evinced higher variability than did those produced by the deposition model.

3.2. Total and stomatal ozone flux

Good correspondence between the deposition model and the gradient method was observed during the 2008 and 2009 growing seasons (Fig. 3). For July to August 2008, mean (± standard deviation) total ozone flux calculated by the gradient method was 7.72 ± 4.26 nmol m^{-2} s^{-1} and mean total ozone flux modelled by the deposition model was 7.09 ± 3.07 nmol m^{-2} s^{-1}. A comparison of mean stomatal flux, total ozone flux, and stomatal uptake during the 2007, 2008, and 2009 growing seasons revealed no distinctive differences (Table 1).

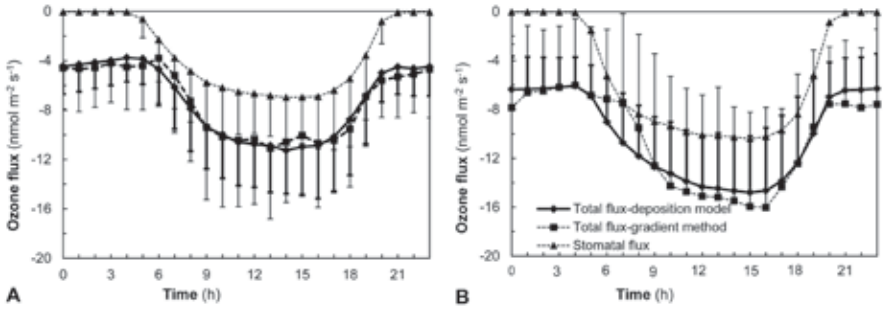

Fig. 2. *Mean daily courses of total and stomatal ozone fluxes as modelled using the deposition model and total ozone flux calculated based on gradient ozone measurements in a Norway spruce forest at the Bílý Kříž experimental site during July–August 2008* (**A**) *and May–September 2009* (**B**). *Means (points) and standard deviations (bars) are presented.*

Table 1. *Modelled stomatal and total ozone fluxes (means ± standard deviation) and stomatal uptake (defined as % of total deposition) estimated for a Norway spruce forest at the Bílý Kříž experimental site during the 2007–2009 vegetation periods.*

Vegetation period	**Stomatal flux** (nmol $m^{-2} s^{-1}$)	**Total flux** (nmol $m^{-2} s^{-1}$)	**Stomatal uptake** (%)
May–September 2007	4.0 ± 3.3	9.7 ± 4.4	29.2
April–September 2008	3.9 ± 3.1	9.5 ± 4.1	27.3
May–September 2009	4.0 ± 2.8	10.1 ± 3.4	28.4
May–September 2009	4.0 ± 2.8	10.5 ± 6.7*	27.6
Mean vegetation period	4.0 ± 3.1	9.7 ± 4.0	29.2

** Mean total ozone flux calculated using the gradient method.*

The results of the models calculating ozone deposition fluxes were in good agreement. Our mean modelled estimate of stomatal uptake, 29.2% of total ozone deposition during the 2007, 2008, and 2009 vegetation periods (Table 1), corresponds to the estimate for stomatal uptake by Mikkelsen et al. (2004) of 30.2% in July and 30.5% in August during 5 years of continuous measurement above a Norway spruce forest in West Jutland, Denmark. Similarly, Fowler et al. (2001) estimated stomatal uptake to be lower than 30% during 4 years of continuous measurement above vegetation dominated by moorland species. Similar data had been reported also by Keronen et al. (2003).

Table 2. *Accumulated exposure to ozone over the threshold value of 40 nmol mol^{-1} (AOT40) and accumulated stomatal flux without (POD_0) and with (POD_1) an hourly threshold of uptake estimated at the Bílý Kříž experimental site during the 2007–2009 vegetation periods.*

Vegetation period	**AOT40** (nmol mol^{-1} h)	**POD_0** (mmol m^{-2})	**POD_1** (mmol m^{-2})
May–September 2007	10,672	15.8	14.3
April–September 2008	12,429	18.8	16.8
May–September 2009	11,562	15.8	14.1

3.3. Indices of ozone exposure and uptake

Ozone exposure exceeded the critical level of 5,000 nmol mol^{-1} h (suggested for forest protection, the threshold for potential ozone hazard conditions), and the ozone dose absorbed by vegetation during measured periods exceeded the critical flux level of 8 mmol m^{-2} (ICP Vegetation 2010) in all growing seasons (Table 2). Examples of AOT40 and POD_Y at the Bílý Kříž experimental research site from July to August 2008 and May to August 2009 are shown in Fig. 3.

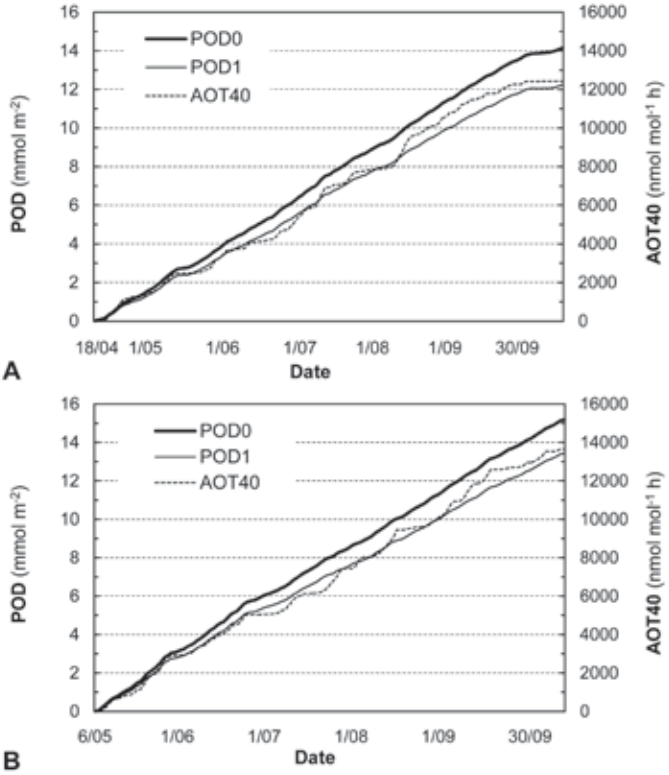

Fig. 3. *Development of accumulated exposure to ozone over the threshold value of 40 nmol mol^{-1} (AOT40) and accumulated stomatal flux without (POD_0) and with (POD_1) an hourly threshold of uptake at the Bílý Kříž experimental site from 18 April to 30 September 2008* (**A**) *and from 6 May to 30 September 2009* (**B**).

POD_1 during the 2007–2009 vegetation periods substantially exceeded the threshold of 8 mmol m^{-2} suggested by ICP Vegetation (2010) for the protection of Norway spruce forests. According to Zapletal et al. (2012), despite the increasing exceedance of AOT40 with the predicted growth of tropospheric background O_3 concentration, exceedance of POD might be lower for Norway spruce in a future climate due to increased stomatal closure. That closure would be related in particular to elevated CO_2 concentration in the atmosphere (see Chapter 7 of this book) and/or expected water restrictions during vegetation seasons (see chapters 2 and 6 of this book for details).

3.4. Relationships with net ecosystem production

Ozone had a significant negative effect on NEP values in both tested forms (concentrations, stomatal flux). Table 3 displays the results of the models tested for predicting NEP values from May to August 2009. All of the models explained more than 97% of the variability in the NEP data, with radiation accounting for the greatest part of the variability in all models. Interactions between ozone and climatic factors were significant only for stomatal ozone flux but not for ozone concentrations. NEP predictions were made based on statistical models for different values of ozone concentration, stomatal flux, radiation, humidity, and mean temperature in a growing season (12°C) (Fig. 4). The decrease in NEP values with increasing ozone was faster for lower humidity (40%) than it was for higher humidity (80%).

Our results indicate that NEP could be reduced by stomatal ozone uptake during the growing season (Zapletal et al. 2011). NEP decrease, based upon stomatal ozone flux rather than ozone concentration, had previously been confirmed for *Pinus ponderosa* and *Citrus* spp. plantation plants (by as much as 12–19%), whereas a Mediterranean forest did not display reductions in NEP-related ozone flux or concentration (Fares et al. 2013b).

Reduced carbon assimilation by forests has been proven globally as contributing substantially to indirect radiative forcing of the climate by ozone (Sitch et al. 2007). It is likely that this will remain a threat to terrestrial ecosystems at least throughout the current century. Wittig et al. (2009) assume that in the Northern Hemisphere after a rise in ozone concentration the current carbon sink, which presently is offsetting a great portion of fossil fuel CO_2 emissions, could be diminished in future. According to Lombardozzi et al. (2015), global terrestrial gross primary production will decrease by 8–12% due to O_3 exposure and the largest decrease – by as much as 20% – will occur at middle latitudes in the eastern United States and Europe. It is apparent that high ozone concentrations and high stomatal ozone fluxes during hot sunny days may contribute to a reduction in carbon uptake by forest stands, as has been described by Urban et al. in Chapter 6 of this book.

Depending upon many micrometeorological parameters, ozone could react via various reactions. Therefore, estimation of different ozone sinks for each site could help to secure human health and welfare. Worldwide, a number of experiments have been conducted in open-top chambers or enclosures under standard conditions. However, the particular conditions in chambers differ from (high air turbulence, higher temperature), and could change plant response comparison to, field conditions (Nussbaum & Fuhrer 2000). Thus, scaling up of leaf-level observations to complex whole-ecosystem measurements is needed. Such real-world measurements with consequent mathematical modelling approaches, as in this study, are greatly appreciated for both model validations and improvements, which are closely linked to better understanding the biosphere–chemosphere continuum of the forest ecosystem at a given site.

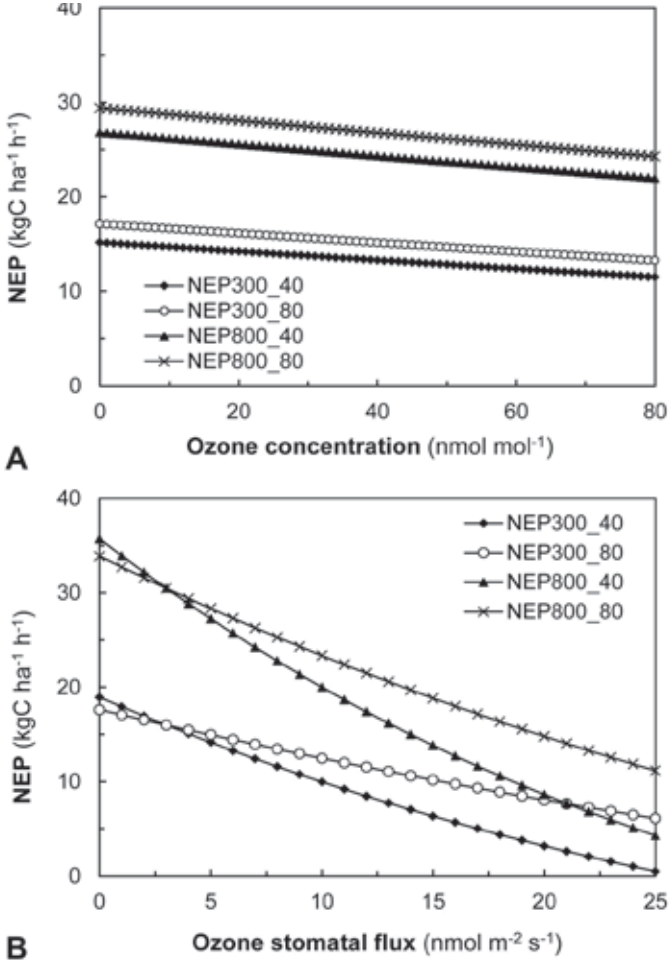

Fig. 4. *Changes in net ecosystem production (NEP) based on regression models for different values of O_3 concentration (***A***) and stomatal ozone flux (***B***) estimated for two levels of global radiation (300 and 800 W m^{-2}), two levels of air humidity (40% and 80%), and air temperature of 12ºC. See Table 3 for an explanation of the models.*

Table 3. *The results of regression models for predicting net ecosystem production using O_3 concentration at 15 m above ground level (O_3 model) and stomatal ozone flux (Stom model) as predictors. Predictors with non-significant effect (n.s.) were not included into the model.*

Model	Predictors	coef.	st. coef.	*F*	*p*
O3 model, $R^2 = 0.976$, $df = 7$, F = 17,426, $p < 10^{-6}$					
	Constant	0.30855	–	13.3	$<10^{-3}$
	radiation	0.06521	1.583	23295.8	$<10^{-6}$
	radiation^2	−0.00099	−0.631	3483.3	$<10^{-6}$
	temperature	−0.01127	−0.166	172.6	$<10^{-6}$
	temperature^2	0.00013	0.068	27.0	$<10^{-6}$
	humidity	0.32319	0.784	254.3	$<10^{-6}$
	humidity^2	−0.02014	−0.837	287.2	$<10^{-6}$
	O_3 concentration	−0.00105	−0.030	40.6	$<10^{-6}$
	O_3 concentration^2	–	–	-	n.s.
	O_3*radiation	–	–	-	n.s.
	O_3*temperature	–	–	-	n.s.
	O_3*humidity	–	-	-	n.s.
Stom model, $R^2 = 0.980$, $df = 10$, F = 15,109, $p < 10^{-6}$					
	Constant	0.82304	–	50.4	$<10^{-6}$
	radiation	0.06475	1.572	4457.1	$<10^{-6}$
	radiation^2	−0.00087	−0.552	468.6	$<10^{-6}$
	temperature	−0.00828	−0.122	93.0	$<10^{-6}$
	temperature^2	−0.00017	−0.088	42.4	$<10^{-6}$
	humidity	0.21754	0.528	72.0	$<10^{-6}$
	humidity^2	−0.01490	−0.619	111.3	$<10^{-6}$
	stom	−0.05183	−0.505	111.1	$<10^{-6}$
	stom^2	–	–	–	n.s.
	stom*radiation	−0.00051	−0.118	28.7	$<10^{-6}$
	stom*temperature	0.00163	0.326	719.1	$<10^{-6}$
	stom*humidity	0.00334	0.254	49.4	$<10^{-6}$

*^2 = 2nd order polynomial, * = interaction, coef. = regression coefficient, st. coef. = standardized regression coefficient, F = F ratio, p = significance level, stom = stomatal flow.*

4. CONCLUSIONS

Daily variation in ozone deposition flux to a Norway spruce forest was estimated using the gradient method. Results from measurements and the model were in good agreement. During the 2007–2009 vegetation periods, POD_1 substantially exceeded the threshold value of 8 mmol m^{-2} suggested by ICP Vegetation (2010) for the protection of Norway spruce forests.

Global carbon models that do not take into account the NEP reduction caused by ozone may result in overestimation. Until now, only a few studies have incorporated this NEP loss (Lombardozzi et al. 2015). From the perspective of the precautionary principle to sustain wood stock productivity, it seems important to include an ozone risk assessment into the awareness of local policy decision makers.

Acknowledgement

This study was funded by the Ministry of Education, Youth and Sports of the Czech Republic within the National Programme for Sustainability I, grant No. LO1415. Thanks are extended to Jaroslav Kulveit for both discussing and reviewing this manuscript and to Zbyněk Večeřa, Pavel Mikuška, and Iva Hůnová for their scientific cooperation.

References

Braun, S., Schindler, C. & Rihm, B. (2014) Growth losses in Swiss forests caused by ozone: Epidemiological data analysis of stem increment of *Fagus sylvatica* L. and *Picea abies* Karst. *Environmental Pollution,* **192**, 129–138.

Cieslik, S. (2004) Ozone uptake by various surface types: a comparison between dose and exposure. *Atmospheric Environment*, **38**, 2409–2420.

Cudlín, P., Seják, J., Pokorný, J., Albrechtová, J., Bastian, O. & Marek, M. (2013) Forest ecosystem services under climate change and air pollution. *Climate Change, Air pollution and Global Challenges: Understanding and Perspectives from Forest Research. Developments in Environmental Science Vol. 13* (eds R. Matyssek, N. Clarke, P. Cudlín, T.N. Mikkelsen, J.-P. Tuovinen, G. Wiesner & E. Paoletti), pp. 521–546. Elsevier, Oxford.

Emberson, L.D., Ashmore, M.R., Cambridge, H., Simpson, D., Tuovinen & J.-P. (2000) Modelling stomatal ozone flux across Europe. *Environmental Pollution*, **109**, 403–414.

Fares, S., Matteucci, G., Scarascia Mugnozza, G. et al. (2013a) Testing of models of stomatal ozone fluxes with field measurements in a mixed Mediterranean forest. *Atmospheric Environment*, **67**, 242–251.

Fares, S., Vargas, R., Detto, M. et al. (2013b) Tropospheric ozone reduces carbon assimilation in trees: Estimates from analysis of continuous flux measurements. *Global Change Biology,* **19**, 2427–2443.

Fowler, D. & Duyzer, J. (1989) Micrometeorological techniques for the measurement of trace gas exchange. *Exchange of Trace Gates Between Terrestrial Ecosystems and the Atmosphere* (eds M.O. Andrea & D.S. Schumel), pp. 189–207. Wiley, London.

Fowler, D., Flechard, C., Cape, J.N., Storeton-West, R.L. & Coyle, M. (2001) Measurements of ozone deposition to vegetation quantifying the flux, the stomatal and non-stomatal components. *Water, Air, and Soil Pollution*, **130**, 63–74.

Fuhrer, J., Skarby, L. & Ashmore, M.R. (1997) Critical levels for ozone effects on vegetation in Europe. *Environmental Pollution*, **97**, 91–106.

Gerosa, G., Finco, A, Mereu, S., Marzuoli, R. & Ballarin-Denti, A. (2009) Interactions among vegetation and ozone, water and nitrogen fluxes in a coastal Mediterranean maquis ecosystem. *Biogeosciences Discussions*, **6**, 1453–1495.

Hicks, B.B., Baldocchi, D.D., Meyers, T.P., Hosker, Jr.R.P. & Matt, D.R. (1987) A preliminary multiple resistance routine for deriving dry deposition velocities from measured quantities. *Water, Air, and Soil Pollution*, **36**, 311–330.

Hummelshoj, P. (1994) *Dry Deposition of Particles and Gases*. Risoe National Laboratory, Denmark.

ICP Vegetation (2009) *Flux-based Assessment of Ozone Effects for Air Pollution Policy*. ICP Vegetation Expert Panel Meeting, 9–12 November, 2009, JRC-Ispra, Italy.

ICP Vegetation (2010) *Minutes of the 23rd Task Force Meeting*. ICP Vegetation 23rd Task Force Meeting, 1–3 February, 2010, Tervuren, Belgium.

Karlsson, P.E., Selldén, G. & Pleijel, H. (2003) *Establishing Ozone Critical Levels II´*. UNECE Workshop Report 2003. Swedish Environmental Research Institute, Gothenburg, Sweden.

Keronen, P., Reissell, A., Rannik, U. et al. (2003) Ozone flux measurement over a Scots pine forest using eddy covariance method: performance evaluation and comparison with flux-profile method. *Boreal Environment Research*, **8**, 425–443.

Klingberg, J., Engardt, M., Karlsson, P. E., Langner, J. & Pleijel, H. (2014) Declining ozone exposure of european vegetation under climate change and reduced precursor emissions. *Biogeosciences*, **11**, 5269–5283.

Lombardozzi, D., Levis, S., Bonan, G., Hess, P.G. & Sparks, J.P. (2015) The influence of chronic ozone exposure on global carbon and water cycles. *Journal of Climate*, **28**, 292–305.

Matyssek, R., Wieser, G., Nunn, A.J. et al. (2004) Comparison between AOT40 and ozone uptake in forest trees of different species, age and site conditions. *Atmospheric Environment*, **38**, 2271–2281.

Mikkelsen, T.N., Ro-Poulsen, H., Hovmand, M.F., Jensen, N.O., Pilegaard, K. & Egelov, A.H. (2004) Five-year measurements of ozone fluxes to a Danish Norway spruce canopy. *Atmospheric Environment*, **38**, 2361–2371.

Mölder, M., Grelle, A., Lindroth, A. & Halldin, S. (1999) Flux-profile relationships over a boreal forest - roughness sublayer corrections. *Agricultural and Forest Meteorology*, **98–99**, 645–658.

Nussbaum, S. & Fuhrer, J. (2000). Difference in ozone uptake in grassland species between open-top chambers and ambient air. *Environmental Pollution*, **109**, 463–471.

Paoletti, E., Bytnerowicz A., Andersen C. et al. (2007) Impacts of air pollution and climate change on forest ecosystems – emerging research needs. *The Scientific World Journal*, **7**(S1), 1–8.

Paoletti, E., Schaub, M., Matyssek, R. et al. (2010) Advances of air pollution sciences: from forest decline to multiple stress effects on forest ecosystem services. *Environmental Pollution*, **158**, 1896–1989.

Pleijel, H., Danielsson, H., Emberson, L., Ashmore, M.R. & Mills, G. (2007) Ozone risk assessment for agricultural crops in Europe: Further development of stomatal flux and flux-response relationships for European wheat and potato. *Atmospheric Environment*, **41**, 3002–3040.

Potier, E., Ogée, J., Jouanguy, J. et al. (2015) Multilayer modelling of ozone fluxes on winter wheat reveals large deposition on wet senescing leaves. *Agricultural and Forest Meteorology*, **211–212**, 58–71.

Pretzsch, H., Dieler, J., Matyssek, R. & Wipfler, P. (2010) Tree and stand growth of mature Norway spruce and European beech under long-term ozone fumigation. *Environmental Pollution*, **158**, 1061–1070.

Sicard, P., De Marco, A., Dalstein-Richier, L., Tagliaferro, F., Renou, C. & Paoletti, E. (2016) An epidemiological assessment of stomatal ozone flux-based critical levels for visible ozone injury in Southern European forests. *Science of the Total Environment*, **541**, 729–741.

Sitch, S., Cox, P.M., Collins, W.J. & Huntingford, C. (2007) Indirect radiative forcing of climate change through ozone effects on the land-carbon sink. *Nature*, **448**, 791–794.

Stevenson, D., Dentener, F.J., Schultz, M.G. et al. (2006) Multimodel ensemble simulations of present-day and near-future tropospheric ozone. *Journal of Geophysical Research*, **111**, D08301.

UNECE (2005). *The Condition of Forests in Europe*. Executive Report, UNECE, Geneva.

Urban, O., Janouš, D., Acosta, M. et al. (2007) Ecophysiological controls over the net ecosystem exchange of mountain spruce stand: Comparison of the response in direct versus diffuse solar radiation. *Global Change Biology*, **13**, 157–168.

Wittig, V.E., Ainsworth, E.A., Naidu, S.L., Karnosky, D.F. & Long, S.P. (2009). Quantifying the impact of current and

future tropospheric ozone on tree biomass, growth, physiology and biochemistry: a quantitative metaanalysis. *Global Change Biology*, **15**, 396–424.

Young, P.J., Archibald, A.T., Bowman, K.W. et al. (2013) Pre-industrial to end 21st century projections of tropospheric ozone from the Atmospheric Chemistry and Climate Model Intercomparison Project (ACCMIP), *Atmospheric Chemistry and Physics*, **13**, 2063–2090.

Zapletal, M., Cudlín, P., Chroust, P. et al. (2011) Ozone flux over a Norway spruce forest and correlation with net ecosystem production. *Environmental Pollution*, **159**, 1024–1034.

Zapletal, M., Pretel, J., Chroust, P. et al. (2012) The influence of climate change on stomatal ozone flux to a mountain Norway spruce forest. *Environmental Pollution*, **169**, 267–273.

Chapter 14

Impact of anticipated climate change on recovery from acidification of an acid-sensitive forested catchment

Jakub Hruška[1], Anna Lamačová[1], Filip Oulehle[1], Pavel Krám[1], Aleš Farda[2], Tomáš Chuman[1]

[1] *Department of Biogeochemical and Hydrological Cycles, Global Change Research Centre, Czech Academy of Sciences, Bělidla 4a, CZ-60300 Brno, Czech Republic*

[2] *Department of Climate Modelling, Global Change Research Centre, Czech Academy of Sciences, Bělidla 4a, CZ-60300 Brno, Czech Republic*

1. INTRODUCTION

Climate change and acidification both ultimately involve chemical changes in the atmosphere, and we should therefore not be surprised to find strong links between the two processes. This study focuses in particular upon how climate change might delay or accelerate the recovery of an acidified aquatic ecosystem. Chronic emissions of S and N compounds into the atmosphere, long-range transport, and the resulting deposition of S and N pollutants have caused acidification of freshwaters over large parts of Europe and eastern North America (e.g. Overrein et al. 1980). Within Europe, S emissions reached their peak in the late 1970s and early 1980s. Since that time, S emissions have decreased substantially even as N emissions have declined much more modestly. Although the past two decades have seen chemical recovery as surface waters have responded to the declines in S and N emissions (e.g. Garmo et al. 2014; Helliwell et al. 2014), climatic variations continue to affect acidification and recovery of surface waters (Wright et al. 2010). There are many processes in terrestrial and aquatic ecosystems that influence the amount and chemical composition of runoff. The combined effects of these processes can be quantified using process-oriented biogeochemical models. One such model is the Model of Acidification of Groundwater in Catchments (MAGIC; Cosby et al. 2001; Oulehle et al. 2012). This model has been used to evaluate the potential effect of climate change on soil and water chemistry. Wright et al. (2006) used MAGIC to examine the relative influence of major climate-sensitive processes on the recovery of soil and water from acidification, and they identified runoff and temperature changes as important drivers. The BROOK90 hydrological model (Federer et al. 2003) has been used to estimate future changes in runoff under expected climate change (Benčoková et al. 2011). Combining the two models provides a unique opportunity to estimate the combined effect of climate change and declines in acidic deposition on the future stream-water and soil chemistry of an acidified acid-sensitive forest catchment.

2. MATERIALS AND METHODS

2.1. Site description

The Lysina catchment (Table 1) is located in the Slavkov Forest, within a mountainous region in the western Czech Republic (Fig. 1). Lysina is an acid-sensitive site underlain by base-poor bedrock and soil with evenly aged Norway spruce (*Picea abies*) plantations. The local soil is classified as Folic Albic Skeletic Podzol with a sandy loam structure and depth of about 120 cm. Organic layer thickness typically varies

between 4 and 7 cm. Soil pHw increases with depth from 3.4 to 4.2 (Banwart et al. 2012; Regelink et al. 2015). Lysina is part of several catchment monitoring networks, including GEOMON (Oulehle et al. 2008) and the International Cooperative Programme (ICP) on Integrated Monitoring and ICP Waters (Holmberg et al. 2013; Garmo et al. 2014).

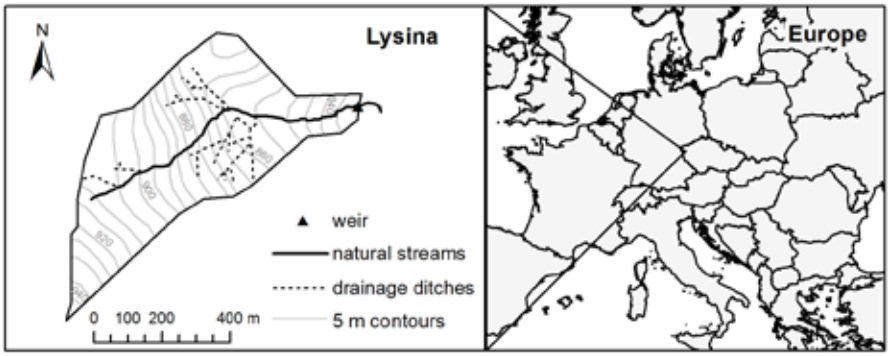

Fig. 1. *Map of Europe showing Lysina catchment with natural streams and drainage ditches.*

Table 1. *Characteristics of Lysina catchment*

Location	50°03'N, 12°40'E
Altitude (m)	829–949
Drainage area (km²)	0.273
Mean slope (%)	11.5
Aspect	North-east
Annual average temperature (°C)	5.0
Dominant tree species	Norway spruce (>99%)
Average age of spruce forest (yr)	50
Dominant soil type	Folic Albic Podzol (Skeletic), 45% of catchment
Bedrock	Leucogranite

2.2. BROOK90

BROOK90 (Federer et al. 2003) is a deterministic, process-oriented, lumped-parameter hydrological model with daily time step. The model generates stream flows through different flow paths. It stores water as intercepted rain, intercepted snow, snow on the ground, soil water from 1–25 layers, and groundwater. Snow accumulation and melt are controlled by a degree-day method with cold content (Linsley 1949). Evaporation is modelled as the sum of five components: intercepted-rain, intercepted-snow, snow, soil evaporation, and transpiration. Transpiration and soil evaporation from sparse canopies and intercepted-rain evaporation are separated in the model using the method proposed by Shuttleworth & Wallace (1985). Actual transpiration is reduced below potential when water supply to the plant is limited.

Model inputs are daily precipitation, maximum and minimum air temperatures, average daily wind speed,

daily solar radiation, and daily average vapour pressure. Six parameter sets are required: canopy, location, soil, flow, initial and fixed parameters. The model includes 47 free parameters in total.
Discharges measured at the Lysina outlet during 1990–1997 were used for calibration, and 1998–2006 data were used to validate BROOK90 performance. Model performance was assessed using Pearson's correlation coefficient and the Nash–Sutcliffe criterion (Nash & Sutcliffe 1970) while comparing measured and simulated stream flows.

2.3. Climatic data

Meteorological data measured at the Mariánské Lázně Úpravna Vody climatic station of the Czech Hydrometeorological Institute (691 m a.s.l., 49°59′N, 12°42′E, located 5 km from Lysina) were used as inputs to BROOK90 after modifications. Air temperature data were modified based on local minimum and maximum temperature lapse rates to represent the average catchment elevation (Benčoková et al. 2011). Precipitation data were modified by the local precipitation–elevation gradient (1.35 mm per year per meter) (Yu et al. 2015). Daily global radiation was calculated from sunshine duration using the Klabzuba approach (described in Trnka et al. 2005). BROOK90 estimated daily average vapour pressure data using saturated vapour pressure at minimum temperature.
Precipitation, maximum and minimum air temperature, global radiation, and wind speed for 2021–2050 and 2071–2100 from the ALADIN-Climate/CZ regional climate model coupled to the ARPEGE-Climate global circulation model and forced with the SRES A1B emissions scenario of the Intergovernmental Panel on Climate Change were used as future forcing data. Grid resolution was ca 10 km. Model outputs were statistically corrected according to observed values using the percentile approach proposed by Dequé (2007). Gridded observed data used for the correction were produced by the Czech Hydrometeorological Institute. The control period was 1961–1990. Data were derived by spatial interpolation of point measurements (Štěpánek et al. 2011).
Mean elevation of the grid covering the Lysina catchment was 739 m a.s.l. (50°03′N, 12°40′E), and so the precipitation and temperature time series were corrected using the same precipitation–elevation gradient and lapse rates as in recent data (see above) to better represent the catchment's elevation of 829–949 m a.s.l.

2.4. The MAGIC model

2.4.1. Model description

MAGIC is a lumped-parameter model of intermediate complexity, developed to predict the long-term effects of acidic deposition on soil- and surface-water chemistry (Cosby et al. 2001; Oulehle at al. 2012). The model simulates soil- and surface-water chemistry in response to changes in such drivers as S and N deposition, silvicultural practices, and climate. For each time step (monthly time steps in this study), MAGIC calculates the concentrations of major ions while assuming simultaneous reactions involving SO_4^{2-} adsorption, cation exchange, dissolution–precipitation–speciation of Al, and dissolution–speciation of inorganic and organic carbon compounds. MAGIC accounts for the mass balance of major ions in the soil by considering the fluxes from atmospheric inputs, chemical weathering, net uptake in biomass, and loss to runoff. Data inputs required for MAGIC calibration comprise catchment characteristics, soil chemical and physical characteristics, water input and output fluxes, concentrations of major ions, and net uptake of base cations and N by vegetation.

2.4.2. MAGIC calibration

Measured data for catchment characteristics, soil, deposition, and stream-water volume and chemistry were used to calibrate MAGIC. Fixed parameters (constant values that must be specified) were measured or estimated (such as in the cases of soil depth and cation exchange capacity) or obtained through optimization as part of the calibration procedure (such as for cation exchange coefficients and base cation weathering rates) (Table 2). Cosby et al. (2001) provide definitions and details. MAGIC was calibrated to the average stream- and soil-water chemistry for 1990–1991. Calibration proceeded through sequential steps. The first steps involved calibration of the strong acid anions. Cl^-, SO_4^{2-}, and NO_3^- were calibrated by adjusting the deposition inputs and/or ecosystem uptake as described by Wright & Cosby (2003). This procedure resulted in the modelled sum of strong acid anions in water being equal to the observed sum. The next steps involved calibration of the base cations Ca^{2+}, Mg^{2+}, Na^+, and K^+. In these steps, the model was run from an assumed steady-state condition from 1870 to 2012. A trial and error process was used to adjust the weathering rates of Ca^{2+}, Mg^{2+}, Na^+, and K^+ and the initial soil-exchange pools of these four cations until modelled concentrations of base cations in stream and soil water and modelled pools of base cations in soil matched the observed data for the calibration period of 1990–2012. This step calculated the soil–soil-water selectivity coefficients for base cations and Al exchange as well as the weathering rates for the four base cations (Table 2). At this point, the modelled sum of base cations (SBC) equalled the observed SBC for the calibration period, and so the modelled acid-neutralizing capacity also equalled the observed capacity. The final step entailed calibration of the weak acids (as represented by dissolved organic carbon) such that the simulated concentrations of H^+, Al^{n+}, and organic anions (A^-) matched observations. This was achieved by adjusting the dissociation constants for organic acids; aluminium hydroxide, fluoride, and sulphate species; and organic Al complexes. We used a tri-protic model for organic acids with dissociation constants given by Hruška et al. (2003; Table 2).

3. RESULTS AND DISCUSSION

3.1. Hydrology

BROOK90 reproduced the flow patterns at Lysina well. Pearson's correlation coefficients for daily data were 0.75 ($r_{crit} = 0.20$, $n = 2{,}922$, $p = 0.05$) for the calibration period and 0.74 ($r_{crit} = 0.20$, n = 3,287, $p = 0.05$) for the validation period. For monthly data, Pearson's correlation coefficient was 0.91 ($r_{crit} = 0.20$, $n = 108$, $p = 0.05$) for the validation period. The Nash–Sutcliffe coefficients were for daily data 0.47 ($n = 2{,}922$) in the calibration period and 0.45 ($n = 3{,}287$) in the validation period, and for monthly data it was 0.78 ($n = 108$) in the validation period.

According to ALADIN-Climate/CZ projections, mean annual temperature will increase from 5.0°C (1990–2011) to 6.3°C (2021–2050) and 8.0°C (2071–2100). Mean annual precipitation is projected to decrease from the recent 1,035 mm (1990–2011) to 960 mm (2021–2050) and 932 mm (2071–2100). The anticipated change in temperature and precipitation will result in a notable reduction in runoff from 453 mm (1990–2011) to 391 mm (2021–2050) and 338 mm (2071–2100). The impact on the seasonal runoff pattern will be even more substantial with large decreases in spring runoff maxima as well as in summer to autumn runoff values, and particularly in August and September (Fig. 2).

Table 2. *Selected fixed and adjusted parameters used to calibrate MAGIC to Lysina. DOC = dissolved organic carbon, CEC = cation-exchange capacity.*

Fixed parameters	**Units**	**Value**
CATCHMENT		
Discharge, annual	*m*	*0.432*
Precipitation, annual	*m*	*0.95*
SOIL		
Bulk density (fraction <2 mm)	*kg m^{-3}*	*530*
CEC	*meq kg^{-1}*	*59*
$Al(OH)_3$ solubility constant	*log 10*	*7.7*
SO_4 adsorption half saturation	*meq m^{-3}*	*500*
SO_4 maximum adsorption capacity	*meq kg^{-1}*	*3*
pCO_2	*atm*	*2.2*
Temperature	*°C*	*5*
Site density of DOC	*mmol m^{-3}*	*3.4*
pK_1 of organic acids	*–log 10*	*2.5*
pK_2 of organic acids	*–log 10*	*4.1*
pK_3 of organic acids	*–log 10*	*6.7*
STREAM		
$Al(OH)_3$ solubility constant	*log 10*	*7.1*
pCO_2	*atm*	*1.3*
Site density of DOC	*mmol m^{-3}*	*3.4*
pK_1 of organic acids	*–log 10*	*2.5*
pK_2 of organic acids	*–log 10*	*4.1*
pK_3 of organic acids	*–log 10*	*6.7*
Adjusted parameters		
SOIL		
Weathering Ca	*meq m^{-2} per year*	*29.6*
Weathering Mg	*meq m^{-2} per year*	*11.5*
Weathering Na	*meq m^{-2} per year*	*21.1*
Weathering K	*meq m^{-2}per year*	*4.3*
Weathering Σ(Ca+Mg+K+Na)	*meq m^{-2}per year*	*66.5*
Selectivity coefficient Al–Ca	*log*	*0.75*
Selectivity coefficient Al–Mg	*log*	*1.16*
Selectivity coefficient Al–K	*log*	*–0.75*
Selectivity coefficient Al–Na	*log*	*–4.41*
Ca initial condition	*% of CEC*	*17.5*
Mg initial condition	*% of CEC*	*5.5*
Na initial condition	*% of CEC*	*1.2*
K initial condition	*% of CEC*	*3.3*
Initial base saturation Σ(Ca+Mg+K+Na)	*% of CEC*	*27.5*

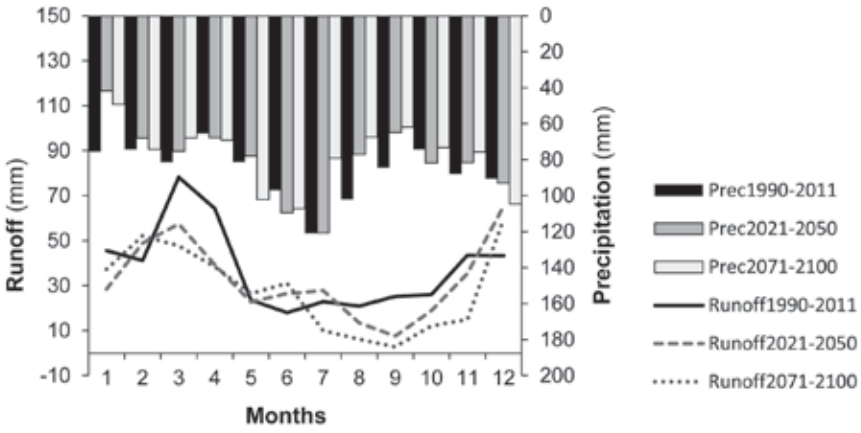

Fig. 2. *Future mean monthly precipitation (prec) and runoff estimated by the ALADIN-Climate/CZ and BROOK90 models for 2021–2050 and 2071–2100 compared with recently measured precipitation and runoff for 1990–2011.*

For biogeochemical modelling purposes, stream-water runoff was estimated for each month for 2020–2100 and two scenarios were taken into account:

a. "Current climate" – continuation of ambient measured monthly runoff patterns until 2100, and

b. "Climate change" – monthly runoff estimated by ALADIN-Climate/CZ and BROOK90.

3.2. Atmospheric deposition

The Lysina catchment had been strongly acidified by atmospheric deposition during the second half of the 20th century (Hruška & Krám 2003; Krám et al. 2012). As estimated by throughfall fluxes, S and N deposition peaked in the late 1980s. S deposition then declined from 30–34 kg ha^{-1} to 5–7 kg ha^{-1} for 2008–2012. Inorganic N deposition decreased from 12–14 kg ha^{-1} to 7–10 kg ha^{-1} for the same period.

Historical deposition fluxes were estimated according to historical S and N emissions in the Czech Republic derived from Kopáček & Veselý (2005) for 1860–1990. Constant deposition as observed during 2010–2012 was applied for 2013–2100 because anthropogenic emissions and atmospheric SO_4 and NO_3^- deposition have been stable in the 2010s and further reduction is not expected.

3.3. Stream-water chemistry

3.3.1. Sulphate

Change in S deposition had been the main factor driving changes in biogeochemical patterns. The amount of historical S deposition was estimated as proportional to regional coal mining for 1851–1990. We verified our estimates of SO_4 concentrations in past runoff by examining historical data published by Hanaman in 1896 (Hruška et al. 2002). Monthly variations in SO_4 concentrations (Fig. 3) as well as fluxes (Fig. 4) were caused mainly by hydrological fluctuations in combination with S adsorption/desorption in soil.

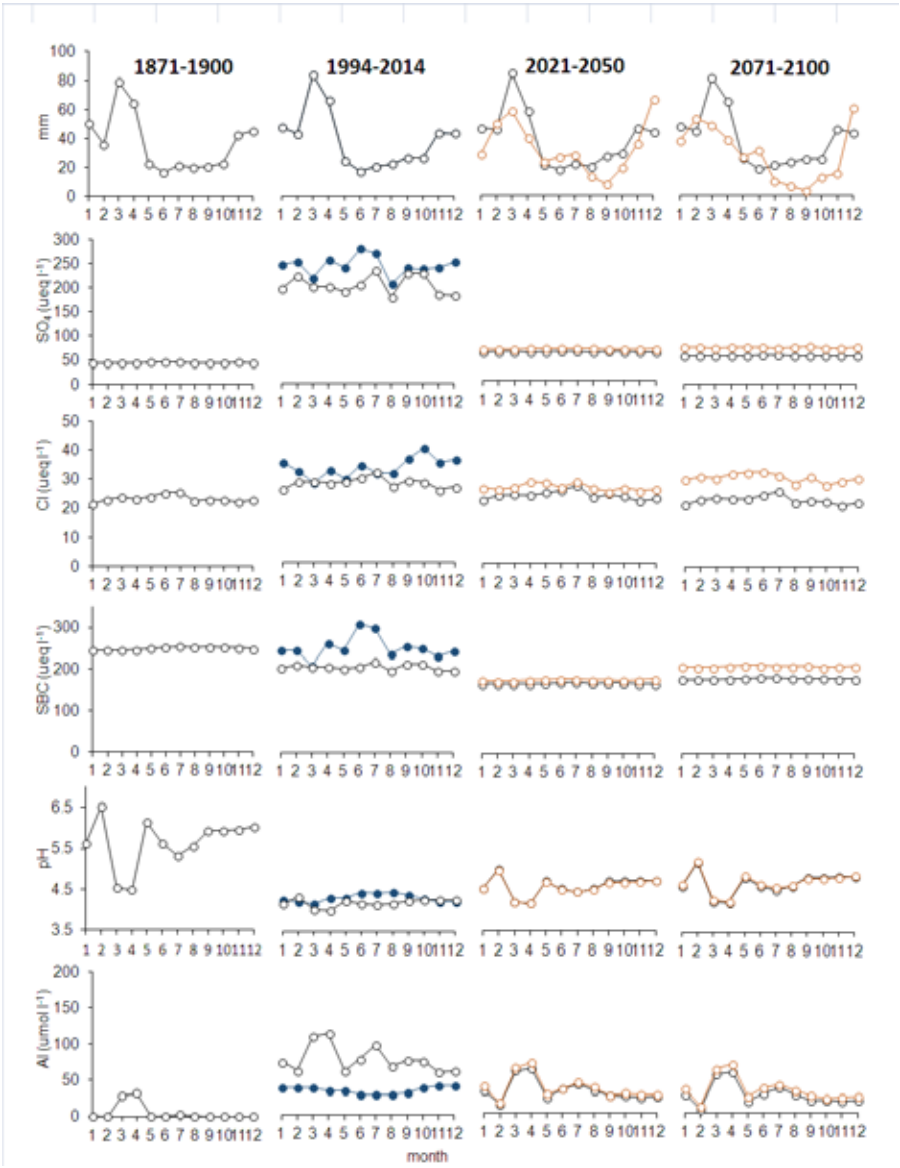

Fig. 3. *Simulated and observed mean monthly concentrations of different solutes in stream water at Lysina for 1871–1900, 1994–2014, 2021–2050, and 2071–2010. Black lines with open circles depict simulations with the "Current climate" scenario. Orange lines with open circles depict the "Climate change" scenario. Blue lines with filled circles depict measured data for 1994–2014. SBC = sum of base cations.*

If atmospheric deposition remains at 2010–2012 values, predicted stream-water SO_4 concentrations will decrease to ca 65 µeq l^{-1} for 2021–2050. The "Climate change" scenario would result in ca 5% higher SO_4 concentration, due to slightly reduced runoff (Fig. 2) during this period. A larger difference was predicted for 2071–2100 mostly due to a more pronounced decline in runoff. SO_4 would decline to ca 56 µeq l^{-1} (Fig. 3) for the "Current climate" scenario, but the "Climate change" scenario predicted substantially higher concentrations (73 µeq l^{-1}). Both values would be higher than the estimated pre-industrial concentration of 45 µeq l^{-1}. Two main causes drive this pattern: a) the S deposition in 2010 was still slightly higher than was the pre-industrial estimate for 1850, and b) the modelled SO_4 desorption caused a lag in the response of SO_4 fluxes in runoff to decreasing SO_4 deposition. The store of adsorbed SO_4 in the soil is predicted to decrease rapidly, however, and by around 2020 soil-adsorbed SO_4 will approach a new steady state with S deposition.

There were no distinct differences in modelled SO_4 fluxes (Fig. 4) between the two scenarios, and so the difference in concentration was caused mostly by reduced runoff under anticipated climate change.

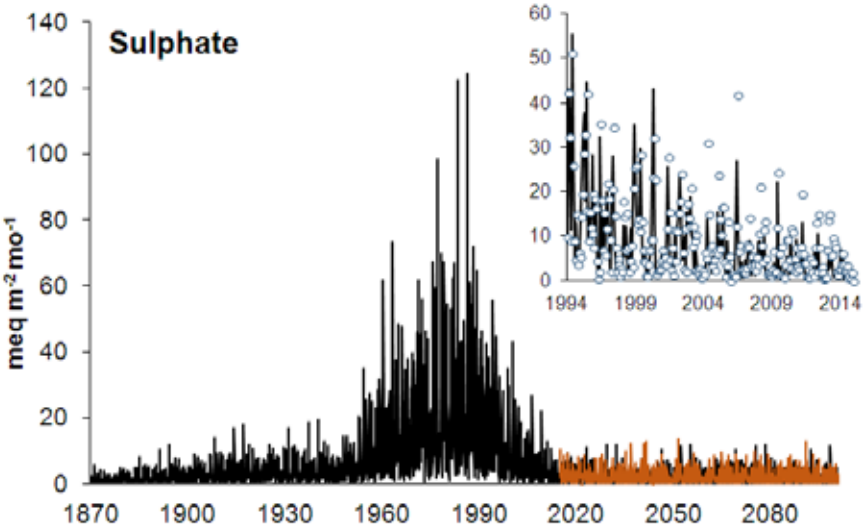

Fig. 4. *Simulated and observed monthly SO_4 fluxes in stream water at Lysina for 1870–2100. Black lines depict the simulation with the "Current climate" scenario. Orange lines depict the "Climate change" scenario from 2021. Blue circles in the inset depict measured monthly data for 1994–2014.*

3.2.2. Base cations

Modelled base cations (Ca, Mg, K, Na) in runoff increased gradually, while SO_4 increased over the historical period of 1851–1991 (Fig. 3) similarly as did SBC fluxes (Fig. 5). Following this period, SBC declined and then decreased further while following the decline in SO_4 (Figs. 3 and 4). At Lysina, 240 µeq l^{-1} was simulated as the historic pre-industrial SBC concentration, and the model simulation for the 1980s was near 500 µeq l^{-1}. During the 1990s, both modelled and observed SBC declined to 200–220 µeq l^{-1} (Fig. 3). Under the "Climate change" and "Current climate" scenarios, concentrations of ca 170–180 µeq l^{-1} will be recorded between 2021 and 2050. For 2071–2100, the model predicts a slight increase to ca 180 µeq l^{-1} for

"Current climate" and a more pronounced increase to ca 205 µeq l^{-1} for "Climate change". All of the aforementioned predictions involved concentrations substantially lower than was the historical estimate of 240 µeq l^{-1}. The two scenarios did not differ substantially in SBC fluxes (Fig. 5).

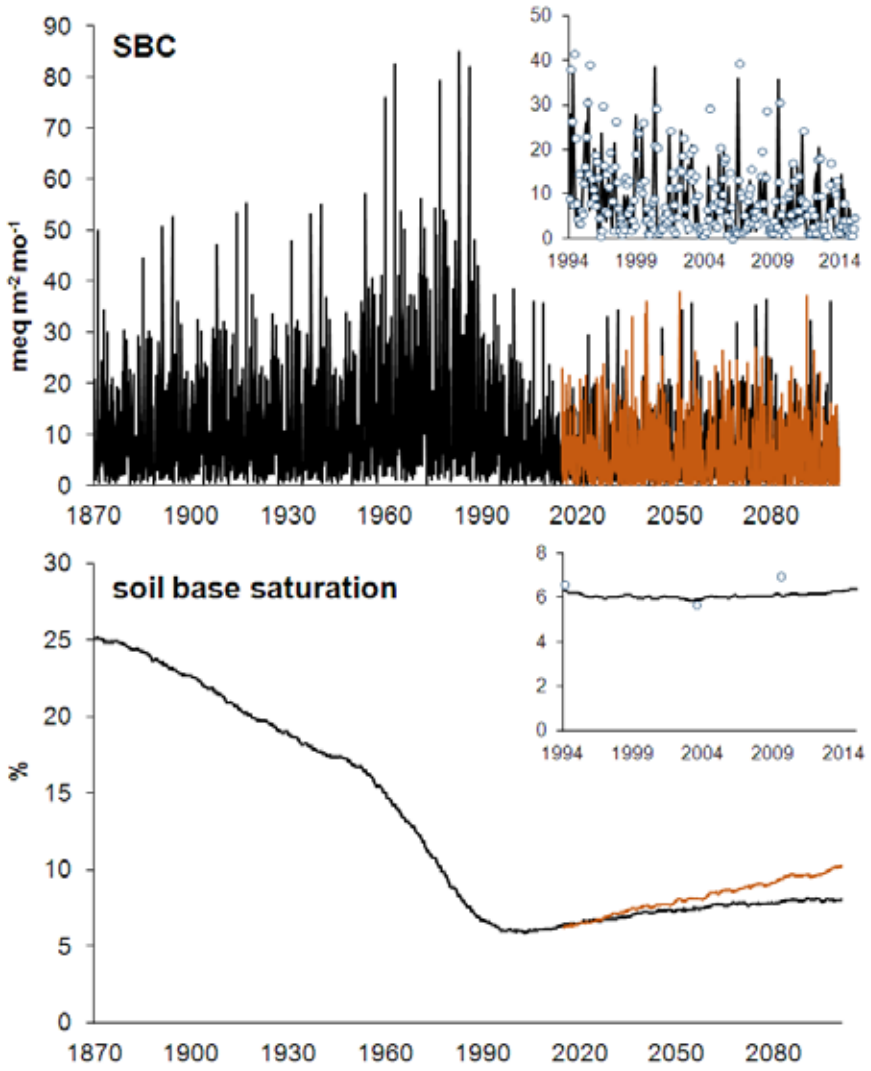

Fig. 5. *Simulated and observed monthly fluxes of sum of base cations (SBC; Na + K + Ca + Mg) in stream water and % of soil base saturation at Lysina for 1870–2100. Black lines depict the simulation with the "Current climate" scenario. Orange lines depict the "Climate change" scenario from 2021. Blue circles in the inset depict measured monthly data for 1994–2014.*

The low supply of base cations from the soil exchange complex and weathering was a major factor contributing to the severe acidification of soils and stream water at Lysina.

Weathering rates (Table 2) were estimated within the MAGIC calibration procedure together with historic soil base saturation. The calibrated annual weathering rate of 65 meq m^{-2} per year for Lysina seems to be realistic given the catchment's geology, morphology, and climate. Langan et al. (2001) had published 15 weathering rates estimated for granitic areas in northern Europe calculated in different ways (mineral index, PROFILE model, Sr isotopes, depletion) ranging between 10 meq m^{-2} and 85 meq m^{-2} annually.

Modelled soil base saturation at Lysina decreased from 25% in 1870 to the 6.8% measured in 1994. Loss of base cations from cation-exchange sites was an important mechanism for neutralizing incoming acidity, and during the peak of acidic deposition (from the 1950s to the 1990s) cation exchange was the dominant source of base cations in the stream (Figs. 3 and 5). Base saturation of 6.5–7.0% was simulated for 2021–2050, an increase from the minimum of 6.0% modelled for 1997–2002 (Fig. 5). The difference between the two climatic scenarios was negligible for 2021–2050. A more substantial difference was estimated for 2071–2100. Base saturation increased to 10.0% for the "Climate change" scenario compared to 8.0% for the "Current climate" scenario (Fig. 5). While the expected increase in soil base saturation is unquestionably desirable and marks the onset of true recovery from acidification, the actual maximum of 10% by 2100 is still low compared to 25% in 1870. The two major reasons for the loss of base cations from the soil at Lysina were deposition of strong acids and forest growth. There is, however, an important difference in the dynamics of these two processes. Base-cations leaching first increased and then decreased with deposition (Figs. 3 and 5), whereas forest uptake was less variable. At present and into the future, however, uptake will be greater than runoff loss at Lysina. Net annual uptake (in bark and bole wood) was calculated as 18.2 meq m^{-2} in 1994. It was dominated by Ca (12.5 meq m^{-2}), while uptake of Na (0.1 meq m^{-2}) was negligible (Table 2). Base-cation uptake by vegetation represents ca 30% of the annual weathering rate, and therefore this amount cannot be used to mitigate acidification within the soil (Hruška et al. 2002).

In future, vegetation uptake will be the dominant net sink of base cations at Lysina, because stream-water output will be similar to or lower than that during the pre-industrial period and part of the weathering and deposition will be consumed to recharge the soil cation exchanger. Thus, spruce harvesting will have been responsible for one-third of SBC loss for the entire modelled period of 1851–2030 (for more details see Hruška et al. 2002). Expected climate change may help to recharge the soil cation exchanger due to slightly declining streamwater flux.

pH and aluminium

Lysina is a typical catchment where historical depletion of base cations from the soil has led to chronic acidification as characterized by pH decline (Figs. 3 and 6) and Al mobilization (Figs. 3 and 6). Extremely elevated Al in stream water at Lysina was documented in detail by Krám et al. (2009, 2012). Modelled pre-industrial pH varied between 4.5 and 6.5 (Figs. 3 and 6), thus showing the expected susceptibility of granitic catchments to anthropogenic acid loading. The great pH variability was caused by increasing organic acids (humic and fulvic acids represented by dissolved organic carbon) and decreased base cations during high flow events, and large amounts of dissolved organic carbon (data not shown) had produced low stream-water pH prior to the onset of acidic deposition. As a result of S deposition and long-term soil base cation depletion, pH declined to a minimum annual discharge-weighted average of 3.87 during the 1980s (Fig. 6). Stream water became chronically acidic and lost its original preindustrial variability due to the presence of very high H^+ concentrations under all runoff conditions. After two decades of declining S

deposition, measured and modelled pH were both around 4.1 between 1994 and 2014 (Fig. 3). Under projections for 2021–2050, modelled pH rose slightly to 4.4 for both climatic scenarios and then more slowly to 4.5 in 2100 and pH variability partly recovered. There was no difference between climatic scenarios. The increase in base cations as a result of declining runoff (Fig. 3) was compensated by a similar increase in SO_4. Thus, the acid/base character of the stream water was not significantly affected and predicted pH did not differ between climatic scenarios.

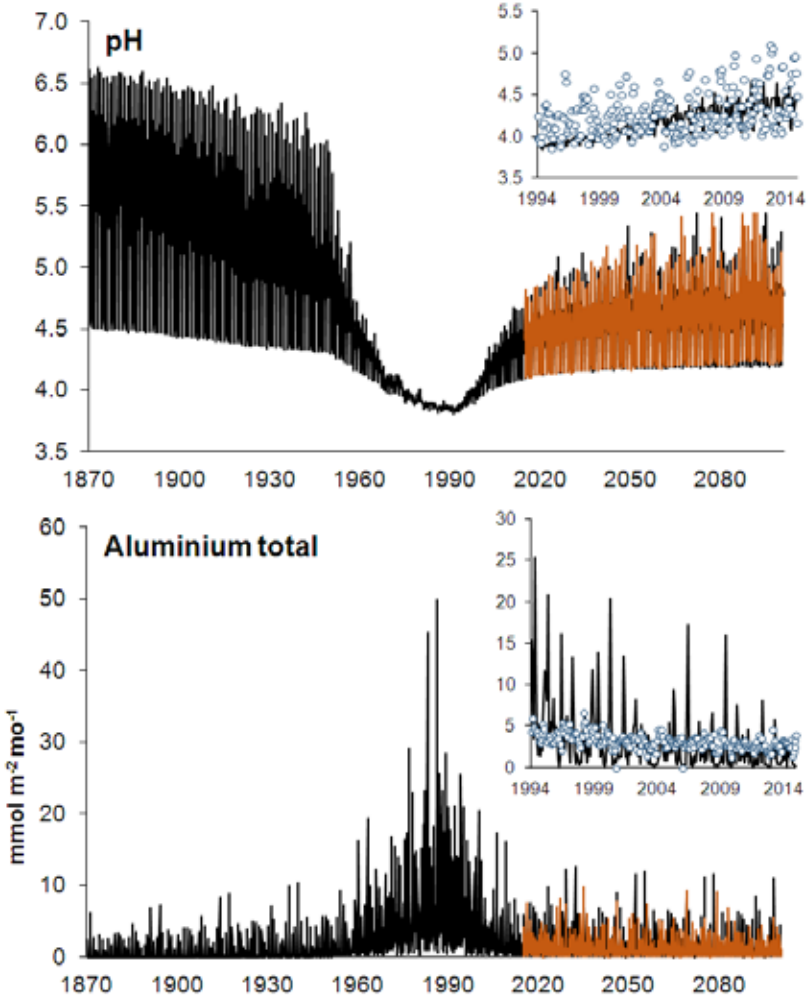

Fig. 6. *Simulated and observed pH and monthly Al fluxes at Lysina for 1870–2100. Black lines depict the simulation with the "Current climate" scenario. Orange lines depict the "Climate change" scenario from 2021. Blue circles in the insets depict measured monthly data for 1994–2014.*

Total Al concentrations in MAGIC are controlled by Al(OH)3 solubility. The Al(OH)3 solubility constant for Lysina was optimized using data measured between 1990 and 2000. Using fitted $-pK_{Al(OH)3} = 7.1$ (Table 2), it was possible to reproduce satisfactorily the measured Al and pH, but this constant seems to be low in view of the mineral soil thickness and amount of soil organic matter. For a more detailed explanation, see Hruška et al. (2002).

The MAGIC forecast estimated a small decline in total Al during 2021–2050, from ca 100 μmol l^{-1} in 1994–2014 (Fig. 3) to ca 40 μmol l^{-1}. Thereafter, Al would decline further albeit slightly to ca 30 μmol l^{-1} for 2071–2100. Al solubility is strictly controlled by water pH, and so differences in Al concentrations are also negligible between the two climatic scenarios.

4. CONCLUSIONS

According to BROOK90 and subsequent MAGIC simulations, projected climate change will not have a substantial impact on the chemistry of surface water at Lysina even though the projected decline in stream runoff would be substantial. The explanation lies in the presently marked acidity due to the considerable level of historic anthropogenic acidification within this naturally vulnerable catchment. The main factor controlling the stream-water chemistry was the change in acidic deposition. The environmental conditions of the studied stream would probably remain unsatisfactory, with the dominant influences being from atmospheric acid deposition and forest management in the area.

Acknowledgement

This work was supported by the Ministry of Education, Youth and Sports of the Czech Republic within the National Programme for Sustainability I, grant No. LO1415.

References

Banwart, S., Menon, M., Bernasconi, S.M. et al. (2012) Soil processes and functions across an international network of Critical Zone Observatories: Introduction to experimental methods and initial results. *Comptes Rendus Geoscience*, **344**, 758–772.

Benčoková, A., Krám, P. & Hruška, J. (2011) Future climate and changes in flow patterns in Czech headwater catchments. *Climate Research*, **49**, 1–15.

Cosby, B.J., Ferrier, R.C., Jenkins, A. & Wright, R.F. (2001) Modelling the effects of acid deposition: Refinements, adjustments and inclusion of nitrogen dynamics in the MAGIC model. *Hydrology and Earth Systems Sciences*, **5**, 499–517.

Dequé, M. (2007) Frequency of precipitation and temperature extremes over France in an anthropogenic scenario: model results and statistical correction according to observed values. *Global Planet Change*, **57**, 16–26.

Federer, C.A., Vörösmarty, C. & Fekete, B. (2003) Sensitivity of annual evaporation to soil and root properties in two models of contrasting complexity. *Journal of Hydrometeorology*, **4**, 1276–1290.

Garmo, O.A., Skjelkvåle, B., de Wit, H.A. et al. (2014) Trends in surface water chemistry in acidified areas in Europe and North America from 1990 to 2008. *Water, Air and Soil Pollution*, **225**, 1880.

Helliwell, R.C., Wright, R.F., Jackson-Blake, L.A. et al. (2014) Assessing recovery from acidification of European surface waters in the year 2010: Evaluation of projections made with the MAGIC model in 1995. *Environmental Science and Technology*, **48**, 13280–13288.

Holmberg, M., Vuorenmaa, J., Posch, M. et al. (2013) Relationship between critical load exceedances and empirical impact indicators at Integrated Monitoring sites across Europe. *Ecological Indicators*, **24**, 256–265.

Hruška, J. & Krám, P. (2003) Modelling long-term changes in stream water and soil chemistry in catchments with contrasting vulnerability to acidification (Lysina and Pluhuv Bor, Czech Republic). *Hydrology and Earth System Sciences,* **7**, 525–539.

Hruška, J., Köhler, S., Laudon, H. & Bishop, K. (2003) Is a universal model of organic acidity possible: Comparison of the acid/base properties of dissolved organic carbon in the boreal and temperate zones. *Environmental Science and Technology*, **37**, 1726–1730.

Hruška, J., Moldan, F. & Krám, P. (2002) Recovery from acidification in Central Europe- observed and predicted changes of soil and streamwater chemistry in the Lysina catchment, Czech Republic. *Environmental Pollution*, **120**, 261–274.

Kopáček, J. & Veselý, J. (2005) Sulfur and nitrogen emissions in the Czech Republic and Slovakia from 1850 till 2000. *Atmospheric Environment*, **39**, 2179–2188.

Krám, P., Hruška, J., Driscoll, C.T., Johnson, C.E. & Oulehle, F. (2009) Long-term changes in aluminum fractions of drainage waters in two forest catchments with contrasting lithology. *Journal of Inorganic Biochemistry*, **103**, 1465–1472.

Krám, P., Hruška, J. & Shanley, J.B. (2012) Streamwater chemistry in three contrasting monolithologic catchments. *Applied Geochemistry*, **27**, 1854–1863.

Langan, S., Hodson, M., Bain, D. et al. (2001) The role of mineral weathering rate determination in generating uncertainties in the calculation of critical loads of acidity and their exceedance. *Water, Air, and Soil Pollution: Focus*, **1**, 229–312.

Linsley, R.K. (1949) Applied hydrology. McGraw-Hill, New York

Nash, J.E. & Sutcliffe, J.V. (1970) River flow forecasting through conceptual models. 1. A discussion of principles. *Journal of Hydrology*, **10**, 282–290.

Oulehle, F., Cosby, B.J., Wright, R.F. et al. (2012) Modelling soil nitrogen: The MAGIC model with retention linked to carbon turnover using decomposer dynamics. *Environmental Pollution*, **156**, 158–166.

Oulehle, F., McDowell, W.H., Aitkenhead-Peterson, J.A. et al. (2008) Long-term trends in stream nitrate concentrations and losses across watersheds undergoing recovery from acidification in the Czech Republic. *Ecosystems*, **11**, 410–425.

Overrein, L., Seip, H.M. & Tollan, A. (1980) Acid precipitation — Effects on forest and fish. Final report of the SNSF-project 1972–1980. FR 19-80, SNSF project, Ås, Norway.

Regelink, I.C., Stoof, C.R., Rousseva, S. et al. (2015) Linkages between aggregate formation, porosity and soil chemical properties. *Geoderma*, **247–248**, 24–37.

Shuttleworth, W.J. & Wallace, J.S. (1985) Evaporation from sparse crops — an energy combination theory. *Quarterly Journal of the Royal Meteorological Society*, **111**, 839–855.

Štěpánek, P., Zahradníček, P. & Huth, R. (2011) Interpolation techniques used for data quality control and calculation of technical series: an example of a Central European daily time series. *Időjárás – Quarterly Journal of the Hungarian Meteorological Service*, **115**, 87–98.

Trnka, M., Žalud, Z., Eitzinger, J. & Dubrovský, M. (2005) Global radiation in Central European lowlands estimated by various empirical formulae. *Agricultural and Forest Meteorology*, **131**, 54–76.

Wright, R.F., & Cosby, B.J. (2003) Future recovery of acidifed lakes in southern Norway predicted by the MAGIC model. *Hydrology and Earth System Sciences*, **7**, 467–485.

Wright, R.F., Aherne, J., Bishop, K. et al. (2006) Modelling the effect of climate change on recovery of acidified freshwaters: relative sensitivity of individual processes in the MAGIC model. *Science of the Total Environment*, **365**, 154–166.

Wright, R.F., Aherne, J., Bishop, K. et al. (2010) Interaction of climate change and acid deposition. Climate Change Impacts on Freshwater Ecosystems (eds M. Kernan, R.W. Battarbee & B. Moss), pp. 152–179. Wiley-Blackwell, A John Wiley and Sons, Ltd., Chichester, UK.

Yu, X., Lamačová, A., Duffy, C. et al. (2015) Modelling long-term water yield effects of forest management in a Norway spruce forest. *Hydrological Sciences Journal*, **60**, 174–191.

Chapter 15

Global change effects on insect diversity with examples from butterflies in the High Sudetes

Karolína Bílá, Pavel Kindlmann

Department of Biodiversity Research, Global Change Research Centre, Czech Academy of Sciences, Prokišova 7, CZ-370 01 České Budějovice, Czech Republic

1. INTRODUCTION

Two major threats to insect diversity are currently in particular research focus: climate change and land-cover change (Sala et al. 2000; Thomas et al. 2006; Jetz et al. 2007; Bowler et al. 2015; Mantyka-Pringle et al. 2015; Visconti et al. 2015). These changes are caused by either natural processes or anthropogenic activities. It is assumed that the threats' effects interact and amplify such of their impacts as habitat loss and fragmentation, reduced ability for species to adapt to modified land-cover, and spread of invasive species (Sutherst 2000; Opdam & Wascher 2004; de Chazal & Rounsevell 2009). Although we lack empirical data and can only infer what these interactions mean for ecosystems (Vinebrooke et al. 2004; Brook et al. 2008; Felton et al. 2009; Oliver & Morecroft 2014), these factors, climate change and land-cover change, have nevertheless been studied intensively but individually in recent decades.

Climate change is followed by alterations to many environmental factors, such as increased temperature, reduction of the winter season, decline in precipitation during the summer season, and more frequent extreme meteorological events (droughts or torrential rainfalls) (European Commission 2013). Climate change is a long-term process and acts as one of the limiting factors for species distribution and in determining the margins of species' ranges (Hill et al. 2002; Hill & Preston 2015; Mason et al. 2015). Due to climate warming, many taxonomic groups evidence pole- and upward shifts in species geographic distributions or phenology adaptations (Parmesan & Yohe 2003; Hickling et al. 2006; Chen et al. 2011; Callinger et al. 2013; Bowler et al. 2015). Climate change can also affect population abundances, which might be even more apparent than the distribution shift (Saether et al. 2000; Parmesan 2006; Devictor et al. 2008; Cahill et al. 2013).

The other major threat to biodiversity, land-cover change, is a consequence of both climate change and anthropogenic activities. It affects species diversity in terms of habitat loss and fragmentation. Fragmented populations are more prone to extinction (Sala et al. 2000; Jetz et al. 2007; de Chazal & Rounsevell 2009), while isolated sub-populations are enabled to migrate within former species range (Bílá et al. 2012). In this context, species attempting to track suitable life conditions might become isolated in a fragmented habitat (Thomas et al. 2004; Keith et al. 2008; Brook et al. 2009; Mantyka-Pringle 2015). This process of isolation began naturally at the beginning of the last postglacial period when cold-adapted species dispersed to their present territories and after progressive climate warming became trapped on the highest mountain summits, which are today's alpine habitats (Gutierrez 1997; Hewitt 1999; Varga & Schmitt 2008). The roles of alpine habitat isolation and possible future reduction in those habitats' size are widely discussed (Dennis & Shreeve 1997; Isaac & Williams 2007; Bílá et al. 2012).

Remarkable alpine habitats occur in the High Sudetes Mountains, which form the northern border of the

Czech Republic. Treeless arctic–alpine tundra rises to 1,300–1,600 m a.s.l. in these mountains and occupies a narrow belt above the timberline extending several dozen to several hundred metres below the summits (Treml & Banaš 2000; Bílá et al. 2012). In mountainous parts of Central Europe, arctic–alpine tundra generally forms only isolated sites comparable to islands, while in Northern Europe it occupies much larger areas (Soukupová et al. 1995; Jeník 1998; Jeník & Štursa 2003; Bílá et al. 2012). The alpine environment is not very favourable climatically, and therefore alpine grasslands are generally species-poor in comparison with those in lower altitudes (Dennis et al. 1995; Fleishman et al. 1998; Gutierrez & Menendez 1998; Strathdee & Bale 1998; Bílá et al. 2012). The High Sudetes, however, host specific lepidopteran fauna, as three ecoregions meet here: alpine, Carpathian, and boreal (Liška & Skyva 1997; Beneš et al. 2000; Laštůvka & Liška 2005; Bílá et al. 2012). Furthermore, the Sudetes are the northernmost outpost of some European mountain species (e.g. *Blastesthia mughiana, Catoptria petrificella, Erebia sudetica, Elophos operarius, Psodos quadrifarius*), while the boreal tortricid *Sparganothis rubicundana* has here an isolated south-western outpost of its global distribution (Liška 2000; Kuras & Helová 2002; Bílá et al. 2012).

These alpine habitats are unique and highly vulnerable because their existence depends on abiotic conditions, island phenomena, and postglacial history (Taberlet et al. 1998; Schmitt & Haubrich 2008). There nevertheless are few studies as to the effects of biotic factors in determining the composition of communities in such habitats during their postglacial development. It is highly likely that competitive species determined the community's structure and survival of other species (Maron & Vilà 2001). A typical species of Central European mountains is dwarf pine (*Pinus mugo*). It is usually dominant at the lower margin of the subalpine altitudinal zone. Dwarf pine limits the distribution of many other plants and animals within the alpine zone (Cavalli et al. 2011; Zeidler et al. 2012). This successful colonist spreads not only at locations within its indigenous distribution area but in particular at mountain summits where it was artificially planted (Dullinger et al. 2003; Treml et al. 2010). The spread of dwarf pine negatively affects alpine zones by overgrowing the native treeless area, fragmenting the habitat and increasing its isolation, decreasing the amount of food available for insects, and changing the microclimate (Svoboda 2001).

Climate and vegetation changes have contributed to increasing disjunctions in species distribution, and consequent isolation of particular populations has led to their gradual differentiation (Jahn et al. 1997; Liška 1997, Liška & Skyva 1997; Beneš et al. 2000; Liška 2000; Kuras et al. 2000, 2001, 2003, 2009; Čížek et al. 2003). In this study, we endeavoured to quantify the effects on Lepidoptera diversity at both local (Czech Republic) and regional (Central Europe) levels. The aim of our study was to suggest future scenarios of Lepidoptera diversity in alpine habitats of the High Sudetes, including to identify the most vulnerable locations.

2. MATERIALS AND METHODS

2.1. Research synthesis

We performed an extensive literature search through Web of Science during 2015 using the following key words: global change / climate / warming / land-cover use / insect, Lepidoptera / butterfly / moth / upward shift / pole shift / habitat fragmentation / alpine habitat. Information was collected from scientific papers, research articles, short communications, reports, and scholars' research. Selected materials were screened for data about global change and its effects on insects, and in particular the order Lepidoptera. References in preselected papers led to further relevant articles. We used internet sources to learn more about global

change indicators, prognoses, and policies applied to the regional level of the Central Europe: EU Strategy on adaptation to climate change (http://ec.europa.eu/clima), Biodiversity Indicators Partnership (http://www.bipindicators.net), and European Environment Agency (http://www.eea.europa.eu). All findings were summarized and conclusions applied to our example field study.

2.2. Field study

Our field study was conducted in the High Sudetes Mountains. These are middle-high mountains in Central Europe which form a natural border between the Czech Republic and Poland (Jeník 1961). They comprise three mountain ranges: the Krkonoše, Hrubý Jeseník, and Kralický Sněžník mountains (Fig. 1). We selected all alpine sites of the High Sudetes and specified the degree of isolation and origin of *Pinus mugo* (indigenous/artificially planted/absent) (see Table 1 and Fig. 2). We carried out the same procedure for the geographically nearest alpine habitats, which means Babia Góra Mountain in Slovakia and Poland and the Harz Mountains in Germany (see Fig. 1), in order to study global changes and consequent differences in species composition at a wider, regional scale.

Fig. 1. *Map of Europe with selected Central European alpine sites.*

The experiments were carried out in the Hrubý Jeseník and Kralický Sněžník mountains and concentrated on butterflies, which comprise a group of invertebrates with high conservation as well as bio-indication importance. We identified numbers of individuals per species and measured each trap's distance from the tree line (in metres). We also classified vegetation at the alpine sites according to the Habitat Catalogue of the Czech Republic (Chytrý et al. 2010), where habitats are specified in terms of the dominant, diagnostic,

and other plant species present. There are five apparent types of habitat at the alpine sites studied: (1) alpine heathland dominated by *Calluna vulgaris*; (2) subalpine *Vaccinium* vegetation dominated by *Vaccinium myrtillus* and *Vaccinium vitis-idaea*; (3) alpine grassland dominated by *Avenella flexuosa*, *Nardus stricta*, and *Festuca supina*; (4) subalpine tall-herb vegetation dominated by *Molinia coerullea*; and (5) *Pinus mugo* scrub dominated by dwarf pine. These habitats occurred at all those sites studied.

Table 1. *Area, extent of cover, and origin of Pinus mugo at alpine sites.*

Alpine site	Area (ha)	Pinus mugo (%)	Pinus mugo origin*
HJ – Šerák	21.9	36.0	0
HJ – Mravenečník–Vřesník	46.7	0.0	0
HJ – Malý Děd	55.0	24.7	0
HJ – Červená hora	65.7	35.7	0
HJ – Keprník	80.1	37.3	0
HJ – Praděd	142.5	22.1	0
HJ – Vysoká hole	678.5	14.3	0
Kralický Sněžník	89.6	12.5	0
Krkonoše-East	3,212.6	46.0	1
Krkonoše-West	2,116.1	57.0	1
Harz	131.0	5.0	0
Babia Góra	194.0	75.0	1

*HJ = Hrubý Jeseník; *Pinus mugo origin: 1 = occurs naturally in the area, 0 = planted or absent.*

We tested the association of species abundances with the environmental variables measured. Vegetation types (*Calluna, Vaccinium, Avenella, Molinia*, and *Pinus* spp.), alpine site area (ha), and distance to the alpine tree line (m) were considered as explanatory variables. The relationship between species abundance and *Pinus mugo* cover was tested using a generalized linear model.

Faunal structure and its historical development in the presence and absence of *Pinus mugo* was tested using methods based on diagnostic lepidopteran species, i.e. alpine and boreal species with an exclusive affinity for alpine habitats or generally unlikely to be found below the tree line (Patočka & Kulfan 2009). From an eco-zoogeographical point of view (Krampl 1992), this means species with euboreal, boreo–alpine, arctic–alpine, and subalpine distributions with disjunct and very narrow dispersal ranges within Central European mountains. All literature sources related to these mountain ranges were critically reviewed with regard to recent findings (Soffner 1960; Krampl 1992; Jahn et al. 1997; Liška 1997; Liška & Skyva 1997; Liška 2000; Kuras et al. 2009) and the following diagnostic species were identified: *Argyresthia amiantella, Blastesthia mughiana, Callisto coffeella, Catoptria maculalis, Catoptria petrificella, Chionodes viduellus, Clepsis rogana, Clepsis steineriana, Elachista dimicatella, Elachista kilmunella, Elophos operarius, Epichnopterix ardua, Erebia epiphron, Erebia sudetica, Glacies alpinatus, Incurvaria vetulella, Kessleria zimmermanni, Lampronia rupella, Olethreutes obsoletanus, Psodos quadrifarius, Rhigognostis senilella, Sparganothis rubicundana*, and *Xestia alpicola*.

Fig. 2. *Alpine sites in the High Sudetes resembling islands in the matrix of spruce wood and expanding Pinus mugo (dark green inside red lines).*

3. RESULTS AND DISCUSSION

Pinus mugo significantly affected the fauna and flora of alpine sites in Central European mountains during their postglacial development (Jeník 1961; Gutierrez 1997; Čížek et al. 2003). During the Holocene climatic optimum, the conditions for alpine species were even less favourable than they are now because the mountain summits were covered with dwarf pine or spruce (Rybníček & Rybníčková 2004). Therefore, species confined to treeless habitats could survive only at a very few locations, such as glacial cirques, stone debris fields, rocks, and wind-swept summits. We also recorded significant differences in lepidopteran fauna at those alpine sites differing by the origin of *Pinus mugo* there.

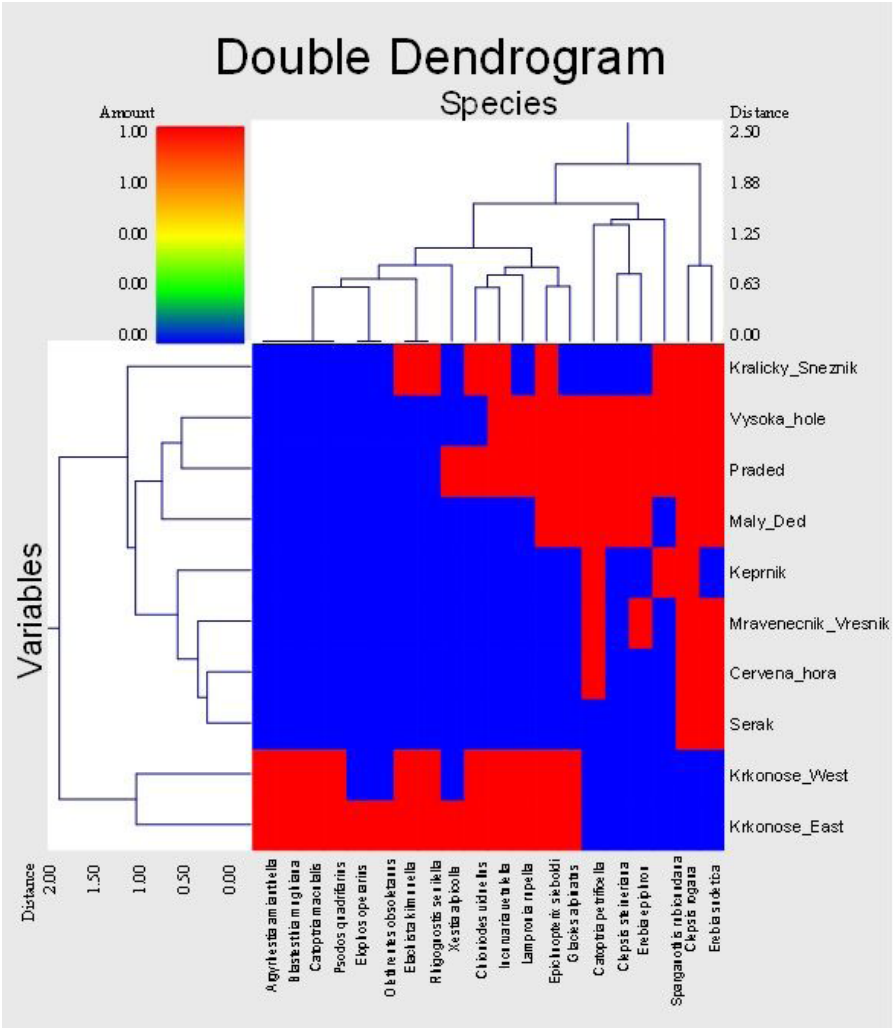

Fig. 3. *Similarity analyses distinguishing alpine sites according to species occurrence.*

Alpine sites with naturally occurring *Pinus mugo*, which most probably in the past covered the summits of these mountains completely or at least in large part, hosted predominantly those lepidopteran species that are able to feed on *Pinus* or those that survived in glacial cirques or stone debris fields. Alpine sites where dwarf pine was not present were covered with dwarf spruce, which does not form such dense formations as dwarf pine. Thus, lepidopteran species associated with grassy tundra could survive at such sites until colder conditions resulted in the tree line's occurring at lower altitudes.

Based on a similarity analysis (Fig. 3), three different groups of alpine sites were identified in the Czech Republic. The first cluster is obvious and consists of alpine habitats with naturally occurring *Pinus mugo*

(Krkonoše-East and Krkonoše-West). The second cluster includes Šerák, Červená hora, Mravenečník-Vřesník, and Keprník (located in the Hrubý Jeseník Mountains), which are small areas with dense cover of planted *Pinus mugo*. The third cluster links alpine summits in the Hrubý Jeseník Mountains (i.e. Vysoká hole, Praděd, and Malý Děd) which are presumably associated with the presence of planted *Pinus mugo*. The last cluster includes Kralický Sněžník, a small site almost overgrown with dwarf pine.

Afforestation with *Pinus mugo* started at the end of the 19th century (Jeník & Hampel 1992) and resulted in the species colonizing the area. Dwarf pine recently reached coverage of about 63% of former alpine habitats (Treml et al. 2010), and this process is continuing. Climate change is now favouring the spread of planted *Pinus mugo* into alpine sites where it previously did not occur.

We next attempted to quantify the potential of dwarf pine to change treeless sites and increase their degree of isolation. We tested the effect of the area covered by *Pinus mugo* on lepidopteran-species abundance using a generalized linear model. Only 15 species were captured during the field sampling: *Aglais urticae, Boloria dia, Coenonympha pamphilus, Erebia epiphron silesiana, Erebia euryale, Erebia ligea, Erebia sudetica sudetica, Gonepteryx rhamni, Inachis io, Issoria lathonia, Lycaena hippothoe, Pieris brassicae, Pieris napi, Pieris rapae*, and *Polygonia c-album*. Species migrating from lower altitudes and captured in numbers of only a few individuals were not evaluated statistically. The most abundant species with exclusive affinity for alpine and montane habitats were *Erebia* spp.: *E. epiphron silesiana, E. euryale, E. ligea*, and *E. sudetica sudetica* (comprising 94.2% of those individuals sampled) (see Fig. 4).

Fig. 4. *Species with exclusive affinity for alpine habitats in the High Sudetes.*

Adult butterflies are highly mobile organisms, and according to our findings (Fig. 5) *Pinus mugo* might be a barrier to their dispersal (Kuras et al. 2001; Konvička et al. 2002). Furthermore, dwarf pine overgrowing alpine vegetation changes the habitat's characteristics by altering the food available for adult butterflies and the quantity of plants suitable for caterpillars (Zeidler et al. 2012) or by causing a decrease in the area of native grass-herbaceous vegetation within the alpine tundra. Over the past 30 years, the extent of cover of planted dwarf pine has increased by 63%; moreover, the percentage cover at small alpine sites in the Hrubý Jeseník Mountains is currently more than 30% and continuing to rise (Fig. 6) (Treml et al. 2010).

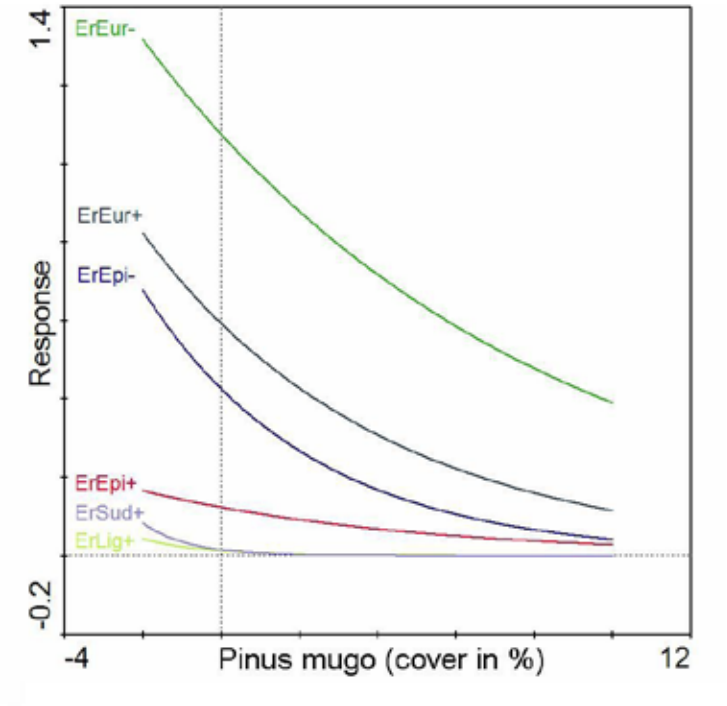

Fig. 5. *Relationship between Erebia species abundance and Pinus mugo cover. ErEur = Erebia euryale, ErEpi = Erebia epiphron, ErSud = Erebia sudetica, ErLig = Erebia ligea; + = female, – = male.*

Our field study provides an example of the interaction between climate change and land-cover change. The two factors acting together can exacerbate the impact of habitat loss and fragmentation on species diversity. We might expect dwarf pine to shift northwards under recent climate warming. The responsible authorities must be attentive to conservation planning and intervention on alpine sites of the High Sudetes, as otherwise we might witness catastrophic declines in species richness due to highly competitive species supported by more favourable climate conditions.

Fig. 6. *Pinus mugo overgrowing alpine sites in the High Sudetes.*

4. CONCLUSIONS

Alpine sites are generally ranked among the most threatened of habitats influenced by anthropogenic activities (Grabherr et al. 1995; Boggs & Murphy 1997; Jeník & Štursa 2003) and climate change (Thomas et al. 2004; Isaac & Williams 2007; European Commission 2013; Bowler et al. 2015). Recent predictions suggest that a temperature increase might cause indigenous alpine species to become endangered or even extinct as a result of the loss of alpine areas due to forest encroachment, habitat fragmentation, invasion of introduced species, and direct climate effects. Therefore, alpine ecosystems constitute a conservation priority. Our results highlight the need for more diversity-response studies to consider global change interactions if we wish to improve conservation policies and strategies.

Acknowledgement

This work was supported by the Ministry of Education, Youth and Sports of the Czech Republic within the National Programme for Sustainability I, grant No. LO1415.

References

Beneš, J., Kuras, T. & Konvička, M. (2000) Assemblages of mountainous day-active Lepidoptera in the Hrubý Jeseník Mts., Czech Republic. *Biologia Bratislava*, **55**, 159–167.

Bílá, K., Kuras, T., Šipoš, J. & Kindlmann, P. (2012) Lepidopteran species richness of alpine sites in the High Sudetes Mts.: effect of area and isolation. *Journal of Insect Conservation*, **17**, 257–267.

Boggs, C.L. & Murphy, D.D. (1997) Community composition in mountain ecosystems: climatic determinants of montane butterfly distributions. *Global Ecology and Biogeography,* **6**, 39–48.

Bowler, D.E., Haase, P., Kröncke, I. et al. (2015) A cross-taxon analysis of the impact of climate change on abundance trends in central Europe. *Biological Conservation*, **187**, 41–50.

Brook, B.W., Akçakaya, H.R., Keith, D.A., Mace, G.M., Pearson, R.G. & Araújo, M.B (2009) Integrating bioclimate with population models to improve forecasts of species extinctions under climate change. *Biology Letters*, **11**, 723–725.

Brook, B.W., Sodhi, N.S. & Bradshaw, C.J.A. (2008) Synergies among extinction drivers under global change. *Trends in Ecology & Evolution*, **23**, 453–460.

Cahill, A.E., Aiello-Lammens, M.E., Fisher-Reid, M.C. et al. (2013) How does climate change cause extinction? *Proceedings of the Royal Society B: Biological Sciences*, **280**, 20121890.

Callinger, K.M., Queensborough, S. & Curtis, P.S. (2013) Herbarium specimens reveal the footprint of climate change on flowering trends across north-central America. *Ecology Letters*, **16**, 1037–1044.

Cavalli, R., Pellegrini M., Grigolato, S. & Bietresato, M. (2011) A strategy for the management of abandoned mountain pasture land colonised by dwarf pine. *Italian Journal of Forest and Mountain Environments*, **66**, 383–393.

Chen, I.C., Hill, J.K., Ohlemuller, R., Roy, D.B. & Thomas, C.D. (2011) Rapid range shifts of species associated with high levels of climate warming. *Science*, **333**, 1024–1026.

Chytrý, M., Kučera, T., Kočí, M., Grulich, V. & Lustyk, P. (eds) (2010) *Habitat Catalogue of the Czech Republic*, Nature Conservation Agency of the Czech Republic.

Čížek, O., Bakešová, A., Kuras, T., Beneš, J. & Konvička, M. (2003) Vacant niche in alpine habitat: the case of an introduced population of the butterfly *Erebia epiphron* in the Krkonoše Mountains. *Acta Oecologica*, **24,** 15–23.

de Chazal, J. & Rounsevell, M.D.A. (2009) Land-use and climate change within assessments of biodiversity change: a review. *Global Environmental Change-Human and Policy Dimensions*, **19**, 306–315.

Dennis, R.L.H. & Shreeve, T.G. (1997) Diversity of butterflies on British islands: ecological influences underlying the roles of area, isolation and the size of the faunal source. *Biological Journal of the Linnean Society*, **60**, 257–275.

Dennis, R.L.H., Shreeve, T.G. & Williams, W.R. (1995) Taxonomic differentiation in species richness gradients among European butterflies (*Papilionoidea*, *Hesperioidea*): contribution of macroevolutionary dynamics. *Ecography*, **18**, 27–40.

Devictor, V., Julliard, R., Couvet, D. & Jiguet, F. (2008) Birds are tracking climate warming, but not fast enough. *Proceedings of the Royal Society B: Biological Sciences*, **275**, 2743–2748.

Dullinger, S., Dirnböck, T. & Grabherr, G. (2003) Patterns of shrub invasion into high mountain grasslands of the Northern Calcareous Alps, Austria. *Arctic, Antarctic, and Alpine Research*, **35**, 434–441.

European Commission (2013) *The EU strategy on adaptation to climate change strengthening Europe's resilience to the impacts of climate change*. Brussels, ISBN 978-927-9329-753.

Fleishman, E., Austin, G.T. & Weiss, AD. (1998) An empirical test of Rapoport's rule: Elevational gradients in montane butterfly communities. *Ecology,* **79**, 2482–2493.

Grabherr, G., Gottfried, M., Gruber, A. & Pauli, H. (1995) Patterns and current changes in alpine plant diversity. *Arctic and alpine biodiversity: patterns, causes and ecosystem consequences* (eds F.S. III Chapin & C. Körner), pp. 167–181. Springer, Berlin.

Gutierrez, D. (1997) Importance of historical factors on species richness and composition of butterfly assemblages (Lepidoptera: Rhopalocera) in northern Iberian mountain range. *Journal of Biogeography*, **24**, 77–88.

Gutierrez, D. & Menendez, R. (1998) Stability of butterfly assemblages in relation to the level of numerical resolution and altitude. *Biodiversity and Conservation*, **7**, 967–979.

Hewitt, G.M. (1999) Post-glacial re-colonization of European biota. *Biological Journal of the Linnean Society*, **68**, 87–112.

Hickling, R., Roy, D.B., Hill, J.K., Fox, R. & Thomas, C.D. (2006) The distributions of a wide range of taxonomic groups are expanding polewards. *Global Change Biology*, **12**, 450–455.

Hill, J.K., Thomas, C.D., Fox, R. et al. (2002) Responses of butterflies to twentieth century climate warming: implications for future ranges. *Proceedings of the Royal Society B: Biological Sciences*, **269**, 2163–2171.

Hill, M.O. & Preston, C.D. (2015). Disappearance of boreal plants in southern Britain – habitat loss or climate change? *Biological Journal of the Linnean Society,* **115**, 598–610.

Felton, A., Fischer, J., Lindenmayer, D. et al. (2009) Climate change, conservation and management: an assessment of the peer-reviewed scientific journal literature. *Biodiversity and Conservation*, **18**, 2243–2253.

Isaac, J.L. & Williams, S.E. (2007) Climate change and extinctions. *Encyclopaedia of biodiversity* (ed Levin, S.). Elsevier Press.

Jahn, A., Kozlowski, S. & Pulina, M. (1997) *Masyw Snieznika: Zmiany w srodowisku przyrodniczym* [Massif of Kralicky Sneznik: Changes in natural environment]. Polska agencija ekologiczna s.a.

Jeník, J. (1961) *Alpinská vegetace Krkonoš, Kralického Sněžníku a Hrubého Jeseníku: teorie anemo-orografických systémů* [Alpine vegetation of the High Sudetes: theory of Anemo-Orographic systems]. Nakladatelství ČSAV, Prague.

Jeník, J. (1998) Biodiversity of the Hercynian Mountains in central Europe. *Pirineos*, **151**, 83–99.

Jeník, J. & Hampel, R. (1992) *Die Waldfreien Kammlagen des Altvatergebirges: Geschichte und Ökologie* [Treeless areas in the Hruby Jesenik Mts.: History and Ecology]. Mährisch-Schlesischer Sudetengebirgsverein, Kirchheim/Teck.

Jeník, J. & Štursa, J. (2003) Vegetation of the Giant Mountains, Central Europe. *Alpine biodiversity in Europe (ecological studies)* (eds L. Nagy, G. Grabherr, C. Körner & D.B.A. Thompson), pp. 47–51. Springer, Berlin.

Jetz, W., Wilcove, D.S. & Dobson, A.P. (2007) Projected impacts of climate and land-use change on the global diversity of birds. *PLoS Biology*, **5**, 1211–1219.

Keith, D.A., Akçakaya, H.R., Thuiller, W. et al. (2008) Predicting extinction risks under climate change: coupling stochastic population models with dynamic bioclimatic habitat models. *Biological Letters*, **4**, 560–563.

Konvička, M., Beneš, J. & Kuras, T. (2002) Microdistribution and diurnal behaviour of two sympatric mountain butterflies (*Erebia epiphron* and *E. euryale*): relations to vegetation and weather. *Biologia Bratislava*, **57**, 223–233.

Krampl, F. (1992) Boreal macro-moths in Central Europe (Czechoslovakia) and their eco-geographical characteristics (Lepidoptera: Geometridae, Noctuidae, Notodontidae). *Acta Entomologica Bohemoslovaca*, **89**, 237–262.

Kuras, T., Beneš, J., Fric, Z. & Konvička, M. (2003) Dispersal patterns of endemic alpine butterflies with contrasting population structures: *Erebia epiphron* and *E. sudetica*. *Population Ecology*, **45**, 115–123.

Kuras, T., Beneš, J. & Konvička, M. (2000) Differing habitat affinities of four *Erebia* species (Lepidoptera: Nymphalidae, Satyrinae) in the Hrubý Jeseník Mts, Czech Republic. *Biologia Bratislava*, **55**, 169–175.

Kuras, T., Beneš, J. & Konvička, M. (2001) Behaviour and within-habitat distribution of adult *Erebia sudetica sudetica*, endemic of the Hrubý Jeseník Mts., Czech Republic (Nymphalidae, Satyrinae). *Nota Lepidopterologica*, **24**, 69–83.

Kuras, T. & Helová, S. (2002) Relict occurrence of the leaf-roller *Sparganothis rubicundana* in Central Europe (Lepidoptera, Tortricidae). *Časopis Slezského Muzea Opava (A)*, **51**,199–204.

Kuras, T., Konvička, M., Beneš, J. & Čížek, O. (2001) *Erebia sudetica* and *Erebia epiphron* (Lepidoptera: Nymphalidae, Satyrinae) in the Czech Republic: review of present and past distribution, conservation implication. *Časopis Slezského Muzea Opava (A)*, **50**, 57–81.

Kuras, T., Sitek, J., Liška, J., Mazalová, M. & Černá, K. (2009) Motýli (Lepidoptera) národní přírodní rezervace Praděd (CHKO Jeseníky): implikace poznatků v ochraně území [Lepidoptera of the Praded National Nature Reserve (Jeseniky Protected Landscape Area): conservation implications]. *Časopis Slezského Muzea Opava (A)*, **58**, 250–288.

Laštůvka, Z. & Liška, J. (2005) Seznam motýlů České republiky (Insecta: Lepidoptera) [Checklist of Lepidoptera of the Czech Republic (Insecta: Lepidoptera)]. http://www.lepidoptera.wz.cz/Lepidoptera.pdf. Accessed 26 Oct 2015.

Liška, J. (1997) Motýlí fauna Úpského a Černohorského rašeliniště v Krkonoších [Lepidoptera of the Úpské and Černohorské rašeliniště bogs in the Krkonoše Mts.]. *Geoekologiczne problemy Karkonoszy*. Materialy z sesji naukowej w Przesiece 15.–18. X. Wydawnictwo Acarus, Poznan.

Liška, J. (2000) Pokus o srovnání motýlí fauny subalpinských poloh Vysokých Sudet [Attempt of comparing lepidopteran fauna of subalpine areas of the High Sudetes]. *Opera Corcontica*, **37,** 286–290.

Liška, J. & Skyva, J. (1997) Historical and recent occurrence of Lepidoptera in mountains sites of the Giant Mountains (Czech Republic). *Biologia Bratislava*, **52**, 163–165.

Mantyka-Pringle, C.S., Visconti, P., Di Marco, M., Martin, T.G., Rondinini, C. & Rhodes, J.R. (2015) Climate change modifies risk of global biodiversity loss due to land-cover change. *Biological Conservation*, **187**, 103–111.

Maron, J.L. & Vilà, M. (2001) When do herbivores affect plant invasion? Evidence for the natural enemies and biotic resistance hypotheses. *Oikos,* **95**, 361–373.

Mason, S.C., Palmer, G., Fox, R. et al. (2015) Geographical range margins of many taxonomic groups continue to shift polewards. *Biological Journal of the Linnean Society*, **115**, 586–597.

Oliver, T.H. & Morecroft, M.D. (2014). Interactions between climate change and land use change on biodiversity: attribution problems, risks, and opportunities. *Wiley Interdisciplinary Reviews: Climate Change*, **5**, 317–335.

Opdam, P. & Wascher, D. (2004). Climate change meets habitat fragmentation: linking landscape and biogeographical scale levels in research and conservation. *Biological Conservation*, **117**, 285–297.

Parmesan, C. (2006) Ecological and evolutionary responses to recent climate change. *Annual Review of Ecology and Systematics*, **37**, 637–669.

Parmesan, C. & Yohe, G. (2003) A globally coherent fingerprint of climate change impacts across natural systems. *Nature*, **421**, 37–42.

Patočka, J. & Kulfan, J. (2009) *Motýle Slovenska (bionomia a ekologia)* [Lepidoptera of Slovakia (bionomics and ecology)]. Vydavatelstvo VEDA, Bratislava, Slovakia.

Rybníček, K. & Rybníčková, E. (2004) Pollen analyses of sediments from the summit of the Praděd range in the Hrubý Jeseník Mts (Eastern Sudetes). *Preslia*, **76**, 331–347.

Saether, B.E., Tufto, J., Engen, S., Jerstad, K., Rostad, O.W. & Skatan, J.E. (2000) Population dynamical consequences of climate change for a small temperate songbird. *Science*, **287**, 854–856.

Sala, O.E., Chapin, F.S., Armesto, J.J. et al. (2000) Biodiversity – global biodiversity scenarios for the year 2100. *Science*, **287**, 1770–1774.

Schmitt, T. & Haubrich, K. (2008) The genetic structure of the mountain forest butterfly *Erebia euryale* unravels the late Pleistocene and postglacial history of the mountain coniferous forest biome in Europe. *Molecular Ecology*, **17**, 2194–2207.

Soffner, J. (1960) Schmetterlinge aus dem Riesengebirge [Lepidoptera of the Giant Mts.]. *Zeitschrift der Wiener Entomologischen Gesellschaft*, **45**, 70–91.

Soukupová, L., Kociánová, M., Jeník, J. & Sekyra, J. (eds) (1995) Arctic—alpine tundra in the Krkonoše, the Sudetes. *Opera Corcontica*, **32**, 5–88.

Strathdee, A.T. & Bale, J.S. (1998) Life on the edge: insect ecology in Arctic environments. *Annual Review of Entomology*, **43**, 85–106.

Sutherst, R.W. (2000) Climate change and invasive species – a conceptual framework. *Invasive Species in a Changing World* (eds Mooney, H.A. & Hobbs, R.J), pp. 211–240. Island Press, Washington, DC.

Svoboda, M. (2001) The effects of *Pinus mugo* (Turra) plantations on alpine-tundra microclimate, vegetation distribution, and soils in Krkonoše National Park, Czech Republic. *Opera Corcontica*, **38**, 189–206.

Taberlet, P., Fumagalli, L., Wust-Saucy, A.-G. & Cosson, J.-F. (1998) Comparative phylogeography and postglacial colonization routes in Europe. *Molecular Ecology*, **7**, 453–464.

Thomas, C.D., Cameron, A., Green, R.E. et al. (2004) Extinction risk from climate change. *Nature*, **427**, 145–148.

Thomas, C.D., Franco, A.M.A. & Hill, J.K. (2006). Range retractions and extinction in the face of climate warming. *Trends in Ecology & Evolution*, **21**, 415–416.

Treml, V. & Banaš, M. (2000) Alpine Timberline in the High Sudetes. *Acta Universitatis Carolinae. Geographica,* **35**, 83–99.

Treml, V., Wild, J., Chuman, T. & Potůčková, M. (2010) Assessing the change in cover of non-indigenous dwarf pine using aerial photographs, a case study from the Hrubý Jeseník Mts., the Sudetes. *Journal of Landscape Ecology*, **4**, 90–104.

Varga, Z. & Schmitt, T. (2008) Types of oreal and oreotundral disjunctions in the western Palearctic. *Biological Journal of the Linnean Society,* **93**, 415–430.

Vinebrooke, R.D., Cottingham, K.L., Norberg, J. et al. (2004) Impacts of multiple stressors on biodiversity and ecosystem functioning: the role of species co-tolerance. *Oikos,* **104**, 451–457.

Visconti, P., Bakkenes, M., Baisero, D., Brooks, T., Butchart, S.H., Joppa, L., Alkemade, R., Marco, M.D., Santini, L. & Hoffmann, M. (2015). Projecting global biodiversity indicators under future development scenarios. *Conservation Letters*. doi: 10.1111/conl.12159

Zeidler, M., Duchoslav, M., Banaš, M. & Lešková, M. (2012) Impacts of introduced dwarf pine (*Pinus mugo*) on the diversity and composition of alpine vegetation. *Community Ecology*, **13**, 213–220.

Chapter 16

Effect of global change on orchid diversity: A meta-analysis

Iva Traxmandlová, Pavel Kindlmann, Zuzana Štípková

Department of Biodiversity Research, Global Change Research Centre, Czech Academy of Sciences, Prokišova 7, CZ-370 01 České Budějovice, Czech Republic

1. INTRODUCTION

Over the past 50 years, organisms and ecosystems have become increasingly vulnerable to extinction (Koopowitz et al. 2003). One of the reasons for this is climate change, which is currently considered a major threat to biodiversity, and numerous species extinctions and range shifts are predicted under a range of scenarios (Thomas et al. 2004; Pereira et al. 2010). Moreover, both direct and indirect effects of climate change on organisms may vary among habitats because these effects result from interactions between large-scale changes in climate and local changes in habitat conditions (Brook et al. 2009; Nicole et al. 2011; Bütof et al. 2012; Peery et al. 2012).

Orchids comprise one of the two largest families of flowering plants, embracing between 21,950 and 26,049 currently accepted species within 880 genera (Stevens 2012; WCSP 2015) and representing approximately 10% of all named plants. Orchids are especially predisposed to extinction risks (Koopowitz et al. 2003) because they already suffer from an uncertain future due to overexploitation and habitat loss from human activities. The impact of climate change only adds to this threat (Barman & Devadas 2013). Because most orchid species are greatly endangered, orchids have enormous species diversity, and orchids exist almost everywhere in the world, orchids constitute a very good group for studies of the effect of climate change on endangered plants.

In this study, we carried out a meta-analysis of published literature on the relationship between orchids' persistence, shifts in their life histories, and their population dynamics in order to consider possible consequences and specific threats that might affect the survival of these endangered plants. We concluded that assisted translocation/migration represents a new challenge in the face of climate change. Species, and in particular orchids, will need artificial assistance to migrate from hostile environments across ecological barriers.

2. MATERIALS AND METHODS

In order to determine and compare possible effects of global change on orchid diversity, we undertook a meta-analysis in Web of Science using the keywords "orchid*" and "climate change". We found 123 papers, of which we chose the 18 papers most relevant to the current study's topic. Although the remaining papers contained the two keywords requested, they mentioned climate change only marginally.

In addition, we reviewed another 28 papers which added some context to the issue studied but were not part of the aforementioned search. These were selected from our own database of orchid papers and were used to explain further details and contexts of the issues studied.

We synthesize below the body of knowledge we have about the topic studied and propose actions to be taken in order to preserve the biodiversity of this endangered plant group.

3. RESULTS AND DISCUSSION

3.1. Effects of climatic change on orchid life cycles

Climatic variation may affect many parts of plants' life cycles, including germination (Levine et al. 2008), flowering dynamics (Inouye et al 2002; Pfeifer et al. 2006) and survival probability (Simons et al. 2010). Climatic changes might differ in their effects upon vital rates, and influences may sometimes even act in opposite directions (Hutchings 2010; Nicole et al. 2011).

Climate change operates upon plant populations at larger temporal scales and may affect both phenology and individual fitness components, thus leading to altered long-term population dynamics (Sparks & Menzel 2002; Hedhly et al. 2009; Hornemann et al. 2012). Likewise, a specific management practice may improve some vital rates while worsening others (Sletvold et al. 2013). The potential effects of climate change on orchids are difficult to predict, and some ecosystems are likely to be more vulnerable to climate change than are others (Seaton et al. 2010).

Some changes in orchid life cycles have even attracted the attention of the general public. For example, the BBC reported* that "Orchid spotters are helping to map climate change in a major UK citizen science survey". The project mentioned was initiated in 2015 at the start of the orchid flowering season by the Natural History Museum in London and the University of Oxford's Zooniverse. The organizers plan to use records of orchid flowering times around country to study the effects of climate change upon plant phenology. This research was undertaken following evidence that the peak flowering time of early spider orchids (*Ophrys sphegodes*) advances by about 6 days per 1ºC rise in temperature during spring. The effects of climate change create "winners" and "losers". Among the "winners", bee orchids (*Ophrys apifera*) and pyramidal orchids (*Anacamptis pyramidalis*) have broadened their ranges, moved to the north, and possibly also grown in abundance. Other species, such as the vulnerable sword-leaved helleborine (*Cephalanthera longifolia*), are suffering under climate changes, and very few man orchid (*Orchis anthropophora*) populations are safe and secure. This research should add to understanding of how climate change affects species diversity within the UK.

Molnár et al. (2012) investigated what traits may predict terrestrial orchids' phenological response to climate change. They studied a set of about 40 orchid species in Hungary using data on flowering dates from 1837 to 2009 from herbarium specimens. They found that across all taxa, flowering time advanced by 3 days over 50 years compared to the mean time prior to 1960, and by 7.7 days in those species showing significant advancement in flowering time.

But what might explain the variation in flowering time advancement among the orchid species they studied? They found the greatest advancement among species reproducing autogamously or using deceptive pollination, as well as other such important factors as the season in which the species begins to flower and its lifespan. This last factor is interesting from an evolutionary perspective. One would think that species with shorter lifespans would have greater potential for flowering time selection, but the Hungarian research team found the opposite to be true. They suggested that phenotypic plasticity may be to blame rather than an evolutionary response to climate change.

* http://www.bbc.com/earth/story/20150520-orchid-spotters-help-map-climate-change

3.2. Effects of changes in ambient environmental conditions

Orchids are well known for their strict habitat requirements, a factor which contributes to their rarity (Cribb et al. 2003). Projected increases in precipitation and evaporation rate would result in decreased soil moisture (Bates et al. 2008). This change would likely have the greatest effect on terrestrial orchids. The long-term survival of orchids is threatened by droughts which occur due to climate change and are leading to demise of the genus *Melaleuca* (Swarts & Dixon 2009). Not all orchids will have the same reaction to global warming, and some may be better adapted to cope with future changes.

Regarding epiphytic orchids, those in forest canopies may be not only exceptionally sensitive to desiccation (Benzing 2004) but also affected indirectly. Orchids make up only one component of a complex web of interactions with other epiphytes in the canopy. These other epiphytes may in turn show different effects from changes in light, nutrients, and moisture availability.

Comparing species from the closely related genera *Paphiopedilum* and *Cypripedium* in China revealed that these species displayed different physiological adaptations and survival strategies (Hu Hong, unpublished data). Evergreen *Paphiopedilum* species have adapted to environments with fewer resources by reducing their rates of photosynthesis and growth, while the deciduous *Cypripedium* species displayed higher rates of photosynthesis and more rapid growth during their active periods. Increased atmospheric CO_2 could lead to increased rates of photosynthesis as described in Chapter 7 of this book, but so far the effects of temperature changes are not completely certain and more research on this topic is needed.

3.3. Vertical shifts of species distribution ranges

Species and population responses to climate change depend on species biology and the population's geographic location (Barman & Devadas 2013). In general, populations on flat terrain move toward the poles in response to warming (Jackson et al. 1987) while those in mountainous areas with mild slopes migrate upwards along the elevation gradient (Thompson 1990). In regions with complex habitats and steep and uneven slopes, however, rare species may face shrinking population sizes and even local extinction (Maschinski et al. 2006).

It is predicted that increasing temperature may result in vegetation zones gradually moving vertically toward mountain tops and as a consequence lowland species could migrate upwards and upland species be gradually eliminated (Foster 2001). Apart from this, warming will bring differences in cloudiness, which will hamper orchid populations. Those on or close to the tops of mountains may be similarly vulnerable to climate warming. Penetration of light and heat into forests depends on vegetation thickness and leaf area index as described in chapters 4 and 6 of this book. Many orchids in upper forest canopies are sensitive to desiccation due to heat (Benzing 2004).

There is evidence that vegetation zones on tropical mountains are strongly controlled by temperature (Primack & Corlett 2005; Seaton et al. 2010). Orchid populations on or close to the tops of limestone mountains in the Yachang Orchid Nature Reserve in Guangxi, China provide an example of potential vulnerability to climatic warming (Liu et al. 2010).

3.4. Loss of habitat due to drifts in species distributions

European terrestrial orchid numbers have declined dramatically over the past 30 years or more due to a combination of factors, including habitat loss and fragmentation. In the UK, however, *Himantoglossum hircinum* and *Ophrys sphegodes* have recently begun increasing again. It has been suggested that the

increase in *H. hircinum* may be due to climate change (see references in Kull & Hutchings 2006; Seaton et al. 2010).

We surveyed all available historical and recent databases of terrestrial orchid locations within South Bohemia and selected at random 192 of those locations that according to the databases hosted some of the five most common orchid species: *Dactylorhiza majalis, Epipactis helleborine, Epipactis palustris, Anacamptis morio*, and *Platanthera bifolia*. Four of these species live in meadows, while *E. helleborine* is a forest species and was included for comparison. We distinguished between "historical sites", those reported before 2000, and "recent sites", those reported since 2000. The choice of 2000 as the border between "historical" and "recent" sites was arbitrary. Fig. 1 depicts the numbers of locations with living orchids, those currently with no orchids, and those that could not be found. Our results indicate that for all species studied there was a strong decline in the number of locations with living orchids. For these locations, however, the decline was mainly due to agricultural intensification rather than climate change. More intensive use of fertilizers caused eutrophication of many sites such that stronger competitors subsequently outcompete orchids. In other cases, the orchid sites were destroyed completely by humans constructing new buildings or roads.

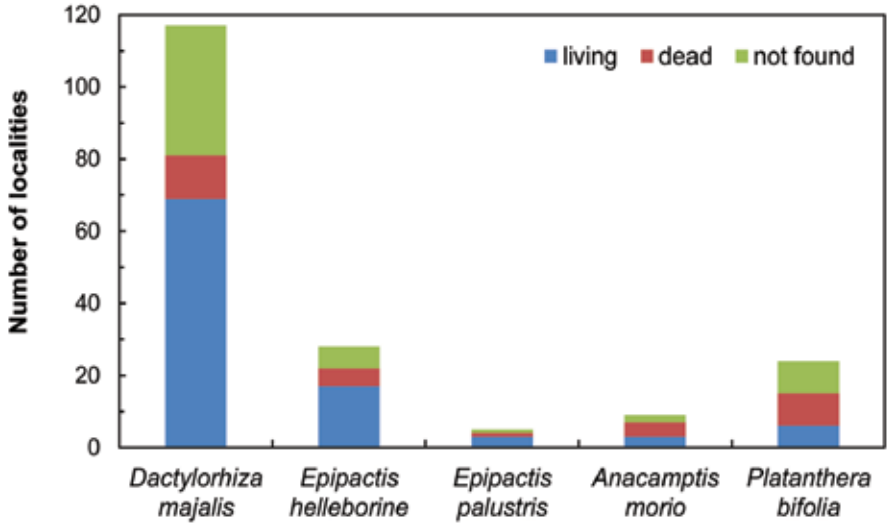

Fig. 1. *Numbers of locations in South Bohemia with selected living orchids, locations currently with no orchids, and locations that could not be found.*

In the Yachang Orchid Nature Reserve, 65 orchid species (47% of the total) currently have very small populations and 20 species (14%) have narrow distributional ranges. These orchids, which face high extinction risk even without climate change (Rabinowitz 1981), may also meet an even higher level of threat from climate change, and in particular if they are found on hilltops because they would not have any higher places to which they could migrate. This category includes *Bulbophyllum tianguii, Cymbidium*

goeringii, Cymbidium longibracteatum, Cymbidium nanulum, Cymbidium tracyanum, Dendrobium officinale, Paphiopedilum micranthum. In addition, populations which are on the southern limit of their species distributions (34 orchid species, 25% of species in Yachang) are also vulnerable to local extinction (Lavergne et al. 2006).

3.5. Loss of interactions with symbionts

It is important, too, to be mindful of the potential effects climate change may have on orchids' fungal partners. One example of the complex relationship that may exist among orchids and other members of their environments can be seen in the underground orchid *Rhizanthella gardneri* of Western Australia. This plant has an obligate mycorrhizal relationship with *Melaleuca uncinata*, specialist-pollinator relationships with a fungus gnat and a termite, and a relationship with a specialist marsupial which acts as a dispersal agent of its berrylike indehiscent seeds.

3.6. Uncoupling of synchronization in pollination systems

The majority of orchid species have specialized insect pollination systems that rely on one to a few pollinator species (Cingel 2001; Tremblay et al. 2005; Liu et al. 2010; Pemberton 2010). Some biologists had previously raised concerns that a warming world would gradually provoke the uncoupling of important species interactions.

For example, a potential disruption of pollination in a sexually deceptive orchid by climatic change was reported by Robbirt et al. (2014). They showed that a sexually deceptive orchid (*Ophrys sphegodes*) and the solitary bee (*Andrena nigroaenea*) upon which it depends for pollination will diverge in phenology as spring temperature increases. Analysis of museum specimens (1893–2007) and field-based records (1975–2009) showed that the bee's flight date was advanced more by higher temperatures than was the orchid's flowering date.

The past two decades have seen several papers speculating on why and how uncoupling might occur (Memmott et al. 2007; Hegland et al. 2009; Wilmer 2014) and where it might be the most serious and lead to species extinctions. The worst effects might occur in entomophilous plants with specialist pollinators and those that flower in early spring.

Field data from at least five decades show that bees emerge earlier in warmer springs (Gordo & Sanz 2006) and that there exists a roughly linear relationship between temperature and phenology. There are also informative data from experimental shifts in flowering time (Rafferty & Ives 2011), although ten bee species in North America showed no evidence of their phenology varying in relation to their preferred flowers (Bartomeus et al. 2011).

It is logical to expect that specialized pollination relationships, such as those between orchids and their pollinators, will be more vulnerable to such mismatches than will more generalist interactions (Ashworth et al. 2004; Dixon 2009). This vulnerability is due in part to the skewed relationships between orchids and pollinators, with the orchid being much more dependent on the pollinators than *vice versa* (Dixon 2009; Liu et al. 2010; Pemberton 2010; Vereecken et al. 2010).

3.7. Potential solutions

Figure 2 displays the sequence of those abiotic and biotic factors which affect terrestrial orchid population (or species) persistence on a continuum from immediate-term impacts (1–2 years for mycorrhizas) to

long-term effects for such factors as climate change, ranked from the most immediate effect to that with the longest delay.

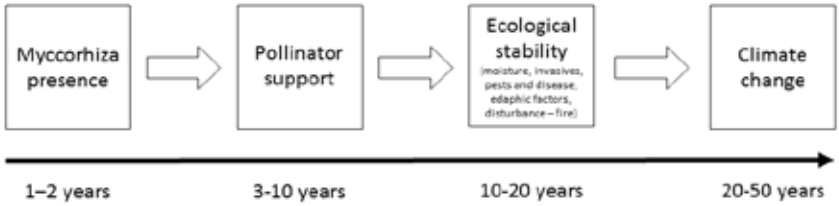

Fig. 2. *Sequence of abiotic and biotic factors affecting terrestrial orchid population (or species) persistence along a continuum from immediate-term impacts (1–2 years for mycorrhizas) to long-term effects for such factors as climate change (adapted from Swarts & Dixon 2009).*

Thus, changes in temperature or other environmental conditions may affect orchid symbionts (mycorrhizas) within one or two seasons. Uncoupling of orchid–pollinator interactions due to different responses to changing environmental conditions may occur within 3–10 years. More complex effects, depending on changes in entire ecosystems, take 10–20 years, and the real effect of climate change (assuming slow changes in temperature) may take as long as 50 years.

A number of strategies pursued to conserve the orchids against the threat from climate change. We present below a list suggested by Barman & Devadas (2013) with some adaptations to make it more appropriate to the current situation.

Restoring and maintaining native ecosystems. Recreating previous habitats or ecosystems in which orchids formerly grew is very difficult due to increasing human population, habitat fragmentation, over-collection of exotic species, extinction of native species, and land conversion for human activities.

Managing habitats in order to support orchids. Sometimes orchids require special management, such as regular mowing. Continuous monitoring is also essential to preserve a population in a good shape.

Ranking species vulnerability. A ranking system can aid in species selection and identification. Restoration can be carried out actively while giving priority to more vulnerable species.

Long-term phenological monitoring of plants and their pollinators. Global warming has a great impact on the phenology of plants and pollinators. Changes in species' range and tropic relationships in relation to warming affect their interactions. Inasmuch as most orchids are cross-pollinated, matching orchid flowering with pollinator visits is important.

Assisted migration. This must be applied differentially, on a case-by-case basis, based on monitoring and stress assessment, in order to mitigate unforeseen problems.

Symbiotic seed germination and seedling propagation. This is a method of saving populations that became extinct in the wild or are close to this. Mycorrhizal associations are essential here.

Seed storage and banking. This is a good safeguard so that some species do not go extinct due to unforeseeable events. Seed banking also enables seed exchanges among research institutes.

4. CONCLUSIONS

In conclusion, climate change will negatively affect many attributes of orchid life, resulting in declining population numbers and the ultimate extinction of many species. Fig. 3 displays a schematic diagram showing the complexity of interactions leading to climate change's strong negative effect on orchid species diversity.

Orchids have strict demands for habitat conditions. They need suitable soil conditions and specific mycorrhizal fungi for germinating as well as appropriate habitats (e.g. climate conditions and management). Many orchids are also dependent on specific pollinators, and climate change is a major threat to pollination services and networks. Thus, there is a need to conserve the plant communities in which orchids live.

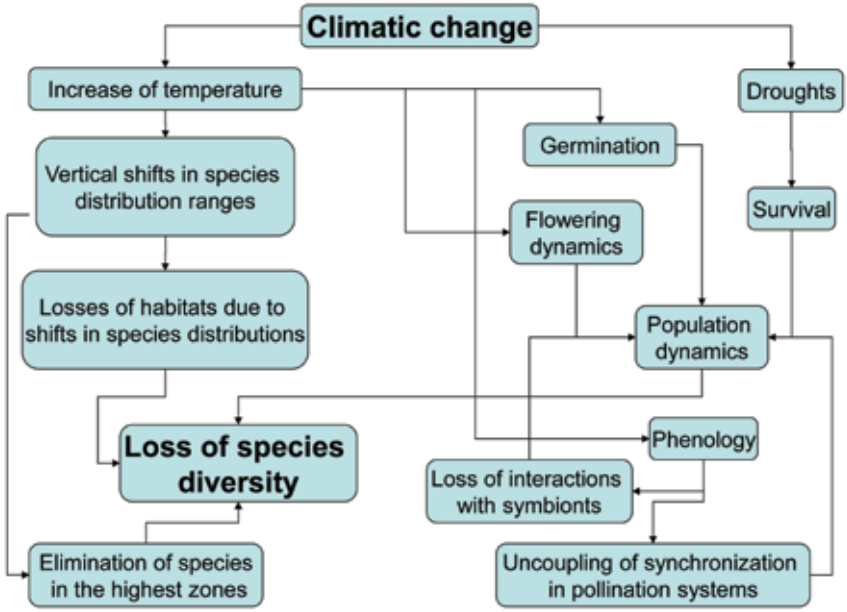

Fig. 3. *A schematic diagram showing the complexity of interactions leading to climate change's strong negative effect on orchid species diversity.*

Conservation through reserves alone is now considered unlikely to achieve protection of those plant species necessary to mitigate direct habitat losses and the pervasive impact of global climate change. Assisted translocation/migration represents a new challenge in the face of climate change: species, and in particular orchids, will need artificial assistance to migrate from hostile environments across such ecological barriers as farmlands and constructed infrastructure to new climatically buffered sites.

Acknowledgement

This work was supported by the Ministry of Education, Youth and Sports of the Czech Republic within the National Programme for Sustainability I, grant No. LO1415.

References

Ashworth, L., Aguilar, R., Galetto, L. & Aizen, M.A. (2004) Why do pollination generalist and specialist plant species show similar reproductive susceptibility to habitat fragmentation? *Journal of Ecology*, **92**, 717–719.

Barman, D. & Devadas, R. (2013) Climate change on orchid population and conservation strategies: A review. *Journal of Crop and Weed*, **9**, 1–12.

Bartomeus, I., Ascher, J.S., Wagner, D. et al. (2011) Climate-associated phenological advances in bee pollinators and bee-pollinated plants. *Proceedings of the National Academy of Sciences of the United States of America*, **108**, 20645–20649.

Bates, B.C., Kundzewics, Z.W., Wu, S. & Palutikof, J.P. (eds) (2008) Climate change and water. IPCC Secretariat, Geneva.

Benzing, D. (2004) Vascular epiphytes. *Forest canopies* (eds M.D. Lowman & H.D. Rinker), pp. 175–211, 2nd edition, Elsevier Academic Press.

Brook, B.W., Akcakaya, H.R., Keith, D.A., Mace, G.M., Pearson, R.G. & Araujo, M.B. (2009) integrating bioclimate with population models to improve forecasts of species extinctions under climate change. *Biology Letters*, **5**, 723–725.

Bütof, A., von Riedmatten, L.R., Dormann, C.F., Scherer-Lorenzen, M., Welk, E. & Bruelheide, H. (2012) the responses of grassland plants to exprerimentally simulated climate change depend on land use and region. *Global Change Biology*, **18**, 127–137.

Cingel, N.A. (2001) An atlas of orchid pollination: America, Africa, Asia, and Australia. A.A. Balkema, Rotterdam, Netherlands.

Cribb, P.J., Kell, S.P., Dixon, K.W. & Barrett R.L. (2003) *Orchid conservation: a global perspective*. (eds K.W. Dixon, S.P. Kell, R.L. Barrett & P.J. Cribb), pp. 1–24, Natural History Publications, Kota Kinabalu, Sabah.

Dixon, K.W. (2009) Pollination and restoration. *Science*, **325**, 571–573.

Foster, P. (2001) The potential negative impacts of global climatic change on tropical montane cloud forest. *Earth Science Reviews*, **55**, 73–106.

Gordo, O. & Sanz, J.J. (2006) Temporal trends in phenology of the honey bee *Apis mellifera* (L.) and the small white *Pieris rapae* (L.) in the Iberian Peninsula (1952–2004). *Ecological Entomology*, **31**, 261–268.

Hedhly, A., Hormaza, J.I. & Herrero, M. (2009) Global warming and sexual plant reproduction. *Trends in Plant Science*, **14**, 30–36.

Hegland, S.J., Nielsen, A., Lázaro, A., Bjerknes, A.-L. & Totland, O. (2009) How does climate warming affect plant-pollinator interactions? *Ecology Letters*, **12**, 184–195.

Hornemann, G., Michalski, S.G. & Durka, W. (2012) Short-term fitness and long-term trends in the orchid *Anacamptis morio*. *Plant Ecology*, **213**, 1583–1595.

Hutchings, M.J. (2010) The population biology of the early spider orchid *Ophrys sphegodes* Mill. III. Demography over three decades. *Journal of Ecology*, **98**, 867–878.

Inouye, D.W., Morales, M.A. & Dodge, G.J. (2002) Variation in timing and abundance of flowering by *Delphinium barbeyi* Huth (Ranunculaceae): the roles of snowpack, frost, and La Nina, in the context of climate change. *Oecologia,* **130**, 543–550.

Jackson, G., Webb I.I., T., Grimm, E.C., Ruddiman, W.F. & Wright Jr, H.E. (1987) North America and adjacent oceans during the last deglaciation. *Geological Society of America*, **3**, 277–288.

Koopowitz, H., Lavarck, P.S. & Dixon, K.W. (2003) The nature of threats to orchid conservation. *Orchid conservation* (eds K.W. Dixon, S.P. Kell, R.L. Barrett & P.J. Cribb), pp. 25–42, Natural History Publications, Kota Kinabalu, Sabah.

Kull, T. & Hutchings, M.J. (2006) A comparative analysis of decline in the distribution ranges of orchid species in Estonia and the United Kingdom. *Biological Conservation*, **129**, 31–39.

Lavergne, S., Molina, J. & Debussche, M. (2006) Fingerprints of environmental change on the rare mediterranean flora: a 115 year study. *Global Change Biology*, **12**, 1466–1478.

Levine, J.M., McEachern, A.K. & Cowan, C. (2008) Rainfall effects on rare annual plants. *Journal of Ecology*, **96**, 795–806.

Liu, H., Feng, C.-L., Luo, Y.-B., Chen, B.-S. & Wang, Z.-S. (2010) Potential challenges of climate change to orchid conservation in a wild orchid hotspot in southwestern China. *Botanical Review*, **76**, 174–192.

Maschinski, J., Baggs, J.P.E., Quintana, A. & Menges, E. (2006) Using population viability analysis to predict the effects of climate change on the extinct risk of an endangered limestone endemic shrub, Arizona cliffrose. *Conservation Biology*, **20**, 218–228.

Memmott, J., Craze, P.G., Waser, N.M. & Price, M.V. (2007) Global warming and the disruption of plant-pollinator interactions. *Ecology Letters*, **10**, 710–717.

Molnár, A.V., Tökölyi, J., Végvári, Z., Sramkó, G., Sulyok J. & Barta, Z. (2012) Pollination mode predicts phenological response to climate change in terrestrial orchids: a case study from central Europe. *Journal of Ecology*, **100**, 1141–1152.

Nicole, F., Dahlgren, J.P., Vivat, A., Till-Bottraud, I. & Ehrlén, J. (2011) Interdependent effects of habitat quality and climate on population growth of an endangered plant. *Journal of Ecology*, **99**, 1211-1218.

Peery, M.Z., Guriérrez, R.J., Kirby, R., LeDee, O.E. & LaHaye, W. (2012) Climate change and spotted owls: potentially contrasting responses in the Southwestern United States. *Global Change Biology*, **18**, 865–880.

Pemberton, R.W. (2010) Biotic resource needs of specialist orchid pollinators. *Botanical Review*, **76**, 275–292.

Pereira, H.M., Leadley, P.W., Prenca V. et al. (2010) Scenarios for global biodiversity in the 21st century. *Science*, **330**, 1496–1501.

Pfeifer, M., Heinrich, W. & Jetschke, G. (2006) Climate, size and flowering history determine flowering pattern of an orchid. *Botanical Journal of the Linnean Society*, **151**, 511–526.

Primack, R. & Corlett, R. (2005) Tropical rainforest: An ecological and biogeographical comparison. Blackwell, U.K.

Rabinowitz, D. (1981) Seven forms of rarity. *The biological aspects of rare plant conservation*. (ed J.H. Synge), pp. 205–217. Wiley, New York.

Rafferty, N.E. & Ives, A.R. (2011). Effects of experimental shifts in flowering phenology on plant-pollinator interactions. *Ecology Letters,* **14**, 69–74.

Robbirt, K.M., Roberts, D.L., Hutchings, M.J. & Davy, A.J. (2014) Potential disruption of pollination in a sexually deceptive orchid by climatic change. *Current Biology*, **24**, 2845–2849.

Seaton, P.T., Hu, H., Perner, H. & Pritchard, H.W. (2010) Ex situ conservation of orchids in a warming world. *Botanical Review,* **76**, 193–203.

Simons, A.M., Goulet, J.M. & Bellehumeur, K.F. (2010) The effects of snow depth in overwinter survival in *Lobelia inflata*. *Oikos*, **119**, 1685–1689.

Sletvold, N., Dahlgren, J.P., Øien, D.-I., Moen, A. & Ehrlén, J. (2013) Climate warming alters effects of management on population viability of threatened species: results from a 30-year experimental study on a rare orchid. *Global Change Biology,* **19**, 2729–2738.

Sparks, T.H. & Menzel, A. (2002) Observed changes in seasons: an overview. *International Journal of Climatology*, **22**, 1715–1725.

Swarts, N.D. & Dixon, K.W. (2009) Terrestrial orchid conservation in the age of extinction. *Annals of Botany*, **104**, 543–556.

Stevens, P.F. (2012) Angiosperm Phylogeny Website Version 9. Missouri Botanical Garden. http://www.mobot.org/mobot/research/apweb/welcome.html. Retrieved 31 October 2015.

Thomas, C.D., Cameron, A., Green, R.E. et al. (2004) Extinction risk from climate change. *Nature,* **427**, 145–148.

Thompson, R.S. (1990) Late quaternary vegetation and climate in the Great Basin. *The last 40,000 Years of Biotic Change*. (eds J.L. Betancourt, T.R. Van Devender & P.S. Martin), pp. 200-209. The University of Arizona Press, Tucson, Arizona.

Tremblay, R.L., Ackerman, J.D., Zimmermann, J.K. & Calvo, R.N. (2005) Variation in sexual reproduction in orchids and its evolutionary consequences: a spasmodic journey to diversification. *Biological Journal of the Linnean Society*, **84**, 1–54.

Vereecken, N.J., Dafni, A. & Cozzolino, S. (2010) Pollination syndromes in Mediterranean orchids – implications for speciation, taxonomy and conservation. *Botanical Review*, **76**, 220–240.

Willmer, P. (2014) Climate change: Bees and orchids lose touch. *Current Biology*, **24**, R1133–R1135.

WCSP (2015) World Checklist of Selected Plant Families. Royal Botanic Gardens, Kew, UK. http://apps.kew.org/wcsp/home.do. Retrieved 31 October 2015.

Chapter 17

New approaches to forest above-ground biomass assessment

Olga Brovkina, Jan Novotný, František Zemek

Department of Remote Sensing, Global Change Research Centre, Czech Academy of Sciences, Bělidla 4a, CZ-60300 Brno, Czech Republic

1. INTRODUCTION

The impacts of changing environmental conditions due to climate change on photosynthesis and respiration (see chapters 6, 7, and 12), biomass formation (see chapters 4, 8, and 10), and the carbon cycle in forest ecosystems (see chapters 6, 13, and 14) have been addressed in this book on leaf, tree, and plot scales. For estimating forest biomass on a forest/ecosystem scale, moreover, robust and precise methods have been always required.

Biomass is directly related to the productivity of forests' carbon sequestration and provides valuable information for understanding ecosystem functions and carbon cycling (Penner et al. 1997).

Various approaches have been applied for above-ground biomass (AGB) estimation based on both field methods and remote sensing methods. Traditional approaches using field measurements (see Chapter 4 of this book for details) are the most accurate ways to collect AGB data. A sufficient number of field measurements is a prerequisite for developing AGB estimation models and for evaluating results (Liang et al. 2012). The estimates usually have spatial, attributional, and temporal gaps, however, and field methods are often time consuming, labour intensive, and difficult to implement, especially in remote areas. Remotely sensed data is used to fill these gaps, thereby leading to AGB estimates closer to the actual value. In recent years, remote sensing techniques have become prevalent in estimating AGB due to several factors, including the ability to obtain measurements from all locations in a forest, the speed with which remotely sensed data can be collected and processed, and the relatively low cost of many remote sensing data types. Remote sensing data are available at different scales to provide information that can be related to AGB estimation. Coarse-resolution (pixel >100 m) satellite data (e.g. Moderate-resolution Imaging Spectroradiometer data) is useful for AGB estimation at regional to continental scales inasmuch as their high temporal frequency increases the probability of acquiring cloud-free data for generating consistent data sets over large areas. Such data provides a suite of biophysical products for AGB estimation, including fraction of absorbed photosynthetically active radiation, gross primary production, net photosynthesis, and net primary productivity (Fensholt et al. 2006). Middle-resolution (e.g. Landsat) satellite-based methods for AGB estimation include the developments of empirical or physical models to estimate forest structural or biophysical properties from relationships with spectral reflectance or derived vegetation indices (Woodcock et al. 1994; Dong et al. 2003). In the past, analogue aerial photographs provided an alternative source for AGB assessment. At present, forest-inventory procedures use visual interpretation of digital aerial photography including such stand-level measurements as canopy cover and distribution (Simova et al. 2009), canopy structure, and stand AGB (Kadmon & Harari-Kremer 1999), as well as such tree-level measurements as tree position, height, crown diameter, and allometric estimation of trunk dimensions (Kovats 1997).

Recently, airborne LiDAR (Light Detection and Ranging) scanning has become the most precise technique for estimating forest characteristics. In contrast to the aforementioned imagery data, high-resolution airborne LiDAR senses trees' physical dimensions with which AGB correlates directly. LiDAR-based airborne instruments provide a direct means of estimating tree heights, crown density, and tree location which enable calculation of AGB based on allometric equations (Koch 2010; Luther et al. 2014).
This chapter presents a methodology for estimating forest AGB based on airborne LiDAR data for a case study located in the Beskydy Mountains. The study aims to estimate forest AGB from airborne LiDAR data at tree, plot, and compartment levels and to compare the results with those obtained from a "classical" field survey and forest inventory as currently used in forestry and management practices.

2. MATERIALS AND METHODS

2.1. Site description

The study area (Fig. 1) is located in the Beskydy Mountains of the Czech Republic (49°50′N, 18°54′E, 750–950 m a.s.l.). The area is characterized by managed forest stands of monoculture Norway spruce (*Picea abies*) aged 15–147 years, with mean age of 60 years, along with an admixture of broadleaved trees (22.7%) with mean age of 72 years. The latter comprise mostly European beech (*Fagus sylvatica*) while less abundant species include goat willow (*Salix caprea*), common alder (*Alnus glutinosa*), and individually occurring silver fir (*Abies alba*) trees.

2.2. Data

2.2.1. Airborne data

LiDAR data were acquired on 14 May 2013 using an LMS-Q680i scanner (Riegl Laser Measurement Systems, Horn, Austria). Thirty-five highly overlapping strips were flown at an average flight height of 550 m above ground level, which resulted in a point cloud density of >50 points m^{-2}. The data were post-processed by the vendor. Post-processing encompassed full-waveform decomposition and georeferencing using the RiProcess software package (Riegl Laser Measurement Systems) and an export to LAS format after strip adjustment.

2.2.2. Field data

Field data were collected by the Institute of Forest Ecosystem Research (IFER, Jílové u Prahy, Czech Republic, www.ifer.cz) in 2013 using circular inventory plots, each measuring 500 m^2 (radius of 12.62 m). On each plot, the measurements included tree height, diameter at breast height (DBH), crown length, age and species composition. The variables were collected using Field-Map technology (IFER, www.fieldmap.cz), including electronic callipers for DBH measurements and a laser rangefinder for tree height and tree crown data. We used 29 plots to compare AGB from field data with AGB calculated from LiDAR data at the tree and plot levels.

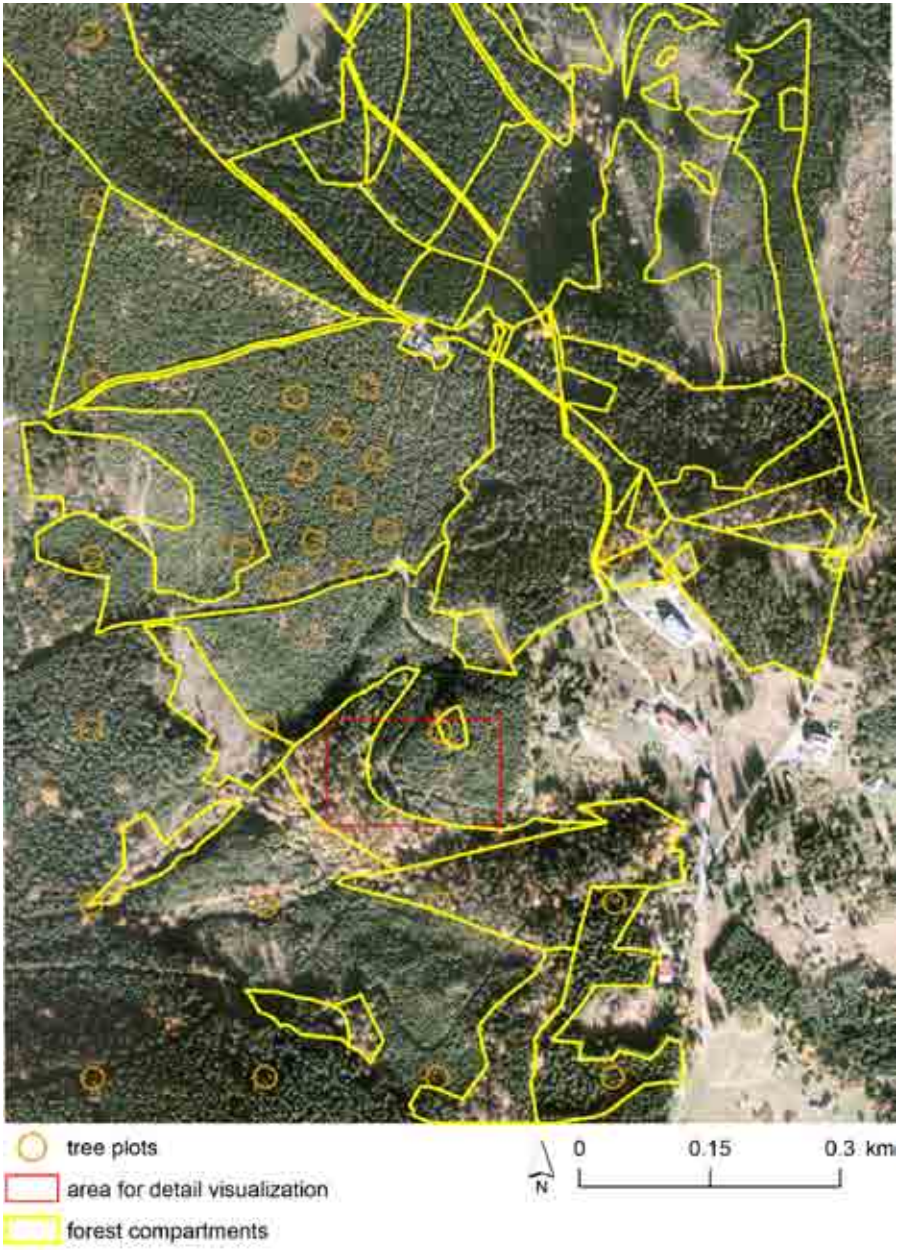

Fig. 1. *Study area with locations of tree plots, forest compartments, and area for detail visualization.*

2.2.3. Forestry map

The Forest Management Institute (Brandýs nad Labem, Czech Republic, www.uhul.cz) provided vector forest inventory maps with attribute tables containing forest management planning data that had been revised in 2010. These data were collected according to the Czech forest management planning standard (Staněk et al. 1997). Merchantable AGB from the inventory data was recalculated from kg m^{-3} per compartment to kg ha^{-1} using basic wood density (420 kg m^{-3} for spruce and 580 kg m^{-3} for beech) and respective compartment area. We selected 29 forest compartments to compare AGB from the forestry inventory with AGB from LiDAR data estimations.

2.3. Method for AGB estimation based on airborne LiDAR data

The steps we used to determine tree-level AGB comprised: 1) creation of a map of species composition; 2) individual tree crown detection, 3) tree height estimation, and 4) AGB estimation using allometric equations. Tree AGB values were summed for each plot and each compartment. Figure 2 depicts this process. Finally, we compared tree-level AGB from LiDAR with field tree AGB estimation, the sum for plot AGB from LiDAR with field plot AGB, and the sum for compartment AGB from LiDAR with compartment AGB from the inventory.

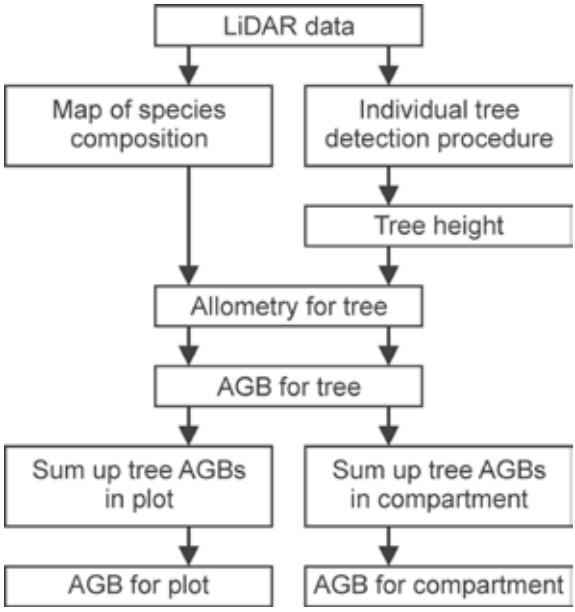

Fig. 2. *Process organization for estimating above-ground biomass from airborne LiDAR data.*

2.3.1. Map of species composition

We used the following full-waveform properties recommended by Heinzel & Koch (2011) for Central European temperate forests: average intensity at top-of-the-canopy level, average echo width from

top-of-the-canopy level, and average number of echoes per pulse. The three-dimensional point cloud was projected onto a two-dimensional raster with spatial resolution of 0.4 m. Recent studies have shown that the most important basic full-waveform parameter for separating species composition is the intensity of the reflection (Lim et al. 2003; Heinzel & Koch 2011). The standard deviation calculated from a moving window of 8 × 8 pixels was used to characterize the intensity texture in the raster. The size of the window was estimated as a modal crown projection of trees in the pilot region. The final multilayer data represented the following five properties from LiDAR data: pulse width, number of echoes per pulse, amplitude, intensity, and intensity texture. We used these parameters as inputs to the classification.

We classified coniferous and broadleaved forest using supervised Mahalanobis Distance Classification in ENVI 5.0 software (Exelis Visual Information Solutions, Boulder, CO, USA). Field data and ground truth observations were used to delineate training samples. All pixels were classified into four classes: "young coniferous", "mature coniferous", "broadleaved", and "artificial objects" (roads and buildings). Post-classification steps included sieving and clump procedures as described below.

The problem of isolated pixels was solved by sieving the classes using a blob grouping procedure with the minimum number of pixels contained in a class group set at 8 and the number of neighbouring pixels set at 4. The clump classes procedure was applied using a morphological operator of 3 × 3 pixels in order to cluster adjacent similarly classified areas. The classification results' accuracy was estimated by calculating a confusion matrix.

2.3.2. Individual tree detection

First, we transformed LiDAR point cloud into a canopy height model (CHM). This was done by subtracting a digital terrain model (DTM) from a digital surface model (DSM). Ground points in the cloud were classified using LAStools software (rapidlasso, Gilching, Germany) with the settings for a natural environment. The DTM was interpolated using the Delaunay triangulation of ground points and the DSM was interpolated using the same methods for the highest points. Second, positions of individual trees were detected in the CHM as local height maxima. We smoothed the CHM using a Gaussian low pass filter and then sought local maxima with a sliding window that varied adaptively in size (Novotny 2014). We saved the coordinates and height of each local maximum to a point shape file for subsequent GIS analysis.

2.3.3. Allometry for AGB estimation

We used allometric equations (1)–(4) to estimate tree-level AGB for spruce and beech (Wirth et al. 2004; Wutzler et al. 2008). These equations were derived from field measurements carried out on trees grown in stand conditions similar to those in our study area:

$$AGB_{spruce} = AGB_{needles} + AGB_{branches} + AGB_{dry\ branches} + AGB_{stem}, \quad (1)$$

where each tree AGB category was calculated as (Wirth et al. 2004):

$$AGB = a \times b \times \exp(c \times \ln(DBH) - d), \quad (2)$$

where $a = 1.0849$, $b = 1.0226$, $c = 1.9162$, $d = 3.19632$ for $AGB_{needles}$;
$a = 1.1332$, $b = 1.0103$, $c = 2.2552$, $d = 3.96201$ for $AGB_{branches}$;
$a = 1.1146$, $b = 1.1107$, $c = 2.04823$, $d = 3.09062$ for $AGB_{dry\ branches}$; and
$a = 1.0142$, $b = 1.0238$, $c = 2.50602$, $d = 2.50602$ for AGB_{stem}.

To retrieve DBH (cm) for spruce trees, we used a parameterized model based on measured tree heights on the sample plots ($R^2 = 0.84$, $n = 257$):

$$DBH = -b/\log\left(\frac{H-1.3}{a}\right), \quad (3)$$

where $a = 64.188$, $b = 30.446$, and H is the height (m) of spruce trees.
We used equation (4) to estimate AGB for beech (Wutzler et al. 2008):

$$AGB_{beech} = 0.0551 * DBH^{2.11} * H^{0.589}, \quad (4)$$

where H is the height (m) of beech trees. DBH model parameters were also derived for beech from equation (3), resulting in $a = 59.567$ and $b = 30.472$ ($R^2 = 0.60$, $n = 447$). Since the number of beech trees at the study site available for measuring height and DBH was limited, we also used field measurements from the CzechTerra landscape inventory program in order to obtain a statistically more representative data set (IFER 2014, unpublished material).

2.3.4. AGB at tree, plot, and compartment levels

The AGB at the tree level was estimated based on the allometry described in section 2.3.3. AGB at the plot and compartment levels was obtained by summing the respective tree-level AGB values in each plot and compartment.

3. RESULTS AND DISCUSSION

3.1. Map of species composition

The accuracy of the classification from LiDAR data was estimated by comparing the classification result with accurate ground information via a confusion matrix. The result demonstrates an overall accuracy of 81% and kappa coefficient of 0.72. The derived map contained "coniferous" and "broadleaved" forest classes with producer accuracies of 86.1% and 72.7%, respectively (Fig. 3). Our study's good overall accuracy is, however, lower than the findings of the study by Heinzel & Koch (2011) on species grouped into coniferous and broadleaved trees (overall accuracy of 91%). To improve species classification for our study area, we recommend separating "beech" and "birch" pixels from the broadleaved group and "spruce" and "fir" pixels from the coniferous group by exploring other such features from LiDAR data as crown shape (Hollaus et al. 2009) or by using hyperspectral imagery (Leckie et al. 2005).

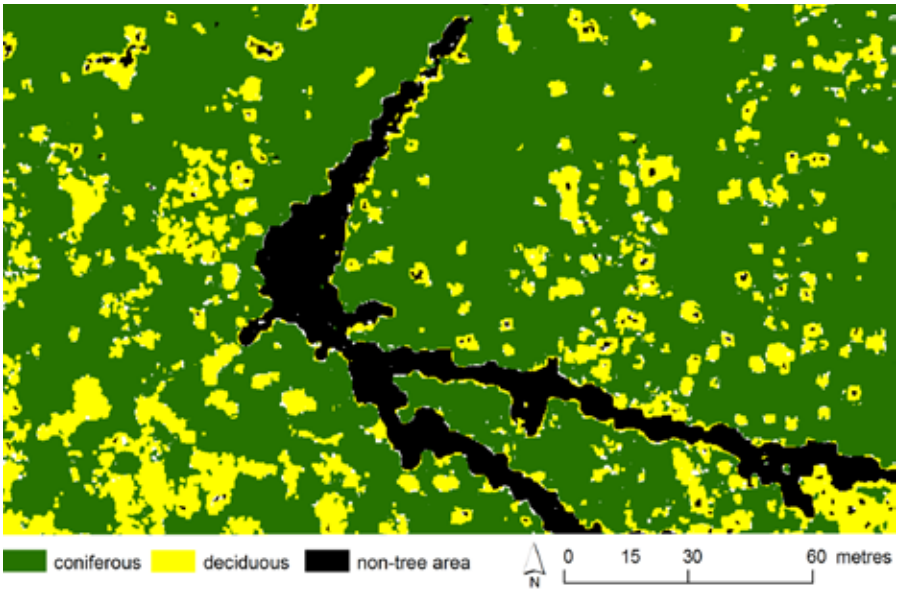

Fig. 3. *Map of species classification based on five LiDAR data properties: pulse width, number of echoes per pulse, amplitude, intensity, and standard deviation of intensity (texture).*

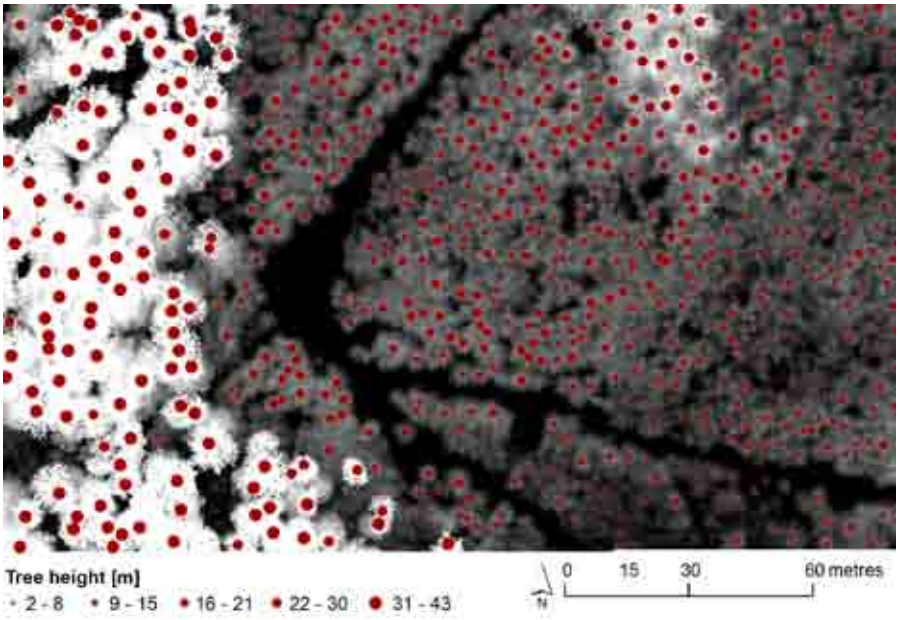

Fig. 4. *Map of tree detection from LiDAR data where circles are trees and the size of circles symbolizes the height (the background is a canopy height model).*

3.2. Individual tree detection

The accuracy of LiDAR input data was estimated by comparing tree heights from LiDAR data with heights measured in the field (Fig. 5) on the 29 plots shown in Fig. 1. Tree heights derived from LiDAR data significantly correlated with field measurements ($R^2 = 0.99$) with a small systematic offset. The offset follows our expectations because laser scanning tends to underestimate tree height. Our results are in agreement with recent studies. For example, Popescu & Wynne (2004) found stronger matching between LiDAR and field measurements in a pine (*Pinus sylvestris*) forest ($R^2 = 0.99$). Luther et al. (2014) predicted black spruce (*Picea mariana*) average height with $R^2 = 0.86$ from airborne laser scanner data.

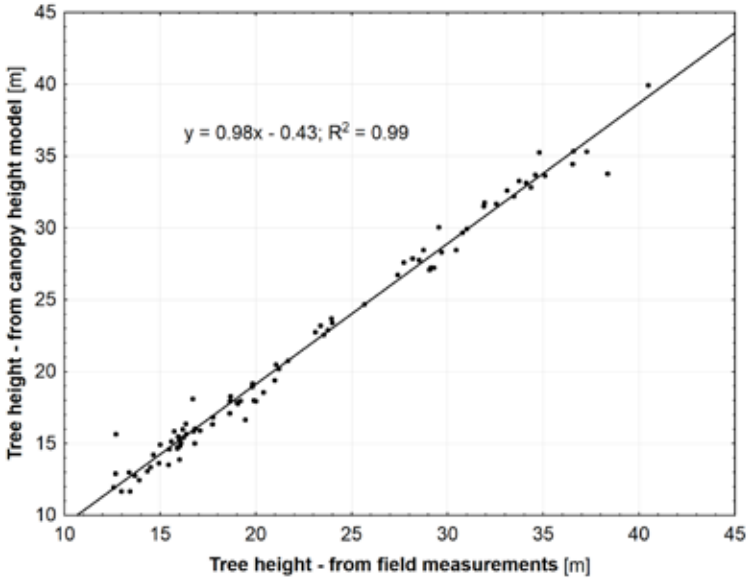

Fig. 5. *Comparison of tree heights derived from laser scanning data and tree heights measured in the field.*

3.3. AGB estimation

The set of AGB values from LiDAR data was retrieved for tree (see e.g. Fig. 6), plot, and compartment levels. AGB is presented in t ha^{-1}. Table 1 summarizes the statistical assessments.

Table 1. *Relationship between AGB from LiDAR data and AGB from field data. n = number of observations, nRMSE = normalized root-mean-square error.*

	Tree level			Plot level	Compartment level
	Spruce	Beech	All		
R^2 (*n*)	0.85 (78)	0.78 (21)	0.81 (99)	0.78 (29)	0.74 (29)
p	<0.01	<0.01	<0.01	<0.01	<0.01
nRMSE (%)	28	48	33	27	28

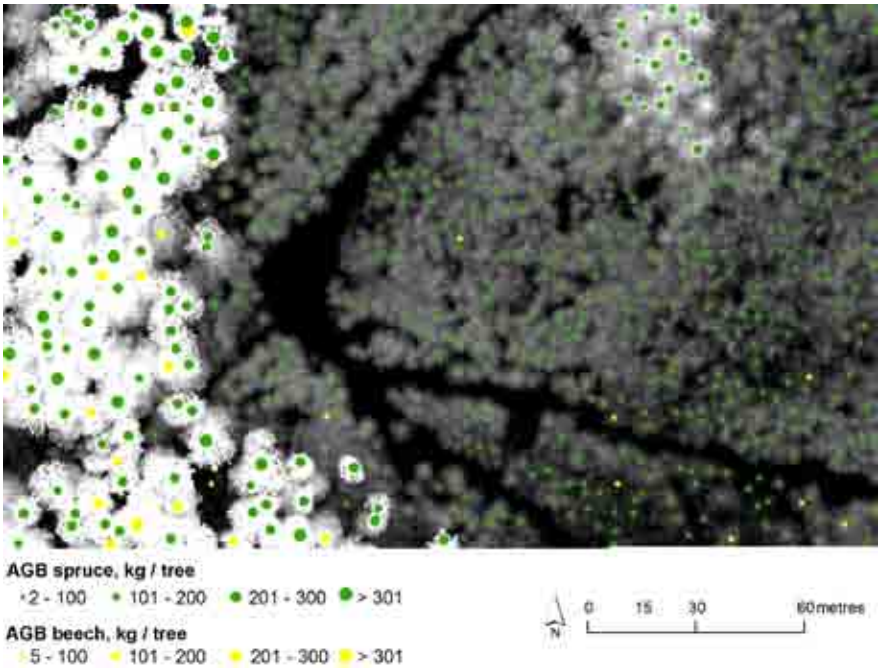

Fig. 6. *Map of above-ground biomass (AGB) from LiDAR data, where circles are identified trees, the two colours symbolize species, and circle size represents AGB amount.*

The results showed relatively high agreement between AGB estimated from "classical" forestry approaches and those from the new geoinformation method established from airborne LiDAR data for all three spatial resolution categories (i.e. tree, plot, and compartment levels).

Comparing tree-level AGB estimations from LiDAR data with those from field data results in $R^2 = 0.85$ for spruce (normalized root-mean-square error [nRMSE] = 28%), 0.78 for beech (nRMSE = 48%), and 0.81 for all trees (nRMSE = 33%) (Table 1). Greater accuracy for an AGB estimation ($R^2 = 0.92$) at tree level has been obtained in a boreal Canadian forest with prevalence of spruce (*Picea mariana, Picea glauca*) and pine (*Pinus contorta*) using airborne LiDAR data (Mora et al. 2013).

A comparison at the plot level revealed agreement between the field forestry inventory and LiDAR-based estimation with $R^2 = 0.78$ (nRMSE = 27%). Kankare et al. (2013) recorded similar results (nRMSE = 24.9%) for plot-level AGB in a boreal forest dominated by Scots pine (*Pinus sylvestris*) and Norway spruce (*Picea abies*).

There was weaker agreement at the compartment level between AGB estimated from LiDAR data and AGB from the forestry map ($R^2 = 0.74$, nRMSE = 28%). This disparity can be explained by the inability to distinguish suppressed and young trees in the understorey when analysing the surface model. However, Zhao et al. (2009) reported an AGB prediction across 1 ha scales with R^2 of 0.80 (RMSE = 14.3 t ha^{-1}) in pine plantations at various age development stages.

Uncertainties in AGB estimates in our study could follow mostly from uncertainties in tree species

classification based on LiDAR data, which classified trees into generalized groups of "coniferous" and "deciduous" without splitting them into various species of spruce, beech, fir, and birch. Although Norway spruce and European beech are the main tree species at our study site, silver birch (*Betula pendula*) and individually occurring silver fir played a minor role. Thus, methods for improving the classification result are a topic for further research. In addition, integration of LiDAR and hyperspectral data is planned for future work in order to expand the study and improve the AGB estimation (Anderson et al. 2008; Latifi et al. 2012; Laurin et al. 2014).

4. CONCLUSION

The study demonstrated that airborne LiDAR data provides AGB estimates with substantially low uncertainty and relatively high accuracy at tree, plot, and compartment levels. The method could potentially be recommended for regional forest inventories.

Acknowledgement

This work was supported by the Ministry of Education, Youth and Sports of the Czech Republic within the National Programme for Sustainability I, grant No. LO1415.

References

Anderson, J.E., Plourde, L.C., Martin, M.E. et al. (2008) Integrating waveform LiDAR with hyperspectral imagery for inventory of a northern temperate forest. *Remote Sensing of Environment,* **112**, 1856–1870.

Dong, J., Kaufmann, R.K., Myneni, R.B. et al. (2003) Remote sensing estimates of boreal and temperate forest woody biomass carbon pools, sources, and sinks. *Remote Sensing of Environment*, **84**, 393–410.

Fensholt, R., Sandholt, I., Rasmussen, M.S., Stisen, S. & Diouf, A. (2006) Evaluation of satellite based primary production modelling in the semiarid Sahel. *Remote Sensing of Environment*, **105**, 173–188.

Heinzel, J. & Koch, B. (2011) Exploring full-waveform LiDAR parameters for tree species classification. *International Journal of Applied Earth Observation and Geoinformation*, **13**, 152–160.

Hollaus, M., Mücke, W., Höfle, B. et al. (2009) Tree species classification based on full-waveform airborne laser scanning. *Proceedings of SilviLaser 2008: 8th international conference on LiDAR applications in forest assessment and inventory* (eds R.A. Hill, J. Rosette & J. Suárez), pp. 54–62. Edinburgh, UK.

Kadmon, R. & Harari-Kremer, R. (1999) Studying long-term vegetation dynamics using digital processing of historical aerial photographs. *Remote Sensing of Environment*, **68**, 164–176.

Kankare, V., Vastaranta, M., Holopainen, M. et al. (2013) Retrieval of forest aboveground biomass and stem volume with airborne scanning LiDAR. *Remote Sensing*, **5**, 2257–2274.

Koch, B. (2010) Status and future of laser scanning, synthetic aperture radar and hyperspectral remote sensing data for forest biomass assessment. *Journal of Photogrammetry and Remote Sensing*, **6**, 581–590.

Kovats, M. (1997) A large-scale aerial photographic technique for measuring tree heights on long-term forest installations. *Photogrammetric Engineering & Remote Sensing*, **63**, 741–747.

Latifi, H., Fanssnacht, F. & Koch, B. (2012) Forest structure modelling with combined airborne hyperspectral and LiDAR data. *Remote Sensing of Environment,* **121**, 10–25.

Laurin, G.V., Chen, Q., Lindsell, J.A. et al. (2014) Above ground biomass estimation in an African tropical forest with LiDAR and hyperspectral data. *ISPRS Journal of Photogrammetry and Remote Sensing*, **89**, 49–58.

Leckie, D.G., Gougeon, F.A., Walsworth, N. & Paradine, D. (2005) Stand delineation and composition estimation using semi-automated tree crown analyses. *Remote Sensing of Environment*, **83**, 355–369.

Liang, S., Li, X. & Wang, J. (2012) *Advanced Remote Sensing:* Terrestrial Information Extraction and Applications. Academic Press, USA.

Lim, K., Treitz, P., Baldwin, K., Morrison, I. & Green, J. (2003) LiDAR remote sensing of biophysical properties of tolerant northern hardwood forests. *Canadian Journal of Remote Sensing*, **29**, 658–678.

Luther, J.E., Skinner, R. Fournier, R.A. et al. (2014) Predicting wood quantity and quality attributes of balsam fir and black spruce using airborne laser scanner data. *Forestry,* **87**, 313–326.

Mora, B., Wulder, M.A., White, J.C. & Hobart, G. (2013) Modeling stand height, volume, and biomass from very high spatial resolution satellite imagery and samples of airborne LiDAR. *Remote Sensing*, **5**, 2308–2326.

Novotny, J. (2014) Tree crown delineation using region growing and active contour: approach introduction. *Proceedings of 20th International Conference on Soft Computing MENDEL 2014*, pp. 213–216. Brno University of Technology, Brno

Penner, M., Power, K., Muhairwe, C., Tellier, R. & Wang, Y. (1997) Canada's forest biomass resources: Deriving estimates from Canada's forest inventory. Information Report BC-X-370, Pacific Forestry Centre, Victoria, B.C., Canada.

Popescu, S.C. & Wynne, R.H. (2004) Seeing the trees in the forest: using LiDAR and multispectral data fusion with local filtering and variable window size for estimating tree height. *Photogrammetric Engineering & Remote Sensing*, **70**, 589–604.

Raupach, M.R., Rayner, P.J., Barrett, D.J. et al. (2005) Model-data synthesis in terrestrial carbon observation: methods, data requirements and data uncertainty specifications. *Global Change Biology*, **11**, 378–397.

Simova, P., Cerny, M., Ciencala, E. et al. (2009) A methodology for classifying aerial photographs within the Czech Terra landscape inventory system: a new approach to generating data for landscape analysis. *Journal of Landscape Studies*, **2**, 43–55.

Staněk, J., Zatloukal, V., Kubu, M. et al. (1997) Lesní zákon v teorii a praxi: úplné znění prováděcích předpisů s komentářem. Matice Lesnická, Písek (in Czech).

Wirth, C., Schumacher, J. & Schulze, E.-D. (2004) Generic biomass functions for Norway spruce in Central Europe – a meta-analysis approach toward prediction and uncertainty estimation. *Tree Physiology*, **24**, 121–139.

Woodcock, C.E., Collins, J.B., Gopal, S. et al. (1994) Mapping forest vegetation using Landsat TM imagery and a canopy reflectance model. *Remote Sensing of Environment*, **50**, 240–254.

Wutzler, T., Wirth, C. & Schumacher, J. (2008) Generic biomass functions for Common beech (*Fagus sylvatica* L.) in Central Europe – predictions and components of uncertainty". *Canadian Journal of Forest Research*, **38**, 1661–1675.

Zhao, K. G., Popescu, S. & Nelson, R. (2009) Lidar remote sensing of forest biomass: A scale-invariant estimation approach using airborne lasers. *Remote Sensing of Environment*, **113**, 182–196.

Chapter 18

Impacts of land use and climate change on ecosystem services in the Czech Republic

Eliška Krkoška Lorencová, Zuzana V. Harmáčková, David Vačkář

Department of Human Dimensions of Global Change, Global Change Research Centre, Czech Academy of Sciences, Bělidla 4a, CZ-60300 Brno, Czech Republic

1. INTRODUCTION

The Millennium Ecosystem Assessment (2005) developed an anthropogenic concept of ecosystem services that are defined as benefits that people obtain from ecosystems. Ecosystem services can be applied as measurable indicators of the functioning and change in the land system, which provide us with tools for management-relevant communications concerning past or potential future states of human-environmental systems (Müller & Burkhard 2012; Rounsevell et al. 2012).

As a whole, ecosystems provide a broad variety of services that are crucial to the existence as well as the social and economic development of human societies (Millennium Ecosystem Assessment 2005; Harrison et al. 2010). Due to its comprehensive integration of various factors, the concept of ecosystem services provides a useful framework for analysing linkages and interdependencies between natural and human systems (Burkhard et al. 2010).

Climate change is perceived as an important driving force in the distribution and functioning of natural ecosystems (Parmesan & Yohe 2003), and it also affects the provisioning of ecosystem services. In order to assess climate change impacts on ecosystem services and potential future trends, climate scenarios are valuable sources of information regarding the suitability of decisions that need to be taken in future.

Moreover, scenarios are not predictions; they are means for illustrating possible future developments while taking into account uncertainty and different interpretations of the current situation. Scenarios should provide consistent and plausible insight into a possible future that informs the main issues of a policy debate (European Environment Agency 2009).

Alcamo (2001) identifies a broad variety of potential scenario applications: (a) So-called baseline scenarios provide insights into future alternative states of the environment that lack additional environmental policies and therefore point to the need to implement environmental policies in order to avoid the negative impacts. (b) Scenarios can raise awareness regarding the connections among different environmental problems in future (e.g. climate change and food security). (c) Scenarios can illustrate how alternative policy pathways would achieve certain targets. (d) Scenarios combine qualitative and quantitative information about the future development of particular environmental problems. (e) Scenarios gauge the robustness of particular environmental policies under different future pathways and can therefore test the best available technology. (f) Scenarios can contribute to decision making, assisting policy makers to "think big" about environmental problems while taking into account the temporal and spatial scales. (g) Scenarios help to raise awareness about newly emerging or intensifying environmental problems over a period of several decades.

Assessment of climate change impacts on ecosystem services provides information necessary for

understanding these impacts and the consequences for the selection of appropriate adaptation and mitigation options. Several comprehensive studies have focused on the assessment of climate change impacts on ecosystem services and biodiversity. For instance, Staudinger et al. (2012) assessed climate change impacts on biodiversity and ecosystem services as an input to the US 2013 National Climate Assessment. These impacts are diverse, ranging from shifts in species and their phenology, to water scarcity and impairment of water quality, and to expansion of coastal areas vulnerable to food security issues.

Metzger et al. (2008) assessed the vulnerability of ecosystem services to environmental changes in Europe. Based on the scenarios used, the vulnerability assessment included ecosystem service indicators for four sectors: agriculture, forestry, nature conservation, and climate regulation.

On a regional level, Shaw et al. (2011) assessed and evaluated climate change impacts on California's ecosystem services. In that study, two ecosystem services, carbon sequestration and forage production, were assessed within the context of various future climate scenarios.

In the present study, we aim to contribute to the assessment of climate change impacts by employing scenarios to quantify the delivery of particular ecosystem services. Moreover, scenarios from the Assessing Large Scale Risks for Biodiversity with Tested Methods (ALARM) project for 2020, 2050, and 2080 are employed to quantify and model in a spatially explicit manner climate change impacts on the future provision of selected ecosystem services (carbon storage and sequestration as well as erosion control and sediment retention) in the Czech Republic.

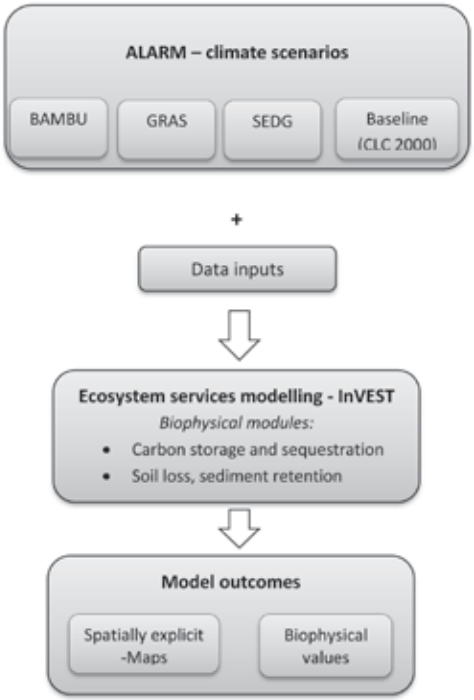

Fig. 1. *Methodological framework for ecosystem services assessment.*

2. MATERIALS AND METHODS

In order to assess climate change impacts on the selected ecosystem services, future scenarios were combined with ecosystem services modelling. Specifically, by combining future projections of ALARM scenarios (for 2020, 2050, and 2080) with Integrated Valuation of Environmental Services and Tradeoffs (InVEST) modelling of ecosystem services, the study aims to evaluate climate change impacts on selected ecosystem services in the Czech Republic. The methodological framework presented in this section is depicted in Fig. 1.

2.1. Application of ALARM scenarios

As mentioned in section 1, scenarios are useful tools for considering the future. Moreover, they can be helpful tools in assessing the future consequences of current environmental problems or the emergence of new future problems (Alcamo 2001).

This study utilized scenarios developed by the ALARM project. The scenarios had been designed originally to explore possible risks to biodiversity in terrestrial and freshwater ecosystems (Spangenberg 2007; Spangenberg et al. 2012). The ALARM scenarios have been statistically downscaled (Dendoncker et al. 2006) to a country-specific level (with a spatial resolution of 250 x 250 m) for the EU 25+2 (Norway and Switzerland) within the project EcoChange – Challenges in assessing and forecasting biodiversity and ecosystem changes in Europe (EcoChange). The ALARM scenarios are land-use scenarios based on Special Report on Emissions Scenarios (SRES) scenarios of the Intergovernmental Panel on Climate Change for 2020, 2050, and 2080 (Spangenberg 2007; Fronzek et al. 2012; Spangenberg et al. 2012).

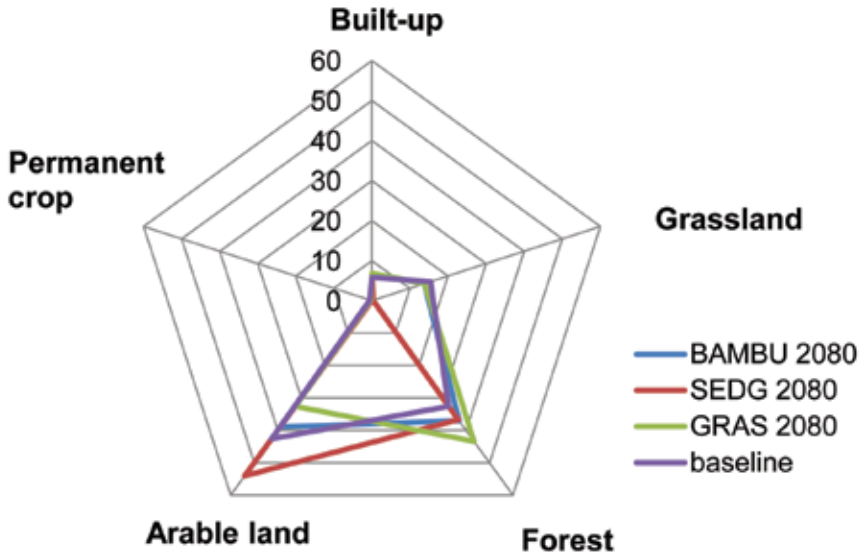

Fig. 2. *Land-use categories in the Czech Republic – BAMBU, SEDG, and GRAS scenarios in 2080 and baseline (CLC 2000).*

The ALARM scenarios comprise three core scenarios that cover a broad range of socioeconomic as well as political characteristics. The BAMBU (Business As Might Be Usual) scenario is based on the A2 SRES scenario, the GRAS (Growth Applied Strategy) scenario is based on the A1FI SRES scenario, and the SEDG (Sustainable European Development Goal) scenario is based on the B1 SRES scenario (Spangenberg 2007; Spangenberg et al. 2012). Table 1 presents the characteristics of each scenario.

Table 1. *Characteristics of ALARM scenarios. Based on Spangenberg (2007) and Fronzek et al. (2012).*

Scenario	Based on IPCC SRES scenario	Scenario description
BAMBU	A2	BAMBU (Business As Might Be Usual) extrapolates expected trends in EU policies and decision making, assessing their sustainability impacts. Climate mitigation and adaptation measures are included in this scenario, but environmental policy is perceived as another technological challenge. Larger regional differences in development occur.
GRAS	A1FI	GRAS (Growth Applied Strategy) focuses on economic growth and market liberalization. It is a free-trade, globalization, and deregulation scenario that focuses mainly on adaptation. Environmental policies focus on damage repair, and economic sustainability is understood mainly as economic growth.
SEDG	B1	SEDG (Sustainable European Development Goal) is a backcasting scenario. SEDG focuses on integrated environmental, social, institutional, and economic sustainability through environmentally oriented policies. As a normative scenario, SEDG is designed to meet specific sustainable development goals, with the aim of 75% reduction in CO_2 emissions by 2050. The SRES B1 scenario used a kind of "climate envelope" while ignoring the socio-economic considerations of that scenario.

The downscaled scenarios cover six land-use and land-cover (LULC) categories: built-up, arable land, permanent crops, grassland, forest, and other. With regard to the current study, these land-use categories (excluding other) were analysed in particular scenarios within the context of the Czech Republic.
Moreover, the BAMBU, GRAS, and SEDG scenarios were analysed for 2020, 2050, and 2080 with respect to the baseline and with the aim of assessing potential future land-use change in the Czech Republic.

2.2. Ecosystem service modelling: applying InVEST

InVEST has been applied to model ecosystem services. InVEST incorporates biophysical and economic information about ecosystem services, focusing on ecosystem services proper rather than on the underlying biophysical processes alone. Moreover, InVEST is a spatially explicit, scenario-driven modelling tool demonstrating the relationships among multiple ecosystem services (Tallis et al. 2011).
InVEST utilizes scenarios to project changes in ecosystem services provision in a changed climate and population. Based on the scenarios, a set of models quantifies and maps ecosystem services that inform managers and policy makers about the impacts of alternative future pathways (Tallis & Polasky 2009)resulting in many unintended consequences. These outcomes often affect society through unaccounted-for ecosystem services. A major challenge in moving to a more ecosystem-based approach to management that would avoid such societal damages is the creation of practical tools that bring a scientifically sound, production function-based approach to natural-resource decision making. A new set of computer-based models is presented, the Integrated Valuation of Ecosystem Services and Tradeoffs tool (InVEST).
Moreover, InVEST is a spatially explicit modelling tool that predicts changes at the ecosystem services, biodiversity conservation, and commodity production levels. This approach of quantifying and spatially determining ecosystem services provision can assist in conservation as well as in making decisions on natural resources more effective, efficient, and defensible (Nelson et al. 2009).

Ecosystem services modelling using InVEST is gaining increasing attention. InVEST has been applied in several studies around the world at global, regional, and local levels (Nelson et al. 2009; Nelson et al. 2010; Cardinale et al. 2012; Goldstein et al. 2012; Johnson et al. 2012; Arkema et al. 2013) in order to analyse future scenarios and project changes in the provision of particular ecosystem services.
In the present analysis, InVEST version 2.4.4 was applied, based on the ALARM scenarios, to assess climate change impacts of selected ecosystem services in the Czech Republic.
InVEST enables modelling of climate change impacts on ecosystem services by analysing scenarios that combine LULC data with climate projections. Climate change will alter the provision of ecosystem services upon which we rely currently. In order to devise appropriate adaptation and mitigation responses, it is necessary to understand how ecosystems and ecosystem services respond to climate change (Lawler et al. 2011).

2.3. Selected ecosystem services

The study also focused on analysing two ecosystem services: (1) carbon storage and sequestration, and (2) erosion control and sediment retention. We consider these services to be "umbrella services", meaning that support for these services indirectly affects support for many other services (Lorencová et al. 2013).
Carbon sequestration is considered a key ecosystem service inasmuch as carbon sequestration is today becoming one of the leading regulating ecosystem services at a national level and is increasingly attracting attention in the international context of climate change mitigation. Compared to other mitigation activities, carbon sequestration is a natural and cost-effective process with numerous ancillary benefits that are immediately applicable but have a finite sink capacity (Lal 2008) process industry, land-use conversion and soil cultivation is an important issue of the twenty-first century. Of the three options of reducing the global energy use, developing low or no-carbon fuel and sequestering emissions, this manuscript describes processes for carbon. Moreover, carbon stored in ecosystems is an important indicator of regulating services potential which is directly related to land-use disturbances and land management practices (Vačkář et al. 2011).
Erosion and sedimentation are natural processes contributing to healthy ecosystems, but excessive levels of these processes can have severe consequences. Severe soil erosion on arable land causes many environmental impacts both on as well as off site. On-site impacts related to soil erosion include loss of topsoil and fertilizers, decline in the supply of such other ecosystem services as food production (decreased crop yield where plants are lost or covered with sediment deposits), and, in the long term, a decrease in soil productivity. Off-site problems are often more obvious and include surface-water pollution with suspended sediments and other pollutants attached to sediment particles, such as phosphates or heavy metals, riverbed silting, and silted reservoirs and ponds with high sediment volume that require costly dredging operations (Verstraeten et al. 2002).

2.4. Data inputs

In order to assess climate change impacts on the selected ecosystem services (carbon sequestration and sediment retention), a variety of data inputs were used to calculate ecosystem service provision in biophysical terms.
Regarding carbon sequestration, InVEST data inputs include current and future land use represented by the ALARM scenarios and carbon pools (above-ground, below-ground, soil, and dead organic matter

carbon) of particular LULC categories based on a literature review. Due to data limitation, no additional optional carbon pools of harvested wood products (such as firewood, charcoal, and house timber) were considered in the analysis.

In the case of the InVEST sediment retention module, the Universal Soil Loss Equation (USLE; Wischmeier & Smith 1978) was utilized to calculate mean annual soil loss erosion in particular areas. In the model, the soil erosion rate was a function of LULC, soil type, rainfall intensity, and topography (Tallis et al. 2011). Data inputs comprised a digital elevation model extracted from the Advanced Spaceborne Thermal Emission and Reflection Radiometer Global Digital Elevation Model, a rainfall erosivity index (*R*-factor) (Krása 2010), and a soil erodibility factor (*K*-factor) (Panagos et al. 2012a,b). The BAMBU, GRAS, and SEDG ALARM scenarios in 2080 as well as the baseline are represented by LULC input. Maps of watersheds and sub-watersheds were obtained from the Digitální Báze Vodohospodářských Dat (Digital Database of Hydrological Data, www.dibavod.cz). The *C*-factor (the USLE's cover and management factor) and *P*-factor (the USLE's management practice factor) were based on a literature review.

3. RESULTS

3.1. Land-use analysis

At the start, land-use changes in the ALARM scenarios within the Czech Republic for 2020, 2050, and 2080 were spatially and quantitatively analysed.

The selected land-use categories were analysed in the context of the Czech Republic. Furthermore, the results of the scenarios for a particular year were quantitatively and spatially compared with the baseline, represented by the current land use according to Corine Land Cover (CLC 2000).

The quantitative results are illustrated by the proportions of land-use categories in the BAMBU, SEDG, and GRAS scenarios in 2080 as well as the baseline (Fig. 2). Compared to the baseline, the most striking changes are seen in the SEDG scenario, where arable land substantially increase in area and grassland and permanent crops almost disappear. In contrast, the BAMBU scenario resembles the baseline.

The BAMBU and GRAS scenarios indicate changes in border regions whereby the arable land in these fringe areas (in particular, the north-western Czech Republic) is replaced by forest and grasslands (Fig. 3). This is valid particularly in the case of the GRAS scenario, which focuses on economic growth and damage repair in environmental policy.

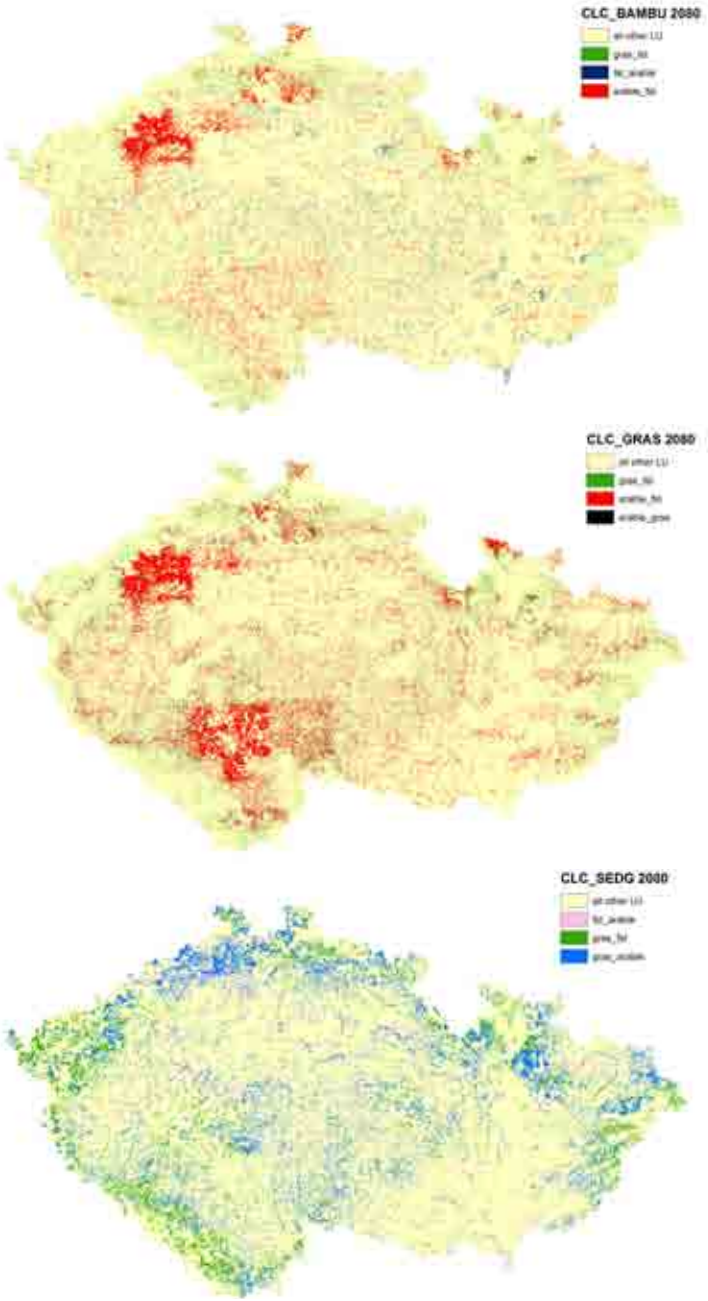

Fig. 3. *Land-use changes between baseline (CLC) and the BAMBU (upper panel), GRAS (middle panel), and SEDG (lower panel) scenarios in 2080.*

As a consequence, the GRAS scenario leads to a decrease in arable land and a potential decline in provisioning of ecosystem services. Major land-use changes in the GRAS scenario show similar features in all scenario years with the changes taking place particularly in the north-western and southern Czech Republic. The GRAS scenario also indicates a 7.7% decrease in arable land between 2020 and 2080, which is a more rapid decline than that in the BAMBU scenario. The decline mainly affects north-western and southern Bohemia and the western Czech Republic. Arable land is mostly replaced by forest, which increases from 35.6% of the total in 2020 to 43.4% in 2080. The proportions of built-up area, permanent crops, and grassland remain the same between 2020 and 2080, accounting for approximately 6.8%, 0.3%, and 13.7%, respectively.

Changes in the GRAS scenarios for 2020, 2050, and 2080 were analysed in comparison with the baseline (CLC 2000). Major changes in land use include a shift from arable land to forest as well as from grassland to forest and arable land to grassland. These changes are most substantial in 2080, where 9% of the total area shifts from arable land to forest, >3% from grassland to forest, and approximately 2% from arable land to grassland. Moreover, the GRAS scenario in 2080 shows an increase in forest area by almost 11% compared with the baseline, with the three major analysed land-use changes covering 14.3% of the total area in 2080.

In general, BAMBU extrapolates current trends in EU policies. In addition to minor regional changes, BAMBU shows a trend relatively similar to that of the baseline scenario. The BAMBU scenario indicates an almost 2% decline between 2020 and 2080 in arable land, however, from 41.8% in 2020 to 39% in 2080. Arable land decreases mainly in the northwestern, northern, and, in part, southern Czech Republic, where it is mostly replaced by forest. Based on these spatial changes, forested area shows an increase by 3% from 34% in 2020 to 37.1% in 2080. Between 2020 and 2080, the proportions of grassland and permanent crops decrease slightly, by 0.2% and 0.1%, respectively. Built-up area remains the same throughout the studied time period, accounting for 6.8% of all land.

In the BAMBU scenario, arable land changing to forest shows the highest rate of change compared with the baseline, amounting to 5% of the total area in 2080. Other major changes include the replacement of grassland by forest, mainly in the northern border and southern regions of the Czech Republic, accounting for approximately 2.5%. Alternatively, within some marginal areas, almost 2% of forest is replaced in 2080 by arable land compared with the baseline. As mentioned above, changes in the BAMBU scenario are not very rapid. By 2080, the three main analysed land-use changes comprise approximately 9.5% of the total area of the Czech Republic.

The SEDG scenario is focused on achieving socially, environmentally, and economically sustainable development (Spangenberg et al. 2012), and, as a result, it differs extensively from the BAMBU, GRAS, and baseline scenarios. In contrast to the previous scenarios, the SEDG scenario indicates replacement of grassland by arable land, which is due to the normative backcasting nature of the scenario designed to meet European sustainable development goals. In 2080, SEDG indicates an almost doubling of arable land compared with the baseline, which may lead to an increase in the provision of agricultural ecosystem services (Lorencová et al. 2013).

SEDG also differs substantially from the other two ALARM scenarios. In contrast to the BAMBU and GRAS scenarios, arable land considerably increases in SEDG compared with the baseline, ranging from 55.2% in 2020 to 54.1% in 2080. Spatially, arable land increases mainly near the northern and southern borders as well as in the central Czech Republic. Moreover, arable land spreads even to mountainous areas

that are in general unsuitable for agricultural activities. Grassland declines to 0.3%, retreating to only marginal areas. Changes in grassland result in the almost complete disappearance of grasslands, which are limited to only small fringes covering around 0.3% of land located in southern and northern Bohemia and partly at the eastern borders of the Czech Republic. Forest increases slightly in respect to the baseline scenario to 35.6% in 2020 and then to 36.7% in 2080. Permanent crops in the SEDG scenario almost disappear and built-up area remains similar to that of the baseline scenario.

Major land-use changes with respect to the baseline result in substantial losses of most grassland, which is largely replaced by arable land (9.5% of the baseline total land makes this shift) and forest (5.9% of the baseline total shifts thusly) in 2080. Moreover, shifts of forest to arable land account for approximately 3.9% of land. The three major analysed land-use changes are the most intensive in the SEDG scenario compared with the other scenarios. By 2080, 19.3% of the total area of the Czech Republic is altered.

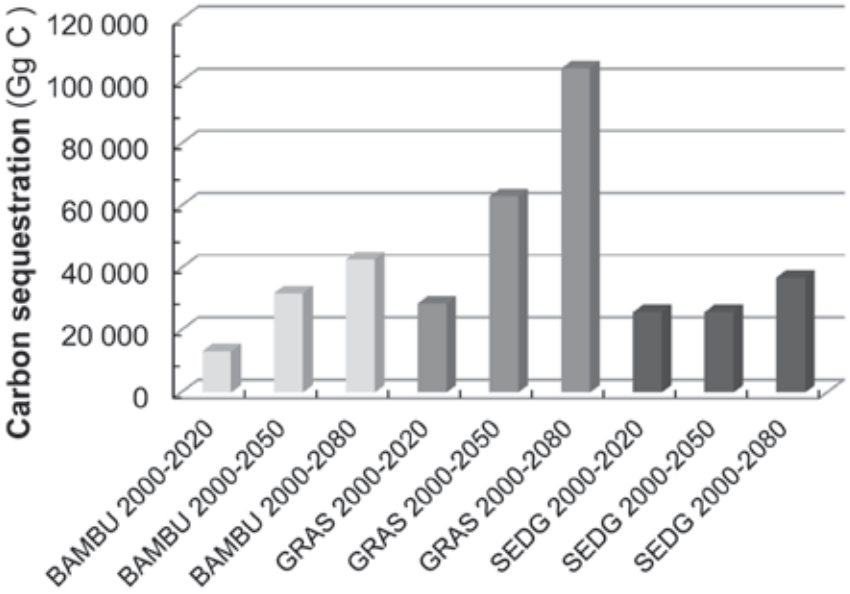

Fig. 4. *Carbon sequestration of BAMBU, GRAS, and SEDG scenarios compared to the baseline, for 2000–2020 (light grey columns), 2000–2050 (dark grey columns), and 2000–2080 (black columns).*

3.2. Carbon storage and sequestration

Based on the results of InVEST ecosystem service modelling, all scenarios (BAMBU, GRAS, and SEDG) show a larger amount of carbon stored in 2020, 2050, and 2080 compared with the baseline (CLC 2000). The most substantial increase in carbon storage is calculated for the GRAS scenario in 2080, where the amount of carbon increases by approximately 33% over the baseline.

On the other hand, the storage levels in the SEDG scenario are more or less stable throughout, showing only a minor increase in carbon storage, from 8% to 12% compared with the baseline.

The highest carbon sequestration rate during 2000–2080 is seen in the GRAS scenario, accounting for 104,224 Gg C and reflecting the substantial increase in forest within this scenario. In contrast, the lowest carbon sequestration rate during 2000–2080 is seen in the SEDG scenario, reaching 37,029 Gg C (Fig. 4). The highest annual carbon sequestration rate during 2000–2080 is displayed by the GRAS scenario, which accounts for 1,303 Gg C per year, while the lowest carbon sequestration rate is in the SEDG scenario, which comes to 463 Gg C per year.

In 2080, the proportion of forest in the GRAS scenario increases by 12.3% compared with the baseline. Also in the GRAS scenario, formerly arable land and grassland are replaced by forest, which has a substantially higher carbon storage rate than do any other land uses. Accordingly, Schulp et al. (2008) had identified land-use change as the most dynamic driving force of terrestrial carbon stock change, it is important to account for the land use changes in modelling carbon stock change.

3.3. Soil loss and sediment retention

Soil loss is represented on an annual basis in t ha^{-1}. The BAMBU, GRAS, and baseline scenarios show a similar range of soil losses, between 0.002 and 13.2 Mg ha^{-1}. The baseline scenario shows patterns similar to those of the BAMBU scenario, with greater soil loss in Moravia, as these scenarios have similar land use (for details see Fig. 5).

Soil loss in the GRAS scenario is relatively low compared with the baseline, particularly in the north-western, northern, and southern regions, which relates to the decrease in arable land that is replaced by forest in these areas.

SEDG scenarios in 2080 show the highest annual soil loss rates, amounting to as much as 31.8 Mg ha^{-1}. These high erosion rates occur mainly in the areas of substantial changes in land use in the northern and eastern border regions and Moravia, as in this scenario a considerable portion of the Czech Republic (over 13%) is transformed into arable land.

Based on the InVEST results, mean sediment retention in the sub-watersheds ranges between 0 and 678.2 Mg ha^{-1} annually. In contrast to the soil loss results, mean sediment retention shows no striking differences between particular scenarios and the baseline, although there are clear differences within given sub-watersheds. These changes are nevertheless related to changes in land use and the spatial distribution of reservoirs. While analysing the amount of sediment retained in the context of particular subwatersheds' prevailing land use, we confirm a strong relationship between these two values.

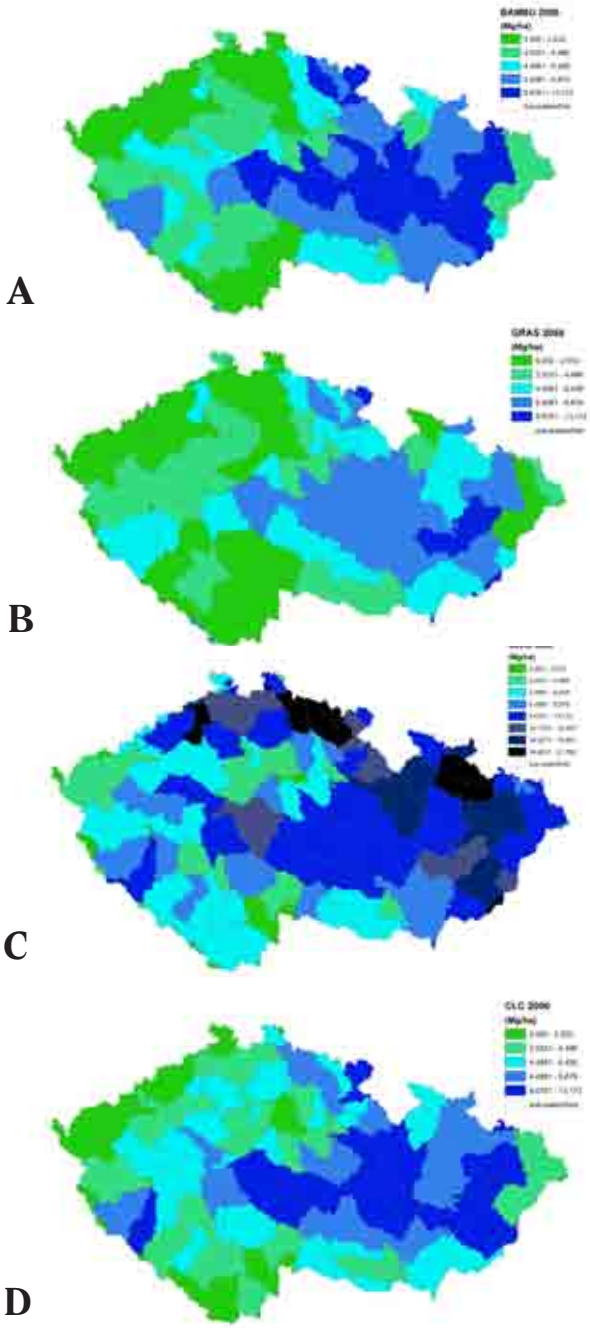

Fig. 5. *Annual soil loss (Mg ha^{-1}) estimated for BAMBU 2080 (***A***), GRAS 2080 (***B***), SEDG 2080 (***C***), and CLC 2000 (***D***).*

All the scenarios show a similar pattern within sub-watersheds with the lowest mean sediment retained occurring in the central and southern Czech Republic, where arable land prevails.
In contrast, there is higher sediment retention in the border region as these areas have mainly permanent vegetation, such as forest, which has considerably lower soil erosion and higher retention rates. The GRAS scenario shows the highest sediment retention rate in those sub-watersheds within the forested border regions.

4. DISCUSSION

4.1. Scenarios

Rubin (2013) suggests that society resembles a hologram consisting of a variety of small details, each interacting with one another as well as with the whole. The hologram is composed of such phenomena as social and natural events and human emotions and behaviour. We are accustomed to calling this holographic process reality. Compared with historical times, reality is rapidly changing, with increasing complexity and abstraction of social events and ongoing changes and impacts on natural systems.
As the present is characterized by uncertainty, innovation, and change, increasing attention is being devoted to scenario-planning techniques because of their usefulness in times of uncertainty and complexity (Schoemaker 1991). Moreover, scenario planning stimulates strategic thinking and, by constructing multiple futures, helps to overcome thinking limitations (Amer et al. 2013).
With respect to past land-use changes in the Czech Republic, the scenarios show fairly diverse pathways. During 1990–1999, the amount of arable land shrunk by 4%. In contrast, meadows and pastures substantially increased, by 15% and 11%, respectively, followed by permanent cultures with a rise of almost 5%. The intensity of agriculture declined and the increase in forest slowed slightly (Bičík et al. 2001).

4.2. Carbon storage and sequestration

Based on the national greenhouse gas inventory data, the so-called LULUCF (land use, land-use change and forestry) greenhouse gas inventory sector removed 987 Gg C in 1990 and 1,505 Gg C in 2010 (NIR 2012). When estimating annual carbon removals based on the period of carbon sequestration, the scenarios show comparable results in the range of national greenhouse gas inventory data. In all cases, LULC in the BAMBU, GRAS, and SEDG scenarios in the Czech Republic represent a net carbon sink. For instance, the annual removal is the lowest in the SEDG scenario, at an estimated 463 Gg C per year. Conversely, the GRAS scenario is estimated as accounting for the largest sink, with approximately 1,303 Gg C removed annually. Although it is necessary to be aware of limitations while comparing these different approaches to calculating carbon sequestration, this comparison aims to provide a context for these results.
Interestingly, the SEDG scenario shows the lowest provision of the carbon sequestration service, even though this scenario is focused on sustainable development. The SEDG scenario is a normative backcasting scenario and shows a considerable increase in arable land in the Czech Republic compared to the baseline (Spangenberg et al. 2012). The increase in arable land might lead to an expansion of agricultural ecosystem services (particularly such provisioning services as food production) while the regulating service of carbon sequestration declines substantially.

4.3. Soil loss, sediment retention

The BAMBU, GRAS, and baseline scenarios show similar ranges for soil loss of between 0.22 and 8.5 Mg ha^{-1} annually. The baseline shows patterns very similar to the BAMBU scenario, mainly due to the relatively comparable land-use proportions. The GRAS scenario has lower soil loss compared to the baseline, as forests have a very high protective function against soil erosion (Cebecauer & Hofierka 2008). A decline in soil loss is particularly evident in the north-western, northern, and southern Czech Republic. These areas of decline are associated with land-use change, where the arable land area is replaced by forest.

According to Cerdan et al. (2010), the mean erosion rate in Europe is 1.2 Mg ha^{-1} per year and the estimated mean regional erosion rate in the Czech Republic is 2.6 Mg ha^{-1} per year. These rates are comparable with those of the baseline, BAMBU, and GRAS scenarios. The SEDG scenario shows substantially higher soil loss rates, mainly due to rapid changes in land use. The SEDG scenario in 2080 shows the highest annual soil loss rates, amounting to as much as 24 Mg ha^{-1} per year.

With regard to soil loss in the Czech Republic, Krása et al. (2010) had calculated the amount of sediment lost due to run-off from arable land. Total annual sediment loss amounted to 3,175,280 Mg, which represents an annual loss of 0.565 m^3 of soil per hectare of arable land. Furthermore, mean long-term soil loss on agricultural land was calculated at approximately 2.34 Mg ha^{-1} annually, which is within the range of our soil loss estimates.

4.4. Climate change vulnerability

As vulnerability to climate change varies across sectors and regions, a key challenge will be to make adaptation context- and location-specific (European Environment Agency 2010).

In this respect, this study's results have the potential to identify regions vulnerable to climate change impacts and target delivery of particular ecosystem services (carbon storage and sequestration as well as erosion control and sediment retention) in the Czech Republic. Moreover, the spatially explicit results from this analysis can be used as a valuable body of evidence for preparing appropriate adaptation plans and measures in order to provide more specific information for decision making.

However, further research needs to be conducted within the Czech Republic to explore future adaptation pathways and to consider the design and implementation of adaptation measures and strategies in a changing climate.

4.5. Limitations and uncertainties

Uncertainties related to climate change scenarios, models, and adaptation measures need to be dealt with in a consistent manner, as various types of uncertainty can be observed, including scientific and methodological uncertainty (European Environment Agency 2012).

It is generally recognized that there will always be uncertainty regarding particular scenario assumptions. In particular, uncertainty can arise from the system's dynamics or may be associated with assumptions about the future development of driving forces (Alcamo 2001). After all, outcomes of human activities are by their nature highly unpredictable (Spangenberg et al. 2012).

Another limitation can be identified within the relatively broad classification of the ALARM scenario land-use categories in that they combine a variety of LULC classes into single categories. To the best of our knowledge, however, climate land-use scenarios with finer-scale land-use categories having the requisite distinctiveness and resolution are not currently available for the Czech Republic. This limitation needs to be taken into account when analysing the results. On the other hand, this limitation also provides an opportunity for further research into scenario development.

Moreover, the study focuses on analyses of two ecosystem services which are considered "umbrella services", meaning that support for these services indirectly influences support for many other services. Thus, these services are representative for the purposes of our study.

Another uncertainty is introduced by the assumption of linear ecosystem services availability even though in reality the provision of services is rather non-linear, as these services are conditioned by highly dynamic processes in nature for which quantitative measures are generally unavailable (Koch et al. 2009).

Application of the InVEST carbon sequestration and sediment retention models also has its limitations which need to be taken into account when considering the results.

With regard to carbon storage and sequestration, Tallis et al. (2011) mention some model limitations that originate in oversimplification of the carbon cycle and that thereby enable the model to run with relatively little information. It is assumed that all LULC types are at a fixed mean storage level and so changes in carbon storage over time are due only to changes in the LULC type or from wood product harvest. The resultant detail depends upon which LULC classification is used. Another limitation is that the model does not capture carbon that moves from one pool to another (e.g. when trees die). In addition, carbon emissions due to management activities (e.g. tractors burning fuel, fertilizer additions, livestock use) are not included into the assessment. Finally, the model assumes a linear change in carbon storage even though most sequestrations follow a non-linear path.

Due to data limitations, harvested wood products were not considered in the analysis, and this can lead to overestimation of carbon storage and sequestration. The aforementioned limitations need to be taken into account when making such estimates. Even considering the model's limitations, it nevertheless has the potential to provide reasonable spatially explicit information on ecosystem service quantities.

Concerning the InVEST sediment retention model, the USLE method is a standard method for calculating soil loss. It has several limitations, however, inasmuch as it predicts erosion from sheet-erosion alone (in-stream processes are ignored) and is more applicable to agricultural land and lowlands because it has been verified only in areas with slopes of 1–20°. Another simplification consists in the grouping of LULC classes. For instance, when all forest is combined into one LULC class (as is the case with the ALARM scenarios), then the difference in soil retention between old and newly planted forest land is neglected (Conte et al. 2011; Tallis et al. 2011).

Examination of these issues demonstrates that it is necessary to understand and present the calculated biophysical values of ecosystem services as indicative, not absolute. While bearing that in mind, this study provides a quantitative as well as spatially explicit analysis of climate change impacts on selected ecosystem services at the national level on the basis of the future climate scenarios. As far as we are aware, such an assessment had not previously been performed in the Czech Republic. Another added value of this study lies in its combining of future climate and land-use projections in the Czech Republic (ALARM scenarios) with the InVEST modelling tool for ecosystem services. Combining these methods enables us to analyse long-term land-use trends along with spatial changes in the delivery of particular ecosystem services.

5. CONCLUSIONS

This study aimed to provide quantitative and spatially explicit information regarding projected changes in land use as well as climate change impacts on selected ecosystem services (carbon storage and sequestration as well as erosion control and sediment retention) in the Czech Republic. Depending on the characteristics of the particular scenario, the analysis shows a variety of trends in projected LULC in the Czech

Republic that are spatially explicit. The BAMBU scenario shows a spatial pattern resembling that of the baseline scenario. In 2080, however, 7.52% of arable land and grassland is replaced by forest land, mainly in the north-western and northern Czech Republic. In the GRAS scenario, the main land-use changes are a substantial increase in forest land. By 2080, 12.25% of arable land and grassland is replaced by forest land. Major changes in forest increases occur in the north-western, southern, and eastern border regions of the Czech Republic. The SEDG scenario shows the largest changes, including substantial increases in arable land distributed across the entire country. Arable land spreads even to regions that had not been predominantly agricultural due to unsuitable geographical and soil conditions. By 2080, arable land covers 54.1% of the Czech Republic and grasslands decline to 0.3%, retreating to only marginal areas in the southern and northeastern regions.

The ecosystem service assessment indicates that the spatial distribution of the provision of the selected ecosystem services reflects the scenarios of land-use changes. In the case of carbon sequestration, the SEDG scenario shows the lowest carbon sequestration rates, accounting for 37,030 Gg C during 2000–2080. The substantial increase in arable land under this scenario leads to a decline in carbon sequestration potential. In contrast, the GRAS scenario has the largest amount of carbon sequestered during 2000–2080, reaching 104,224 Gg C, which is almost three times that in the SEDG scenario. Spatial distribution of carbon sinks and sources reflects the land-use patterns of particular scenarios. In the case of sediment retention, the link between land use and magnitude of ecosystem service delivered is not so straightforward. Stable vegetation cover is nevertheless one of the factors playing an important role in the amount of sediment retained and erosion avoided. In general, annul mean sediment retention in sub-watersheds ranges between 10.7 and 363.5 Mg ha^{-1}.

Although this study adopts an integrated interdisciplinary approach that has several limitations and uncertainties as discussed, it has the potential to contribute to ongoing discussions concerning climate impacts on particular ecosystem services. Application of future climate and land-use projections together with ecosystem services modelling provides us with interesting quantitative and spatial insights into future trends in the delivery of such services in the Czech Republic.

Acknowledgements

This work was supported by the Ministry of Education, Youth and Sports of the Czech Republic within the National Programme for Sustainability I, grant No. LO1415. The authors thank Kateřina Gdulová for her valuable support with ArcGIS data processing and Leanne Ezzy for assistance with language. We thank the authors of the ALARM scenarios, which have been downscaled within the EcoChange project.

References

Alcamo, J. (2001) Scenarios as tools for international environmental assessments. Environmental issue report No 24. European Environment Agency, Copenhagen.

Amer, M., Daim, T.U. & Jetter, A. (2013) A review of scenario planning. *Futures*, **46**, 23–40.

Arkema, K.K., Guannel, G., Verutes, G. et al. (2013) Coastal habitats shield people and property from sea-level rise and storms. *Nature Climate Change*, **3**, 1–6.

Bičík, I., Jeleček, L. & Štěpánek, V. (2001) Land-use changes and their social driving forces in Czechia in the 19th and 20th centuries. *Land Use Policy*, **18**, 65–73.

Burkhard, B., Petrosillo, I. & Costanza, R. (2010) Ecosystem services – bridging ecology, economy and social sciences. *Ecological Complexity*, **7**, 257–259.

Cardinale, B.J., Duffy, J.E., Gonzalez, A. et al. (2012) Biodiversity loss and its impact on humanity. *Nature*, **486**, 59–67.

Cebecauer, T. & Hofierka, J. (2008) The consequences of land-cover changes on soil erosion distribution in Slovakia. *Geomorphology*, **98**, 187–198.

Cerdan, O., Govers, G., Le Bissonnais, Y. et al. (2010) Rates and spatial variations of soil erosion in Europe: a study based on erosion plot data. *Geomorphology*, **122**, 167–177.

Conte, M., Ennaanay, D., Mendoza, G. et al. (2011) Retention of nutrients and sediment by vegetation. *Natural Capital: Theory and Practice of Mapping Ecosystem Services* (eds P. Kareiva, H. Tallis, T.H. Ricketts, G.C. Daily & S. Polasky), pp. 89–110. Oxford University Press, New York.

Dendoncker, N., Bogaert, P. & Rounsevell, M. (2006) A statistical method to downscale aggregated land use data and scenarios. *Journal of Land Use Science*, **1**, 63–82.

European Environment Agency (2009) *Looking back on looking forward: a review of evaluative scenario literature*. Copenhagen, Denmark.

European Environment Agency (2010) T*he European Environment, State and Outlook 2010: Adapting to climate change*. Copenhagen, Denmark.

European Environment Agency (2012) *Climate change, impacts and vulnerability in Europe 2012: An indicator-based report*. Copenhagen, Denmark.

Fronzek, S., Carter, T.R. & Jylhä, K. (2012) Representing two centuries of past and future climate for assessing risks to biodiversity in Europe. *Global Ecology and Biogeography*, **21**, 19–35.

Goldstein, J.H., Caldarone, G., Duarte, T.K. et al. (2012) Integrating ecosystem-service tradeoffs into land-use decisions. *Proceedings of the National Academy of Sciences of the United States of America*, **109**, 7565–7570.

Harrison, P.A., Vandewalle, M., Sykes, M.T. et al. (2010) Identifying and prioritising services in European terrestrial and freshwater ecosystems. *Biodiversity and Conservation*, **19**, 2791–2821.

Holland, R.A., Eigenbrod, F., Armsworth, P.R. et al. (2011) Spatial covariation between freshwater and terrestrial ecosystem services. *Ecological Applications*, **21**, 2034–2048.

Johnson, K.A., Polasky, S., Nelson, E. & Pennington, D. (2012) Uncertainty in ecosystem services valuation and implications for assessing land use tradeoffs: An agricultural case study in the Minnesota River Basin. *Ecological Economics*, **79**, 71–79.

Koch, E.W., Barbier, E.B., Silliman, B.R. et al. (2009) Non-linearity in ecosystem services: temporal and spatial variability in coastal protection. *Frontiers in Ecology and the Environment*, **7**, 29–37.

Krása, J. (2010) *Empirical models for water erosion in the Czech Republic*. Habilitation Thesis. Czech Technical University in Prague, Prague.

Lal, R. (2008) Carbon sequestration. *Philosophical Transactions of the Royal Society of London Series B*, **363**, 815–30.

Lawler, J.J., Nelson, E., Conte, M., Shafer, S.L., Ennaanay, D. & Mendoza, G. (2011) Modelling the impacts of climate change on ecosystem services. *Natural Capital: Theory and Practice of Mapping Ecosystem Services*. (eds P. Kareiva, H. Tallis, T.H. Ricketts, G.C. Daily & S. Polasky), pp. 323–338. Oxford University Press, New York.

Lorencová, E., Frélichová, J., Nelson, E. & Vačkář, D. (2013) Past and future impacts of land use and climate change on agricultural ecosystem services in the Czech Republic. *Land Use Policy*, **33**, 183–194.

Millennium Ecosystem Assessment (2005) *Ecosystems and human well-being. Synthesis*. Island Press, Washington, DC

Metzger, M.J., Schroeter, D., Leemans, R. & Cramer, W. (2008) A spatially explicit and quantitative vulnerability assessment of ecosystem service change in Europe. *Regional Environmental Change*, **8**, 91–107.

Müller, F. & Burkhard, B. (2012) The indicator side of ecosystem services. *Ecosystem Services*, **1**, 26–30.

Nelson, E., Mendoza, G., Regetz, J. et al. (2009) Modeling multiple ecosystem services, biodiversity conservation, commodity production, and tradeoffs at landscape scales. *Frontiers in Ecology and the Environment*, **7**, 4–11.

Nelson, E., Sander, H., Hawthorne, P. et al. (2010) Projecting global land-use change and its effect on ecosystem service provision and biodiversity with simple models. *PloS ONE*, **5**, e14327.

NIR (2012) *National Greenhouse Gas Inventory Report of the Czech Republic (reported inventories 1990–2010)*. Czech Hydrometeorological Institute, Praha-Komořany.

Panagos, P., van Liedekerke, M., Jones, A. & Montanarella, L. (2012a) European Soil Data Centre: Response to European policy support and public data requirements. *Land Use Policy*, **29**, 329–338.

Panagos, P., Meusburger, K., Alewell, C. & Montanarella, L. (2012b) Soil erodibility estimation using LUCAS point survey data of Europe. *Environmental Modelling & Software*, **30**, 143–145.

Parmesan, C. & Yohe, G. (2003) A globally coherent fingerprint of climate change impacts across natural systems. *Nature*, **421**, 37–42.

Raudsepp-Hearne, C., Peterson, G.D. & Bennett, E.M. (2010) Ecosystem service bundles for analyzing tradeoffs in diverse landscapes. *Proceedings of the National Academy of Sciences of the United States of America*, **107**, 5242–5247.

Rodriguez, J.P., Beard, T., Douglas, J. et al. (2006) Trade-offs across space, time and ecosystem services. *Ecology and Society*, **11**, 28.

Rounsevell, M.D.A., Pedroli, B., Erb, K.-H. et al. (2012) Challenges for land system science. *Land Use Policy*, **29**, 899–910.

Rubin, A. (2013) Hidden, inconsistent and influential: Images of the future in changing times. *Futures*, **45**, S38–S44.

Shaw, M.R., Pendleton, L., Cameron, D.R. et al. (2011) The impact of climate change on California's ecosystem services. *Climate Change*, **109**, 465–484.

Schoemaker, P.J. (1991) When and how to use scenario planning: a heuristic approach with illustration. *Journal of Forecasting*, **10**, 549–564.

Schulp, C.J.E., Nabuurs, G.-J. & Verburg, P.H. (2008) Future carbon sequestration in Europe – Effects of land use change. *Agriculture, Ecosystems and Environment*, **127**, 251–264.

Spangenberg, J.H. (2007) Integrated scenarios for assessing biodiversity risks. *Sustainable Development*, **15**, 343–356.

Spangenberg, J.H., Bondeau, A., Carter, T.R. et al. (2012) Scenarios for investigating risks to biodiversity. *Global Ecology and Biogeography*, **21**, 5–18.

Staudinger, M.D., Grimm, N.B., Staudt, A. et al. (2012) *Impacts of Climate Change on Biodiversity, Ecosystems, and Ecosystem Services: Technical Input to the 2013 National Climate Assessment. Cooperative Report to the 2013 National Climate Assessment*. United States Global Change Research Program, Washington, D.C.

Tallis, H. & Polasky, S. (2009) Mapping and valuing ecosystem services as an approach for conservation and natural-resource management. *Annals of the New York Academy of Sciences*, **1162**, 265–83.

Tallis, H., Ricketts, T., Guerry, A. et al. (2011) InVEST 2.4.4 User´s Guide: Integrated Valuation of Environmental Services and Tradeoffs. The Natural Capital Project, Stanford University, University of Minnesota, The Nature Conservancy, and World Wildlife Fund.

Vačkář, D., Melichar, J. & Lorencová, E. (2011) Ecosystem services of grasslands in the Czech Republic. Nature Conservation Agency of the Czech Republic. Prague.

Verstraeten, G., van Oost, K., van Rompaey, A. et al. (2002) Evaluating an integrated approach to catchment management to reduce soil loss and sediment pollution through modelling. *Soil Use and Management*, **18**, 386–394.

Wischmeier, W.H. & Smith, D. (1978) *Predicting rainfall erosion losses: a guide to conservation planning*. Agriculture Handbooks No. 537, USA.

ENGLISH EDITORIAL SERVICES

We take life science seriously.

IMPACT

The **Life Sciences Practice** at **English Editorial Services** provides high-impact editing, translation, publishing and communications services for serious life scientists.

Our clients do great science. We help them to communicate it with impact. **English Editorial Services** provides:

- Expert editing and translation of scientific articles, monographs and grant applications.
- Communications tools and publishing services for life science firms and institutions.

We provide scientific editing with impact to dozens of top scientists at more than 40 research institutes, universities and research hospitals in the Czech Republic. Can we help you, too?

Contact us in Czech or in English:
Gale A. Kirking
Editor-in-Chief
Tel: +420 545 212 872
gale@englisheditorialservices.com
www.EnglishEditorialServices.com